ON WALL-BOUNDED TURBULENT SHEAR FLOWS

by

Martin Wosnik

A dissertation submitted to the
Faculty of the Graduate School of the
State University of New York at Buffalo
in partial fulfillment of the requirements for the degree of

Doctor of Philosophy

May 2000

Department of Mechanical and Aerospace Engineering

To Lynn

ON WALL-BOUNDED TURBULENT SHEAR FLOWS

by

Martin Wosnik

Dissertation Advisor: Dr. William K. George

Abstract

Several *turbulent* wall-bounded flows are investigated by means of similarity analysis, the Asymptotic Invariance Principle and Near-Asymptotics. The flows include pipe and channel flows, plane wall jets, thermal boundary layers and zero pressure gradient boundary layers. Inner and outer regions of these flows can be matched at finite Reynolds number, but become asymptotically independent of it, and reduce to similarity solutions of the inner and outer boundary layer equations in the limit.

A new theory for pipe and channel flow is developed, where Reynolds number dependent logarithmic overlap profiles and a logarithmic friction law provide an excellent description of experimental velocity and skin friction data over more than three and a half decades in Reynolds number. Since the overlap velocity profile is a logarithm in $y+a$, logarithmic behavior inside $y^+ \approx 300$ cannot be established unless the *mesolayer* and offset a^+ are explicitly accounted for.

A new theory is proposed for the plane wall jet, leading to new scaling parameters, i.e. the Reynolds shear stress in the outer layer scales to first order with u_*^2, so that the outer layer is governed by two velocity scales, U_m and u_*. Velocity profiles in the overlap region and the friction law exhibit power law behavior, with coefficients which depend on local Reynolds number. New scaling laws for the turbulence quantities are derived from the Reynolds stress equations. Excellent agreement with all the

experimental data is achieved. The hypothesis that the inner flow of all wall-bounded turbulent flows is the same appears to be supported.

The similarity analysis of George & Castillo (1997) for the isothermal zero pressure-gradient turbulent boundary layer on a flat plate is extended to the thermal boundary layer of forced convection. A new outer temperature scaling is derived. Temperature profiles in the overlap region and the heat transfer law are also power laws.

New developments are reported for the zero pressure gradient boundary layer originally treated by George/Castillo. The scaling of Zagarola & Smits (1998*b*) is found to be consistent with the fundamental scaling laws, and it is derived from a separability hypothesis. It is suggested that δ_*/δ is independent of local Reynolds number and uniquely determined by the initial/upstream conditions. A higher order solution for the boundary layer parameters is derived, and tools to distinguish between the classical log-law and the George/Castillo theory are explored.

Acknowledgements

I would like to thank, first of all, my advisor Professor William K. George for his support and guidance throughout the course of this work. This dissertation would not have been possible without the many enlightening discussions with him and his continued support. My years in his laboratory at UB have taught me a lot, not just about turbulence. Thank you, Bill, you set the standard for any young scientist.

I would also like to thank Prof. Dale B. Taulbee and Prof. William J. Rae for being on my dissertation defense committee. I want to thank Professor Rolf Karlsson of the Royal Institute of Technology, Sweden, for being the outside reader.

I would like to express my appreciation to the faculty of the Department of Mechanical and Aerospace Engineering at the University of Buffalo for providing such an international and open-minded academic environment.

I am grateful to the following people for making their data available to me (in alphabetical order): Dr. H. Abrahamsson (Volvo Aerospace), Dr. J. Eriksson (Vattenfall Uetveckling), Prof. R. Karlsson (KTH), Prof. J. Kim (UCLA), Prof. L. Loefdahl (Chalmers University of Technology), Dr. J. Oesterlund (KTH), Prof. L. Smits (Princeton University), Prof. I. Wygnanski (Univ. of Arizona), Dr. M. Zagarola (Creare Inc.), and M. Zhou (Univ. of Arizona).

I would like to thank Prof. Hanjalic in the Applied Physics department at TU Delft, The Netherlands, for the opportunity to (once again) work on on natural convection flows as a guest researcher during the summer of 1998.

I want to thank the department of Thermo and Fluid Dynamics at Chalmers University of Technology, Sweden, for the opportunity to work on wall jets while being a guest in Gothenburg in 1999.

I also want to thank Prof. Nagib for inviting me to the Illinois Institute of Technology, Chicago, to work on boundary layer data bases in December 1999.

Financial support from the Department of Mechanical and Aerospace Engineering at the University of Buffalo, the UB Research Foundation, the Fulbright Commission, Millard Fillmore College, the Danish Center for Applied Mathematics and Mechanics, UB's The Center for Industrial Effectiveness, my parents, even certain friends and anonymous donors is gratefully acknowledged.

On a more personal note I want to thank my fellow students and staff in the Turbulence Research Laboratory for their friendship, helpful discussions and fun times. I want to mention our senior researchers Scott and Jim, who are the foundations of the laboratory. Debbie, who always brings good news ... The "old guard": Dan, Luciano, Joe and Asad. Stephan, Daehan, Honglu — who will keep the fire burning. Thanks, April and Bill, for showing me Europe from the water.

Being a graduate students sometimes makes you feel (and act) like a lonely warrior, but I would not have succeeded without my family, especially my parents, and friends and their unconditional support and encouragement ... (I'm afraid I might forget somebody if I start listing names, so — if you actually happen to be reading this — be *ascertained* that this 'thank you' goes out to YOU!) My dear friends, it may not always have been obvious, but your support meant a lot to me and I am truly grateful for it...

Finally, I wish to extend my warmest and deepest gratitude to Lynn for her loving support and infinite patience. There were times when we both thought this day would never come. Without her I would not be here.

Contents

List of Figures

List of Tables

Nomenclature

A, A_1, A_2: Parameters occurring in solution of Reynolds number dependence

A_i, A_o : $= f(\delta_T^+)$. Coefficients for mean temperature profile (chapter 6)

A' : Parameter for thermal boundary layer (chapter 6)

B_i, B_o : $= f(R^+)$. Coefficients for mean velocity profile in pipe/cahnnel flow

B, B_1 : Constants for mean velocity profile in pipe/channel flow

C_i, C_o : $= f(\delta^+)$. Coefficients for mean velocity profile

C, D : Constants

c : Specific heat

c_p : Specific heat at constant pressure

c_v : Specific heat at constant volume

e : Internal (thermal) energy per unit mass

F_s : Local scale for turbulent heat flux

F_w : $= \frac{q_w}{\rho c_p}$. Kinematic wall heat flux

f : Functional form for mean streamwise velocity

g : Gravitational acceleration

g : Ratio of inner and outer velocity scale (Appendix B)

g : Functional form for mean temperature (chapter 6)

H : $\equiv \delta_*/\theta$. Shape factor

h : $= \frac{q_w}{T_w - T_\infty}$. Heat transfer coefficient

h : Functional form for turbulent heat flux (chapter 6)

h : "h-function" of George & Castillo (1997)

i, j, k : Indeces in index notation

k : Thermal conductivity

L : Characteristic streamwise length

m : parameter for coordinate transformation, overlap anlysis

n : Exponents (Similarity of the outer equations)

P : Mean static pressure

P_∞ : Hydrostatic pressure at infinite distance from the wall

p : fluctuating pressure (or pressure in general)

q_w : $= -k\left(\frac{\partial T}{\partial y}\right)_{y=0} = h(T_w - T_\infty)$. Wall heat flux

R_S : Local scale for Reynolds' stress

T : Mean temperature (or temperature in general, Appendix A)

T_s : Temperature scale

T_w : Wall (surface) temperature

T_∞ : Temperature at infinite distance from the wall

ΔT : $= T - T_\infty$. Temperature difference

t : Fluctuating temperature

U : Mean streamwise velocity

U_i : Vector of mean velocity

U_M : Maximum velocity

U_s : Velocity scale

U_∞ : Free stream velocity in forced convection boundary layer

u : Streamwise fluctuating velocity

u_* : $\equiv \sqrt{\tau_w/\rho}$. Friction velocity

V : Mean cross-stream velocity

v : Cross-stream fluctuating velocity

W : Mean transverse velocity (in the z-direction)

w : Transverse fluctuating velocity (in the z-direction)

x : Streamwise coordinate

y : Cross-stream coordinate perpendicular to wall

$\overline{y}$: $= \frac{y}{\delta}$. Outer variable, similarity variable

y^+ : $= \frac{y}{\eta}, \frac{y}{\eta_T}$. Inner variable, similarity variable

z : Transverse coordinate, parallel to wall

Greek Symbols

α : parameter in solution for Reynolds number dependence

α : $= \frac{k}{\rho c_p}$. Thermal diffusivity

β : $= -\frac{1}{\rho}\left(\frac{\partial \rho}{\partial T}\right)_{p=const.}$. Coefficient of thermal expansion

δ : Outer cross-stream lengthscale, boundary layer thickness

$\delta_{99,95,90}$: Boundary layer thickness, defined by percent free stream velocity reached

δ_* : $\equiv \int_0^\infty (1 - U/U_\infty)\, dy$. Displacement thickness

η : Inner cross-stream lengthscale

κ : parameter for logarithmic overlap region.

(called the "von Karman constant" in old theory.)

μ : Dynamic (absolute) viscosity

ν : $= \frac{\mu}{\rho}$. Kinematic viscosity

ρ : Fluid density

τ_w : $= \mu\left(\frac{\partial U}{\partial y}\right)_{y=0}$. Wall shear stress

θ : $\equiv \int_0^\infty (1 - U/U_\infty)\, U/U_\infty dy$. Momentum thickness

ϵ : Dissipation of turbulent kinetic energy

Nondimensional Parameters and Characteristic Numbers

M : $= \frac{U}{a}$. The Mach number (Appendix A)

Pe_x : $= Re_x \cdot Pr$. The Peclet number

Pr : $= \frac{\nu}{\alpha}$. The Prandtl number

R^+ : $\equiv R/\eta = Ru_*/\nu$. a Reynolds number.

Re_x : $= \frac{U_S x}{\nu}$. The Reynolds number

St : $\equiv Nu/RePr = \Delta T_w u_*/F_w$. The Stanton number

St^* : $= St(U_\infty/u_*)$. Modified Stanton number

$y^+_{1/2}$: $\equiv y_{1/2}/\eta = y_{1/2}u_*/\nu$. a Reynolds number.

δ^+ : $\equiv \delta/\eta = \delta u_*/\nu$. a Reynolds number.

Parameter for Near-Asymptotics

δ_T^+ : $\equiv \delta_T/\eta_T = \delta u_*/\alpha$. a Reynolds number.

Parameter for Near-Asymptotics in thermal BL

Subscripts

i : Quantities asssociated with the inner layer

o : Quantities associated with the outer layer

s : Scaling function

w : Evaluated at the wall

∞ : Evaluated at infinite distance from the wall

Relation Symbols

$\sim$: "has the same x-dependence as"

$\equiv$: "defined as" (equivalent to)

$\cong$: "approximately equal to"

Acronyms and Abbreviations

AIP : Asymptotic Invariance Principle

AJL : Abrahamsson *et al.* (1994)

CTA : Constant Temperature Anemometry

EKP : Eriksson *et al.* (1998)

GC : George & Castillo (1997)

LDA : Laser Doppler Anemometry

WKH : Wygnanski *et al.* (1992)

ZS : Zagarola & Smits (1998*b*)

Chapter 1

Introduction

If you would be a real seeker after truth, it is necessary that at least once in your life you doubt, as far as possible, all things.
– René Descartes (1596-1650), French philosopher

1.1 Fluid Mechanics: Omnipresence

We live our lives constantly immersed in fluid, usually air or water. Fluid mechanics problems surround us, literally: when we exhale, the flow closely resembles a turbulent round jet; wind in our faces increases the rate of heat removed from the skin; submerged in a bath tub the pressure the water exerts on us — integrated over the surface of our bodies — results in a higher buoyancy force than we are used to from an air environment. Besides providing countless daily personal experiences, fluid mechanics is at the core of many engineering applications and applied physics investigations.

The equations governing momentum conservation in fluid flow, the Navier-Stokes equations[1], have been known for well over a century. For a full description of a flow one can also write equations for conservation of mass and energy, constitutive equa-

[1]Named after Navier (1827) and Stokes (1845), who derived them independently.

tions relating fluid stress to rate of strain (e.g. for a Newtonian fluid in the case of the Navier-Stokes equations) and the heat flux vector to the temperature field. Combined with two equations of state, describing e.g. pressure p and internal energy per unit mass e as a function of density ρ and temperature T ($p = p(\rho, T)$, $e = e(\rho, T)$), a well-posed, closed set[2] of equations for the quantities of interest in a flow field (u_i, ρ, p, e, T) is obtained. Unfortunately, a general solution to this closed set of coupled, partial differential equations is not known due to the nonlinearity contained in the convective terms of the Navier-Stokes equations.[3] Only a handful of exact solutions exist. These become possible if the nonlinear terms vanish due to kinematic restrictions (e.g. fully developed laminar pipe flow), or if global symmetries in a two-dimensional flow allow a transformation to a new set of independent variables, in which the nonlinear partial differential equations become nonlinear ordinary differential equations. This is referred to as a *similarity solution* and will be discussed in chapter 2.

1.2 Turbulence: The Enigma

When the forces driving a flow become large compared to the forces slowing it down, disturbances are no longer dampened and the flow becomes turbulent. This ratio of forces[4] is the Reynolds number Re, very likely the most important dimensionless parameters in fluid mechanics. Turbulent flow is always three-dimensional, rotational, time-dependent and characterized by random fluctuations. Turbulent flows are easily observed in the environment, e.g. the (usually buoyant) jets exhausting from smoke stacks. Turbulence is also characterized by different sizes (scales) of eddies; the range of scales present in a turbulent flow increases with Reynolds number.

Although the set of governing equations for the *instantaneous* (or *stochastic*) tur-

[2] In a well-posed problem the number of unknowns is equal to the number of equations available.

[3] When changing the momentum equation from an Eulerian description (fixed in space) to a Lagrangian frame of reference (following the fluid particle) the nonlinearity would occur in the stress term (when written with a symmetric stress tensor — the second Piola-Kirchhoff stress tensor).

[4] The Reynolds number can also be interpreted as a ratio of length or time scales.

bulent motion is still well-posed (a fact which is taken advantage of in Direct Numerical Simulations), it is now analytically intractable since no kinematic simplifications can be made. Usually mean values of velocity, pressure, temperature, etc. can be observed, and these quantities can be decomposed into a *mean* and a *fluctuating* part, where the mean value of the fluctuating part is zero by definition. In many engineering applications the average, or mean, values of e.g. shear forces or dissipation are of interest. Upon substituting the decompositions into the set of governing equations and averaging (time- or ensemble-averaging), something is gained *and* lost. On one hand, now kinematic simplifications can again be applied to the resulting mean (or *statistical*) quantities, but on the other hand the averages of non-linear occurrences (correlations) of the fluctuating quantities are not equal to zero and create new unknowns, without any new governing equations. For example, in the case of the Navier-Stokes equations, the so called Reynolds stresses $< u_i u_j >$, a symmetric second order tensor, arise from the averaging of the fluctuating convection terms, thus creating six new unknowns. A transport equation for the Reynolds stresses $< u_i u_j >$ can be derived, but even more new unknowns are created in the process. This is known as the "turbulence closure problem" and has been at the heart of industrial and fundamental research for the past half century. A general solution to the turbulence problem remains elusive. The quote "Turbulence is the last great unsolved problem of classical physics." is at different times attributed to either Einstein, Heisenberg or Feynman.

1.3 Wall-Bounded Turbulent Flows

When a (turbulent) flow occurs near a solid wall, a boundary layer[5] develops in which the velocity changes from its free stream value to zero at the wall. No matter how

[5]The term "boundary layer" is used loosely here. Later a distinction will be made between flows unconstrained in the wall-normal direction (e.g. flat plate boundary layer) and fully developed pipe and channel flows.

high the Reynolds number, or how large the scales of motion in the outer part of the boundary layer, the scales of motion near the wall remain small to maintain the no-slip condition. Outside a thin region near the wall, molecular viscosity effects become negligible and turbulent transfer of momentum dominates. Thus a so-called "inner" and "outer" region can be identified in wall-bounded turbulent flows.

Accurate prediction of boundary layer parameters such as wall shear stress is crucial for controlling the flow, e.g. avoiding flow separation and the associated increase in drag. An accurate description of how flow parameters change with Reynolds number all the way to their asymptotic limit is of great interest to both physicists and engineers, e.g. for the "scaling-up" of industrial mixing processes. Any similarity solution to a flow problem describes the proper asymptotic state.

Although it is generally agreed upon that the Navier-Stokes equations describe turbulence[6], they have been used only in a fleeting manner in the development of theories for wall-bounded flows, or in the validation of experimental data bases. Here, the Reynolds-averaged Navier-Stokes equations and the Reynolds stress transport equations will be used as the primary tool for evaluating theories and experiments for various wall bounded flows.

1.4 Dissertation Outline

This dissertation largely builds upon the theoretical concepts developed by George and co-workers over the past decade. In that sense (and in a historical perspective), it can be viewed as a third-generation work. An initial effort to raise questions about the classical boundary layer analysis was made in the late 1980's and early 1990's, e.g. George (1988) or George (1990). Simultaneously, a new approach to similarity analyses of turbulent flows was suggested by George (1989). The second generation consists of an application of these ideas to turbulent boundary layers, e.g. Knecht

[6] at least for a single-phase, Newtonian fluid.

(1990), George (1995) and Castillo (1997). The most important article is the one by George & Castillo (1997), where the theory for zero pressure-gradient boundary layer is developed. This work begins where the aforementioned article ended. Thus, for completeness most of its results are reviewed in appendix A.

In chapter 2 of this dissertation, important concepts such as similarity solutions, the Asymptotic Invariance Principle and Near-Asymptotics are explained. In chapter 3, new developments for the zero pressure gradient turbulent boundary layer are considered. A higher order solution to the constraint equation arising from Near-Asymptotics and a displacement thickness scaling and its implications are presented and tested against new experimental data. In chapter 4 a theory for fully developed pipe and channel flow is developed. Chapter 5 outlines a similarity theory for the plane turbulent wall jet and chapter 6 extends the boundary layer analysis to thermal boundary layers with temperature as a passive scalar.

Chapter 2

Similarity Concepts and Methodology

Every man takes the limits of his own field of vision for the limits of the world.
– Arthur Schopenhauer (1788-1860), German philosopher

2.1 Motivation

There have been several recent developments which make reconsideration of similarity theory of wall-bounded turbulent shear flows timely:

- George (1989) showed that the single length and velocity scale approach (in the literature referred to as "self-preservation" or "self-similarity") to the similarity of *free* shear flows was almost never correct since it over-constrained the governing equations, and proposed the more general approach which will be applied here.

- George (1995) suggested an Asymptotic Invariance Principle which not only could be applied to free shear flows, but allowed the inner and outer portions

of boundary layer flows to be considered separately, then matched at *finite* Reynolds numbers.

- Oberlack (1997) applied a Lie-group analysis to the equations governing the velocity fluctuations transport (and to equations derived from them) in plane parallel turbulent shear flows and demonstrated that both logarithmic *and* algebraic (power-law) profiles were among a class of invariant solutions for the mean velocity.

- New data, of greater accuracy and/or at higher Reynolds number, has become available for various flows over the past decade (e.g. Zagarola, 1996; Eriksson, Karlsson & Persson, 1998; Österlund, 1999), sparking renewed theoretical interest in the overlap region of wall-bounded turbulent flows (e.g. Barenblatt, 1993; George & Castillo, 1997; Zagarola, Perry & Smits, 1997; Wosnik, Castillo & George, 2000). The classical log-law (e.g. Millikan, 1938), long thought to be one of the cornerstones of turbulence theory, has come under intense scrutiny due to its various shortcomings (c.f. A.1.1) and its inability to account for finite Reynolds number effects.

- George & Castillo (1997) successfully applied the approach outlined in George (1995) to the zero pressure gradient boundary layer and correlated the results with boundary layer data. The requirement that inner and outer equations separately admit to similarity solutions in the infinite Reynolds number limit, led to different inner and outer velocity scales[1]. Upon matching at finite Reynolds number, power-law overlap profiles with Reynolds number dependent coefficient and exponent were obtained — in contrast to the classical theory.

[1]It will be shown in subsequent chapters that this is always the case for wall bounded flows which are inhomogeneous in the streamwise direction. Pipe and channel flows (chapter 4) are different, since the convection terms in the mean momentum equation are identically zero due to the streamwise homogeneity (a kinematic simplification).

2.2 Similarity Solutions

In all of the fundamental flow configurations considered here, "similarity" represents a (mathematical) symmetry in the problem, which can be extracted by non-dimensionalizing the quantities of interest into a new set of "similarity variables". If a similarity solution exists, then one should be able to bring the profiles into congruence ("collapse them") using a scaling function which depends only on one of the new variables. An immediate consequence would be that the governing equations become independent of this variable. The functional dependence of the equations is then reduced by one variable, which is extremely helpful when dealing with a two-dimensional or axisymmetric flow field. The governing equations for a two-dimensional flow can thus be reduced from nonlinear partial differential equations to nonlinear ordinary differential equations. Similarity solutions were first introduced to fluid dynamics by Blasius (1908), who applied them in laminar boundary layer theory leading to the well-known "Blasius-equation".

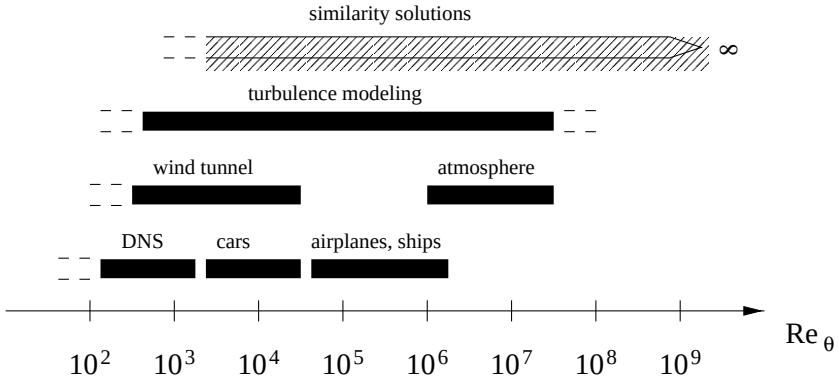

Figure 1: Typical Reynolds numbers of applications, experimental facilities and numerical simulations of boundary layers (given in terms of the boundary layer Reynolds number based on momentum thickness $Re_\theta = U_\infty \theta / \nu$)

It might be asked: Who cares whether similarity solutions to the governing equations exist or not, since most flows of industrial interest do not satisfy the simple boundary conditions of the fundamental flow configurations? The answer is the same as for any turbulent flow under consideration. Only a similarity solution provides an

unambiguous test of a turbulence model independent of computational constraints and experimental uncertainty. It does not depend on computational grid, domain, or differencing schemes, nor does it depend on difficulties in realizing and measuring a laboratory flow. It exists independent of closure approximations, and thus the scaling laws it offers can be used to test closure hypotheses. Its straightforward boundary conditions are free from the finite limits of experimental facilities or computer memories, and thus its profiles provide an ideal reference for testing the effects of enclosure. Most importantly, there is no upper Reynolds number limit for application of similarity solutions. From the moderate Reynolds numbers at which they become approximately valid, to infinite Reynolds number, similarity solutions can be compared to DNS, results from turbulence modeling, wind tunnel experiments to real-life large scale applications alike (c.f. Figure 1).

An alternative definition is given by George (1989): "A flow is said to be self-preserving if solutions to its governing equations and boundary conditions exist, for which all quantities of dynamical significance have the same relative value at the same relative location. The flow then has reached some kind of equilibrium where all of its dynamical influences evolve together. Thus self-preservation is an asymptotic state attained by a flow once its internal readjustments are complete."

Analytical approaches to the Reynolds-averaged equations governing wall-bounded turbulent flow have traditionally abandoned full similarity solutions at the outset, and instead *hypothesized* the existence of "local similarity solutions." The phrase "local similarity solutions" is somewhat misleading, since these are actually not "solutions" at all, but scaling laws proposed on purely dimensional grounds. Inner and outer flow were then analyzed with a single velocity scale. The classical idea of "self-preservation" in turbulent flows (in contrast with George (1989)) usually refers to a single velocity *and* single length scale approach.

In the analysis presented here, however, *full similarity solutions* will be sought for inner and outer sets of equations separately. A very important aspect of the theory

presented here is that no scaling laws are defined *a priori*; each statistical quantity will be allowed to have its own scale. These similarity solutions will then be substituted into the governing equations, and similarity conditions are found by demanding that all terms have the same streamwise (x) dependence. These conditions for similarity determine the asymptotically proper[2] scales for the flow under investigation. Obviously, these *similarity solutions* are quite different from the "local similarity" and "self-preservation" approaches. Applied this way, similarity theory can provide significant insight and new results without addressing directly the turbulence closure problem.

2.3 The Asymptotic Invariance Principle

The reduced inner and outer set of equations describing wall-bounded turbulent flow (for example, the momentum equations for ZPG-TBL A.12 and A.13) are exactly valid only in the limit of *infinite Reynolds number*. Therefore similarity solutions to these equations are also valid exactly only in the limit of *infinite Reynolds number* (c.f. Tennekes & Lumley (1972)). Seen another way, the equations have neglected terms which are Reynolds number dependent and lose these terms only in the limit. Therefore solutions to them must likewise be Reynolds number dependent and lose this dependence only at infinite Reynolds number. This idea was referred to as the *Asymptotic Invariance Principle* (AIP) by George (1995).

The Asymptotic Invariance Principle has always been applied to turbulent *free* shear flows, although not called by this name. Similarity solutions for those flows (when they exist) are infinite Reynolds number solutions because the equations from which they are derived are strictly valid only at infinite Reynolds number (George, 1989; Tennekes & Lumley, 1972). The difference in application here is that for wall-bounded turbulent flows, there are two sets of solutions — one which reduces to a

[2]In the limit of infinite Reynolds number.

full similarity solution of the outer equations, and another which reduces to a full similarity solution of the inner equations.

For finite Reynolds numbers, the Reynolds number dependence of the equations themselves, however weak, dictates that the solutions can not be similarity solutions anywhere[3]. Thus, the Reynolds number enters the problem as an additional variable. There now is one variable too many in the similarity transformation. Symbolically,

$$(x, y, Re) \longrightarrow (\xi, Re) \tag{2.1}$$

where $\xi \equiv y/\delta(x)$ and $\delta(x)$ is a *local* length scale. The AIP then requires that a functional form $F(\xi, Re)$ reduce to a function *of* ξ *only* in the limit as $Re \to \infty$, i.e.

$$F(\xi, Re) \longrightarrow F_\infty(\xi) \tag{2.2}$$

Therefore exact similarity solutions are only possible in this limit. Any scaling function *derived* from the condition for similarity must be an asymptotically correct scale, independent of how successful it is at collapsing data at finite Reynolds number, since it indeed produces solutions to the equations of motion which evolve no further in similarity variables. More elaborate scaling functions can be introduced to capture the Reynolds number dependence, but even these must reduce to the asymptotically correct scales in the limit (e.g. Zagarola & Smits (1998*b*), discussion in section 3.2)[4]. George (1989) suggested the existence of a similarity state which retains a dependence on initial (or upstream) conditions, and shows evidence for turbulent jets and wakes. There now seems to be evidence, contrary to the conventional wisdom, that this is also true for boundary layer flows, c.f. Castillo (2000) and Castillo, Walker

[3]But, as noted above, this is no different than for free shear flows which only asymptotically show Reynolds number independence.

[4]Scaling functions like that would arise from a similarity solution which includes Reynolds number dependence, i.e. a similarity solution to the full boundary layer equations. These functions can of course *not be derived* from reduced inner and outer equations, which are only exact at infinite Reynolds number.

and Wosnik (2000). The asymptotic dependence on initial or upstream conditions[5], denoted here as '$*$', is reflected in the AIP as

$$F(\xi, Re, *) \longrightarrow F_\infty(\xi, *) \tag{2.3}$$

In the following chapters, the Asymptotic Invariance Principle will be applied to the single-point, Reynolds-averaged equations governing the zero pressure gradient boundary layer (new developments in chapter 3, review of George & Castillo (1997) in appendix A), turbulent pipe and channel flows (chapter 4), the plane wall jet (chapter 5) and thermal boundary layers (chapter 6). Solutions will be sought which reduce to full similarity solutions of the equations in the limit of infinite Reynolds number, first for the inner layer and then for the outer. The form of these solutions will determine the appropriate scaling laws for finite as well as infinite Reynolds number, since alternative scaling laws could not be independent of Reynolds number in the limit. Once the method has been established by application to the equations governing the mean momentum, the same principle will be applied to equations governing the Reynolds stress equations and the statistical quantities appearing in them.

2.4 Near-Asymptotics: Finite vs. Infinite Reynolds Number

Appropriate inner and outer scaled versions of the velocity profile can be defined as two families of curves with parameter δ^+; i.e. for the zero pressure gradient turbulent boundary layer,

$$\frac{U}{U_{Si}(x)} = F_i(y^+, \delta^+) \tag{2.4}$$

[5]Initial or upstream conditions can be e.g. the wind tunnel speed (free stream velocity), the size and location of the trip wire or any recent flow history, i.e. how the flow got to the test section.

and

$$\frac{U - U_\infty}{U_{So}(x)} = F_o(\overline{y}, \delta^+) \tag{2.5}$$

where $\delta^+ = u_*\delta/\nu$. The outer velocity has been referenced to the free stream velocity at the centerline, U_∞, to avoid the necessity of accounting for viscous effects over the inner layer when the limits are taken later. Here y^+ and $\overline{y}$ are the cross-stream variable y normalized with an inner and outer length scale, respectively. The parameter δ^+ is a *local* Reynolds number; it is also the ratio of outer to inner length scales $y^+/\overline{y}$. Note that both length scales remain to be determined from the analysis.

The actual mean velocity profile at finite Reynolds number is the average of the instantaneous solutions to the Navier-Stokes equations and boundary conditions. This profile, whether determined from a real flow by measurement, a direct numerical simulation, or not at all, exists, at least in principle, and is valid everywhere *regardless of how it is scaled.* Therefore it is important to note that both families of curves described by equations 2.4 and 2.5, $F_i(y^+, \delta^+)$ and $F_o(\overline{y}, \delta^+)$, represent the *entire* velocity profile, at least as long as the dependence on δ^+ is retained (as long as δ^+ is finite). In other words, they represent the same solutions to the governing equations, and have simply been scaled differently.

F_i and F_o are quite unlike their limiting forms, $F_{i\infty}$ and $F_{o\infty}$, which are only infinite Reynolds number solutions for the inner and outer equations respectively. If F_i and F_o are considered instead of $F_{i\infty}$ and $F_{o\infty}$ (as is usually done), the problem of determining whether an overlap region exists is quite different from the usual asymptotic matching where infinite Reynolds number inner and outer solutions are extended and matched in an overlap region if one exists. The objective here is to determine *whether the fact that these scaled finite Reynolds number solutions (to the whole flow) degenerate at infinite Reynolds number in different ways* can be used to determine their functional forms in the common region they retain in the limit. The methodology of matching profiles at *finite* Reynolds number, termed *Near-Asymptotics*,[6] was first utilized by

[6] *Near-Asymptotics* should not be confused with *Intermediate Asymptotics* as developed by Baren-

George (1995) (see also George & Castillo, 1997; Wosnik & George, 1995; Wosnik, Castillo & George, 2000; Gamard & George, 2000; George, Abrahamsson, Eriksson, Karlsson, Löfdahl & Wosnik, 2000, for applications). It is necessary because the traditional approach cannot account for the possibility of the matching parameter tending to zero, as might be the case. By making it possible to include the Reynolds number dependence, it also makes the results easier to compare to experiments since most are carried out far from asymptotic conditions. The methodology of Near-Asymptotics will be applied to the overlap layer of various wall-bounded turbulent flows in the following chapters.

blatt (1996), where one interpolates between infinite Reynolds number solutions.

Chapter 3

Zero Pressure-Gradient Turbulent Boundary Layer: New Developments

Many a man had taken the first step. With every additional step you enhance immensely the value of your first.
– Ralph Waldo Emerson (1803-1882), American Philosopher

3.1 Introduction

The ideas introduced in the previous chapter were first applied to the zero pressure gradient boundary layer by George & Castillo (1997). Their work is reviewed in appendix A. In this chapter, some new insights and extensions of the analysis by George & Castillo (1997) are presented: The displacement thickness scaling for the velocity deficit suggested by Zagarola & Smits (1998*b*) is reconciled with the George/Castillo theory. Also, improvements are made to the parameters in the George/Castillo theory by means of a higher order solution (for the equation constraining C_i, C_o and γ). Finally, diagnostic tools for distinguishing between logarithmic and power law regions

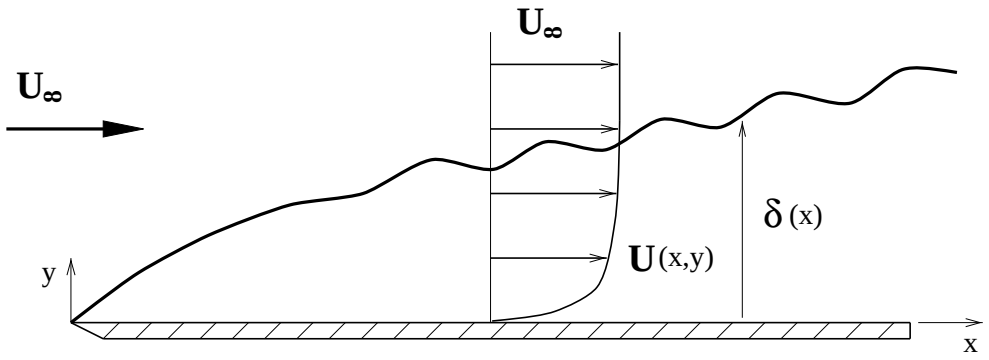

Figure 1: Definition sketch of the zero pressure gradient turbulent boundary layer.

are discussed.

The zero pressure-gradient turbulent boundary layer (shown in Figure 1) has been extensively investigated. It has very simple boundary conditions, yet contains the essential physics of the subject of wall-bounded turbulent flows, and is therefore the canonical problem. George & Castillo (1997) state: "...any general principles which apply to it should be applicable to all [wall-bounded flows] — if they are in fact principles and general..." Only new developments for the zero pressure gradient turbulent boundary layer are discussed here. For a review of previous work c.f. George & Castillo (1997) or appendix A.

3.2 Reconciling the Zagarola/Smits Scaling with the George/Castillo Theory

Recently, a new approach to the scaling of the velocity deficit for turbulent boundary layers which also departs from using the friction velocity as an outer velocity scale[1] was proposed by Zagarola & Smits (1998*b*). In apparent contradiction to George & Castillo (1997), they show striking experimental collapse of the velocity deficit normalized with a new scale defined as $U_s = U_\infty \delta_* / \delta$, where δ_* is the displacement thickness. In fact, using this scaling, near perfect collapse is also achieved for a range of δ^+ from 10^3 to 10^6 (and beyond) for theoretical velocity profiles calculated from the composite solution suggested by George and Castillo. This section shows that there really is no contradiction and how the two points of view can be reconciled. It also shows how the Zagarola/Smits scaling can be derived from the definition integral of the displacement thickness.

3.2.1 The Velocity Scaling of Zagarola and Smits

Zagarola & Smits (1998*b*) find *on empirical grounds* that the velocity deficit profile collapses with a velocity scale given by

$$U_{So} = U_\infty \frac{\delta_*}{\delta} \tag{3.1}$$

The experimental data is shown in figure 2 with this new velocity scale and the collapse in the outer part of the boundary layer is remarkable. Theoretical profiles of George & Castillo (1997) are shown in figure 3, also with this new velocity scale and for the same range of Reynolds numbers, δ^+, as in figure 2. The profiles collapse perfectly. It will be explored below why this scaling works so well.

[1] George & Castillo (1997) derived from similarity arguments that the asymptotically proper outer velocity scale is the free stream velocity, U_∞.

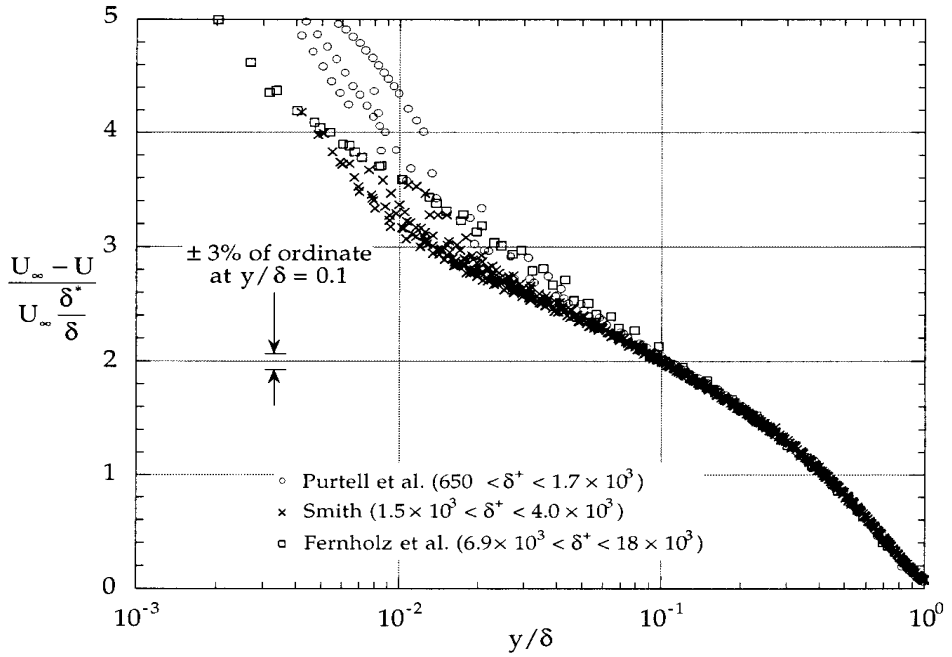

Figure 2: Velocity profiles normalized with new velocity scale based on displacement thickness suggested by Zagarola and Smits. Figure adapted from Zagarola and Smits (1998).

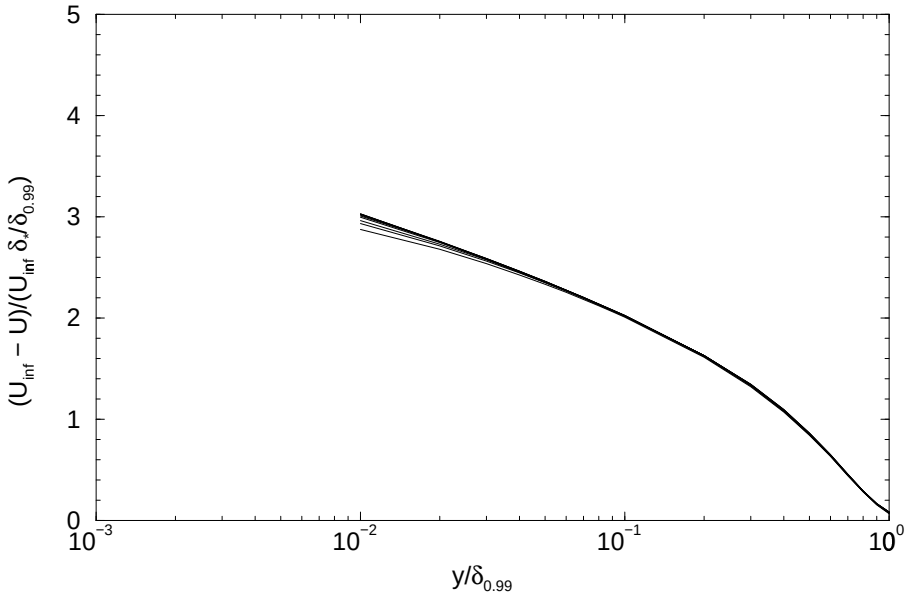

Figure 3: Velocity deficit profiles calculated from George/Castillo outer flow region profile and normalized with $U_\infty \delta_*/\delta$. The range of δ^+ is approximately the same as in the previous figure with experimental data

In the classical theory (Millikan, 1938; Clauser, 1954) the outer velocity scale was *assumed* to be the friction velocity, u_*, and it was shown to be related to the displacement thickness scaling

$$u_* \sim \frac{\delta_*}{\delta} U_\infty \tag{3.2}$$

The fact that $\delta_*/\delta\ U_\infty$ collapses the data remarkably well in the outer region and that u_* doesn't (c.f. figure 2 of Zagarola & Smits, 1998*b*) is further proof[2] that the Millikan/Clauser approach is wrong.

3.2.2 Displacement Thickness Scaling Applied to Velocity Deficit Profiles of Similarity Theory

The velocity deficit profiles of George & Castillo (1997) will be normalized with both U_∞ and the displacement thickness scaling $\delta_*/\delta\ U_\infty$, as shown in figures 4 and 5, respectively. The values for the similarity theory parameters given by George & Castillo (1997) are used. Using the data of Purtell *et al.* (1981) and Smith and Walker (1959), George & Castillo (1997) estimated the asymptotic values for the boundary layer parameters to be $\gamma_\infty = 0.0362$, $C_{o\infty} = 0.897$, $C_{i\infty} = 55$, $A = 2.9$, $\alpha = 0.46$ and $a^+ = -16$. In addition, they suggested on empirical grounds that

$$\frac{C_o}{C_{o\infty}} = 1 + 0.283 \exp(-0.00598\delta^+) \qquad \text{eqn.}(A.84)$$

To compensate for the difference between the actual velocity profile and the overlap profile outside the overlap layer, Coles (1956) (see also Coles 1968) define a "wake function". George & Castillo (1997), for reason of easy integrability, adapted a slightly different "wake function" as

$$w\left(\overline{y}, \delta^+\right) \;=\; \frac{U}{U_\infty} - C_o(\delta^+)\left(\frac{y+a}{\delta}\right)^{\gamma(\delta^+)}$$

[2] aside from the arguments made in George & Castillo (1997)

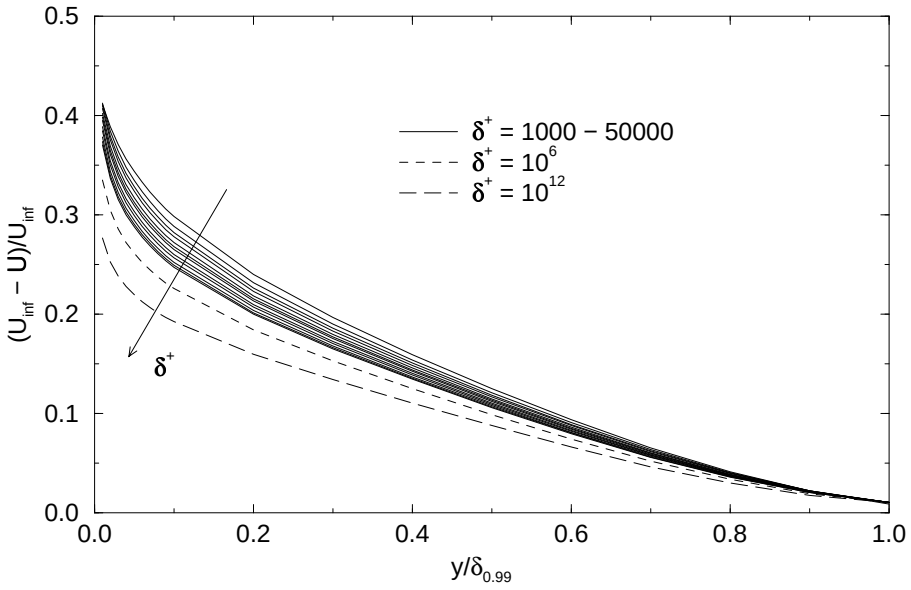

Figure 4: Velocity deficit profiles calculated from George/Castillo outer flow region profile and normalized with U_∞.

$$= \quad (1 - C_o)\,\overline{y}\sin B\overline{y} \tag{3.3}$$

Thus the semi-empirical velocity profile for the entire outer flow is given by

$$\begin{aligned} \frac{U}{U_\infty} &= 1 + f_o\left(\overline{y}, \delta^+\right) + w\left(\overline{y}, \delta^+\right) \\ &= C_o\left(\overline{y} + \overline{a}\right)^\gamma + (1 - C_o)\,\overline{y}\sin B\overline{y} \end{aligned} \tag{3.4}$$

which is shown in Figure 4 for a range of Reynolds numbers δ^+, normalized by the free stream velocity U_∞.

George and Castillo were also able to deduce on theoretical grounds that $\delta_*/\delta \to const. > 0$. In fact, by integrating a composite velocity profile using equation 3.4 they were able to obtain an explicit relation for δ_*/δ (and θ/δ) given to leading order in $1/\delta^+$ by

$$\frac{\delta_*}{\delta} = 1 - \frac{C_o}{1+\gamma} - 0.436(1 - C_o) \tag{3.5}$$

δ^+ (given)	C_o (eqn.A.84)	C_i (eqn.A.82)	γ (eqn.A.81)	u_*/U_∞ (eqn.A.83)
500	0.910	8.97	0.1288	0.0455
1,000	0.898	9.66	0.1156	0.0418
2,000	0.897	10.40	0.1052	0.0388
5,000	0.897	11.32	0.0947	0.0354
10,000	0.897	11.97	0.0884	0.0332
20,000	0.897	12.59	0.0831	0.0313

δ^+ (given)	δ_*/δ (eqn.3.5)	θ/δ (eqn.3.7)	R_θ (eqn.3.9)
500	0.155	0.113	1,244
1,000	0.151	0.112	2,669
2,000	0.144	0.108	5,581
5,000	0.136	0.104	14,725
10,000	0.131	0.102	30,621
20,000	0.127	0.100	63,608

Table 3.1: Parameters for George/Castillo theory as a function of δ^+

$$\begin{aligned} \frac{\theta}{\delta} &= 1 - \frac{C_o}{1+\gamma} - 0.436(1 - C_o) \\ &= -\left[1 - \frac{2C_o}{1+\gamma} + \frac{{C_o}^2}{1+2\gamma} - 0.582(1 - C_o)^2\right] \end{aligned} \tag{3.6}$$

where

$$\frac{\delta_*}{\delta} \longrightarrow 0.0894 \tag{3.7}$$

and

$$\frac{\theta}{\delta} \longrightarrow 0.0767 \tag{3.8}$$

as $\delta^+ \longrightarrow \infty$. Note that since C_o and γ are specified by the above equation as a function of δ^+, the parameters can easily be constructed on a spreadsheet as shown in table 3.1, where

$$R_\theta = \frac{U_\infty}{u_*}\frac{\theta}{\delta}\delta^+. \tag{3.9}$$

Since George & Castillo (1997) provide explicit analytical solutions for the velocity profile for all Reynolds numbers, it is possible to investigate whether the Zagarola/Smits scaling works for these theoretical profiles as well as it appears to for experimental data. In Figures 4 and 5 a total of 12 values of δ^+ ranging from 1×10^3 to 5×10^4 are plotted using the parameters shown in table 3.1. As a comparison, the currently highest Reynolds number experimental data are the measurements of Fernholz *et al.* (1995) Fernholz *et al.* (1995) on the wall of the German–Dutch wind tunnel with a δ^+ of 1.8×10^4. Note that results for δ^+ of 10^6 and 10^{12} are also shown to illustrate the asymptotic behavior of these theoretical profiles.

Figure 5 shows the Zagarola/Smits scaling, $U_{So} = U_\infty \delta_* / \delta$, applied to the theoretical profiles of George/Castillo (of Figure 4), where δ_*/δ was calculated from equation 3.5. The theoretical profiles show striking collapse. In fact the differences between the profiles are almost not discernible, and the collapse is even better than for experimental data. For comparison with experiment, the 70 profiles of Österlund (1999) are also shown in deficit scaling using $U_{So} = U_\infty$ (Figure 6) and in the displacement scaling using $U_{So} = U_\infty \delta_* / \delta$ (Figure 7). The same observations are made here. Obviously, both the George/Castillo and Zagarola/Smits results must be regarded as equivalent.

3.2.3 Why the Displacement Scaling Works

If we hypothesize that the dependence on Reynolds number and cross-stream position of the velocity deficit profile (overlap + "wake") is separable (for $\overline{y} > 0.1$ approximately), then we can write

$$\begin{aligned} \frac{U - U_\infty}{U_\infty} &= f_o\left(\overline{y}, \delta^+, *\right) + w\left(\overline{y}, \delta^+, *\right) \quad ; \quad \text{all } \overline{y} \\ &= G\left(\delta^+, *\right)\left[f_{o\infty}(\overline{y}) + w_\infty(\overline{y})\right] \quad ; \quad \overline{y} > 0.1 \text{ approx.} \end{aligned} \tag{3.10}$$

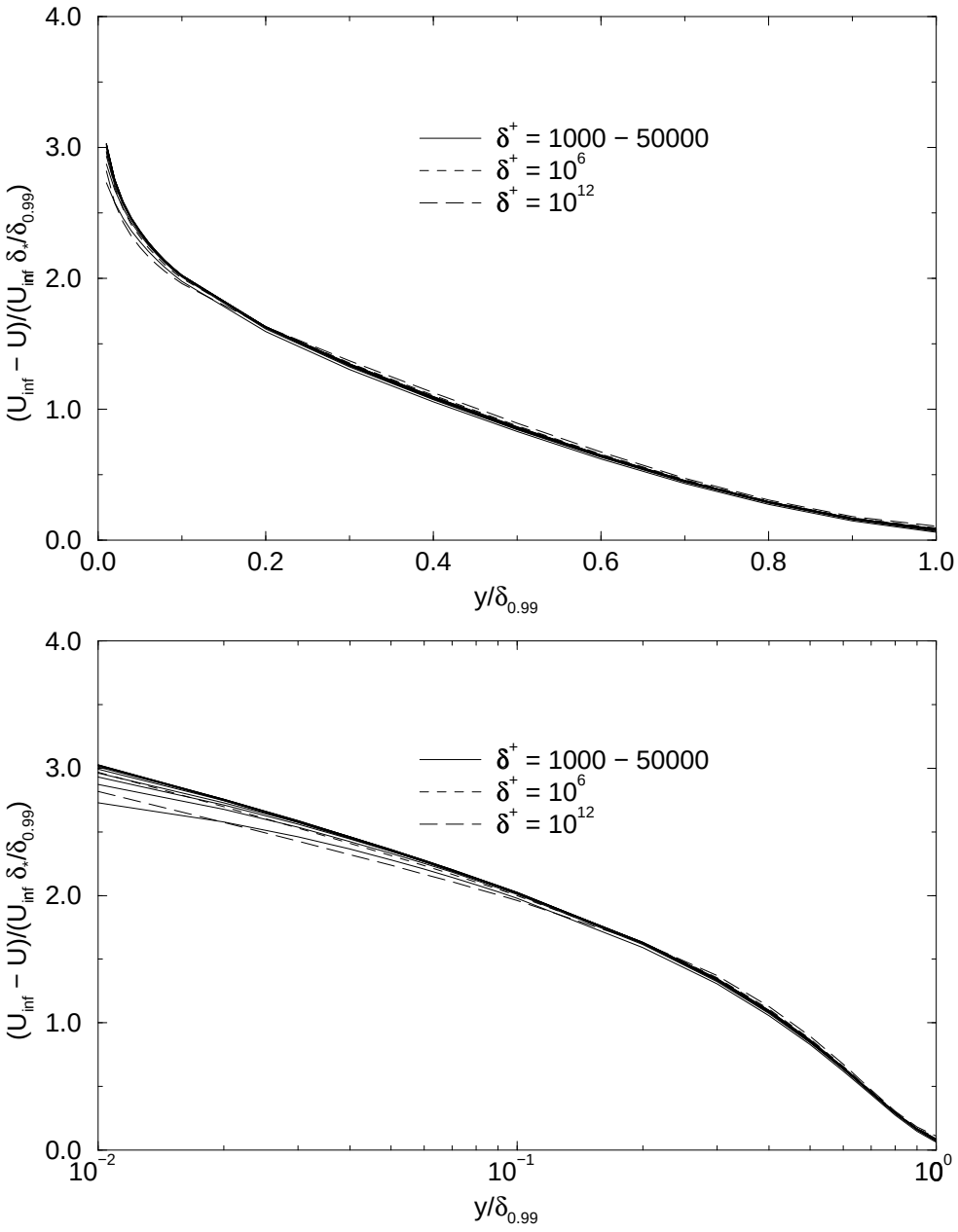

Figure 5: Velocity deficit profiles calculated from George/Castillo outer flow region profile and normalized with $U_\infty \delta_*/\delta$.

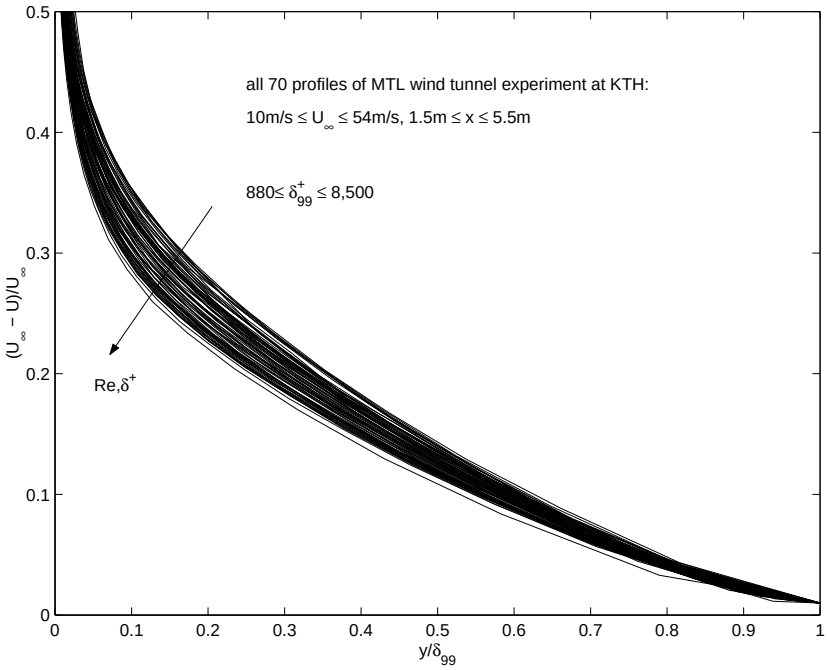

Figure 6: Experimental evaluation of displacement thickness scaling: Velocity deficit profiles of Österlund (1999) normalized with U_∞.

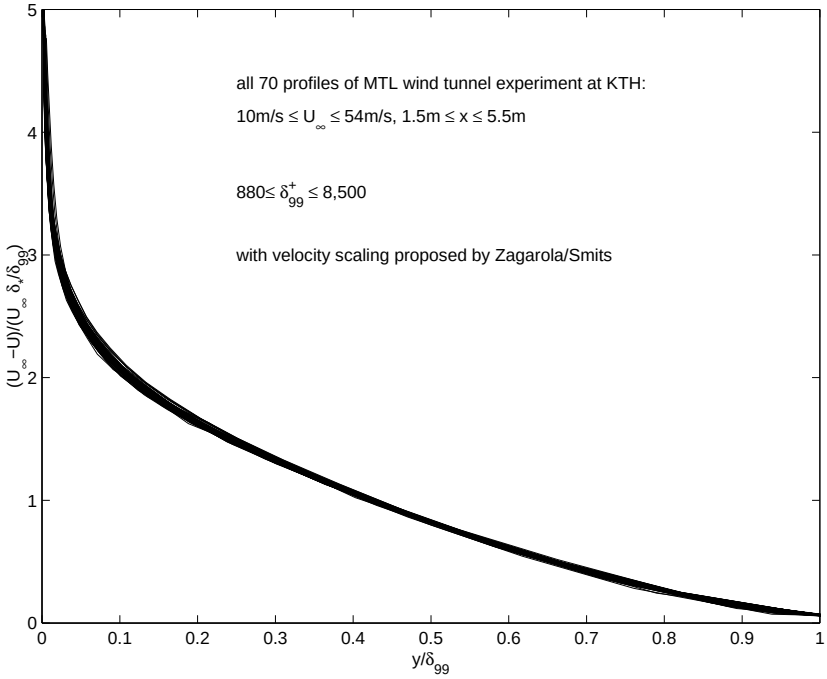

Figure 7: Experimental evaluation of displacement thickness scaling: Velocity deficit profiles of Österlund (1999) normalized with $U_\infty \delta_* / \delta$.

where the arguments inside the similarity function f_o and wake function w are the outer similarity coordinate, $\overline{y} = y/\delta_{99}$, the Reynolds number dependence, $\delta^+ = \delta u_*/\nu$, and any possible dependence on the upstream conditions, $*$, respectively. "Upstream conditions" can be e.g. the wind tunnel speed, the size and location of the trip wire or any recent flow history. The term in square brackets is a universal profile independent of δ^+ (i.e. independent of Reynolds number), and is in fact the limiting George/Castillo profile at infinite Reynolds number (i.e. $f_{o\infty}(\overline{y})$).

From substitution into the definition of the displacement thickness, δ_*/δ, it follows immediately that

$$\begin{aligned} \frac{\delta_*}{\delta} &\equiv \int_0^\infty \left(1 - \frac{U}{U_\infty}\right) d\overline{y} = \\ &\approx -G\left(\delta^+, *\right) \int_0^\infty \left[f_{o\infty}(\overline{y}) + w_\infty(\overline{y})\right] d\overline{y} \end{aligned} \tag{3.11}$$

In the limit as $\delta^+ \to \infty$ the contribution from the inner part vanishes identically. Moreover, the integral on the right-hand side is just $\lim_{\delta^+\to\infty} \delta_*/\delta$. Hence, in the limit as $\delta^+ \to \infty$,

$$\lim_{\delta^+\to\infty} G(\delta^+, *) \longrightarrow 1 \tag{3.12}$$

i.e.,

$$\lim_{\delta^+\to\infty} \frac{\delta_*}{\delta} \equiv \left.\frac{\delta_*}{\delta}\right|_\infty \tag{3.13}$$

George and Castillo (1997) estimated $\delta_*/\delta|_\infty = const. = 0.0894.$, from the data available to them. Therefore, the function $G(\delta^+, *)$, which contains all the Reynolds number dependence (at least according to the hypothesis above), has to be proportional to

$$G\left(\delta^+, *\right) = \frac{\delta_*/\delta}{\lim_{\delta^+\to\infty} \delta_*/\delta} \propto \frac{\delta_*}{\delta} \tag{3.14}$$

It follows immediately that the "effective" velocity scale for the mean velocity deficit profile is $\delta_*/\delta\ U_\infty$, exactly as Zagarola & Smits (1998*b*) claim.

This is not surprising, since the Reynolds number dependence of the h-function used by George and Castillo (and manifested in C_o and γ) is equivalent to that which is present in δ_*/δ, as long as the separability hypothesis is approximately valid.

The success of the Zagarola/Smits scaling suggests an alternative way to find the George/Castillo h-function. If it is *assumed* that δ_*/δ and θ/δ are known from experimental data, then equations 3.5 and 3.7 can be solved analytically for $\gamma(\delta^+)$ and $C_o(\delta^+)$. But since these equations and the data for δ_*/δ and θ/δ were used in the regression to obtain h originally, no new information can be gained. What will be seen to be surprising, however, is that it is the initial condition dependence, $*$, that determines δ_*/δ. In fact, it will be argued that δ_*/δ is nearly independent of local Reynolds number, δ^+, and uniquely characterizes the upstream conditions.

3.2.4 Variation of δ_*/δ with Reynolds Number

The idea that there might be a separate dependence on Reynolds number and initial conditions was introduced by George (1989) for free turbulent shear flows. There now is some evidence that this is also the case for turbulent boundary layers (c.f. Castillo & George, 2000; Castillo, Walker & Wosnik, 2000). If the upstream/initial conditions[3] are fixed and the Reynolds number is increased by simply moving the probe downstream, then the velocity data in outer variables will collapse with U_∞ only.

Examples of such surveys are the experiments by Wieghardt (1943) and the ongoing work of Johansson & Castillo (2000), and their velocity data in outer variables are shown in figures 8 and 9, respectively.

Examples of surveys where the upstream/initial conditions were changed by leaving the probe at a fixed location and increasing the free stream velocity are the experiments by Smith & Walker (1959) and Österlund (1999) and their velocity data

[3]Initial or upstream conditions can be e.g. the wind tunnel speed (free stream velocity), the size and location of the trip wire or any recent flow history, i.e. how the flow got to the test section.

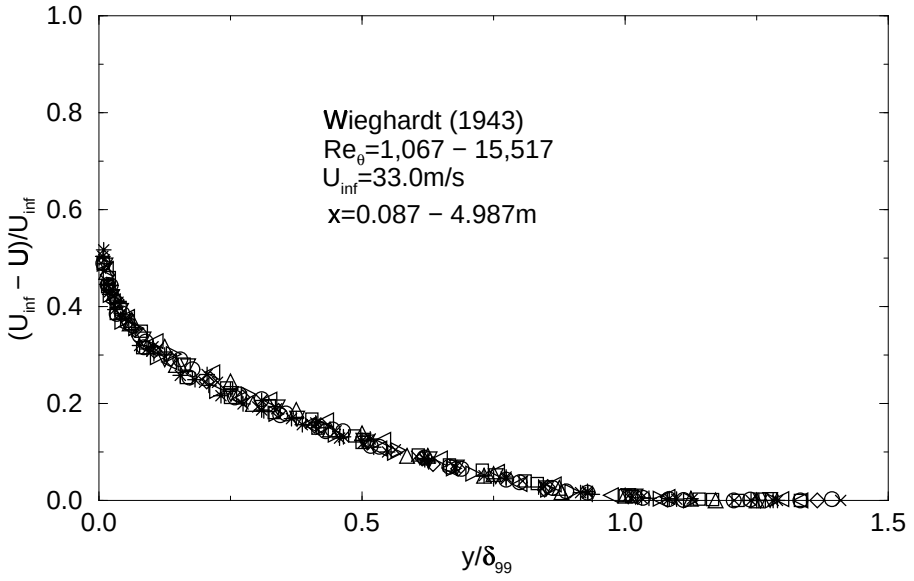

Figure 8: Mean velocity deficit profiles of Wieghardt (1943) normalized by U_∞ and δ_{99} for fixed upstream conditions.

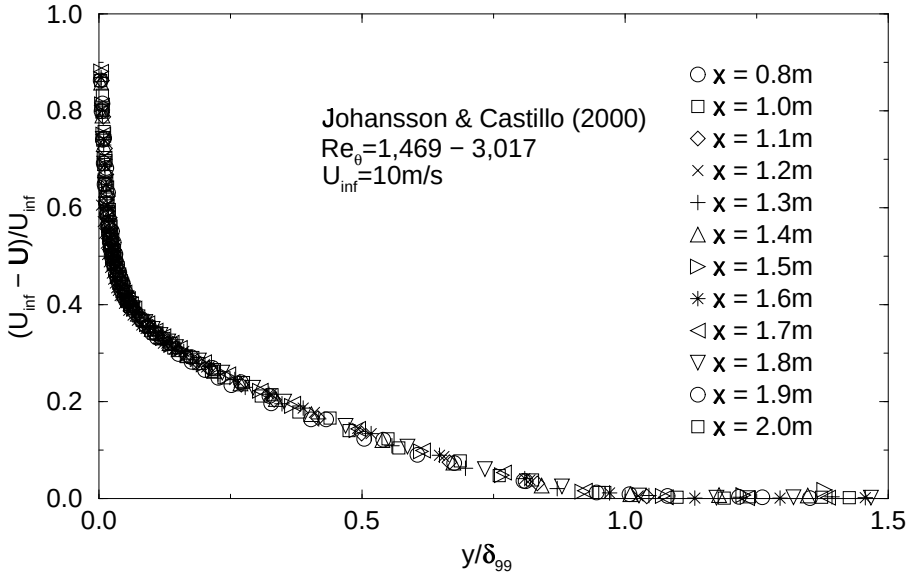

Figure 9: Mean velocity deficit profiles of Johansson & Castillo (2000) normalized by U_∞ and δ_{99} for fixed upstream conditions.

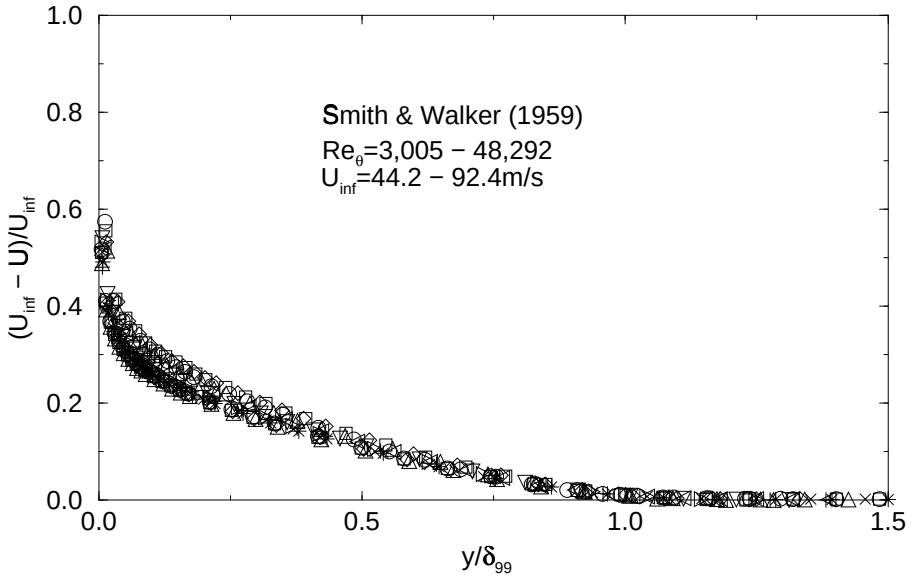

Figure 10: Mean velocity deficit profiles of Smith & Walker (1959) normalized by U_∞ and δ_{99} for varying upstream conditions.

are shown in figures 10 and 6, respectively.

Since all data in figures 8, 9, 10 and 6 collapse equally well with the Zagarola/Smits scaling, the conclusion is that for fixed upstream/initial conditions δ_*/δ must be independent of Reynolds number. Evidence of this is shown in figures 11 and 12, respectively. The data in figure 11 (LDA) is believed to be more accurate than the data in figure 12 (pitot tube), due to the well-known pitot tube errors in turbulent flow (c.f. Blake, 1983). As the turbulence intensity increases, the value of δ_* computed from velocities measured with pitot tubes would decrease compared to its true value. The value of this constant ratio δ_*/δ is determined by the upstream/initial conditions.

Since the displacement thickness scaling collapses the data only in the outer part of the boundary layer, it would be more appropriate to use a modified displacement thickness $\tilde{\delta}_*$, where the integration is performed only over the outer layer

$$\frac{\tilde{\delta}_*}{\delta} \equiv \int_{0.1}^{\infty} \left(1 - \frac{U}{U_\infty}\right) d\overline{y} \tag{3.15}$$

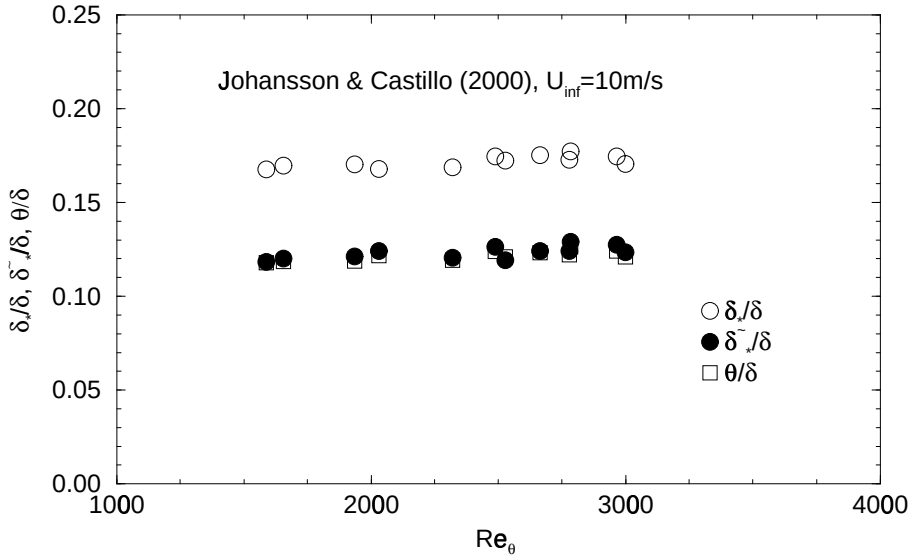

Figure 11: Variation of displacement thickness δ_*, modified displacement thickness $\tilde{\delta}_*$ and momentum thickness θ with Reynolds number for fixed upstream conditions. Data of Johansson & Castillo (2000).

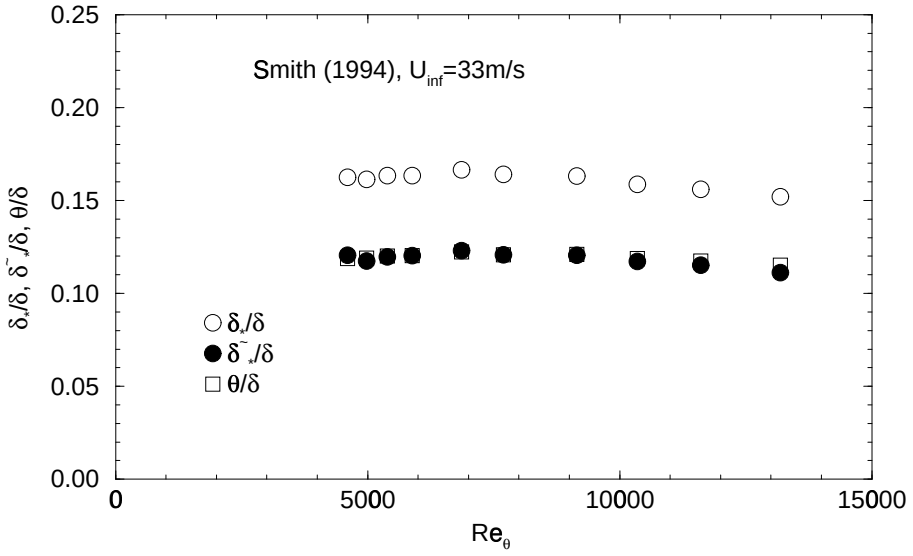

Figure 12: Variation of displacement thickness δ_*, modified displacement thickness $\tilde{\delta}_*$ and momentum thickness θ with Reynolds number for fixed upstream conditions. Data of Smith (1994).

This modified displacement thickness, $\tilde{\delta}_*$, is also plotted in figures 11 and 12, and is seen to be independent of Reynolds number. This new integral thickness, $\tilde{\delta}_*$, is very close in value to the momentum thickness, since for the momentum thickness the multiplier U/U_∞ acts like a filter — filtering out the inner and overlap layer contribution to the integral.

3.2.5 Summary

The Zagarola/Smits scaling is seen to be *consistent with* the George/Castillo theory. The collapse of the profiles using $U_S = U_\infty \delta_*/\delta$ and the success of George and Castillo in fitting the same profiles indicates that the separability hypothesis put forth here is an adequate (even *excellent*) description of the data, even though analytical separation of the George/Castillo profiles is *not* possible, at least not in their present form. This lack of separability of the George/Castillo profiles is exclusively a consequence of treating the outer flow with a wake function which is the difference between the mean velocity and the overlap solution, which strictly speaking applies only for $\overline{y} \leq 0.1$. While the wake function proposed by George and Castillo is in excellent agreement with the data, there is no theoretical justification for its use, historical precedent notwithstanding.

The fact that velocity profiles for fixed upstream/initial conditions collapse with U_∞ alone (but also with the new scale $U_\infty \delta_*/\delta$) lead to the conclusion that δ_*/δ is uniquely determined by the upstream conditions and not a function of local Reynolds number, δ^+.

In summary, if it is assumed that f_o is separable, $f_o(y/\delta, \delta^+) = G(\delta^+, *) f_{o\infty}(y/\delta)$, then the Zagarola/Smits result follows directly from the definition of the displacement thickness, since for $\delta^+ \gg 1$ $G(\delta^+, *) = \delta_*/\delta$. Hence both proposals are in essential agreement on two points: (1) the need for including the Reynolds number dependence in the velocity deficit and (2) what this Reynolds number dependence is.

3.3 Higher Order Solution for the Reynolds Number Dependence

Even in view of the Zagarola/Smits scaling discussed in the previous section, the overlap analysis of George & Castillo (1997) remains unchanged. As shown in section A.7, the solution parameters γ, C_o, and C_i are constrained by

$$ln\delta^+ \frac{d\gamma}{d\ln\delta^+} = \frac{d\ln[C_o/C_i]}{d\ln\delta^+} \tag{3.16}$$

where γ is the power-law exponent and C_o and C_i are multiplicative coefficients in the outer and inner overlap solutions, respectively. Both γ and C_o/C_i are functions of $\ln\delta^+$. This constraint equation must be invariant to scale transformations of the form $\delta^+ \rightarrow D\delta^+$ since the physical choice of δ^+ must be arbitrary (e.g., δ_{99}, δ_{95}, etc.). Therefore the Reynolds number dependence of γ and C_o/C_i must also be independent of the choice of δ; transforming from one δ to another would be reflected in D. This will be important in relating the boundary layer parameters to other wall-bounded flows (chapters 4, 5 and 6).

A solution to equation 3.16 can be written in the form

$$\frac{C_o}{C_i} = \exp[(\gamma - \gamma_\infty)\ln\delta^+ + h] \tag{3.17}$$

where the function $h = h(\delta^+)$ remains to be determined, but must satisfy

$$\gamma - \gamma_\infty = -\delta^+ \frac{dh}{d\delta^+} = -\frac{dh}{d\ln\delta^+} \tag{3.18}$$

The advantage of this form of the solution can be seen by substituting equation 3.17 back into equation A.73 to obtain

$$\frac{u_*}{U_\infty} = \exp[-\gamma_\infty \ln\delta^+ + h] \tag{3.19}$$

Now the friction law, u_*/U_∞, is entirely determined by the asymptotic value of the power exponent, γ_∞, and the function $h(\delta^+)$.

3.3.1 GC Solution for the Constraint Equation

George & Castillo (1997) found on empirical grounds that the variation of $\gamma - \gamma_\infty$ and C_o/C_i with δ^+ was described to a very good approximation by (for the data sets investigated)

$$h - h_\infty = \frac{A}{(\ln \delta^+)^\alpha} \tag{3.20}$$

where $\alpha = 0.46$, $A = 2.90$ and $D = 1$ for δ chosen to be δ_{99}. Equation 3.20 can be shown to satisfy the constraints above. From equations 3.18 and 3.17 it then follows that

$$\gamma - \gamma_\infty = \frac{\alpha A}{(\ln \delta^+)^{1+\alpha}} \tag{3.21}$$

$$\frac{C_o}{C_i} = \frac{C_{o\infty}}{C_{i\infty}} \exp[(1+\alpha)A/(\ln \delta^+)^\alpha] \tag{3.22}$$

and

$$\frac{u_*}{U_\infty} = \frac{C_{o\infty}}{C_{i\infty}} [\delta^+]^{-\gamma_\infty} \exp[A/(\ln \delta^+)^\alpha] \tag{3.23}$$

The variation of C_o is described by an empirical expression with two constants found from experimental data,

$$\frac{C_o}{C_{o\infty}} = 1 + 0.283 \exp(-0.00598\delta^+) \tag{3.24}$$

The data of Purtell *et al.* (1981) and Smith and Walker (1959), were found to be consistent with $C_{o\infty} = 0.897$, $C_{i\infty} = 55$ and $\gamma_\infty = 0.0362$. As can be seen from figure 8 in George & Castillo (1997), the empirical fit for C_o of equation 3.24 reached its asymptotic value too rapidly.

3.3.2 Higher Order Solution for the Constraint Equation

A higher order solution will be derived here, which allows a more gradual approach to $C_{o\infty}$ as $\delta^+ \to \infty$. Again, we can write a solution to equation 3.16 in the form of equation 3.17, where $h = h(\delta^+)$ has a *general* form of

$$h - h_\infty = \frac{A}{(\ln \delta^+)^\alpha}\left[1 + \frac{A_1}{(\ln \delta^+)} + \frac{A_2}{(\ln \delta^+)^2} + \ldots\right] \tag{3.25}$$

It follows immediately from equations 3.18 and 3.17 that

$$\begin{aligned} \gamma - \gamma_\infty &= -\frac{dh}{d\ln \delta^+} \\ &= \frac{\alpha A}{(\ln \delta^+)^{1+\alpha}}\left[1 + \frac{\alpha+1}{\alpha}\frac{A_1}{(\ln \delta^+)} + \frac{\alpha+2}{\alpha}\frac{A_2}{(\ln \delta^+)^2} + \ldots\right] \end{aligned} \tag{3.26}$$

Substituting equation 3.26 into the constraint equation 3.16, integrating with respect to $\ln \delta^+$, and taking the exponential of both sides gives

$$\frac{C_o}{C_i} = \frac{C_{o\infty}}{C_{i\infty}} \exp\left\{\frac{(1+\alpha)A}{(\ln \delta^+)^\alpha}\left[1 + \frac{(2+\alpha)A_1}{(1+\alpha)\ln \delta^+} + \frac{(3+\alpha)A_2}{(1+\alpha)(\ln \delta^+)^2} + \ldots\right]\right\} \tag{3.27}$$

This equation can conveniently be split up into two parts the following way

$$\frac{C_o}{C_i} = C_{o\infty} \exp\left\{\frac{(2+\alpha)AA_1}{(\ln \delta^+)^{\alpha+1}} + \frac{(3+\alpha)AA_2}{(\ln \delta^+)^{\alpha+2}}\right\} \cdot \left[C_{i\infty} \exp\left\{-\frac{(1+\alpha)A}{(\ln \delta^+)^\alpha}\right\}\right]^{-1} \tag{3.28}$$

Rewriting the old form of the solution for C_o/C_i, equation 3.22 with the simplification that $C_{o,old} \approx C_{o\infty,old}$

$$\frac{1}{C_i} = \frac{1}{C_{i\infty}} \exp[(1+\alpha)A/(\ln \delta^+)^\alpha] \tag{3.29}$$

shows that the term in square brackets on the right-hand side of equation 3.28 is exactly the old form of C_i, which seemed to describe the data reasonably well and

will be kept as new C_i.

$$C_i = C_{i\infty} \exp\left[-(1+\alpha)A/(\ln \delta^+)^\alpha\right] \tag{3.30}$$

The remainder of the right-hand side of equation 3.28 can therefore be used as a higher order description for C_o

$$C_o = C_{o\infty} \exp\left\{\frac{(2+\alpha)AA_1}{(\ln \delta^+)^{\alpha+1}} + \frac{(3+\alpha)AA_2}{(\ln \delta^+)^{\alpha+2}}\right\}. \tag{3.31}$$

Equations 3.26 and 3.27 can be substitued into the friction law of equation A.73 to obtain a higher order friction law as

$$\begin{aligned} \frac{u_*}{U_\infty} &= \frac{C_o}{C_i} \exp\left\{-\gamma \ln \delta^+\right\} \\ &= \frac{C_{o\infty}}{C_{i\infty}} \left(\delta^+\right)^{-\gamma_\infty} \exp\left\{\frac{A}{(\ln \delta^+)^\alpha}\left[1 + \frac{A_1}{(\ln \delta^+)} + \frac{A_2}{(\ln \delta^+)^2} + \ldots\right]\right\} \end{aligned} \tag{3.32}$$

The higher order form of C_o allows for a much more gradual approach to C_∞ as $\delta^+ \to \infty$. Another advantage of the higher order solution is that, while parameters A_1 and A_2 need to be determined, there no longer is a need for the empirical equation (3.24), thus eliminating the two empirical constants it contains. Therefore, the number of empirically determined constants is actually reduced by one, if only one extra term (A_1) is carried. If higher order terms up to third order are kept (A_1 and A_2), the number of empirical parameters to be determined from data remains the same.

3.3.3 Experimental Friction Data

The friction law of George & Castillo (1997) and equation 3.32 depend only on the ratio of the asymptotic values, $C_{o\infty}/C_{i\infty}$ and do therefore not need the higher order terms. Equation 3.32, using only the first term in square brackets (which reduces it to equation 3.23, the old George/Castillo friction law), will be seen to work very well

with the new friction data of Österlund (1999).

There are only a handful of ways to measure wall shear stress directly without reference to a theory being tested,[4] one of them is measurement by oil-film interferometry, as performed by Österlund (1999). In these measurements, the investigators (Österlund, Johansson, Nagib & Hites, 2000, equation 5) also claim to find support for the classical logarithmic friction law with constant coefficients, where $\kappa = 0.38$, $B = 4.1$ and $B_1 = 3.6$.

An optimization was performed on just the friction data of Österlund (1999) for the parameters derived here (equation 3.32), and the data are consistent with $\alpha = 0.47$, $A = 2.90$ and $D = 1$ for $\delta = \delta_{99}$. Furthermore, $C_{o\infty} = 0.897$, $C_{i\infty} = 56.7$ and $\gamma_\infty = 0.0332$. Multiplication of δ^+ by δ_{99}/δ_{95} is also needed, when comparing the derived friction law, equation 3.32 (the theory was derived based on δ^+_{99}), with the Österlund data (which was given with δ^+_{95} as variable), c.f. discussion on page 31.

In figure 13, power friction law (eqn. 3.32, 3.23) and logarithmic friction law are compared with the oil-film wall shear stress data. Figure 13 uses the same values, but extends the comparison of both theories to higher Reynolds number. It can be seen that — for the given values of the parameters — the logarithmic friction law and the power friction law are almost identical for higher Reynolds number, but the power law describes the data better at low Reynolds number.

Figures 15 and 16 show the same data and power law, but now the constants[5] in the logarithmic friction law have been slightly modified to $\kappa = 0.384$,[6] $B = 4.06$ and $B_1 = 3.6$. Now the log law describes the data better than before at low Reynolds number, but diverges at high Reynolds number. These figures lead to the conclusion that a logarithmic friction law with constant coefficients *does not have the right shape*

[4] e.g., using the "Clauser-method", which assumes the existence of a logarithmic overlap region, to determine the wall shear stress, and then using the same shear stress values in normalizing the data to "prove" the existence of a logarithmic overlap region is clearly *wrong*.

[5] Note that these values would round to the ones previously used.

[6] $\kappa = 0.384$ was also given in Österlund *et al.* (2000), obtained from fitting a friction curve ($\kappa = 0.38$ was obtained from velocity profile fits).

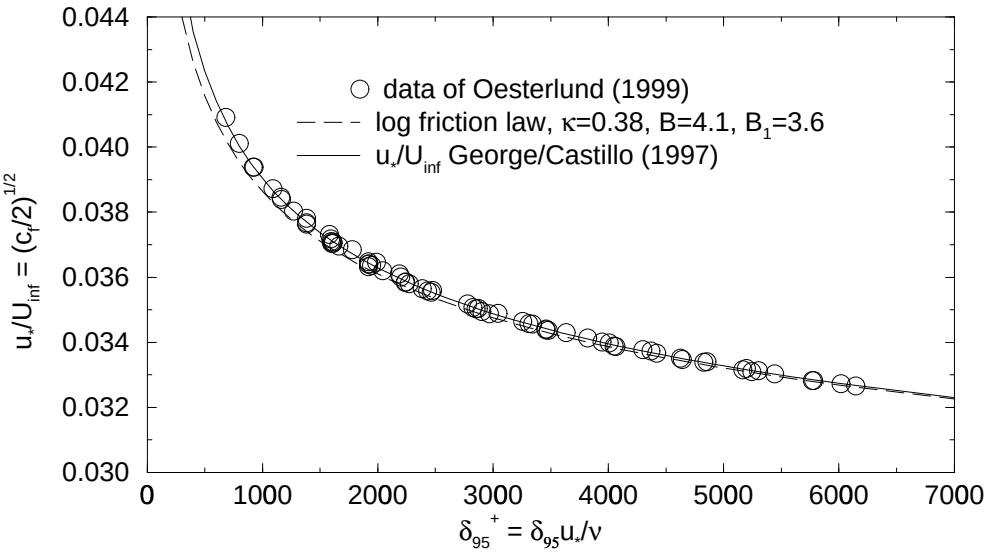

Figure 13: Comparison of friction laws. Shown are the logarithmic law with constant coefficients ($\kappa = 0.38$, $B = 4.1$ and $B_1 = 3.6$, c.f. Österlund *et al.* (2000), eqn.5), and the theory proposed here ($C_{o\infty}/C_{i\infty} = 0.158$), and data obtained with oil-film interferometry (Österlund, 1999).

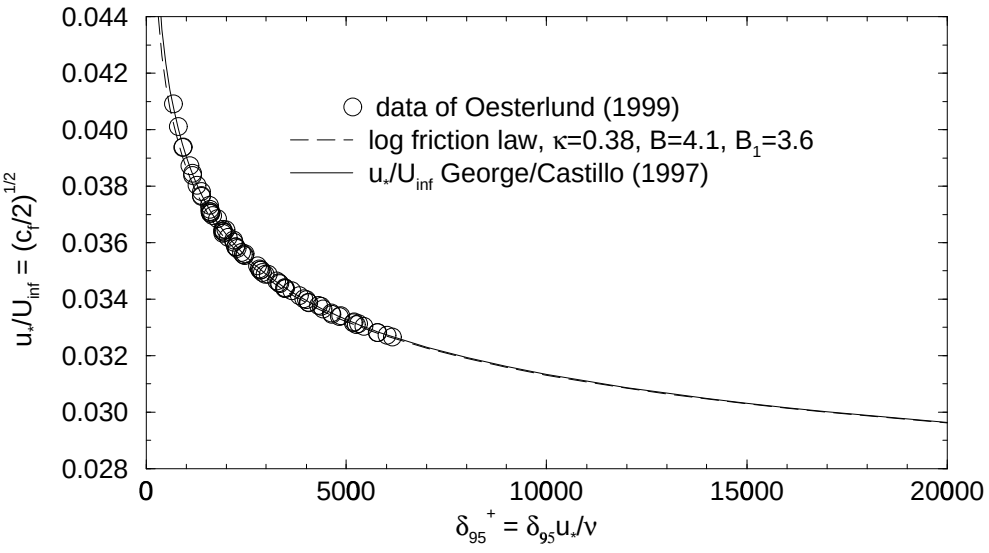

Figure 14: Comparison of friction laws, extended to high Reynolds number. Values for logarithmic friction law are the same as in Figure 13.

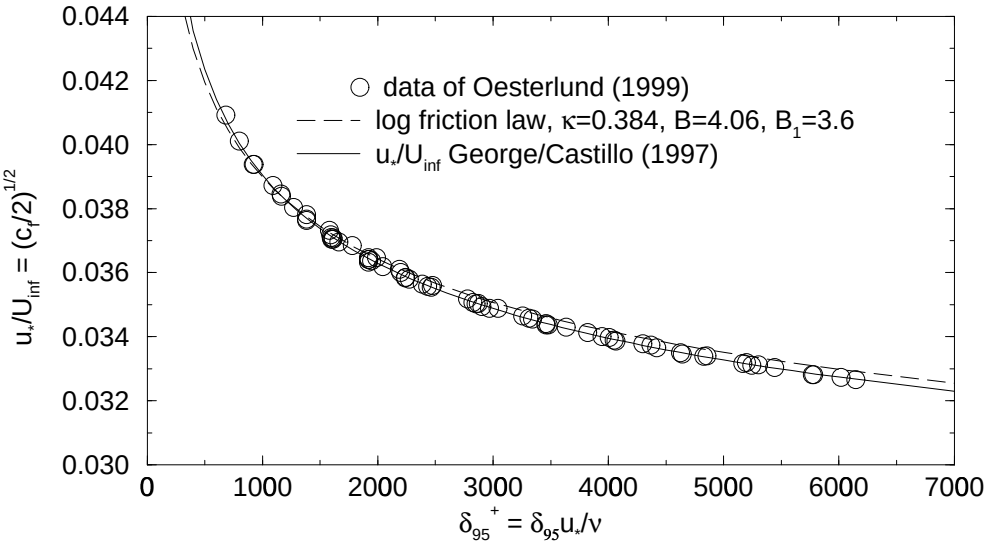

Figure 15: Comparison of friction laws. Shown are the logarithmic law with (slightly different) constant coefficients ($\kappa = 0.384$, $B = 4.06$ and $B_1 = 3.6$, c.f. Österlund *et al.* (2000), eqn.5), and the theory proposed here ($C_{o\infty}/C_{i\infty} = 0.0158$), and data obtained with oil-film interferometry (Österlund, 1999).

to agree with friction data over just one decade in δ_{95}^+. The power law (re-derived in appendix A), on the other hand, is able to predict the data well for its entire range.

The logarithmic friction law still describes the data *fairly well*, but the small deviation observed can be very important for certain applications. For example, in the design phase of commercial passenger airplanes, a small difference (on the order of a percent) in full-scale drag prediction results in a difference of several thousand pounds in gross take-off weight (c.f. Kulfan, 2000). Usually, models that predict the drag for an entire airplane are "tuned" to correctly calculate the base case, the zero pressure gradient boundary layer.[7]

Interestingly, the friction law of George & Castillo (1997) (eqn. 3.23) together with the original parameters given in section 3.3.1 (A.8.1) needs little change to describe the friction data of Österlund (1999) as well as the power law plotted in figures 13–16. It needs to be modified to account for δ_{95} being used as a variable in the experiment

[7]From the plots shown here it is understandable that even correctly calculating the zero pressure gradient boundary layer poses a problem for models calibrated using classical boundary layer theory.

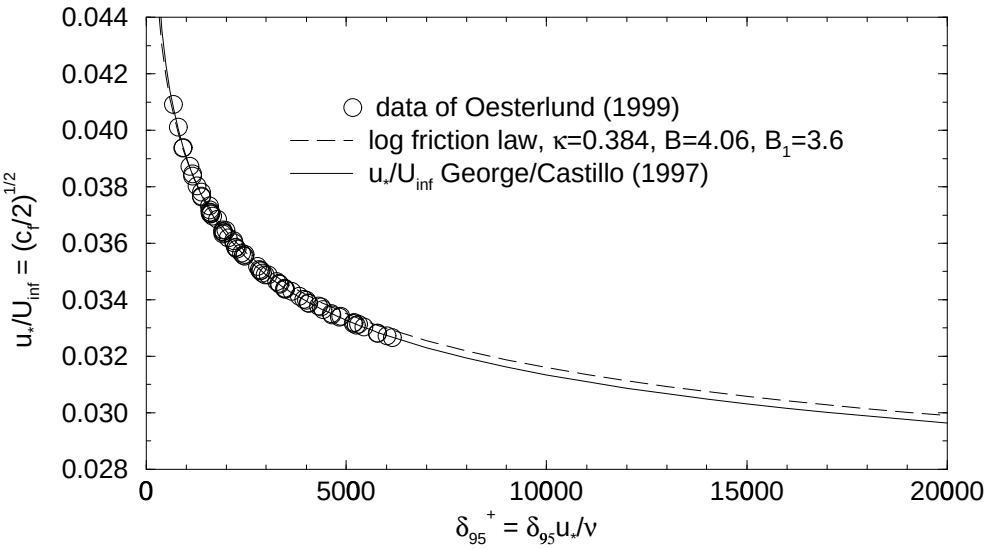

Figure 16: Comparison of friction laws, extended to high Reynolds number. Values for logarithmic friction law are the same as in Figure 15.

(using $D = 1.4$, c.f. section 3.3) and an improved value for $C_{i\infty}$, taken to be 56.7. This value for $C_{i\infty}$ was obtained from a combined optimization for friction data *and* velocity profiles of the high accuracy LDA[8] data of Eriksson *et al.* (1998) taken in a plane wall jet.[9] This curve[10] and the power law plotted in figures 13–16 are virtually indistinguishable for $\delta_{95}^+ < 10,000$.

Accurate determination of the power law profile coefficients C_i and C_o (equations 3.30 and 3.31, respectively) will be possible once accurate near-wall measurements (LDA) become available, in addition to the existing pitot tube (e.g. Smith, 1994) and CTA (e.g. Österlund, 1999) data. Among the ongoing efforts is the experiment by Johansson & Castillo (2000) at Chalmers University of Technology.

[8] Due to well-known errors of pitot tube and hot wire velocity measurements in turbulent flows, the LDA data are believed to be more accurate.

[9] c.f. chapter 5 for discussion on the universality of the inner layer for developing wall-bounded flows.

[10] George/Castillo friction law with original parameter values not shown in plots.

3.4 Distinguishing Between Logarithmic and Power Law Profiles

To investigate whether a power law overlap region exists, data are often plotted using a "power law diagnostic function" Γ (c.f. Österlund, Johansson, Nagib & Hites, 2000, figure 6), which in inner variables is defined as

$$\Gamma = \frac{y^+}{U^+}\frac{dU^+}{dy^+} \tag{3.33}$$

where $y^+ = y/\eta = yu_*/\nu$ and $U^+ = U/u_*$. Suppose the zero pressure gradient velocity profiles were described by a power law of the form

$$U^+ = C\ (y^+)^p \tag{3.34}$$

then equation 3.33 above would simply reduce to $\Gamma = p$. As long as power p is *not* a function of Reynolds number, *all* profiles should exhibit a horizontal tangent with value $p = const.$ over some overlap region when plotted this way. This is what Österlund *et al.* (2000) are testing in their figure 4, where the overlap regions for different Reynolds numbers are averaged together.

George & Castillo (1997) derived an overlap profile (a first-order solution to the governing equations) in inner variables as

$$U^+ = C_i(\delta^+)(y^+ + a^+)^{\gamma(\delta^+)} \tag{3.35}$$

Using Γ in the form of equation 3.33 is, however, not the correct way to test whether experimental data support the power law overlap profiles of George & Castillo (1997), for the following reasons:

- The power γ is a function of Reynolds number, δ^+, therefore different profiles must not be averaged together.

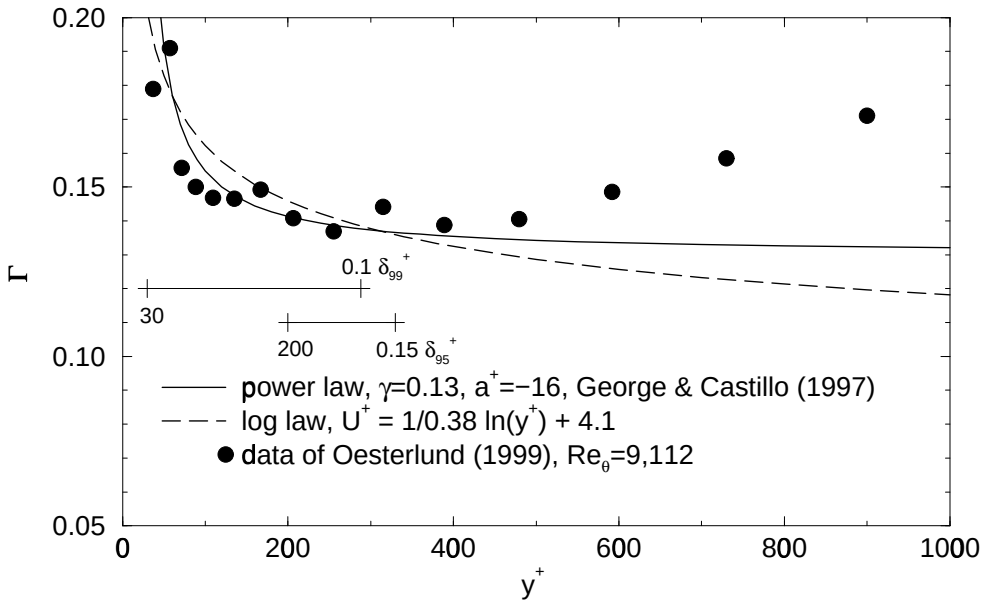

Figure 17: Comparison of experimental data, logarithmic and power law profiles plotted in the form of Γ (equation 3.33).

- Equation 3.35 contains an offset a^+ (c.f. appendix A), therefore Γ becomes[11]

$$\Gamma = \frac{y^+}{U^+}\frac{dU^+}{dy^+} = \frac{y^+}{y^+ + a^+}\gamma \neq const. \tag{3.36}$$

Figure 17 shows data and theory in the from of Γ (equation 3.33).

However, a modified form of this "diagnostic function", Γ^*, becomes useful for individual George/Castillo profiles if defined as follows

$$\Gamma^* = \frac{y^+ + a^+}{U^+}\frac{dU^+}{dy^+} \tag{3.37}$$

so that Γ^* for a George/Castillo profile becomes

$$\Gamma^* = \gamma(\delta^+) \tag{3.38}$$

[11] Γ (equation 3.33) can still be applied to *individual* profiles of power laws with Reynolds number dependent power exponent *without* offset, such as the type proposed by Barenblatt (1993).

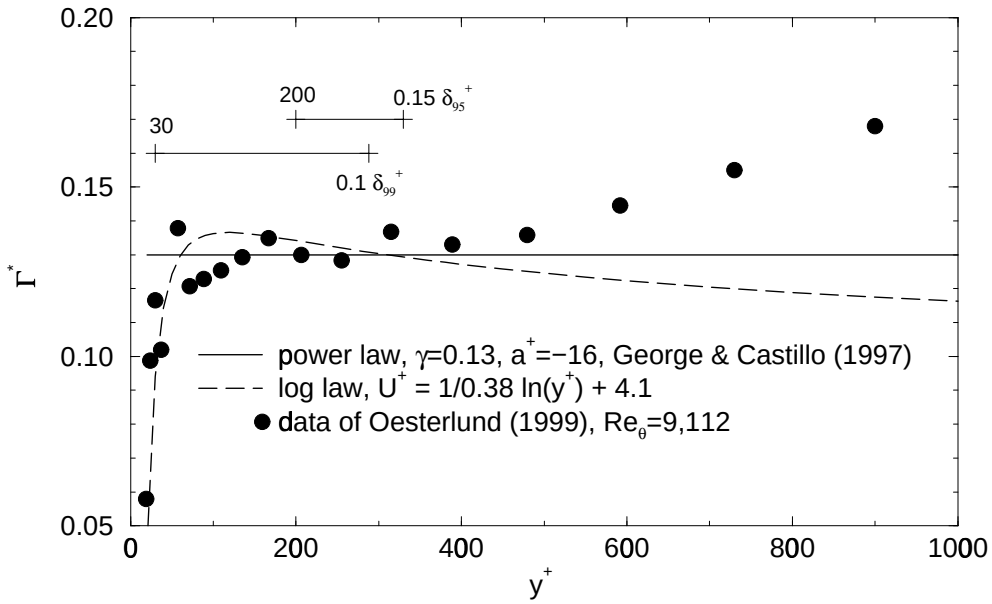

Figure 18: Comparison of experimental data, logarithmic and power law profiles plotted in the form of Γ^* (equation 3.37).

Figure 18 shows data and theory in the from of Γ^* (equation 3.37).

Clearly, from the experimental data one could argue for *either* a logarithmic law with constant coefficients *or* a power law in $(y + a)$ (The narrow regions of applicability of each theory are also shown in the figures). Data alone cannot distinguish between the two proposals, even when derivative plots are made. The "power law diagnostic function", even in its modified form Γ^* which is more appropriate for the George/Castillo profiles, is therefore *not* as useful a tool to sort theories as previously believed.[12]

The closeness of the theoretical profiles can be understood if one expands the power law in terms of a logarithm (or vice versa), as done in section A.16. From equation A.140, it can be argued that the asymptotic power law boundary layer profiles would appear logarithmic to leading order, even for finite values of γ, since the classical Millikan/Clauser (or Österlund *et al.*) logarithmic profile result is recovered

[12]see also section 4.10 for discussion on derivative plots of pipe/channel flow data.

as the first term in the expansion. It is, however, *not* a useful approximation since the higher order terms decay very slowly and are still significant at the Reynolds numbers usually encountered in experiments. In summary: It is very difficult, if not impossible, to tell a logarithm from a weak power using experimental data alone since the small difference — one can always be expanded in terms of the other — is on the order of the scatter in the data.

Chapter 4

Pipe and Channel Flow

The one who relies on authority during a discussion does not use his mind but his memory.

– Leonardo da Vinci (1452-1519), Italian artist, scientist

4.1 Introduction

Pipe and channel flows[1] have recently become the subject of intense scrutiny, thanks in part to new experimental data which has become available from the superpipe experiment at Princeton (Zagarola, 1996; Zagarola & Smits, 1998*a*). In spite of the facts that the scaling laws for pipe and channel flows were established more than 80 years ago (Stanton & Pannell, 1914; Prandtl, 1932) and that the now classical theory of Millikan was offered in 1938 for the friction law and velocity profiles, the subject has remained of considerable interest. Examples from the last 30 years alone include the analyses of Tennekes (1968), Bush & Fendell (1974), Long & Chen (1981), Panton (1990). All of these were essentially refinements on the original Millikan theory in which the functional form of the friction and velocity laws was logarithmic, and

[1]This chapter is largely based on the forthcoming paper by Wosnik *et al.* (2000). (Wosnik, M., Castillo, L. & George, W. K. (2000) A theory for turbulent pipe and channel flows. *J.Fluid Mechanics*, accepted for publication).

only the infinite Reynolds number state was considered. The difficulties presented by the experimental data have recently been extensively reviewed by Gad-el-Hak & Bandyopadhyay (1994).

Barenblatt (Barenblatt, 1993, 1996; Barenblatt & Prostokishin, 1993; Barenblatt, Chorin & Prostokishin, 1997) has suggested that the velocity profiles of pipe, channel *and* boundary layer flows are power laws. By contrast, George and his coworkers (George, 1988, 1990, 1995; George & Castillo, 1993, 1997; George *et al.*, 1992, 1996, 1997; Wosnik *et al.*, 2000; George *et al.*, 2000) have argued that the overlap velocity profiles and friction law for boundary layers are power laws, but that the corresponding relations for pipes and channels are logarithmic. The analysis for boundary layers leading to power-law profiles in the overlap region was presented in the previous chapter.

The purpose of this chapter is to apply the same methodology to pipe and channel flows, and to compare the resulting theory with the new experimental data. The important difference from previous efforts mentioned above is that the effects of finite Reynolds number are explicitly included and the *mesolayer* is accounted for.

4.2 Scaling Laws for Turbulent Pipe and Channel Flow

The stream-wise momentum equation for a fully developed two-dimensional channel flow (c.f. Figure 1) at high Reynolds number reduces to

$$0 = -\frac{1}{\rho}\frac{dP}{dx} + \frac{\partial}{\partial y}\left[< -uv > +\nu\frac{\partial U}{\partial y}\right] \tag{4.1}$$

The convection terms are identically equal to zero due to kinematic simplification. Like the boundary layer, the viscous term is negligible everywhere except very near the wall, so that the core (or outer) flow in the limit of infinite Reynolds number is

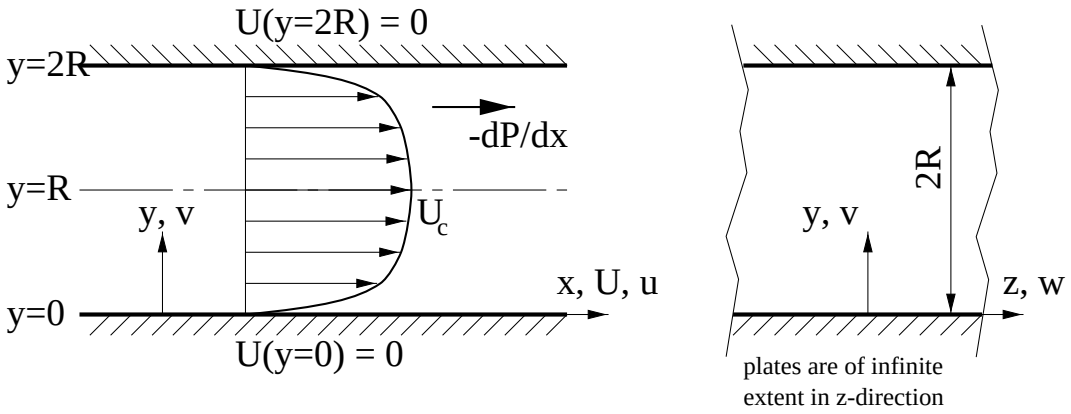

Figure 1: Definition sketch for turbulent channel flow (flow between infinite parallel plates)

exactly governed by

$$0 = -\frac{1}{\rho}\frac{dP}{dx} + \frac{\partial}{\partial y} < -uv > \tag{4.2}$$

In the limit of infinite Reynolds number, the inner layer is exactly governed by

$$0 = \frac{\partial}{\partial y}\left[< -uv > +\nu \frac{\partial U}{\partial y} \right] \tag{4.3}$$

This can be integrated from the wall to obtain the total stress

$$\frac{\tau_w}{\rho} \equiv u_*^2 \equiv \nu \left.\frac{\partial U}{\partial y}\right|_{y=0} = < -uv > +\nu \frac{\partial U}{\partial y} \tag{4.4}$$

where u_* is the friction velocity defined as $u_*^2 \equiv \tau_w/\rho$. The viscous stress vanishes with increasing distance from the wall, and $< -uv > \rightarrow u_*^2$, but only in the infinite Reynolds number limit. At finite Reynolds numbers the pressure gradient causes the total stress to drop linearly until it reaches zero at the center of the channel (or pipe). Hence the Reynolds stress never really reaches the value of u_*^2, but instead reaches a maximum value away from the wall before dropping slowly as distance from the wall is increased.

It is obvious that the inner profiles must scale with u_* and ν since these are the

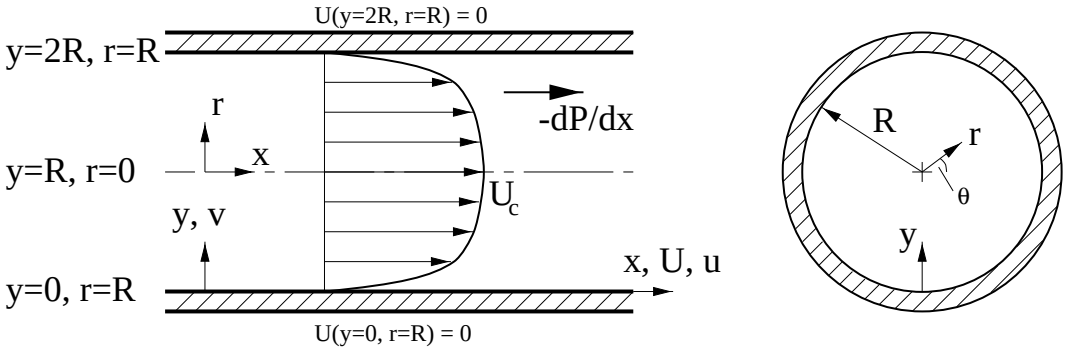

Figure 2: Definition sketch for turbulent pipe flow

only parameters in the inner equations and boundary conditions. Hence, there must be a law of the wall (at least for a limited region very close to the wall). This should not be taken to imply, however, that u_*^2 is an independent parameter; it is not. It is uniquely determined by the pressure drop imposed on the pipe, the pipe diameter and the kinematic viscosity.

Because there is no imposed condition on the velocity, except for the no-slip condition at the wall, an outer scaling velocity must be sought from the parameters in the outer equation itself. Since there are only two, $-(1/\rho)dP/dx$, the externally imposed pressure gradient, and R, the channel half-width, only a single velocity can be formed; namely,

$$U_o = \left(-\frac{R}{\rho}\frac{dP}{dx} \right)^{1/2} \tag{4.5}$$

Unlike the developing boundary layer, the fully-developed pipe or channel flow is homogeneous in the stream-wise direction, so the straightforward similarity analysis of George & Castillo (1997) (c.f. appendix A) using the x-dependence to establish the scaling parameters is not possible. However, because of this stream-wise homogeneity, there is an exact balance between the wall shear stress acting on the walls, and the net pressure force acting across the flow. For fully-developed channel flow, this force equilibrium requires that

$$u_*^2 = -\frac{R}{\rho}\frac{dP}{dx} \tag{4.6}$$

which is just the square of equation 4.5 above; thus, $U_o = u_*$. Therefore, the outer scale velocity is also u_*, and the outer and inner velocity scales are the same. Note that in a pipe flow (c.f. Figure 2) there will appear a factor of 2 in the force balance. This factor can be ignored in choosing the scale velocity, so the same argument and result apply to it as well.

Thus channel and pipe flows differ from boundary layer flows where asymptotic Reynolds number independence and stream-wise *inhomogeneity* demand that the inner and outer scales for the mean velocity be different (George & Castillo, 1997). This consequence of the streamwise homogeneity on the governing equations themselves is fundamental to understanding the unique nature of pipe and channel flows. Homogeneity causes the inner and outer velocity scale to be the same, and this in turn is the reason these flows show a logarithmic dependence for the velocity in the overlap region and for the friction law (c.f. section 4.4). This can be contrasted with wall-bounded flows developing in the streamwise direction, where the inner and outer velocity scales are different because of their inhomogeneity in x, and hence are characterized by power laws (c.f. chapters 3, 5, 6, appendix A).

The analysis presented below will be based on using u_* as the outer velocity scale; however, it should be noted before leaving this section that there are at least two other possibilities which might be considered for an outer velocity scale. Both are formed from the mass averaged (or bulk) velocity defined for the pipe by:

$$U_m \equiv \frac{1}{\pi R^2} \int_0^R U r dr \tag{4.7}$$

The first possibility is to use U_m directly, the second is to use its difference from the centerline velocity, $U_c - U_m$. The former has an advantage in that it is often easier to specify the mass flow in experiments and simulations than the pressure drop (or shear stress), but it has the disadvantage that it does not lend itself easily to the overlap analysis described below. The latter has been utilized with great success by Zagarola & Smits (1998*b*) in removing the Reynolds number dependence of the velocity profiles

in both boundary layers and pipe flows. For the purpose of developing this theory it is sufficient to note that in the limit as $R^+ = u_* R/\nu \to \infty$, $U_c - U_m \to const \cdot u_*$. Hence the fundamental limiting and overlap arguments of the succeeding sections will be the same for both u_* and $U_c - U_m$, only the Reynolds number dependence of the coefficients will differ.

4.3 Finite versus Infinite Reynolds Number

From the dimensional/physical analysis above, it follows that appropriate inner and outer scaled versions of the velocity profile can be defined as two families of curves with parameter R^+; i.e.,

$$\frac{U}{u_*} = f_i(y^+, R^+) \tag{4.8}$$

and

$$\frac{U - U_c}{u_*} = f_o(\overline{y}, R^+) \tag{4.9}$$

where the outer velocity has been referenced to the velocity at the centerline, U_c, to avoid the necessity of accounting for viscous effects over the inner layer when the limits are taken later. The outer length scale is some measure of the diameter of the pipe (say the pipe radius) or the width of the channel (say half-width). Both of these will be denoted as R in the remainder of the chapter.

Since the length scales for inner and outer profiles are different, no single scaling law should be able to collapse data for the entire flow. The ratio of length scales is a Reynolds number, $R^+ = Ru_*/\nu$, therefore the region between the two similarity regimes cannot be Reynolds number independent, except possibly in the limit of infinite Reynolds number. Moreover, since the neglected terms in both inner and outer equations depend on the ratio of length scales (v. Tennekes & Lumley, 1972), then neither set of scaling parameters will be able to perfectly collapse the data in either region at finite values of R^+.

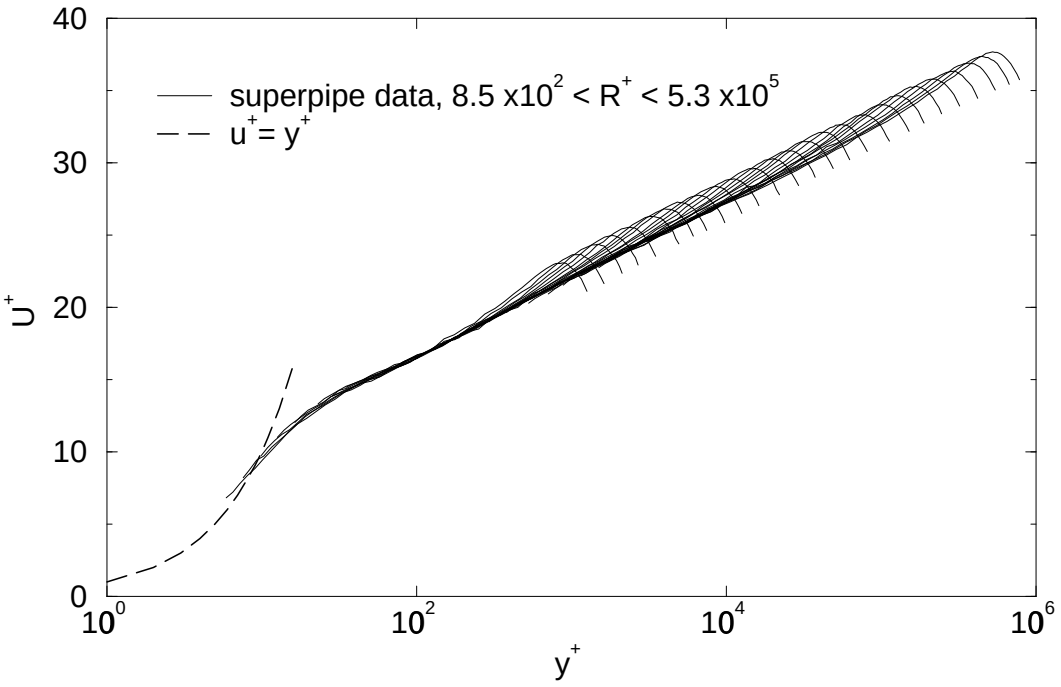

Figure 3: Velocity profiles in inner variables

As explained in section 2.4 both families of curves described by equations 4.8 and 4.9, $f_i(y^+, R^+)$ and $f_o(\overline{y}, R^+)$, represent the *entire* velocity profile as long as R^+ is finite. Properly scaled profiles must, by the Asymptotic Invariance Principle (AIP, section 2.3, George, 1995), become asymptotically independent of R^+ in the limit of infinite Reynolds number; i.e.,

$$\begin{aligned} \lim f_i(y^+, R^+) &\rightarrow f_{i\infty}(y^+) \\ \lim f_o(\overline{y}, R^+) &\rightarrow f_{o\infty}(\overline{y}) \end{aligned}$$

as $R^+ \rightarrow \infty$. Otherwise an inner and outer scaling makes no sense. In fact, these limiting profiles should be solutions to the inner and outer equations respectively (i.e., equations 4.3 and 4.2), which are themselves valid only in the infinite Reynolds number limit.

Figures 3 and 4 show the mean velocity profile data from the Princeton super-

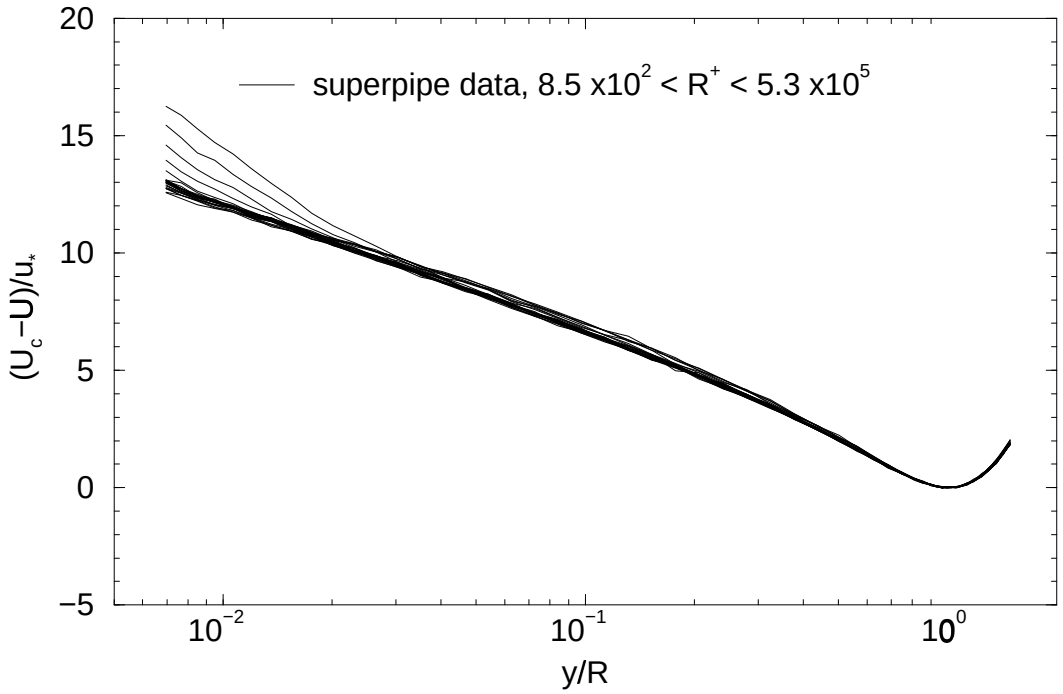

Figure 4: Velocity profiles in outer variables

pipe experiment (Zagarola, 1996; Zagarola & Smits, 1998*a*) in both inner and outer variables. Note the excellent collapse very close to the wall for $y^+ < 100$ in inner variables, and over the core region for $\overline{y} > 0.3$. Note also that the region of approximate collapse in inner variables (Figure 3) increases from the wall with increasing Reynolds number, as does the inward extent of the outer variable collapse (Figure 4). In fact, the parameter R^+ uniquely labels the fanning out of the inner scaled profiles in the outer region and the outer scaled profiles near the wall in Figures 3 and 4.

Finally note that the inner scaling does not collapse the data at all where the outer scaling collapses it best, and vice versa. Both the region of approximate collapse and the region of no collapse are manifestations of the dependence of the scaled profiles on R^+ as argued above.

Unlike boundary layer experiments, the wall shear stress for the fully-developed pipe flow can be determined from the pressure drop in the pipe alone, entirely independent from the velocity profile measurements (c.f. section 4.2). The direct deter-

mination of the shear stress from the pressure drop without choosing it to collapse a "log layer" which can only be assumed to collapse (the so-called "Clauser method") is especially important since, as noted above, there is evidence of a lack of complete collapse of the data in Figure 3 *outside* of $y^+ = 100$, especially for the lowest Reynolds numbers. The lack of collapse is even more apparent for the outer scaling in Figure 4 *inside* of $\overline{y} \approx 0.3$ which includes all of the overlap region discussed below.

4.4 The Overlap Layer: An Application of Near-Asymptotics

As discussed in the preceding section, f_i and f_o are quite unlike their limiting forms, $f_{i\infty}$ and $f_{o\infty}$, which are only infinite Reynolds number solutions for the inner and outer equations respectively. If f_i and f_o are considered instead of $f_{i\infty}$ and $f_{o\infty}$ (as is usually done), the problem of determining whether an overlap region exists is quite different from the usual asymptotic matching where infinite Reynolds number inner and outer solutions are extended and matched in an overlap region if one exists. The objective here is *not* to see if f_i and f_o overlap and match them if they do. Rather, it is to determine *whether the fact that these scaled finite Reynolds number solutions (to the whole flow) degenerate at infinite Reynolds number in different ways* can be used to determine their functional forms in the common region they retain in the limit. The methodology, termed *Near-Asymptotics*, was first utilized by George (1995) (see also George & Castillo, 1997), and is necessary because the traditional approach cannot account for the possibility of the matching parameter tending to zero, as might be the case. It also makes the results easier to compare to experiments since most are carried out far from asymptotic conditions.

The fact that analytical forms for f_i and f_o are not available, and they are only known *in principle* turns out not to be a significant handicap. There are several pieces of information about the two profiles which can be utilized without further

assumptions. They are:

- First, since both inner and outer forms of the velocity profile must describe the flow everywhere as long as the ratio of length scales, $R^+ = R/\eta$, is finite, it follows from equations 4.8 and 4.9 that

$$\frac{1}{g(R^+)} + f_o(\overline{y}, R^+) = f_i(y^+, R^+) \tag{4.10}$$

  where $g(R^+)$ is defined by

$$g(R^+) \equiv u_*/U_c \tag{4.11}$$

- Second, for finite values of R^+, the velocity derivatives from both inner and outer forms of the velocity must also be the same everywhere. This implies that

$$\overline{y}\frac{\partial f_o}{\partial \overline{y}} = y^+\frac{\partial f_i}{\partial y^+} \tag{4.12}$$

  for all values of R^+ and y.

- Third, as noted above, in the limit both f_o and f_i must become asymptotically independent of R^+; i.e., $f_o(\overline{y}, R^+) \rightarrow f_{o\infty}(\overline{y})$ and $f_i(y^+, R^+) \rightarrow f_{i\infty}(y^+)$ as $R^+ \rightarrow \infty$.

Now the problem is that *in the limit* as $R^+ \rightarrow \infty$, the outer form fails to account for the behavior close to the wall while the inner fails to describe the behavior away from it. The question is: In this limit (as well as for all finite values approaching it) does there exist an "overlap" region where equation 4.10 is still valid? (Note that boundary layer flows are quite different from pipe and channel flows since the overlap layer in the latter remains at fixed distance from the wall for all x because of the stream-wise homogeneity, as long as the external parameters — like geometry and Reynolds number — are fixed, while in the former it moves away from the wall with increasing x.)

The question of whether there is a common region of validity can be investigated by examining how rapidly f_o and f_i are changing with R^+, or more conveniently with $\ln R^+$. The relative variation of f_i and f_o with Reynolds number can be related to their Taylor series expansion about a fixed value of R^+; i.e.,

$$\frac{f_i(y^+; R^+ + \Delta R^+) - f_i(y^+; R^+)}{\Delta \ln R^+ f_i(y^+, R^+)} \approx \frac{1}{f_i(y^+, R^+)} \frac{\partial f_i(y^+; R^+)}{\partial \ln R^+}\bigg|_{y^+} \equiv S_i(R^+, y^+) \quad (4.13)$$

and

$$\frac{f_o(\overline{y}; R^+ + \Delta R^+) - f_o(\overline{y}; R^+)}{\Delta \ln R^+ f_o(\overline{y}, R^+)} \approx \frac{1}{f_o(\overline{y}, R^+)} \frac{\partial f_o(\overline{y}; R^+)}{\partial \ln R^+}\bigg|_{\overline{y}} \equiv S_o(R^+, \overline{y}) \quad (4.14)$$

Thus S_i and S_o are measures of the Reynolds number dependence of f_i and f_o, respectively. Both vanish identically in the limit as $\ln R^+ \to \infty$. If y^+_{max} denotes a location where outer flow effects begin to be strongly felt on the inner scaled profile, then for $y^+ < y^+_{max}$, S_i should be much less than unity (or else the inner scaling is not very useful). Similarly, if $\overline{y}_{min}$ measures the location where viscous effects begin to be strongly felt (e.g., as the linear velocity region near the wall is approached), then S_o should be small for $\overline{y} > \overline{y}_{min}$. Obviously either S_i or S_o should increase as these limits are approached. Outside these limits, one or the other should increase dramatically.

The quantities S_i and S_o can, in fact, be used to provide a formal definition of an "overlap" region where both scaling laws are valid. Since S_i will increase drastically for large values of y for given $\ln R^+$, and S_o will increase for small values of y, an "overlap" region exists only if there is a region for which both S_i and S_o remain small simultaneously. In the following paragraphs, this condition will be used in conjunction with equation 4.10 to derive the functional form of the velocity in the overlap region *at finite Reynolds number*, hence the term 'Near-Asymptotics'.

Because the overlap region moves toward the wall with increasing R^+, it is convenient and necessary to introduce an intermediate variable $\tilde{y}$ which can be fixed in the

overlap region all the way to the limit, regardless of what is happening in physical space (v. Cole & Kevorkian, 1981). A definition of $\tilde{y}$ which accomplishes this is given by

$$\tilde{y} = y^+ \delta^{+-n} \tag{4.15}$$

or

$$y^+ = \tilde{y} \delta^{+n} \tag{4.16}$$

Since $R^+ = y^+/\overline{y}$, it follows that

$$\overline{y} = \tilde{y} \delta^{+n-1} \tag{4.17}$$

For all values of n satisfying $0 < n < 1$, $\tilde{y}$ can remain fixed in the limit as $R^+ \to \infty$ while $\overline{y} \to 0$ and $y^+ \to \infty$. Substituting these into equation 4.10 yields the matching condition on the velocity in terms of the intermediate variable as

$$\frac{1}{g(R^+)} + f_o(R^{+n-1}\tilde{y}, R^+) = f_i(R^{+n}\tilde{y}, R^+) \tag{4.18}$$

Now equation 4.18 can be differentiated with respect to R^+ *for fixed* $\tilde{y}$ to yield equations which explicitly include S_i and S_o. The result after some manipulation is

$$\overline{y} \frac{\partial f_o}{\partial \overline{y}}\bigg|_{R^+} = \frac{1}{\kappa} - \left[S_i(y^+, R^+) f_i(y^+, R^+) - S_o(\overline{y}, R^+) f_o(\overline{y}, R^+) \right] \tag{4.19}$$

where

$$\frac{1}{\kappa(R^+)} \equiv -\frac{R^+}{g^2} \frac{dg}{dR^+} = \frac{d(1/g)}{d \ln R^+} \tag{4.20}$$

The first term on the right hand side of equation 4.19 is at most a function of R^+ alone, while the second term contains all of the residual y-dependence.

Now it is clear that if both

$$|S_o| \, f_o << 1/\kappa \tag{4.21}$$

and

$$|S_i|\, f_i << 1/\kappa \tag{4.22}$$

then the first term on the r.h.s. of equation 4.19 dominates. If $1/\kappa \to 0$, the inequalities are still satisfied as long as the l.h.s. of equations 4.21 and 4.22 does so more rapidly than $1/\kappa$. Note that a much weaker condition can be applied which yields the same result; namely that both inner and outer scaled profiles have the same dependence on R^+; i.e., $S_i f_i = S_o f_o$ in the overlap range so only $1/\kappa$ remains. If these inequalities are satisfied over some range in y, then to leading order, equation 4.19 can be written as

$$\overline{y}\frac{\partial f_o}{\partial \overline{y}}\bigg|_{R^+} = \frac{1}{\kappa} \tag{4.23}$$

The solution to equation 4.23 could be denoted as $f_o^{(1)}$ since it represents a first order approximation to f_o. Because $1/\kappa$ depends on R^+ it is *not* simply the same as $f_{o\infty}$, but reduces to it in the limit. Thus, by regrouping all of the y-independent contributions into the leading term, the method applied here has yielded a more general result than the customary expansion about infinite Reynolds number. (It is also easy to see why the usual matching of infinite Reynolds number inner and outer solutions will not work if the limiting value of $1/\kappa$ is zero, which can not yet be ruled out.)

From equations 4.12 and 4.23, it follows that

$$y^+\frac{\partial f_i}{\partial y^+}\bigg|_{R^+} = \frac{1}{\kappa} \tag{4.24}$$

Equations 4.23 and 4.24 must be independent of the origin for y; hence they must be invariant to transformations of the forms $\overline{y} \to \overline{y}+\overline{a}$ and $y^+ \to y^+ + a^+$, respectively, where a is at most a function of the Reynolds number. Therefore the most general

forms of equations 4.23 and 4.26 are:

$$(\overline{y}+\overline{a})\frac{\partial f_o}{\partial(\overline{y}+\overline{a})}\bigg|_{R^+} = \frac{1}{\kappa} \tag{4.25}$$

and

$$(y^+ + a^+)\frac{\partial f_i}{\partial(y^+ + a^+)}\bigg|_{R^+} = \frac{1}{\kappa} \tag{4.26}$$

The solutions to these overlap equations are given by:

$$\frac{U-U_c}{u_*} = f_o(\overline{y}, R^+) = \frac{1}{\kappa(R^+)}\ln[\overline{y}+\overline{a}(R^+)] + B_o(R^+) \tag{4.27}$$

and

$$\frac{U}{u_*} = f_i(y^+, R^+) = \frac{1}{\kappa(R^+)}\ln[y^+ + a^+(R^+)] + B_i(R^+) \tag{4.28}$$

The superscript "(1)" has been dropped; however it is these first order solutions that are being referred to unless otherwise stated. Thus the velocity profiles in the overlap region are logarithmic, but with parameters which are in general Reynolds number dependent.

Note that the particular form of the solution $\ln(y+a)$ has also been identified by Oberlack (1997) from a Lie group analysis of the equations governing homogeneous shear flows. It will be argued in Section 4.8 that a^+ is closely related to the *mesolayer*, just as it is for the boundary layer (George & Castillo, 1997). The data will be found to be consistent with $a^+ \approx -8$. Interestingly, the need for the offset parameter a appears to have first been noticed by Squire (1948) (see also Duncan, Thom & Young, 1970) using a simple eddy viscosity model. (Even his value of $a^+ = 5.9$ does not differ much from the one used here.) George *et al.* (1996) arrived at a similar form from a simple one-equation turbulence model for the mesolayer, as discussed in Section 4.8 below.

A particularly interesting feature of these first order solutions is that the inequalities given by equations 4.21 and 4.22 determine the limits of validity of both equa-

tions 4.25 and 4.26 since either S_o or S_i will be large outside the overlap region. Clearly, the extent of this region will increase as the Reynolds number (or R^+) increases.

The parameters $1/\kappa$, B_i and B_o must be asymptotically constant since they occur in solutions to equations which are themselves Reynolds number independent in the limit (AIP). Moreover, the limiting values, κ_∞, $B_{i\infty}$, and $B_{o\infty}$ cannot all be zero, or else the solutions themselves are trivial. In the limit of infinite Reynolds number the energy balance in the overlap region reduces to production equals dissipation; i.e., $\epsilon^+ = P^+$. In section 4.8 this will be shown to imply that

$$\epsilon \to \frac{du^+}{dy^+} = \frac{1}{\kappa(y^+ + a^+)} \tag{4.29}$$

Since the *local* energy dissipation rate must be finite and non-zero (Frisch (1995)), it follows that $1/\kappa_\infty$ must be finite and non-zero. It will be shown below that these conditions severely restrict the possible Reynolds number dependencies for the parameters κ, B_i and B_o. (Note that the same physical constraint on the boundary layer results required the power exponent for the boundary layer, γ, to be asymptotically finite and non-zero.)

The relation between u_* and U_c follows immediately from equation 4.10; i.e.,

$$\frac{U_c}{u_*} = \frac{1}{g(R^+)} = \frac{1}{\kappa(R^+)} ln R^+ + [B_i(R^+) - B_o(R^+)] \tag{4.30}$$

Thus the friction law is entirely determined by the velocity parameters for the overlap region. However, equation 4.20 must also be satisfied. Substituting equation 4.30 into equation 4.20 implies that κ, B_i, and B_o are constrained by

$$\ln R^+ \frac{d(1/\kappa)}{d \ln R^+} = -\frac{d(B_i - B_o)}{d \ln R^+} \tag{4.31}$$

This is exactly the criterion for the neglected terms in equation 4.19 to vanish iden-

tically (i.e., $S_i f_i - S_o f_o \equiv 0$). Therefore the solution represented by equations 4.27 to 4.31 is, indeed, the first order solution for the velocity profile in the overlap layer at *finite*, but large, Reynolds number. Clearly when y^+ is too big or $\overline{y}$ is too small for a given value of R^+, the inequalities of equation 4.21 and 4.22 cannot be satisfied. Since all the derivatives with respect to R^+ must vanish as $R^+ \to \infty$ (AIP), the outer range of the inner overlap solution is unbounded in the limit, while the inner range of the outer is bounded only by $\overline{y} = -\overline{a}$.

Equation 4.31 is invariant to transformations of the form $R^+ \to D_s R^+$ where D_s is a scale factor which ensures that the functional dependence is independent of the particular choice of the outer length scale (e.g., diameter versus radius). Thus the velocity profile in the overlap layer is logarithmic, *but* with parameters which depend on the Reynolds number, $D_s R^+$. The functions $\kappa(D_s R^+)$, $B_i(D_s R^+)$ and $B_o(D_s R^+)$ must be determined either empirically or from a closure model for the turbulence. Regardless of how they are determined, the results must be consistent with equation 4.31.

4.5 A Solution for the Reynolds Number Dependence

From equation 4.31 it is clear that if either $B_i - B_o$ or $1/\kappa$ are given, then the other is determined (to within an additive constant). Since there is only one unknown function, it is convenient to transform equation 4.31 using the function

$$H(D_s R^+) \equiv (\frac{1}{\kappa} - \frac{1}{\kappa_\infty}) \ln D_s R^+ + (B_i - B_o) \tag{4.32}$$

where $H = H(D_s R^+)$ remains to be determined. If $H(D_s R^+)$ satisfies

$$\frac{1}{\kappa} - \frac{1}{\kappa_\infty} = \frac{dH}{d \ln D_s R^+} \tag{4.33}$$

then equation 4.31 is satisfied. It follows immediately that

$$\frac{1}{g} = \frac{U_c}{u_*} = \frac{1}{\kappa_\infty} \ln D_s R^+ + H(D_s R^+) \tag{4.34}$$

Thus the Reynolds number dependence of the single function $H(D_s R^+)$ determines that of κ, $B_i - B_o$ and g.

The conditions that both $B_{i\infty}$ and $B_{o\infty}$ be finite and non-zero require that:
Either

- B_i, B_o and κ remain constant always;

or

- (i) $1/\kappa \to 1/\kappa_\infty$ faster than $1/\ln D_s R^+ \to 0$, and
- (ii) $H(D_s R^+) \to H_\infty = constant$.

Obviously from equation 4.32,

$$H_\infty = B_{i\infty} - B_{o\infty} \tag{4.35}$$

It is also clear from the constraint equation that the natural variable is $\ln D_s R^+$. Since this blows up in the limit as $R^+ \to \infty$, H can at most depend on inverse powers of $\ln D_s R^+$. Thus the expansion of H for large values of $\ln D_s R^+$ must be of the form:

$$H(D_s R^+) - H_\infty = \frac{A}{[\ln D_s R^+]^\alpha} \left[1 + \frac{A_1}{\ln D_s R^+} + \frac{A_2}{(\ln D_s R^+)^2} + \cdots \right] \tag{4.36}$$

Note that conditions (i) and (ii) above imply that $\alpha > 0$. Although only the leading term will be found to be necessary to describe the data, the rest will be carried in developing the theoretical relations below.

Substituting equation 4.36 in equation 4.34 yields:

$$\frac{U_c}{u_*} = \frac{1}{\kappa_\infty}\ln D_s R^+ + [B_{i\infty} - B_{o\infty}] + \frac{A}{[\ln D_s R^+]^\alpha}\left[1 + \frac{A_1}{\ln D_s R^+} + \frac{A_2}{(\ln D_s R^+)^2} + \cdots\right] \tag{4.37}$$

As $R^+ \to \infty$ this reduces to the classical solution of Millikan (1938). This is reassuring since Millikan's analysis is an infinite Reynolds number analysis of inner and outer profiles scaled in the same way. (Note that this was *not* true for the boundary layer: The Clauser/Millikan analysis *assumed* the same scaling laws applied as for the channel/pipe. George and Castillo argued from the Reynolds-averaged equations that they had to be different, hence the different conclusions.)

The Reynolds number variation of $1/\kappa$ and $B_i - B_o$ can be obtained immediately from equations 4.32, 4.33 and 4.36 as

$$\frac{1}{\kappa} - \frac{1}{\kappa_\infty} = -\frac{\alpha A}{(\ln D_s R^+)^{1+\alpha}}\left[1 + \left(\frac{1+\alpha}{\alpha}\right)\frac{A_1}{\ln D_s R^+} + \left(\frac{2+\alpha}{\alpha}\right)\frac{A_2}{(\ln D_s R^+)^2} + \cdots\right] \tag{4.38}$$

and

$$\begin{aligned}(B_i - B_o) \quad - \quad (B_{i\infty} - B_{o\infty}) \quad &= \\ = \frac{(1+\alpha)A}{(\ln D_s R^+)^\alpha} \qquad &\left[1 + \left(\frac{2+\alpha}{1+\alpha}\right)\frac{A_1}{\ln D_s R^+} + \left(\frac{3+\alpha}{1+\alpha}\right)\frac{A_2}{(\ln D_s R^+)^2} + \cdots\right]\end{aligned} \tag{4.39}$$

Figure 5 shows the friction data of the superpipe experiment of Zagarola & Smits (1998*a*). As the investigators themselves have pointed out, careful scrutiny reveals that the data do not fall on a straight line on a semi-log plot, so a simple logarithmic friction law with constant coefficients does not describe all the data *to within the accuracy of the data itself.* In particular, a log which attempts to fit all of the data dips away from it in the middle range. On the other hand, a log which fits the high Reynolds number range does not fit the low, or vice versa. Figure 5 shows two curves: The first represents a regression fit of equation 4.37 with only the leading term (i.e., $A_1 = A_2 = 0$), while the second shows only the asymptotic log form of equation

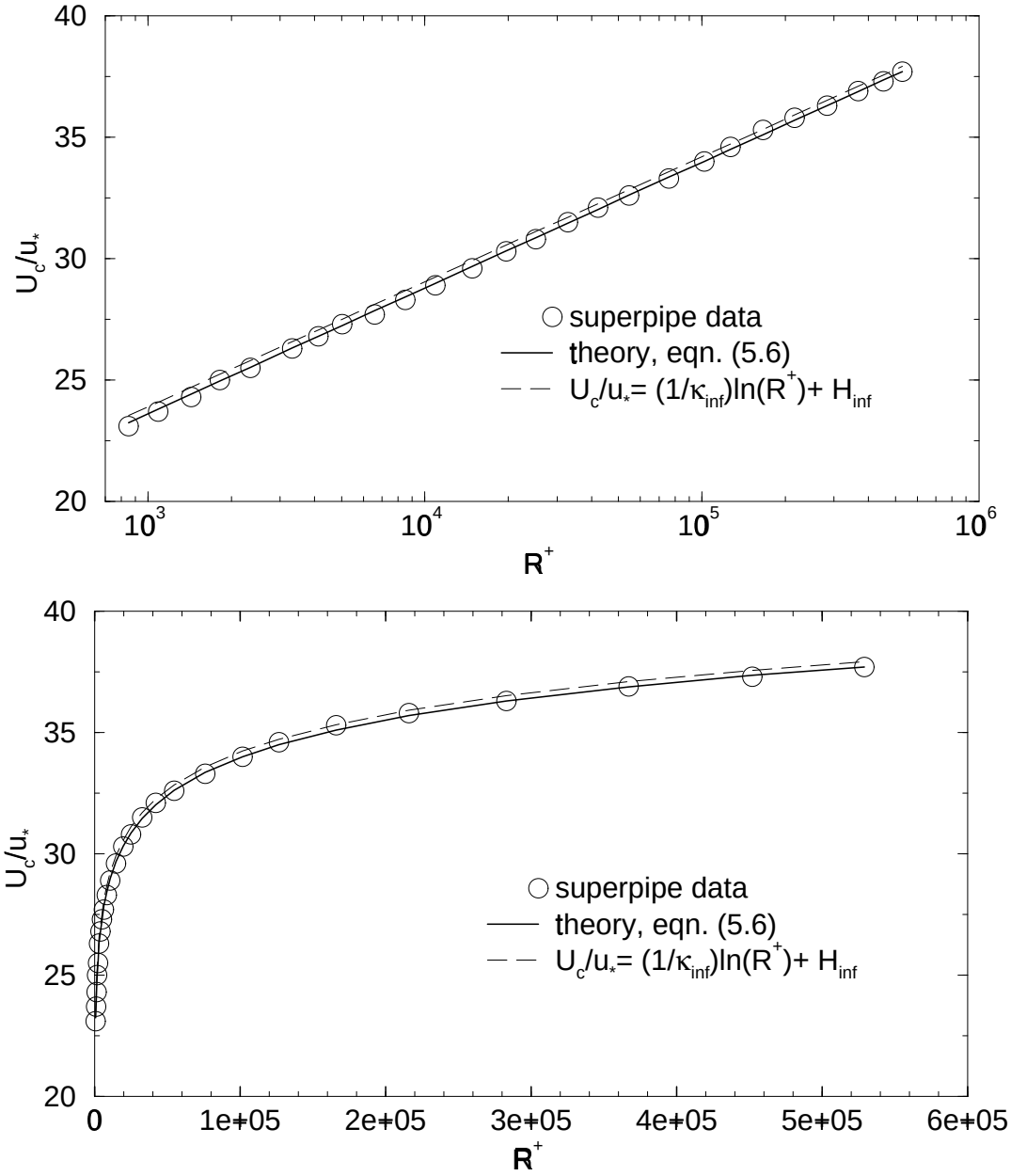

Figure 5: Variation of U_c/u_* with $R^+ = Ru_*/\nu$

4.37. The former provides an excellent fit to the data for *all* Reynolds numbers and asymptotes exactly to the latter, but only at much higher Reynolds numbers. The differences, although slight, are very important since they entirely determine (or reflect) the Reynolds number dependence of the parameters $1/\kappa$, B_i and B_o. The latter will be seen later to be especially sensitive to this dependence. Clearly the simplest of the proposed forms of H captures the residual Reynolds number dependence, while simply using constant coefficients does not.

The values obtained for the asymptotic friction law parameters using optimization techniques are $\kappa_\infty = 0.447$, $B_{i\infty} - B_{o\infty} = 8.45$, while those describing the Reynolds number dependence are $A = -0.668$ and $\alpha = 0.441$. The higher order terms in equation 4.36 were ignored, and will be throughout the remainder of this chapter. The same optimization techniques showed no advantage to using values of the parameter D_s different from unity, hence $D_s = 1$ to within experimental error. Note that the values of $B_{i\infty}$ and $B_{o\infty}$ cannot be determined individually from the friction data, only their difference. Nominal values for κ and $B_i - B_o$ are approximately 0.445 and 8.20 respectively, the former varying by less than 0.5% and the latter by only one percent over the entire range of the data. These values differ only slightly from the values determined by Zagarola (1996) (0.44 and 7.8, respectively) and Zagarola & Smits (1998*a*) (0.436 and 7.66, respectively) using the velocity profiles alone and assuming that the asymptotic state had been reached. In fact it will be shown later from the velocity profiles that B_i is independent of Reynolds number and approximately equal to 6.5. Thus only B_o significantly changes with Reynolds number and then only by about 5% over the range of the data, but even this variation will be seen to be quite important for the outer profile. Note that the friction law is independent of the parameter a.

All the parameters are remarkably independent of the particular range of data utilized. For example, after optimizing the parameters in equation 4.37 for the friction data of all 26 different Reynolds numbers available, the highest 15 Reynolds numbers

could be dropped before a new optimization would even change the second digit of the values of the parameters cited above. This suggests strongly, contrary to the suggestion of Barenblatt *et al.* (1997) (see also Barenblatt & Chorin, 1998; Smits & Zagarola, 1998, for response), that the superpipe data are in fact a smooth curve, uncontaminated by roughness. If the analysis developed herein is correct, then the reason these authors had a problem with the superpipe data is obvious: the data vary logarithmically as *derived* here, and not according to their *conjectured* power law.

For the boundary layer the friction data are not as reliable as those reported here, so the functional form of $h(\delta^+)$ had to be inferred by GC after a variety of attempts to describe the variation of the exponent in a power law description of the velocity profile in the overlap region. Interestingly, the value for α obtained here is almost exactly the value obtained for the boundary layer data (0.46 versus 0.44). Even more intriguing is that both of these are nearly equal to the values found for κ_∞ and $1/(\gamma_\infty C_{i\infty})$. It is not yet clear whether this is of physical significance to this, or whether it is just coincidence.

4.6 Single-point Second-order Turbulence Quantities.

Unlike the boundary layer where the continued downstream evolution imposes certain similarity constraints, for pipe and channel flows there is only a single velocity scale so all quantities must scale with it. An immediate consequence of this is that all quantities scaling with the velocity only will have logarithmic profiles in the overlap region. (It is straightforward to show this by the same procedures applied above to the mean velocity.)

For example, in inner variables, the Reynolds stress profiles are given by

$$< -u_m u_n >^+ = \frac{< -u_m u_n >}{u_*^2} = A_{i,mn}(R^+) \ln(y^+ + a^+) + B_{i,mn}(R^+) \qquad (4.40)$$

As for the velocity, the parameters $A_{i,mn}$ and $B_{i,mn}$ are functions of the Reynolds number and asymptotically constant. Note that the offset a^+ has been assumed to be the same as for the velocity, although this needs to be subjected to experimental verification.

The Reynolds shear stress is particularly interesting since for it more information can be obtained from the mean momentum equation. In the overlap region in the limit as $R^+ \to \infty$, both equations 4.2 and 4.3 reduce to

$$0 = \frac{\partial < -uv >}{\partial y} \tag{4.41}$$

or in inner variables,

$$0 = \frac{\partial < -uv >^+}{\partial y^+} \tag{4.42}$$

It follows from substituting the 1, 2-component of equation 4.40 that

$$0 = \frac{A_{i12}}{y^+ + a^+} \tag{4.43}$$

It is immediately clear that equation 4.42 can be satisfied only if $A_{i12} \to 0$ as $R^+ \to \infty$. A similar argument for the outer profile implies $A_{o12} \to 0$. Thus to leading order, the Reynolds shear stress profile in the overlap region is independent of y; however, the remaining parameters B_{i12} and B_{o12} are only asymptotically constant. From equation 4.4 it is clear that $B_{i12} \to 1$, but only in the limit. Since $< -uv > \to u_*^2$ is also the inner boundary condition on equation 4.2, $B_{o12} \to 1$ in the limit also.

Another quantity of particular interest is the rate of dissipation of turbulence energy per unit mass, ϵ. For the inner part of the flow, the appropriate dissipation scale must be u_*^4/ν on dimensional grounds, since there are no other possibilities. In the outer layer in the limit of infinite Reynolds number, the dissipation is effectively inviscid (as discussed in Section 4.7 below), so it must scale as u_*^3/R. (Note that this only means that profiles scaled as $\epsilon\nu/u_*^4$ vs. y^+ and $\epsilon R/u_*^3$ vs. $\overline{y}$ will collapse in

the limit of infinite Reynolds number in the inner and outer regions, respectively.) It is easy to show by the methodology applied to mean velocity and Reynolds stresses above that the dissipation profile in the overlap region is given by a *power law* with an exponent of -1. Thus

$$\epsilon^+ = \frac{\epsilon\nu}{u_*^4} = \frac{E_i(R^+)}{y^+ + a^+} \tag{4.44}$$

and

$$\overline{\epsilon} = \frac{\epsilon R}{u_*^3} = \frac{E_o(R^+)}{\overline{y} + \overline{a}} \tag{4.45}$$

where both E_o and E_i are asymptotically constant. It has again been assumed that the origin shift a is the same as for the mean velocity. For the dissipation, this can be justified using the production equals dissipation limit as shown in the Section 4.8.

4.7 The Effect of Reynolds Number on the Overlap Region

The asymptotic values of the parameters established for the friction law will be used below to calculate the values of κ, B_i and B_o for each Reynolds number of the superpipe data. Only either of the B's need be established from the experiments since their difference is known from equation 4.32. Before carrying out a detailed comparison with the velocity data, however, it is useful to first consider exactly which region of the flow is being described by the overlap profiles. Also of interest is the question of how large the Reynolds number must be before the flow begins to show characteristics of the asymptotic state.

The overlap layer identified in the preceding sections can be related directly to the averaged equations for the mean flow and the Reynolds stresses. From about $y^+ > 30$ out to about the center of the flow, the averaged momentum equation is given approximately by

$$0 = -\frac{1}{\rho}\frac{dP}{dx} + \frac{\partial < -uv >}{\partial y} \tag{4.46}$$

It has no explicit Reynolds number dependence; and the Reynolds shear stress drops linearly all the way to the center of the flow (v. Perry & Abell, 1975). Inside about $\overline{y} = 0.1$ and outside of $y^+ = 30$, however, the Reynolds shear stress is very nearly constant. In fact, at infinite Reynolds number the pressure gradient term vanishes identically in the constant Reynolds shear stress region and the mean momentum equation reduces to

$$0 = \frac{\partial < -uv >}{\partial y} \tag{4.47}$$

At finite (but large) Reynolds numbers this region is similar to the developing boundary layer where the Reynolds stress is effectively constant. Obviously *the overlap region corresponds to this constant Reynolds shear stress layer* since the Reynolds shear stress gradient is the common term to both inner and outer momentum equations. Note that many low Reynolds number experiments do not have a region where the Reynolds stress is even approximately constant because the pressure gradient term is not truly negligible. Hence it is unreasonable to expect such experimental profiles to display any of the characteristics of the overlap described above, except possibly in combination with the characteristics of the other regions (e.g., through a composite solution).

Even when there is a region of reasonably constant Reynolds stress, however, there remains the Reynolds number dependence of $< -uv >$ itself. And it is this weak Reynolds number dependence which is the reason that κ, B_i, and B_o are only asymptotically constant. The origin of this weak Reynolds number dependence (which is well-known to turbulence modelers) can be seen by considering the Reynolds transport equations. For the same region, $y^+ > 30$, the viscous diffusion terms are negligible (as in the mean momentum equation), so the Reynolds shear stress equations reduce approximately to (Tennekes & Lumley, 1972),

$$0 = -(< p\frac{\partial u_i}{\partial x_k} > + < p\frac{\partial u_k}{\partial x_i} >) - \left[< u_i u_2 > \frac{\partial U_k}{\partial x_2} + < u_k u_2 > \frac{\partial U_i}{\partial x_2}\right] - \frac{\partial < u_i u_k u_2 >}{\partial x_2} - \epsilon_{ik} \tag{4.48}$$

where $U_i = U\delta_{i1}$. Thus viscosity does not appear directly in any of the single point equations governing the overlap region, nor in those governing the outer layer.

Viscosity, however, can be shown to play a crucial role in at least a portion of the constant stress layer, even at infinite Reynolds number. The reason is that the *length scales* at which the dissipation, ϵ_{ik}, actually takes place depend on the *local* turbulence Reynolds number, $R_t = q^4/\nu\epsilon$. For $R_t > 5000$ approximately, the energy dissipation is mostly determined by the large energetic scales of motion. These scales are effectively inviscid, but control the energy transfer through non-linear interactions (the energy cascade) to much smaller viscous scales where the actual dissipation occurs (Tennekes & Lumley, 1972). When this is the case, the dissipation is nearly isotropic so $\epsilon_{ik} \approx 2\epsilon\delta_{ik}$. Moreover, ϵ can be approximated by the infinite Reynolds number relation: $\epsilon \sim q^3/L$ where L is a scale characteristic of the energy-containing eddies. The coefficient has a weak Reynolds number dependence, but is asymptotically constant. Thus, the Reynolds stress equations themselves are effectively inviscid, but only exactly so in the limit. Note that in this limit the Reynolds shear stress has no dissipation at all, i.e., $\epsilon_{12} = 0$.

At very low turbulence Reynolds number, however, the dissipative and energy-containing ranges nearly overlap, and so the latter (which also produce the Reynolds shear stress) feel directly the influence of viscosity. In this limit, the energy and dissipative scales are about the same, so the dissipation is more reasonably estimated by $\epsilon \sim \nu q^2/L^2$, where the constant of proportionality is of order 10. The dissipation tensor, ϵ_{ik} is anisotropic and ϵ_{12}, in particular, is non-zero. (Hanjalic & Launder (1974), for example, take $\epsilon_{12} = (- < u_1 u_2 > \epsilon/q^2)$.)

For turbulence Reynolds numbers between these two limits, the dissipation will show characteristics of both limits, gradually making a transition from $\epsilon \sim \nu q^2/L^2$ to $\epsilon \sim q^3/L$ as R_t increases. This is felt by the Reynolds stresses themselves, which will show a strong Reynolds number dependence. Obviously, in order to establish when (if at all) parts of the flow become Reynolds number independent, it is necessary to

determine how the local turbulence Reynolds number varies across the flow.

Over the outer part of the pipe (which is most of it), $L \approx R/2$ and $q \approx 3u_*$. So when $R^+ > 3,000$, the dissipation in the outer flow is effectively inviscid. Above this value the mean and turbulence quantities in the core region of the flow should show little Reynolds number dependence. This is indeed the case as illustrated by Figure 4. The outer region can, of course, not be entirely Reynolds number independent, except in the limit, and this residual dependence manifests itself in the overlap layer in the slow variations of κ and B_o, for example.

The near wall region is considerably more interesting since in it the scales governing the energy-containing eddies are constrained by the proximity of the wall. Hence, the turbulence Reynolds number, R_t, depends on the distance from the wall, y. In fact, $R_t \sim y^+$ with a coefficient of about 18 (Gibson, 1997); so, in effect, y^+ is the turbulence Reynolds number. Two things are then immediately obvious:

- First, as the Reynolds number increases more of the pipe (in outer variables) will become effectively inviscid and will be governed by the inviscid dissipation relation. Correspondingly, the properly scaled mean and turbulence quantities in at least the outer part of the overlap layer (say, an *inertial sublayer*) will become Reynolds number independent, although very slowly. This cannot be reached until the layer is governed by the infinite Reynolds number dissipation relation and its coefficient has reached the limiting value. Obviously this can happen only when there is a substantial inertial sublayer satisfying $y^+ > 300$ (approximately) and for which the mean pressure-gradient term is negligible, typically $\overline{y} < 0.1$. Thus the asymptotic limits are realized only when $300\nu/u_* << 0.1R$ or $R^+ >> 3000$. Therefore below $R^+ = 30,000$ approximately, even this inertial sublayer should display a Reynolds number dependence, not only in κ, B_o, and B_i, but correspondingly in the behavior of $< u^2 >$, $< uv >$, etc. The lower limit of this inertial sublayer also corresponds (for the same reasons) to the place where a $k^{-5/3}$-region should begin to be observed in the energy spectra.

- Second, at the bottom of the overlap region (or the constant Reynolds shear stress layer) there will always be a *mesolayer*[2] below $y^+ \approx 300$ in which the dissipation can *never* assume the character of a high Reynolds number flow, no matter how high the Reynolds number becomes. This is because the dissipation (and Reynolds stress as well) can never become independent of viscosity in this region. Even though the single-point Reynolds-averaged equations are inviscid above $y^+ \approx 30$, the multi-point equations are not! This fact is well-known to turbulence modelers (v. Hanjalic & Launder, 1974), but the consequences for similarity theory and asymptotic analyses do not seem to have been noticed previously. It is particularly important for experimentalists who have routinely tried to apply asymptotic formulae to data in this region, wrongly believing the mesolayer to be the inertial sublayer.

Thus, as illustrated in Figure 6, the constant stress layer has two separate regions, each having their own unique character: the *constant Reynolds shear stress (or overlap) region* and *the viscous sublayer* where the viscous stress is also important. Each of these has two subregions. The overlap region consists of an *inertial sublayer* ($y^+ > 300$, $\overline{y} < 0.1$) which is nearly inviscid, and a *mesolayer* ($30 < y^+ < 300$) in which the viscous stresses are negligible, but in which viscosity acts directly on the turbulence scales producing the Reynolds stresses. The viscous sublayer is comprised of a buffer layer ($3 < y^+ < 30$) where the Reynolds stress and viscous stress both act directly on the mean flow; and the linear sublayer near the wall ($y^+ < 3$) where the viscous stresses dominate. Of these four regions, the inertial sublayer will be the *last* to appear as the Reynolds number is increased. Thus, the overlap layer itself will be most difficult to identify at the modest Reynolds numbers of most laboratory experiments, unless the properties of the mesolayer are known. In the next section it will be argued that, in fact, it is the offset parameter a^+ which accounts for it. Thus

[2]This appropriates a term from Long (1976) (see also Long & Chen, 1981) who argued strongly for its existence, but from entirely different physical and scaling arguments which we find untenable. Despite the skepticism which greeted his ideas, Long's instincts were correct.

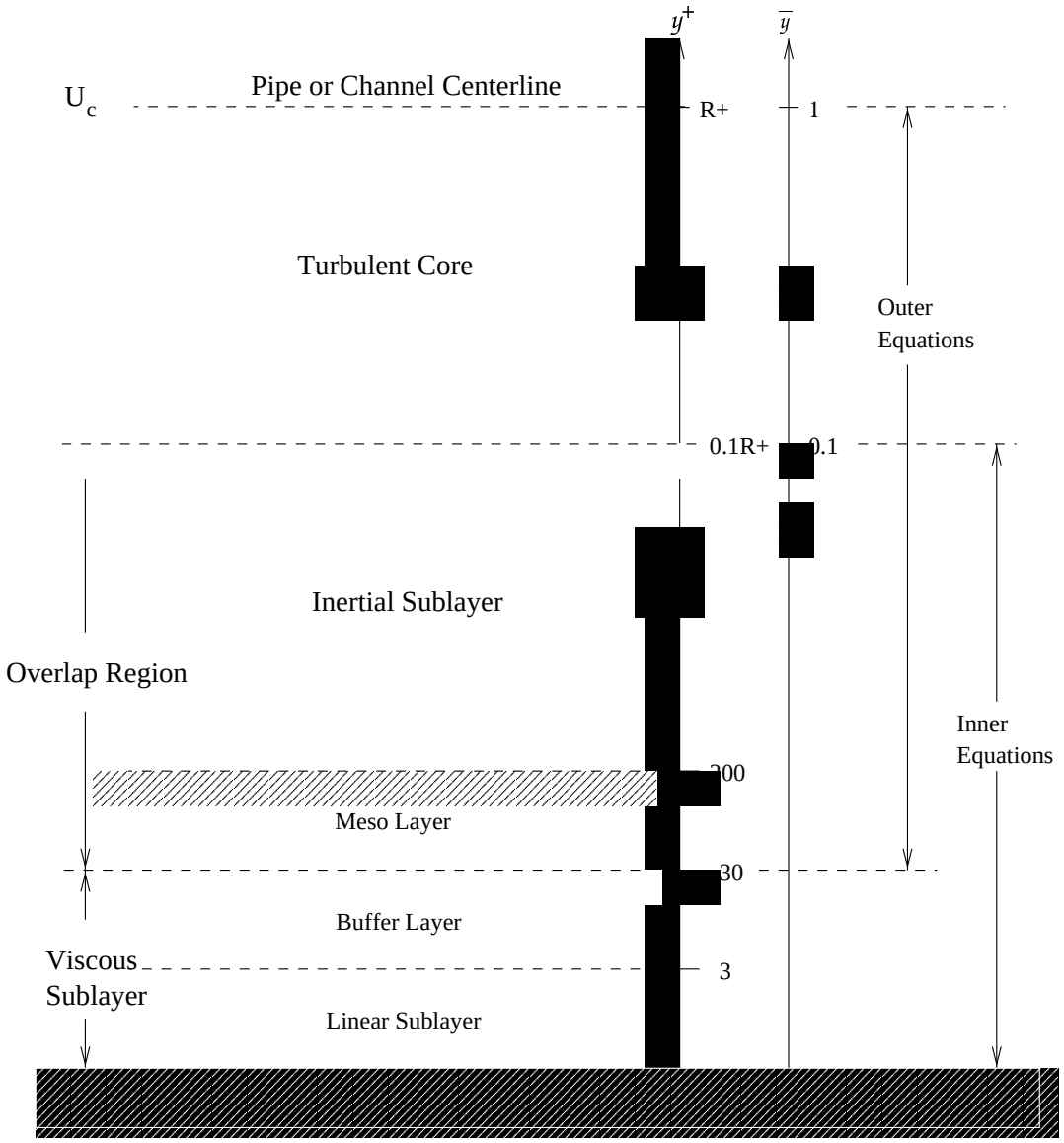

Figure 6: Schematic showing various regions and layers of pipe and channel flows

the inertial sublayer can readily be identified as the region for which $y^+ >> |a^+|$ and the velocity profile in it is primarily a log profile in y alone, the contribution of the offset being negligible; i.e., $\ln(y+a) \approx \ln y$. Attempts to identify logarithmic behavior inside $y^+ = 300$ from straight lines on semi-log plots of u^+ versus y^+ are of little use if the theory presented herein is correct because of the presence of a. They will, of course, always succeed as a local approximation, but coefficients so determined will be incapable of extension to higher values of y^+ as the Reynolds number is increased. And this is indeed the history of attempts to identify the log layer and its parameters from such data.

4.8 A Mesolayer Interpretation of a^+

As noted in Section 4.4 above, Squire (1948) was apparently the first to notice the need for the offset coordinate $y^+ + a^+$. The basis of his argument was that the mixing length could not be taken as proportional to y alone, since the physics incorporated in it could not account for the thickness of the viscous sublayer. Although the overlap analysis presented here depends on different closure assumptions, the invariance to coordinate origin argument presented earlier is not much different, in principle at least. The preceding section argues for the existence of a *mesolayer* below the usual inertial layer in which the well-known scale separation of the energy and dissipative eddies cannot exist. The purpose of this section is to show how these last two ideas are related.

The overlap solution of equation 4.28 can be expanded for values of $y^+ >> |a^+|$

$$\frac{U}{u_*} = f_i(y^+, R^+) = \frac{1}{\kappa}\left\{[lny^+ + \kappa B_i] + \frac{a^+}{y^+} - \frac{1}{2}\frac{a^{+2}}{y^{+2}} + \frac{1}{3}\frac{a^{+3}}{y^{+3}} + \ldots\right\} \tag{4.49}$$

For $y^+ >> 2|a^+|$, this can be approximated by the first three terms as

$$\frac{U}{u_*} \approx \frac{1}{\kappa}\ln y^+ + B_i + \frac{a^+}{\kappa y^+} \tag{4.50}$$

An equivalent expansion in outer variables is given by

$$\frac{U - U_c}{u_*} \approx \frac{1}{\kappa} \ln \overline{y} + B_o + \frac{\overline{a}}{\kappa \overline{y}} \tag{4.51}$$

Equations 4.50 and 4.51 are useful for three reasons: First, they are an excellent approximation to the overlap solutions for values of $y^+ > 2|a^+|$ (or $\overline{y} > 2|\overline{a}|$). Second, they are easier to incorporate into a composite solution which includes the viscous sublayer than is the overlap solution itself since they do not have the singularity at $y^+ = -a^+$ (cf. George & Castillo, 1997). Third, the inner variable version can be shown to offer useful insight into the role of the parameter a^+ as accounting for the *mesolayer*.

In the overlap region the turbulence energy balance reduces to production equals dissipation; i.e., in inner variables, $P^+ \approx \epsilon^+$. This is exactly true in the limit of infinite Reynolds number, and approximately true at finite Reynolds numbers for $30 < y^+ < 0.1R^+$. It follows immediately by substitution of the overlap solutions for velocity, Reynolds stress and dissipation for P^+ and ϵ^+ that

$$P^+ = \frac{B_{i12}}{\kappa(y^+ + a^+)} = \epsilon^+ = \frac{E_i}{(y^+ + a^+)} \tag{4.52}$$

It is clear that the offset a^+ must be the same for both velocity and dissipation, as *assumed* earlier. Hence $E_i = B_{i12}/\kappa \to 1/\kappa$, at least in the limit as $R^+ \to \infty$ since $B_{i12} \to 1$.

Therefore, in this limit the dissipation and velocity derivative profiles are identical (as noted earlier) and equal to the derivative of equation 4.28 with respect to y^+; i.e.,

$$\epsilon^+ = \frac{1}{\kappa(y^+ + a^+)} = \epsilon_o^+ f_T(y^+) \tag{4.53}$$

where

$$\epsilon_o^+ \equiv \frac{1}{\kappa y^+} \tag{4.54}$$

and

$$f_T \equiv [1 + \frac{a^+}{y^+}]^{-1} \approx 1 - \frac{a^+}{y^+} \tag{4.55}$$

where the higher terms in the expansion in a^+ have been neglected. This is identical to the form used by many turbulence modelers for wall-bounded flows (cf. Reynolds, 1976; Hanjalic & Launder, 1974) to account *empirically* for the change in the character of the dissipation near the wall since $R_t \approx 18y^+$ as noted earlier. Thus the interpretation of a^+ as a mesolayer parameter is obvious since it, in effect, modifies the dissipation (and hence the velocity profile) near the wall. The suggested value of $a^+ = -8$ accomplishes this.

A similar form of f_T is obtained if the power law profile of George & Castillo (1997) for the boundary layer is expanded, even though the form of ϵ_o is different. Interestingly, if the order of argument is reversed and any of the simple dissipation models (eg., Reynolds, 1976) are used to deduce the mesolayer contribution to the velocity profile for the boundary layer, they produce a $y^{+^{-1}}$ additive instead of the $y^{+^{\gamma-1}}$ required. Obviously these simple turbulence models, as currently posed, are consistent with the theory developed herein only for homogeneous flows, although the difference is slight.

Note that the common practice of choosing the model constants in equation 4.55 to produce a log profile at $y^+ \approx 30$ is clearly wrong if the proposed theory is correct, since this is the location where the mesolayer only *begins*. As noted in Section 4.7, the mesolayer ends at $y^+ \approx 300$, and the inertial sublayer begins. It follows that a^+ should be chosen to "turn off" the low Reynolds number contribution at about this point (for increasing y^+) and "turn on" the $\ln y$ solution.

4.9 The Superpipe Velocity Data

Now that the approximate region of validity of the overlap solution has been established as $30 < y^+ < 0.1R^+$ it is possible to test the theoretical profiles and the

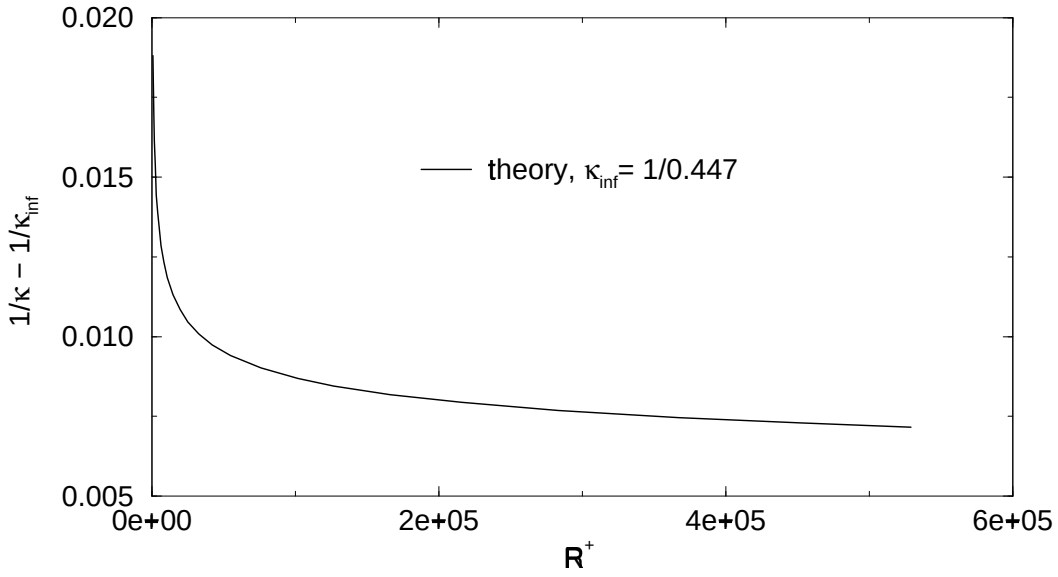

Figure 7: Variation of $1/\kappa - 1/\kappa_\infty$ with R^+, $\kappa_\infty = 0.447$

proposed layer model for the Reynolds number dependence. If they are correct, only an independent determination of either B_i or B_o is necessary to completely specify the profile, the rest of the parameters having been determined from the friction data. Since the superpipe experiments have a substantial range satisfying the conditions for the existence of the inertial sublayer ($300 < y^+ < 0.1R^+$), it should be possible to establish the value of B_i (or B_o) independent from the mesolayer. Also it should be possible to determine whether the parameter a^+ accounts for the mesolayer behavior, at least for those data sets where data are available below $y^+ = 300$.

For all of the data sets it appears $B_i = 6.5$ is nearly optimal (at least for values of $R^+ > 850$, the lowest available in this experiment), so that for the remainder of this chapter it will be assumed that $B_i = B_{i\infty}$. This value is close to the value of 6.15 determined by Zagarola & Smits (1998*a*), who assumed κ fixed at 0.436. Since the difference, $B_{i\infty} - B_{o\infty} = 8.45$, was established from the friction data, it follows that $B_{o\infty} = -1.95$. (Note, however, that the DNS channel data below suggest that $B_{o\infty} = -2.1$ and $B_{i\infty} = 6.35$ might be more appropriate, but the evidence is not conclusive yet.)

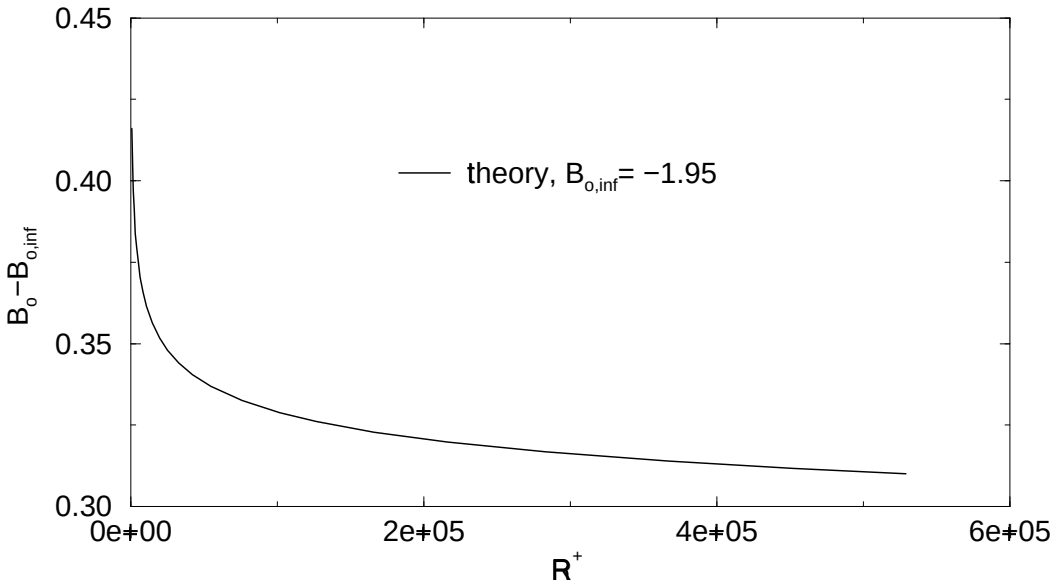

Figure 8: Variation of $B_o - B_{o\infty}$ with R^+, $B_{o\infty} = 8.50$

The constancy of B_i implies that it is B_o which shows all the Reynolds number dependence of the difference given by equation 4.39. Figures 7 and 8 show the theoretical variation of $1/\kappa$ and B_o with Reynolds number (equations 4.32 and 4.33). Clearly both converge very slowly to their asymptotic values. This has far more relative effect on B_o than it does on $1/\kappa$, however, since B_o has achieved only 85% of its asymptotic value at $R^+ = 10^5$. The observed variation of $1/\kappa$ and B_o and the constancy of B_i can be contrasted with the boundary layer results of George *et al.* (1996) and George & Castillo (1997) in which C_o, the outer coefficient was nearly constant while the power exponent γ and the inner coefficient C_i varied over the entire range of Reynolds numbers available.

Therefore the outer profile scaling will show more variation with Reynolds number in the overlap region than the inner where only κ varies. This explains a great deal of the problems historically in establishing what $B_{o\infty}$ is and in determining whether the outer scaling is correct. And it might also explain the conclusion of Zagarola & Smits (1998*a*) that a different scale for the outer flow is required, especially if attention is focused on the overlap region instead of the core region of the flow.

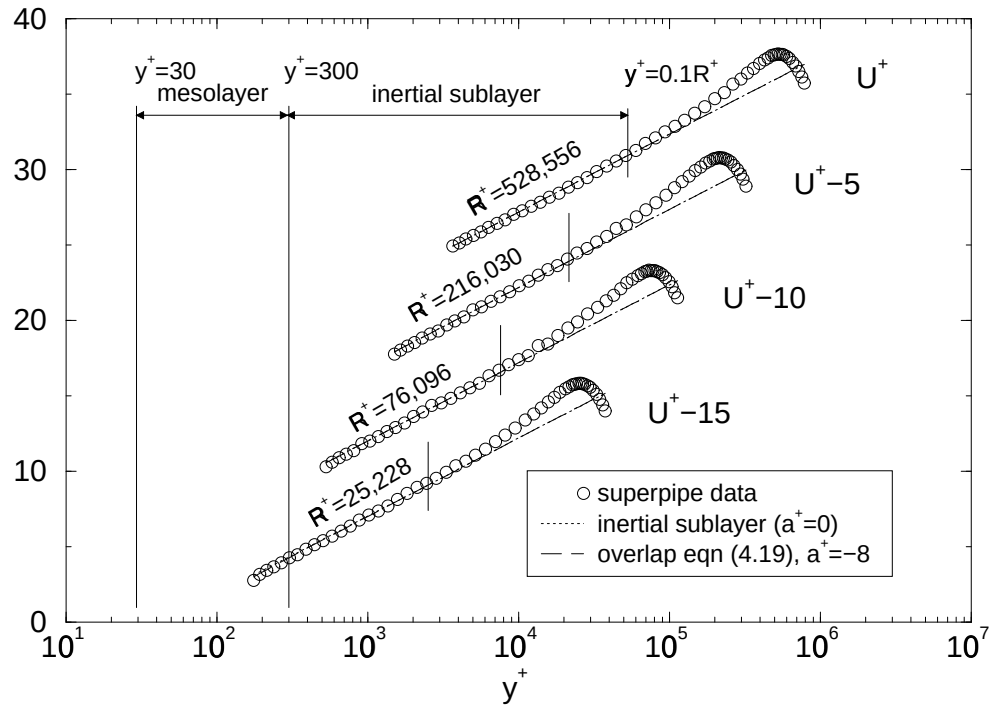

Figure 9: Velocity profiles in inner variables at relatively high Reynolds number

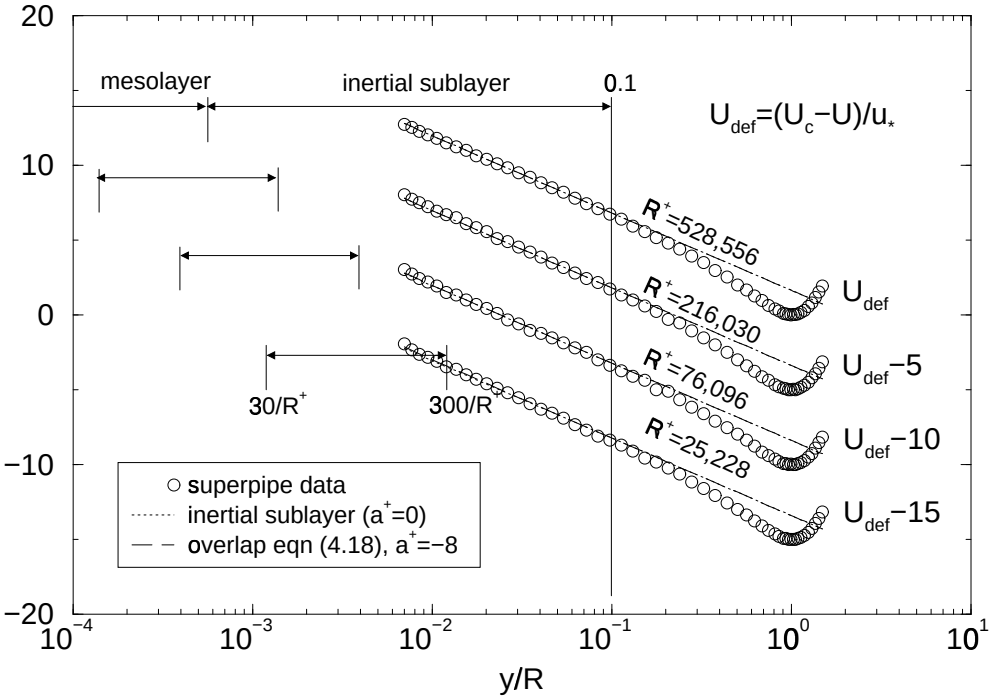

Figure 10: Velocity profiles in outer variables at relatively high Reynolds number

Figures 9, 10,11 and 12 show representative velocity profiles of the superpipe data at high and low Reynolds numbers, respectively. The profiles scaled in inner variables are shown in the upper plots, and the same data scaled in outer variables is shown in the lower plots. Also shown for each profile are the overlap solutions of equations 4.27 and 4.28 together with equations 4.38 and 4.39. The vertical lines on each profile show the suggested bounds for the two sublayers of the overlap region; in particular, the mesolayer ($30 < y^+ < 300$ or $30/R^+ < \overline{y} < 300/R^+$) and the inertial sublayer ($300 < y^+ < 0.1R^+$ or $300/R^+ < \overline{y} < 0.1$). The limits vary with R^+ for each profile. Note that for the highest Reynolds number plots the data were not measured close enough to the wall to see any of the mesolayer; however, they do show clearly the inertial sublayer. For the lowest Reynolds numbers, enough of the near wall region was resolved to clearly see the mesolayer, but the extent of the inertial sublayer was limited or non-existent. The theoretical profiles were computed using the measured value of R^+ and assuming $a^+ = 0$, -8, and -16 (or $\overline{a} = 0$, $-8/R^+$, and $-16/R^+$). (As noted above, the value of $B_{o\infty} = -1.95$ is determined since $B_{i\infty}$ has been chosen as 6.5 and $B_{i\infty} - B_{o\infty} = 8.45$ from the friction data.) Therefore there are *no* adjustable parameters in the outer scaled plot if a^+ is determined from the inner. Thus these outer profiles provide an completely independent test of the theory (and the data as well).

The value of $a^+ = 0$ corresponds to the inertial sublayer solution only, and as expected describes the data well only in the range of $300 < y^+ < 0.1R^+$. The boundary layer value of $a^+ = -16$ (from the power law) is clearly too large, but then there is no reason to expect it to be the same since the homogeneous pipe and inhomogeneous boundary layer flows are fundamentally different, at least in the outer and overlap regions. The best fit to the DNS channel flow data (see below) above $y^+ \approx 30$ is also $a^+ = -8$. It is possible to fit the data to substantially lower values of y^+ by using different values of a^+, but there appears to be no theoretical justification for doing so. Note that the Pitot tube used to make the pipe velocity measurements

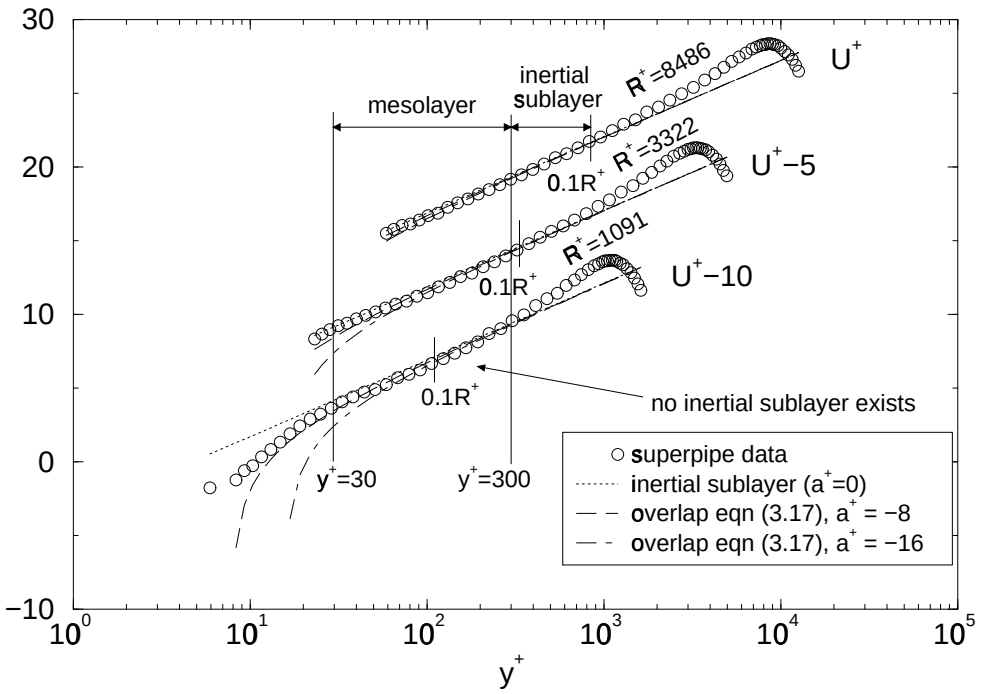

Figure 11: Velocity profiles in inner variables at relatively low Reynolds number

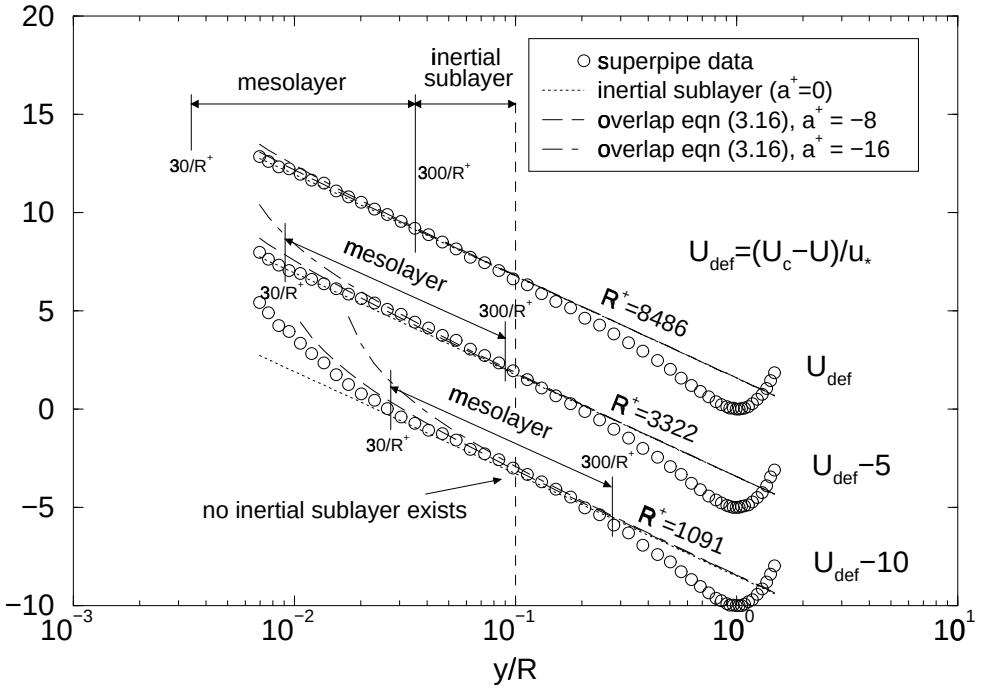

Figure 12: Velocity profiles in outer variables at relatively low Reynolds number

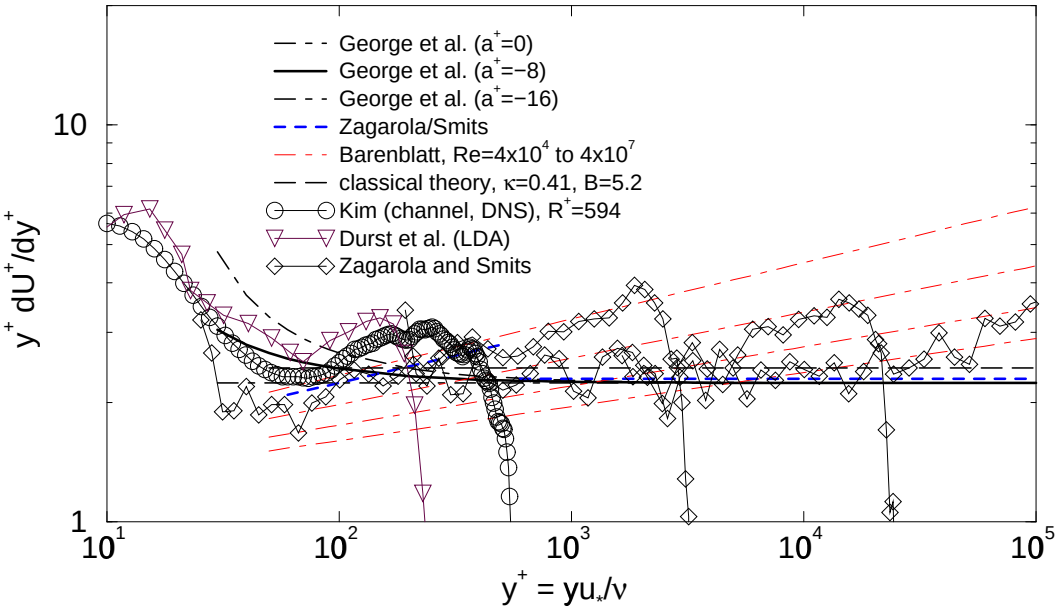

Figure 13: Comparison of data and theories for y^+du^+/dy^+ versus y^+.

could be as much as much as two percent too high at $y^+ = 30$ because of the local turbulence intensity there (since $U_{meas}/U \approx 1 + [< u^2 > + < v^2 > + < w^2 >]/2U^2$). Additional positive errors probably arise when the probes are closest to the wall because of the asymmetry in the streamline pattern around them. In spite of this, the agreement between experiment and theory over the entire overlap region is particularly gratifying since the velocity data were only used to establish B_i and a^+, the remaining parameters having been entirely determined by the friction data.

4.10 Comparison with Other Data and Theories

Figure 13 shows the profiles of y^+dU^+/dy^+ computed from a number of sources, including the LDA experiment of Durst, Jovanovic & Sender (1995) and the DNS data discussed below. Also shown are a comparison of the present theoretical results with the classical theory and the recent contributions of Zagarola & Smits (1998a) and Barenblatt (1993). Only a single $\kappa = 0.447$ is used for the present theory since

in inner variables the parameters are nearly constant, but the same three values of a^+ ($-16, -8$, and 0) are shown. The present theory reduces to a constant in these variables only when $a^+ = 0$. On the other hand for large values of y^+ , $y^+ dU^+/dy^+ \rightarrow 1/\kappa$ for all values of a^+.

The data themselves are not very helpful, especially in the important region from $y^+ = 30$ to 100. The most that can be said from all the data taken together is that the value of a^+ is bounded by these values. A case could be made that -16 is the best choice if the Durst et al. data are used. On the other hand, the DNS channel data discussed below would tend to indicate that zero might better.

There are two reasons for why the data are problematical: First the only reliable data in this region are from experiments or simulations in which the Reynolds is so low that it is impossible to distinguish an overlap region which is reasonably independent of the inner and outer layers. George & Castillo (1997) dealt with this problem for boundary layers by using semi-empirical inner and outer profiles, then building a composite solution so all the effects could be considered. Obtaining such a composite solution certainly should be a focus of future work. Second, as noted above, this is probably the most difficult region in which to measure accurately. *The errors in measurement with virtually every probe are larger than the differences between the theories which are being compared*, especially for the higher Reynolds numbers. Clearly better experiments and/or simulations at higher Reynolds numbers are necessary.

Figure 14 compares velocity profiles in the overlap region of the present theoretical result with the classical theory and the recent contributions of Zagarola & Smits (1998*a*) and Barenblatt (1993). As noted above there is little difference between the present results and that of Zagarola and Smits except below $y^+ < 300 - 500$ for which the latter suggest a power law region exists. Although it can certainly be argued that a power law fits *their* low Reynolds number data in this region, there is reason to doubt both the data and the matching procedure used to obtain the power law result. As

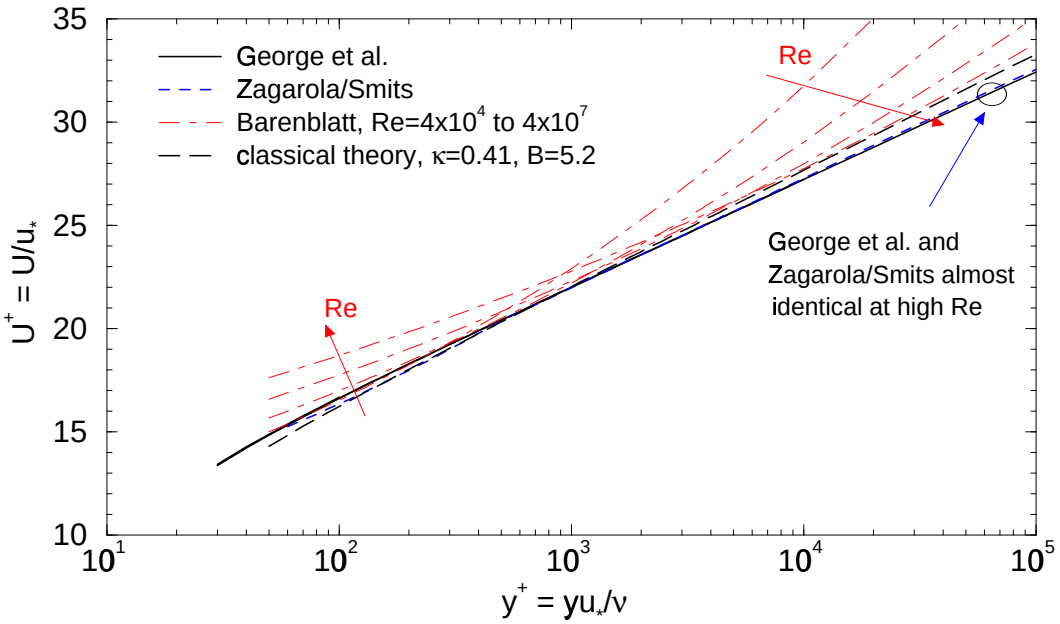

Figure 14: Comparison of Velocity Profiles from Various Theories

noted above, measurements with Pitot tubes close to (or even *on*) the wall might be expected to be in error by the small amounts of interest here. Also, the matching procedure they employ depends on the existence of an outer scale velocity different from that used to obtain the log region. The outer scale they suggest, $U_c - U_m$, is proportional to u_* in the limit in which the matching is carried out, hence only a log profile can result (cf. Appendix I of George & Castillo, 1997).

The family of curves due to Barenblatt can at most be argued to fit a region which moves to the right as the Reynolds number is increased. This is exactly what would be expected if the power law form being fitted were *not* the right choice for an overlap region, a conclusion consistent with the difficulties in this "theory" in accounting for the superpipe friction data as noted earlier.

4.11 Channel versus Pipe Flow

Although both fully-developed channel and pipe flows are homogeneous in the streamwise direction and both scale with u_*, there is no reason, in principle, to expect the outer flow or overlap profiles of channel flow to be the same as for pipe flow. The former is planar and homogeneous in planes parallel to the surface, while the latter is axially symmetric. The geometries are different, but the averaged equations are nearly the same, differing only in the turbulence and viscous transport terms.

The inner regions of both flows have long been known to be quite close (v. Monin & Yaglom, 1971). In fact, they must be exactly the same in the limit as the ratio of the extent of the viscous sublayer to the pipe radius (or channel half-width) goes to zero. Therefore it is reasonable *to hypothesize* that the inner regions of both flows be the same. Then the only differences between channel and pipe flows must appear in the outer flow. If this is true, then all of the parameters governing the *inner* region (including the overlap region in inner variables) must be the same for both pipe and channel flows. In particular, the parameters κ and B_i must be the same, *as well as their dependence on Reynolds number.* Hence even the empirical constants A and α must be identical. Only the parameter B_o and the scale constant D_s can be different. Moreover, since equation 4.31 must be satisfied, the channel flow value of B_o can at most differ by an additive constant from the pipe flow value, since any other difference would affect the Reynolds number-dependent relation between κ and $B_i - B_o$.

Figures 15 and 16 show the mean velocity profile data from the channel flow simulations of Kim, Moin & Moser (1987) and Kim (1989) at values of $R^+ = 180$ and 395, where R in this case is taken to mean the channel half-width. Also shown is the profile of Kim (1997) at $R^+ = 595$.[3] As before the profiles scaled in inner variables are presented in the upper figure, and the same data in outer variables in the lower. By the criteria established earlier, there should be no region which is described by

[3]The authors are very grateful to Professor Kim for making this data available to us. It has since been published as Moser, Kim & Mansour (1999)

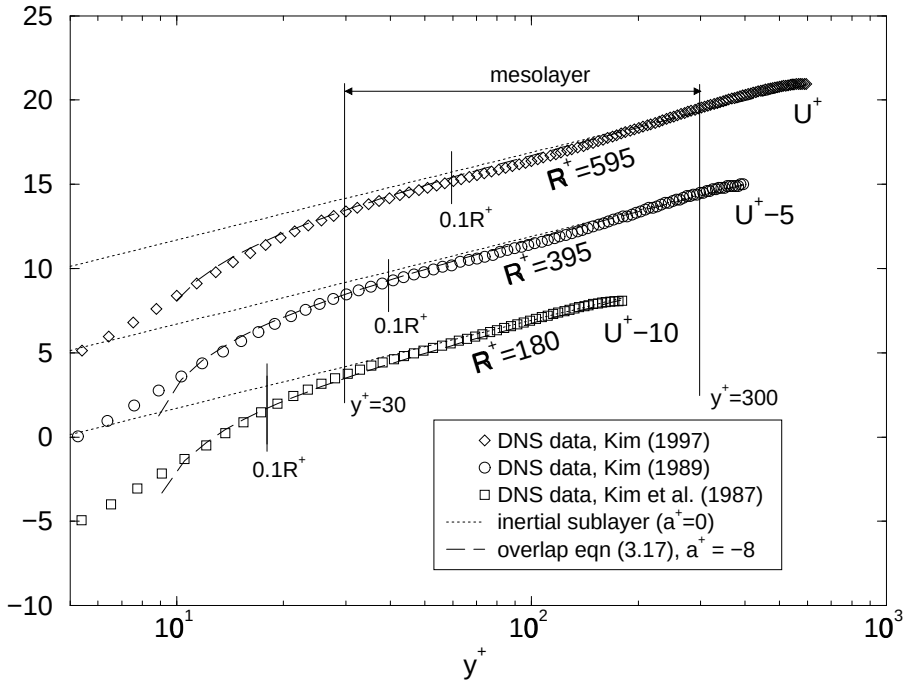

Figure 15: Channel flow DNS data of Kim et al. (1987), Kim (1989) and Kim (1997), inner variables.

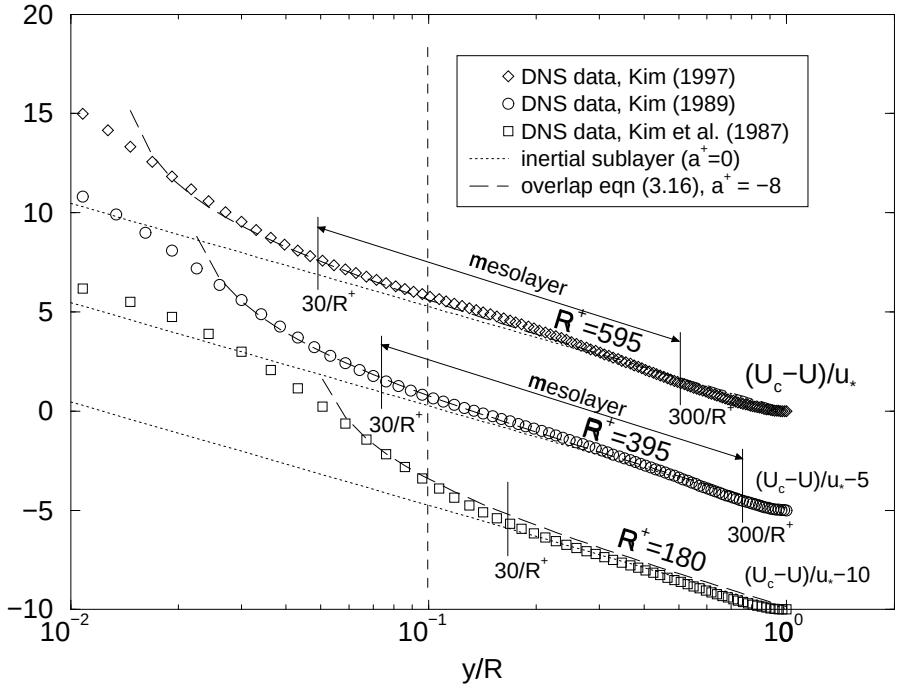

Figure 16: Channel flow DNS data of Kim et al. (1987), Kim (1989) and Kim (1997), outer variables.

a simple logarithmic profile alone without the mesolayer contribution, even at the highest Reynolds number. In fact, as is clear from the vertical lines on the plots, there should not even be a mesolayer region in the lowest Reynolds number profile (since $0.1R^+ < 30$).

Nonetheless, the theoretical overlap solution, equation 4.28, with exactly the parameter values used above for the superpipe data fits all three sets of data in inner variables nicely over the very limited range $30 < y^+ < 0.1R^+$. (In fact, the theoretical curve appears to work well to values of y^+ substantially closer to the wall, even though its use below $y^+ = 30$ cannot be justified theoretically, at least not by the arguments presented earlier.) It is not even necessary to adjust the scale factor D_s which was chosen as unity, just as for the pipe data. This agreement is all the more remarkable because all of the constants have been obtained from the superpipe experiment at much higher Reynolds number.

The theoretical outer velocity profile uses the pipe values for all constants except for $B_{o\infty}$ as noted above. Since $B_{o\infty}$ is quite small for the channel flow, even small uncertainties about its value have a relatively large effect on the outer profile. Therefore the approach taken here has been to first determine $B_{i\infty} - B_{o\infty}$ from the channel friction data, then use the value of $B_{i\infty}$ from the superpipe (since they should be the same as noted above) to determine $B_{o\infty}$ for the channel. Thus the channel flow velocity data scaled in outer variables provide a completely independent test of the theory. Unlike the superpipe data, however, there is much less DNS data available so a sophisticated optimization is not possible. However, there is only a single parameter which needs to be determined. Note that the experimental channel flow data has been avoided entirely because of uncertainties about the shear stress (v. Kim, Moin & Moser, 1987).

The best overall fit to the friction data, U_c/u_*, is achieved by choosing $B_{i\infty} - B_{o\infty} = 7.0$ with the relative errors being 0.18%, 0.57%, and 1.2% for the Reynolds numbers of 595, 395, and 180 respectively. It follows that $B_{o\infty} = -0.5$.

As shown in Figure 16, equation 4.27 provides a reasonable fit to the higher Reynolds number profiles over the same region as for the inner scaling. The fit is especially impressive since there has been no effort to optimize the fit to the velocity profile data. (Recall that all constants but one were determined by the superpipe and the remaining one was chosen from the friction data!) A near perfect fit (not shown) to the two higher Reynolds number profiles can be achieved, however, by using $B_{o\infty} = -0.65$. This will increase the relative error in the friction estimates to 0.089%, 1.3%, and 2.0%, respectively, if B_i is maintained at 6.5. On the other hand, if the value of $B_{i\infty}$ is reduced to 6.35, then both the better friction prediction and the better outer profile fits can be maintained simultaneously (since $B_{i\,\mathrm{inf}} - B_{o\infty} = 7.0$ is maintained), but with little relative change to the inner profile. Note that such a value for B_i would be closer to the value of 6.15 suggested by Zagarola & Smits (1998*a*). The authors have resisted the urge to re-analyze the pipe flow data until higher Reynolds number DNS data confirm the need to do so, but it is clear that the only other effect would be to change the pipe flow value of $B_{o\infty}$ from -1.95 to -2.1 which would hardly be noticeable in the plots.

All of the errors between the calculated and DNS values of U_c/u_* are within the uncertainty of the DNS data itself which is estimated at one to two percent. The reason for the larger discrepancy between the lower Reynolds number profiles is probably that the theory is simply being stretched to Reynolds numbers below where it can reasonably be expected to apply. It is clear that the value of $B_{o\infty}$ is substantially lower for the channel than for the pipe, but this was expected since, as noted above, the differences between the two flows should show up only in the outer flow.

The success of the theory developed herein in accounting for the channel flow data using the pipe flow constants should give considerable confidence in the entire theoretical approach. Moreover, it provides an independent confirmation of the values of the constants and the empirical function utilized for the Reynolds number dependence.

4.12 Summary and Conclusions

The Asymptotic Invariance Principle and the deductions from Near-Asymptotics, together with the recognition of the existence of a mesolayer, have provided an excellent description of the mean velocity and skin friction data from fully-developed channel and pipe flows over more than three and a half decades in Reynolds number. Specifically the theory describes the velocity profile in the region $30 < y^+ < 0.1R^+$ (or $30/R^+ < \overline{y} < 0.1$) for the superpipe experiment ($850 < R^+ < 530,000$) and the low Reynolds number DNS data as well ($R^+ = 180$, 395 and 595). Of the five parameters needed to describe the flow, four could be determined only from the friction data *alone*. Three of these ($\kappa_\infty = 0.447$, $A = -0.67$ and $\alpha = 0.44$) probably apply to any *stream-wise homogeneous* wall-bounded flow. The difference parameter which appears in the friction law, $B_{i\infty} - B_{o\infty}$, is different for pipes and channels (even though $B_{i\infty}$ is the same). From the superpipe experiment, $B_{i\infty} - B_{o\infty} = 8.45$, while from the DNS channel data it was estimated to be 7.0. Both pipe and channel data sets were consistent with constant values of $B_i \approx B_{i\infty} = 6.5$ and $a^+ = -8$. It follows that the outer parameter $B_{o\infty} = -1.95$ for the pipe flow, and -0.5 for the channel flow. A case can also be made that the limiting values of $B_{o\infty}$ should be -2.1 and -0.65 corresponding to $B_{i\infty} = 6.35$, but a final decision can probably not be made until higher Reynolds number DNS data becomes available.

Unlike the boundary layer where both Reynolds number effects and the mesolayer were of equal importance in understanding the data, for pipe and channel flows the Reynolds number dependence was found to be slight. In fact, only B_o shows significant variation over the range of the data, and then only about 5%. The variation of the von Karman parameter, κ, was only about 1%; and both B_i and a^+ were constant to within the accuracy of the data.

On the other hand, the mesolayer concept (and a^+ in particular) proved crucial in understanding where the theory applied and in understanding why previous attempts to verify the log law were less than totally satisfactory. In particular, the overlap mean

velocity profile was found to not be a simple logarithm in y, but instead a logarithm in $y + a$. The most important consequence of this is that attempts to establish $\ln y$ behavior using velocity profile data inside $y^+ = 300$ are doomed to failure and the results misleading unless the mesolayer (and a in particular) are explicitly accounted for. This, of course, explains much of the confusion in the literature about precisely what the log parameters were and where the theory applied — not only was the wrong profile being used, but it was being applied to the wrong region.

It should be noted that for their boundary layer data analysis, George *et al.* (1996) and George & Castillo (1997) used a procedure which was the reverse of that used here. There a series of careful attempts was first made to obtain directly the variation of the parameters from the velocity profiles, then the friction law was inferred and shown to be in agreement with direct measurements. The fact that the procedure followed here has been equally successful lends credibility to both analyses, especially in view of the importance of the subtle difference between the friction law proposed here and a simple log law with constant coefficients.

There are a number of interesting questions which remain. One of these is whether the mesolayer parameter a^+ is indeed constant as it appears it might be. This will require accurate measurements of the velocity profile near $y^+ = 30$ at considerably higher Reynolds numbers than has been possible to-date. Note that the problem is not with the overall flow Reynolds number (which in the superpipe was certainly adequate), but with the inability to resolve the flow near the wall at the higher Reynolds numbers due to probe size limitations. An obvious solution is to increase Reynolds number by increasing the pipe diameter — and not by decreasing viscosity or increasing the pressure drop — so less absolute resolution is required at a given Reynolds number.

Another question arises from the Reynolds number dependence itself which is nearly negligible for channel and pipe, but crucial for boundary layer flows. Is this a subtle consequence of the homogeneity of the former and inhomogeneity of the

latter, or is it simply a reflection of the differing inner and outer velocity scales for the boundary layer with the consequent Reynolds number dependence? Or are these the same thing? Or is the boundary layer's dependence a residual of the dependence on upstream conditions?

Then there is the fact that the parameter, α, which accounts for the Reynolds number dependence is nearly the same as for the boundary layer, and tantalizingly close to κ_∞ and the boundary layer value of $1/(\gamma_\infty C_{o\infty})$. The possible universality of these is particularly interesting, especially given the agreement between theory and experiment for both the homogeneous and inhomogeneous flows. A consequence of this is that the dissipation profiles for the pipe and the *infinite* Reynolds number boundary layer are nearly identical throughout the overlap region, even though they differ substantially for the finite Reynolds numbers of experiments. And, of course, this raises the question for the functions H (for the pipe and channel) and h (for the boundary layer) which contain the essential Reynolds number dependence of the flow: Can they (or alternatives) be derived directly from the underlying physics of the flow, perhaps through symmetry considerations of the turbulence dissipative scales or from the multi-point equations?

In conclusion, unlike the classical boundary layer theory which was shown by George & Castillo (1997) to be fundamentally flawed, the same approach has been able to show that the classical theory for pipe and channel flows is really pretty good. The present analysis has, from purely deductive reasoning using the Reynolds-averaged Navier-Stokes equations, been able to identify why the classical results were not totally successful, and was able to account for recent DNS, LDA and superpipe observations. Thus it would seem that the Navier-Stokes equations indeed apply to turbulence, hardly a novel idea to most, but reassuring nonetheless.

Chapter 5

Two-Dimensional Walljets

... crisis simultaneously loosens the stereotypes and provides incremental data necessary for a fundamental paradigm shift.

– Thomas Kuhn (1923-1996), The Structure of Scientific Revolutions

5.1 Introduction

The flow under consideration is the plane wall jet[1] with no externally imposed flow (Figure 1). It is simulated in the laboratory by a jet of fluid from a high aspect ratio slot at the wall exhausting into a large chamber. The development of a plane wall jet is shown in figure 2 using the data of Eriksson *et al.* (1998). In the *ideal* plane wall jet the flow is of infinite extent in the transverse (z) direction, and unconstrained in either the streamwise (x) or cross-stream (y) directions.

Turbulent wall jets have long been a favorite of experimenters and modelers, both because of their simple boundary conditions and their close resemblance to many flows of engineering importance. Such flows include applications in film cooling, ventilation, and separation control over wings, to cite but a few examples. An abundance of papers

[1]This chapter is largely based on the forthcoming paper by George *et al.* (2000). (George, W. K., Abrahamsson, H., Eriksson, J., Karlsson, R., Löfdahl, L. & Wosnik, M. (2000) A similarity theory for the turbulent plane wall jet without external stream. *J.Fluid Mechanics*, accepted for publication).

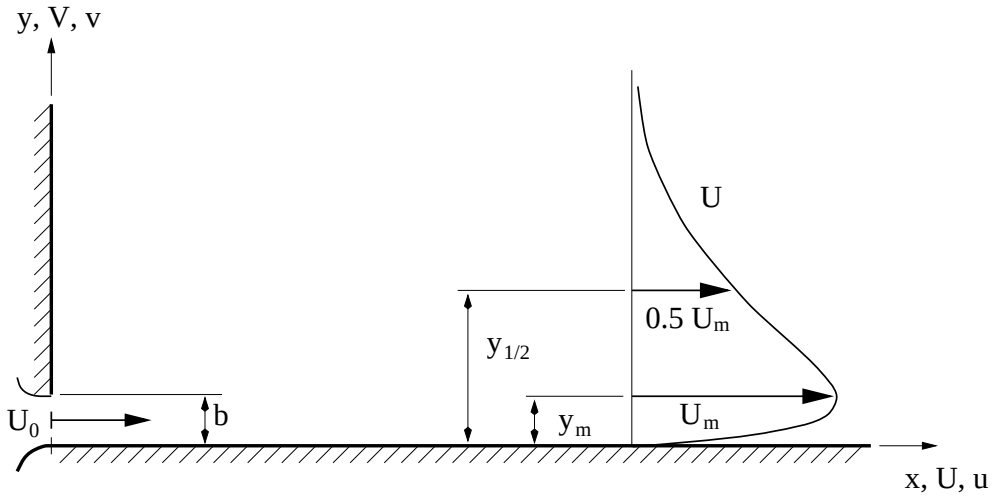

Figure 1: Schematic of the plane wall jet.

have been written about wall jets, and numerous review articles. Noteworthy with regard to this work are the ones by Launder & Rodi (1981, 1983) which provide excellent summaries of the state of knowledge to the early 1980's. Wygnanski, Katz & Horev (1992) (hereafter referred to as WKH) and Abrahamsson, Johansson & Löfdahl (1994) (hereafter referred to as AJL) both extend the reviews to the present, and provide more experimental data of their own.

Recently, Karlsson, Eriksson & Persson (1993*a*,*b*) (hereafter referred to as KEP) and Eriksson, Karlsson & Persson (1997, 1998, 1999) (hereafter referred to as EKP) have provided velocity measurements which resolve both the high turbulence intensity outer flow and the wall region down to $y^+ = 1$ using LDA (in a large water tank). The latter provide, for the first time, direct determination of the wall shear stress *without* reference to the theories being tested.

There has long been the suspicion that there should exist a similarity solution of some type for the plane wall jet; however, attempts to identify the solution have not been totally successful. Irwin (1973) tried to apply the single length and velocity scale methods presented in most text books, and had some success in scaling the outer mean velocity with the velocity maximum, U_m, and the velocity half-width, $y_{1/2}$. The scaling was less successful for the Reynolds stress, and no statement at all could be

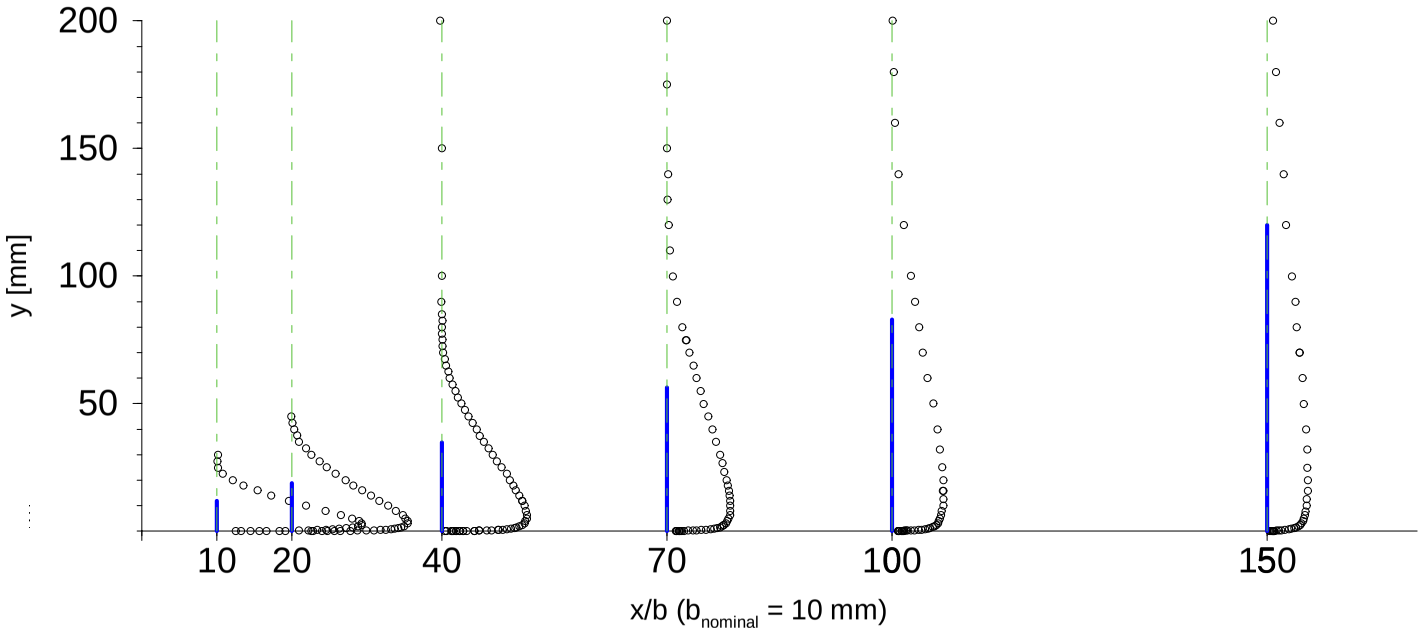
200
150
100
50
y [mm]
10
20
40
70
100
150
x/b (b_nominal = 10 mm)

made about how the outer flow was coupled to the inner flow or what the friction law was, other than empirically. WKH were particularly critical of the use of the familiar law of the wall and log profiles from boundary layer theory for the near wall region.

Here the question of whether the plane wall jet should admit to similarity solutions at all is reconsidered. A new theory based on the principles discussed in chapter 2 is proposed and will be tested against wall jet experiments, and compared step-by-step with the corresponding theory for the zero pressure gradient boundary layer outlined in chapter 3 and by George & Castillo (1997).

Experiments receiving particular attention will be those of KEP/EKP and AJL. The KEP/EKP experiments were carried out in a large water tank at Vattenfall Utveckling AB, Sweden, using two-component burst-mode LDA with statistically uniform seeding. The AJL experiment used hot-wires in an air facility at Chalmers University of Technology, Sweden. The KEP/EKP data are believed to be more accurate than the AJL data because of well-known hot-wires errors close to walls, and also in the high intensity outer turbulent flow where local instantaneous flow reversal can occur. However, both sets of data are useful in this context for several reasons: Both experiments were carefully coordinated and achieved very similar inlet conditions. The hot-wire data have less scatter than the LDA data, making it easier to sort out trends, especially in the second moment data. Also, as will be seen later in section 5.5, the hot-wire errors themselves scale in similarity variables, at least away from the very near wall, so even if the curves differ (usually slightly) from the LDA profiles, they can be used to establish whether the profiles collapse with a given scaling. In the experiments of AJL and KEP/EKP, the aspect ratio (facility width/slot height) was 200:1 and 151:1, respectively.

Usually, experimenters try to achieve low turbulence (potential flow), "top-hat" source (inlet) conditions (c.f. figure 3) by means of turbulence-reducing screens, honey-comb or other flow straighteners and a large contraction. Figure 3 of Eriksson, Karlsson & Persson (1998) shows that a flat inlet velocity profile was achieved over

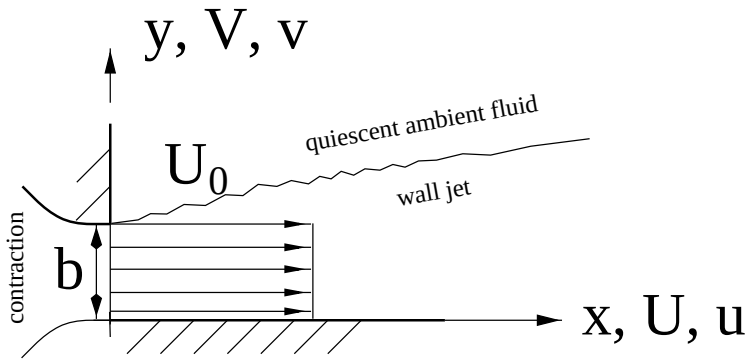

Figure 3: "Top-hat" source conditions for plane wall jet.

approximately 70% of the slot height with a turbulence intensity (u/U_0) of less than 1% . Figure 4 of Abrahamsson, Johansson & Löfdahl (1994) shows that a flat inlet velocity profile was achieved over approximately 90% of the slot height with a turbulence intensity (u/U_o) of about 0.4% . The transverse (spanwise) variation of the mean inlet velocity U_0 in the KEP/EKP and AJL experiments was less than 0.25% and 0.5%, respectively.

Also used in the experimental verification of the analysis were two data sets of WKH without external stream. While the experimental facilities of KEP/EKP and AJL were designed with an "infinite" vertical wall above the inlet slot, the WKH experiment only had a small "lip" above the slot. This does not change the (idealized) boundary conditions for the analysis, however, due to the finite size of the different experimental setups it will change the entrainment field somewhat. The two cases also have to be treated differently in computations. The WKH data was acquired using hot wire (HW) anemometry in air. For the cases considered, the aspect ratio (facility width/slot height) was 120:1.

5.2 Governing Equations and Boundary Conditions

The equation of motion and boundary conditions appropriate to a plane wall jet with constant properties at high Reynolds number are given by (Irwin, 1973)

$$U\frac{\partial U}{\partial x}+V\frac{\partial U}{\partial y}=\frac{\partial}{\partial y}\left[<-uv>+\nu\frac{\partial U}{\partial y}\right]-\left\{\frac{\partial}{\partial x}\left[<u^2>-<v^2>\right]\right\} \tag{5.1}$$

where $U \to 0$ as $y \to \infty$ and $U = 0$ at $y = 0$. This equation has been obtained by integrating the y-momentum equation across the boundary layer to eliminate the pressure. It is the same equation that governs both the plane free jet and the turbulent boundary layer at zero pressure gradient; only the boundary conditions are different.

Equation 5.1 can be integrated across the flow to yield the momentum integral equation given to second order by

$$\frac{d}{dx}\int_0^\infty [U^2+<u^2>-<v^2>]dy=-\frac{\tau_w}{\rho}\equiv -u_*^2 \tag{5.2}$$

where τ_w is the wall shear stress and u_* is the friction velocity. If the flow indeed evolves free from other influences, equation 5.2 can be integrated from the source to yield

$$\underbrace{\int_0^\infty [U^2+<u^2>-<v^2>]dy}_{\text{momentum contained in jet}}=\underbrace{\text{-}M_o}_{\text{m. added at source}}-\underbrace{\int_0^x \frac{\tau_w}{\rho}dx'}_{\text{m. lost to wall}} \tag{5.3}$$

where ρM_o is the rate at which momentum is added per unit length at the source. Thus unlike the plane free jet where the momentum integral is constant, for the plane wall jet there is a slow but continuous loss of momentum to the wall. And unlike the boundary layer, the supply of momentum driving the flow is finite.

The presence of the no-slip condition precludes the possibility of similarity solutions for the entire flow. The normal stresses in equation 5.1 are negligible to second order, and can be omitted for now with no loss of generality (in section 5.6 it will be

shown from the Reynolds stress equations that they also scale in similarity variables). Therefore solutions are sought which asymptotically (at infinite Reynolds number) satisfy the following outer and inner equations and boundary conditions:

- Outer Region

$$U\frac{\partial U}{\partial x} + V\frac{\partial U}{\partial y} = \frac{\partial}{\partial y}\left[< -uv >\right] \tag{5.4}$$

  where $U \to 0$ as $y \to \infty$.

- Inner (or near wall) region

$$0 = \frac{\partial}{\partial y}\left[< -uv > +\nu\frac{\partial U}{\partial y}\right] \tag{5.5}$$

  where $U = 0$ at $y = 0$.

The neglected terms in both inner and outer equations vanish identically only at infinite Reynolds number. However, there is nothing in the development of these equations which precludes their approximate validity from the time the flow undergoes transition.

Just as for the turbulent boundary layer, equation 5.5 for the inner region can be integrated to obtain

$$< -uv > +\nu\frac{\partial U}{\partial y} = \frac{\tau_w}{\rho} \equiv u_*^2 \tag{5.6}$$

where τ_w is the wall shear stress and u_* is the corresponding friction velocity defined from it. It is clear that in the limit of infinite Reynolds number (but only in this limit) the total stress is constant across the inner layer, and hence its name "Constant Stress Layer". The appearance of u_* in equation 5.6 does not imply that the wall shear stress is an independent parameter (like ν or M_o). It enters the problem only because it measures the forcing of the inner flow by the outer; or alternatively, it can be viewed as measuring the retarding effect of the inner flow on the outer. Thus u_* is a *dependent* parameter which must be determined by matching solutions of the inner and outer equations.

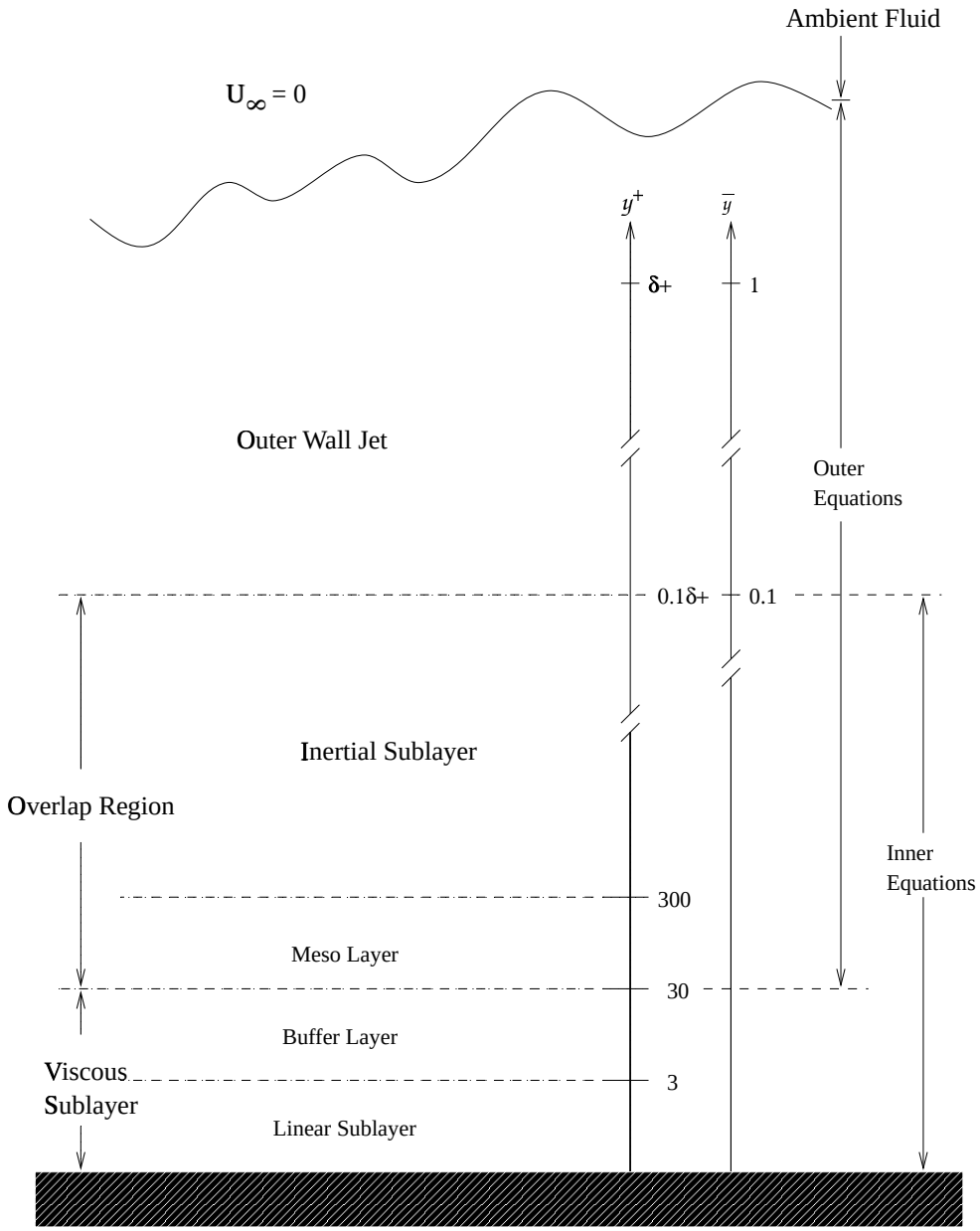

Figure 4: Schematic showing inner and outer regions together with subregions. (For plane wall jet: $\delta^+ \propto {y_{1/2}}^+ = y_{1/2}u_*/\nu$)

The inner and outer regions of the flow are illustrated schematically in Figure 4, which also shows the subregions which will be identified later. As noted above, the inner layer occurs only because of the necessity of including viscosity in the problem so that the no-slip condition can be met. The outer layer, on the other hand, is dominated by inertia and the effects of viscosity enter primarily through the matching to the inner layer. Thus the outer flow is effectively governed by inviscid equations, but with *viscous-dominated inner boundary conditions* set by the inner layer.

As outlined in section 2.3, the traditional approach to the equations for the plane wall jet has been to ignore the presence of the wall and to analyze the outer flow as a single length and velocity scale flow (Irwin, 1973; Townsend, 1976). This approach has been proven to be too restrictive even for a free turbulent shear flow like the plane jet (George (1989)), where the entire flow is treated as "outer" flow.

As explained in section 2.3, here the Asymptotic Invariance Principle will be applied to the inner and outer single-point equations governing the plane wall jet separately. Solutions will be sought which reduce to full similarity solutions of the equations in the limit of infinite Reynolds number, first for the inner equations and then for the outer. The form of these solutions will determine the appropriate scaling laws for finite as well as infinite Reynolds number, since alternative scaling laws could not be independent of Reynolds number in the limit. The AIP will first be applied to the mean momentum equations, then to the Reynolds stress component equations.

5.3 Full Similarity of the Inner Equations

In keeping with the AIP set forth above, Similarity solutions to the infinite Reynolds number inner equations and boundary conditions are sought which are of the form

$$U = U_{si}(x) f_{i\infty}(y^+) \tag{5.7}$$

$$< -uv > = R_{si}(x) r_{i\infty}(y^+) \tag{5.8}$$

where $y^+ \equiv y/\eta$ and the length scale $\eta = \eta(x)$ remains to be determined. The subscript "$i\infty$" is used to distinguish these solutions to the limiting inner equation from the profiles for the entire flow (scaled with the same variables) that are introduced below.

Substitution into equation 5.6 and clearing terms yields

$$\left[\frac{u_*^2}{U_{si}^2}\right] = \left[\frac{R_{si}}{U_{si}^2}\right] r_{i\infty} + \left[\frac{\nu}{\eta U_{si}}\right] f_{i\infty}' \tag{5.9}$$

All of the x-dependence is in the bracketed terms, therefore similarity is possible only if all of these have the same x-dependence; i.e.,

$$\left[\frac{u_*^2}{U_{si}^2}\right] \sim \left[\frac{R_{si}}{U_{si}^2}\right] \sim \left[\frac{\nu}{\eta U_{si}}\right] \tag{5.10}$$

Here the symbol "$\sim$" is *defined* to mean "*has the same x-dependence as*".

Since three parameters are to be determined, and equation 5.10 gives only two independent conditions, one can be chosen arbitrarily. A convenient choice for η is

$$\eta = \nu/U_{si} \tag{5.11}$$

Then the inner velocity scale must be the friction velocity so that

$$U_{si} \equiv u_* \tag{5.12}$$

It follows that

$$\eta = \nu/u_* \tag{5.13}$$

$$R_{si} = u_*^2 \tag{5.14}$$

Substitution into equation 5.9 yields the limiting inner momentum equation as

$$1 = r_{i\infty} + f_{i\infty}' \quad . \tag{5.15}$$

The similarity variables derived above are the usual choices for the inner layer of a turbulent boundary layer, and have previously been used as scaling parameters for the wall jet by most investigators. For finite Reynolds number, however, the solutions for mean velocity and Reynolds stress will retain a Reynolds number dependence, no matter how they are scaled, since the Reynolds averaged Navier-Stokes equations themselves do. It will be convenient later to represent this dependence symbolically by

$$u^+ \equiv \frac{U}{u_*} = f_i(y^+, \delta^+) \tag{5.16}$$

$$\frac{< -uv >}{u_*^2} = r_i(y^+, \delta^+) \tag{5.17}$$

where $\delta^+ = \delta/\eta = u_*\delta/\nu$ is a Reynolds number to be defined later. Note that the evolution of the profiles with x which is *not* removed by the scaling parameters is accounted for by the dependence on δ^+ since $\delta = \delta(x)$ only. In the limit of infinite Reynolds number equations 5.16 and 5.17 reduce to similarity solutions of the inner equations. For finite Reynolds number they are simply a family of scaled profiles for the entire flow characterized by the parameter δ^+ (or $y^+_{1/2}$), like those shown in the plots below.

Figure 5 shows the mean velocity profile from the KEP data scaled in inner variables. These data collapse reasonably for y^+ less than 100 to 200 approximately, depending on distance downstream (or the Reynolds number). KEP and EKP have noted that the linear region next to wall only extends to $y^+ \approx 3$. Outside of this, the Reynolds shear stress begins to be important in the momentum balance until by $y^+ \approx 30$ it dominates the viscous stress completely. This region where the Reynolds shear stress and viscous stress are both important will be referred to as the *buffer*

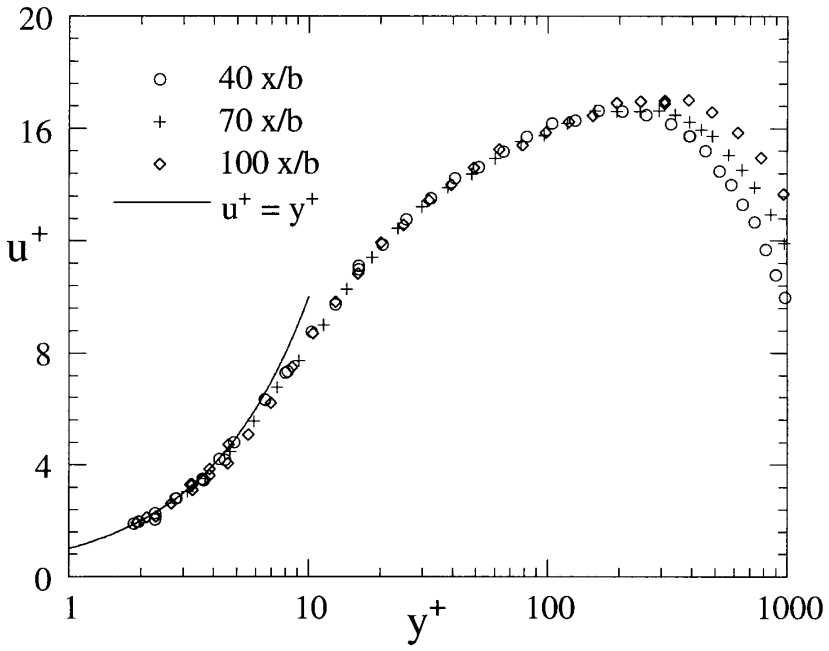

Figure 5: The mean velocity profile in inner scaling: KEP data at 40, 70 and 100 x/b.

region. Figure 4 shows both the linear and buffer layers to comprise the viscous sublayer, so named since viscous stresses play a significant role in the single-point equations. Most importantly, convection effects by the mean velocity are negligible as long as $y_m^+ = y_m u_* / \nu \gg 30$.

Note that application of the AIP to the Reynolds stress equations near the wall shows that u_* and ν are the appropriate quantities for scaling all the single point quantities. From Figure 6 it is obvious that the inner scaling fails completely for $< u^2 >$ outside of $y^+ \approx 7$. Interestingly, this is the outer extent to which the fourth order expansion of u^+ at the wall (i.e. $u^+ = y^+ + c_4 y^{+4}$) can adequately describe the mean velocity , c.f. EKP and section 5.13. Both $< -uv >$ and $< v^2 >$ show similar tendencies as shown in Figure 7, but the curves do not separate as dramatically, perhaps because of the kinematic condition on v at the wall. These results are consistent with the conclusions of GC and Gad-el-Hak & Bandyopadhyay (1994) for the zero pressure gradient turbulent boundary layer.

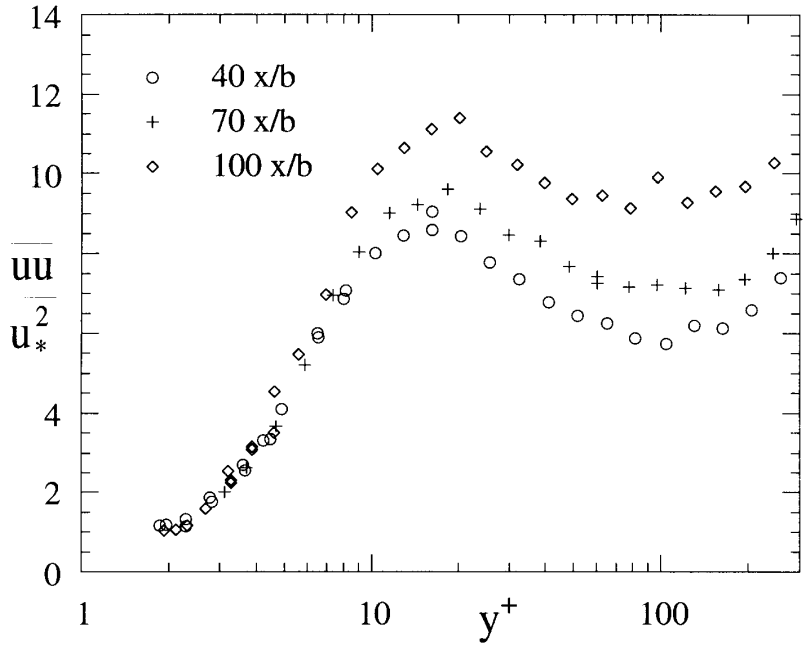

Figure 6: The streamwise normal Reynolds stress in inner scaling: KEP data at 40, 70 and 100 x/b.

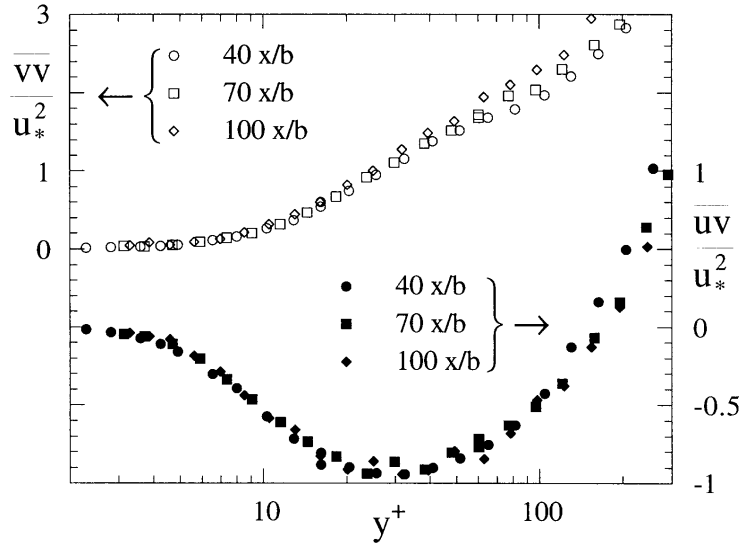

Figure 7: The cross-stream normal and shear Reynolds stress in inner scaling: KEP data at 40, 70 and 100 x/b.

5.4 Full Similarity of the Outer Equations

In accordance with the Asymptotic Invariance Principle, solutions to the outer momentum equation and boundary conditions are sought which reduce to similarity solutions of these equations in the limit of infinite Reynolds number.

$$U = U_{so} f_{o\infty}(\overline{y}) \tag{5.18}$$

$$-< uv > = R_{so} r_{o\infty}(\overline{y}) \tag{5.19}$$

where $\overline{y} = y/\delta$ and U_{so}, R_{so}, and δ are functions of x only. It is important to note that, unlike in the previous analysis of Irwin (1973), *no scaling laws are assumed at the outset*, but will be derived from the conditions for similarity of the governing equations (In particular, it is not assumed that $R_{so} = U_{so}^2$). As before, the subscript "$o\infty$" is used to distinguish these infinite Reynolds number solutions from the Reynolds number dependent profiles scaled in outer variables which will be used later. The velocity could have been written as a deficit using some reference velocity in the outer layer to avoid the necessity of accounting for its variation across the inner layer, however the results can be shown to be the same.

Substitution into equation 5.4 and clearing terms yields

$$\left[\frac{\delta}{U_{so}}\frac{dU_{so}}{dx}\right] f_{o\infty}^2 - \left(\left[\frac{d\delta}{dx}\right] + \left[\frac{\delta}{U_{so}}\frac{dU_{so}}{dx}\right]\right) f_{o\infty}{}' \int_0^{\overline{y}} f_{o\infty}(\xi) d\xi = \left[\frac{R_{so}}{U_{so}^2}\right] r_{o\infty}{}' \tag{5.20}$$

The V-component of velocity has been eliminated by integrating the continuity equation from the wall, thus introducing a contribution from the inner layer which vanishes identically at infinite Reynolds number. The only difference between this equation and the one utilized by Irwin (1973) is the factor of $[R_{so}/U_{so}^2]$ on the right-hand side, but it will be seen to be very important below.

For the type of equilibrium similarity solution suggested by George (1989, 1995) to be possible, the bracketed terms must all have the same $x-$dependence. This is

possible only if

$$\frac{1}{U_{so}}\frac{dU_{so}}{dx} \sim \frac{1}{\delta}\frac{d\delta}{dx} \tag{5.21}$$

and

$$R_{so} \sim U_{so}^2 \frac{d\delta}{dx} \tag{5.22}$$

Note that Irwin (1973) *assumed* at the outset that $R_{so} = U_m^2$; this assumption is not justified. The Reynolds stress scale is not U_{so}^2, but an entirely different scale depending also on the growth rate, $d\delta/dx$. Thus the x-dependence of R_{so} is the same as U_{so}^2 only if the wall jet can be shown to grow linearly. It will be shown below that linear growth is not possible. It can also be shown (see section 5.8) that the inner and outer Reynolds shear stress can match (to first order) only if

$$R_{so} \sim U_{so}^2 \frac{d\delta}{dx} \sim u_*^2 \tag{5.23}$$

The need for such a matching is intuitively obvious, since the only non-zero boundary condition on the Reynolds stress in the outer flow is that imposed by the inner. Thus the outer flow is governed by two velocity scales The similarity constraint of Equation 5.21 is satisfied if U_{so} is a power of δ; i.e.,

$$U_{so} \sim \delta^n \tag{5.24}$$

where the coefficient and the exponent n remain to be determined, but can at most be a function of the source conditions. This is a specific prediction which is easy to test from experiment, but it does not seem to have been noticed previously. Note that equation 5.21 also implies that *if* the velocity scale varies as a power of distance, x, then δ must also vary as a power of x. *But, contrary to popular assumption,* there is no reason to believe *a priori* that either is true, nor will they be found to be except possibly asymptotically.

It is important to note that there is nothing in the equations to suggest that the

bracketed terms of equation 5.20 must be the same for all flows. In other words, while all of the bracketed terms must have the same x-dependence and their ratios must be constant, in principle at least, the constants may vary from flow to flow. Thus, contrary to conventional wisdom, the equations themselves cannot rule out the possibility of an asymptotic dependence on the source (or initial) conditions.

An interesting feature of the mean velocity and Reynolds stress profiles can be seen by rewriting equation 5.20 using the similarity conditions as

$$n f_{o\infty}^2 - (1+n) f_{o\infty}{}' \int_0^{\overline{y}} f_{o\infty}(\xi) d\xi = \left[\frac{R_{so}}{U_{so}^2 d\delta/dx} \right] r_{o\infty}{}' \tag{5.25}$$

The bracketed term on the righthand side can be incorporated as a simple scale factor into the function $r_{o\infty}$ by defining

$$\tilde{r}_{o\infty} \equiv \left[\frac{R_{so}}{U_{so}^2 d\delta/dx} \right] r_{o\infty} \tag{5.26}$$

Equation 5.25 then reduces further to

$$n f_{o\infty}^2 - (1+n) f_{o\infty}{}' \int_0^{\overline{y}} f_{o\infty}(\xi) d\xi = \tilde{r}'_{o\infty} \tag{5.27}$$

The implications of this are striking:

(i) If the value of n is universal, then *properly scaled* mean velocity and Reynolds stress profiles from different wall jets must be exactly the same *even if the x-dependence of $d\delta/dx$ is itself dependent on the initial conditions.* Conversely, collapse of the profiles from different experiments means that n *is* universal, even if the other ratios depend on initial conditions.

(ii) In view of (i), the collapse of the *properly scaled* mean velocity and Reynolds shear stress profiles from different experiments can *not* be taken to imply that the wall jet is asymptotically independent of its initial (or upstream) conditions. Such independence must be established from the other parameters, if it exists

at all.

It should be noted that similar statements are not true, in general, for the other second order and higher moment profiles for which a simple scale change cannot make the profiles independent of source conditions. Thus the outer wall jet shares this characteristic with free shear flows (cf. George, 1989). The data considered below will show that the exponent n appears to be universal; yet the asymptotic wall jet may still be dependent on its source conditions.

Since the only boundary conditions on U are homogeneous, the scale velocity U_{so} can be chosen as the maximum velocity, U_m with no loss of generality. Similarly, the outer length scale δ can be identified with any convenient location in the outer flow; hence it can hereafter be assumed with no loss of generality to be the familiar half-width denoted as $y_{1/2}$.[2] The extension of the AIP to the Reynolds stress equations in Section 5.6 shows that some of the turbulence moments scale with U_m, some with u_*, and some with both. The normal stresses, $< u^2 >$, $< v^2 >$, and $< w^2 >$ scale as U_m^2; hence they are quite different from the Reynolds shear stress.

According to the AIP, the similarity scaling derived above is appropriate for finite Reynolds numbers as well, since only it can be invariant in the limit of infinite Reynolds number. Thus the velocity and Reynolds stress profiles in outer variables are

$$\frac{U}{U_m} = f_o(\overline{y}, y^+_{1/2}) \tag{5.28}$$

and

$$\frac{< -uv >}{u_*^2} = r_o(\overline{y}, y^+_{1/2}) \tag{5.29}$$

where $\delta^+ \equiv y^+_{1/2}$ is the *local* Reynolds number. The profiles scaled in this manner, unlike their infinite Reynolds number limits, are valid for all y until the limit is taken.

[2]Alternatively the outer length scale could have been identified with the position of the velocity maximum, say y_m, since it also occurs in the outer flow, at least if the Reynolds number is high enough. This choice has the disadvantage that it is difficult to determine the precise location of the maximum experimentally because of the slow variation of the velocity around it, quite unlike $y_{1/2}$ where the velocity is changing rapidly.

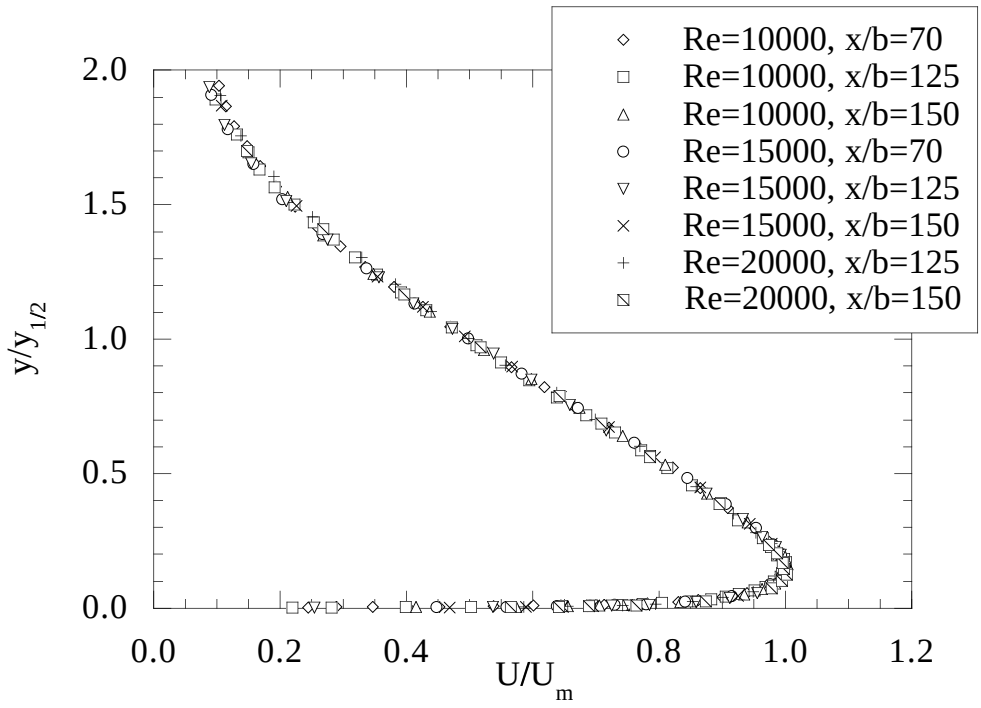

Figure 8: The mean velocity profile in outer scaling: AJL data at different inlet Reynolds numbers and streamwise positions

However, *the scaled data can never collapse perfectly except in the limit,* nor can they be made to collapse with any other Reynolds number independent scaling. Obviously f_o and r_o *converge* to $f_{o\infty}$ and $r_{o\infty}$, respectively, in the limit, and lose in the process their ability to describe the inner flow.

5.5 Experimental Verification of the Outer Flow Analysis

Figure 8 shows the mean velocity data of AJL normalized by U_m and $y_{1/2}$ from $x/b = 70$ to 150 for three different source Reynolds numbers.

Figure 9 shows mean velocity profiles from a number of investigators. Except for

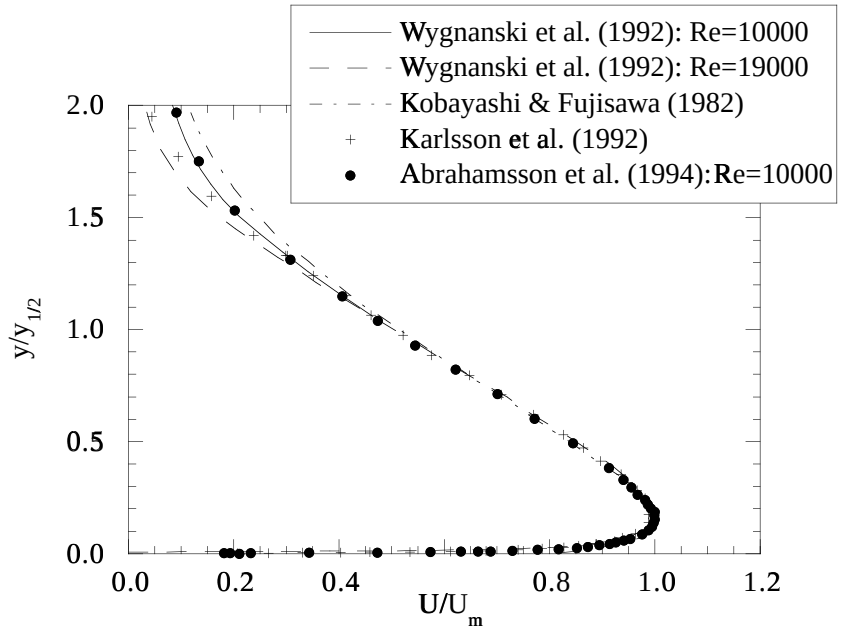

Figure 9: Comparison of mean velocity profiles of various investigators in outer variables.

the extreme outer edge of the flow (beyond $y/y_{1/2} > 1.3$ or so) where external flows, counter-flows, and measurement errors dominate, all the normalized mean velocity profiles are virtually identical. This collapse has been observed by many before (e.g., AJL or the review by Launder & Rodi (1981)). The virtually identical profiles do imply that the exponent n in the similarity relation of equation 5.24 is universal. This will be corroborated below using $y_{1/2}$ and U_m. However, as noted above, they do *not* imply that the flow is independent of source conditions.

Figures 10, 11 and 12 show the Reynolds stresses of AJL normalized both by U_m^2, $y_{1/2}$ and by u_*^2, $y_{1/2}$. While the normal stresses collapse well in the outer flow with U_m^2, the Reynolds shear stress does not. On the other hand, the Reynolds shear stress collapses well with u_*^2, while the normal stresses do not. Thus both the mean velocity and second moments are in striking agreement with the theory presented here. The differences are not as obvious for the LDA data of KEP for which there is not as much variation of u_*/U_m, perhaps due to the presence of the

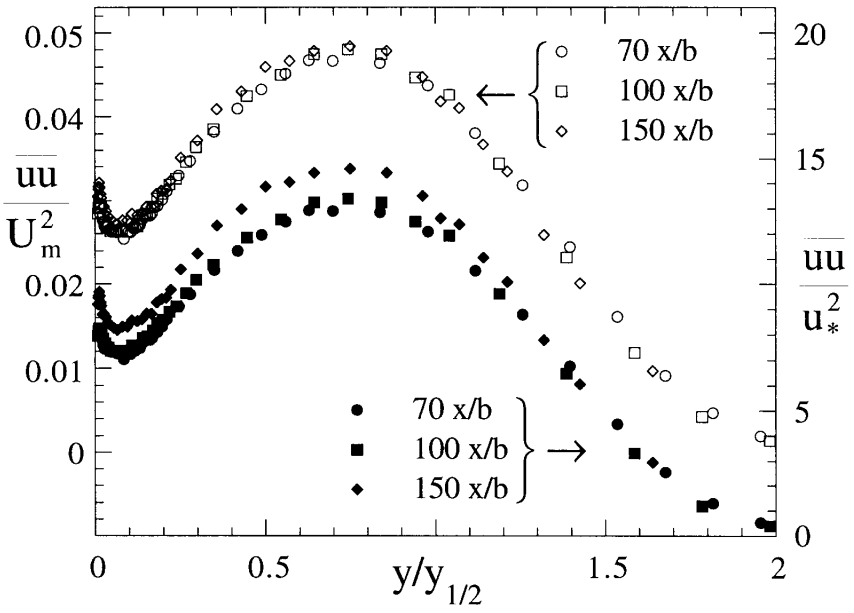

Figure 10: The streamwise normal Reynolds stress in outer scaling: AJL data at 70, 100 and 150 x/b.

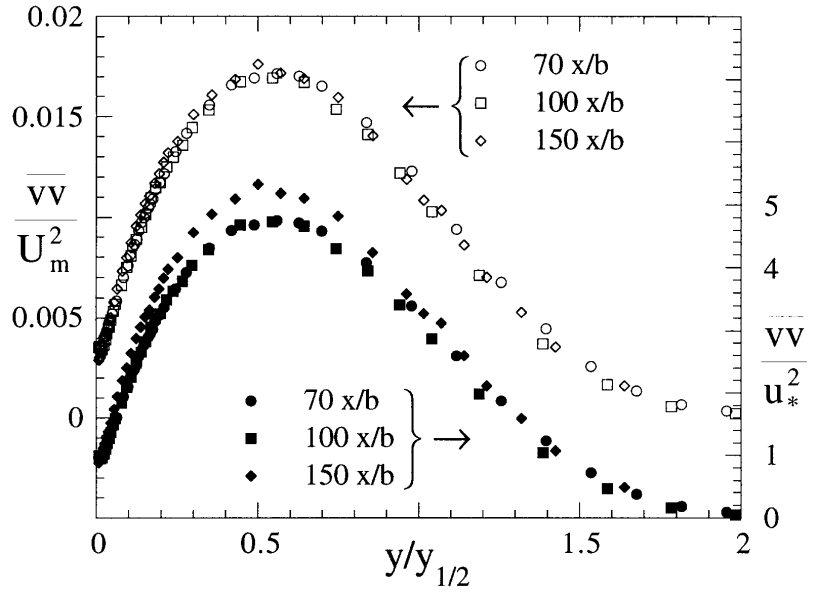

Figure 11: The cross-stream normal Reynolds stress in outer scaling: AJL data at 70, 100 and 150 x/b.

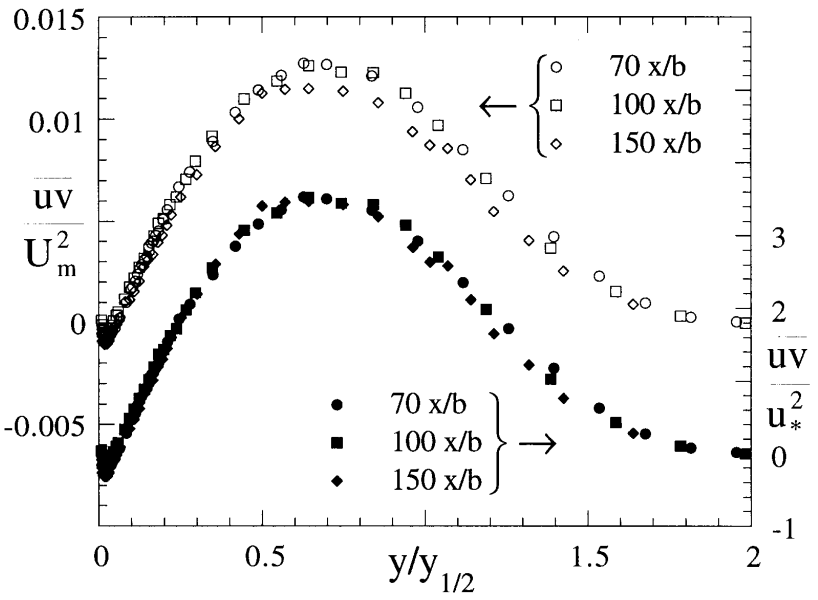

Figure 12: The Reynolds shear stress in outer scaling: AJL data at 70, 100 and 150 x/b.

recirculation at the largest x/b values as noted by the authors. Both AJL and EKP show comparisons with several earlier experiments for all the second-order moments, and there are significant differences, both in profile shape and magnitude. While the latter may indeed represent a sensitivity to upstream conditions, the profile variations suggest that the differences may also be due to the well-known measurement problems with hot-wires in such high intensity flows and the manner in which the wires were employed. A definitive statement on this must await more extensive measurements with the more reliable LDA techniques (as in KEP).

Figure 13 shows a log-log plot of U_m/U_o versus $y_{1/2}/b$ for the data of KEP, AJL and WKH where U_o is the exit velocity at $x = 0$ and b is the width of the source.

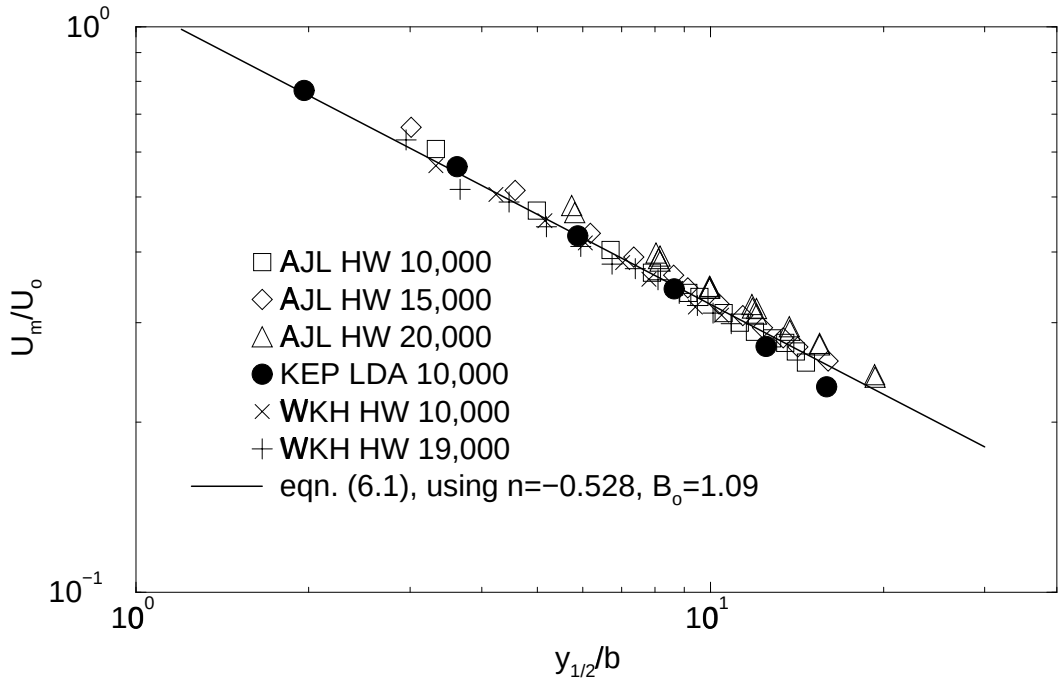

Figure 13: Log-log plot of U_{max}/U_o and $y_{1/2}/b$, KEP, AJL and WKH data.

There is no theoretical justification for this normalization in spite of its widespread use; it does, however, collapse the data to within about 10%. All the data are in excellent agreement with the similarity requirement of a power law relation between U_m and $y_{1/2}$; i.e.,

$$\frac{U_m}{U_o} = B_0 \left[\frac{y_{1/2}}{b}\right]^n \tag{5.30}$$

The line shown has slope $n = -0.528$ and $B_0 = 1.09$, where the former was obtained from the momentum balance of the KEP data for $40 \leq x/b \leq 150$ (discussed in detail in Section 5.15). The best fit slope, n, is nearly the same for all the curves, consistent with the apparently universal velocity profile noted above. The best fit values of B_0 (assuming $n = -0.528$) are 1.10, 1.12, and 1.18 for the AJL data at source Reynolds numbers of $10,000$, $15,000$, and $20,000$ respectively. Note EKP have argued that their data should not all be treated equally because for small values of x/b the flow is still developing, while for $x/b > 100$ the flow is adversely influenced by the return flow in their facility. This will be discussed in Sections 5.15 and 5.16, and accounts

for the slight deviation of the data from the momentum conservation value for large values of x/b.

Some, but not all, of the dependence on source conditions can be eliminated by following Narasimha, Yegna Narayan & Parthasarathy (1973) (see also WKH) who suggested normalization by M_o and ν where M_o is the rate at which momentum per unit mass per unit length is added at the source, since these would be the only parameters available for a line source of momentum. The same reasoning applied here (but *without* the additional *assumption* of a power law in x) yields a nondimensionalized similarity condition as

$$\frac{\nu U_m}{M_o} = B_1 {Y_{1/2}}^n \tag{5.31}$$

where $Y_{1/2}$ is defined as $Y_{1/2} \equiv y_{1/2} M_o/\nu^2$ Note that this normalization does not affect the exponent of the power law relationship between U_m and $y_{1/2}$, since it is already dimensionless. Moreover, unlike power laws *in* x where the origin is arbitrarily chosen, there can be no virtual origin for $y_{1/2}$ since it evolves together with U_m.

It is important to recognize that while the scaling given by equation 5.31 is certainly the appropriate scaling for a line source of momentum, it should not be expected to collapse the data if finite source effects (like the exit profile or exit Reynolds number) are important. As noted earlier, *there is nothing in the equations themselves to suggest that these finite source conditions are NOT important*, and indeed the data appear to reflect that.

Figure 14 shows a log-log plot of the momentum-viscosity normalized KEP, AJL and WKH data. The line represents equation 5.31 using $B_1 = 1.85$ and $n = -0.528$, both determined from the momentum balance of the KEP data alone, again using only data for $40 \leq x/b \leq 150$. The best fit values for B_1 (assuming $n = -0.528$) are 1.87, 1.87 and 2.06 for the AJL $10,000$, $15,000$, and $20,000$ data respectively. The corresponding values are 1.79 and 1.84 for the WKH data at source Reynolds

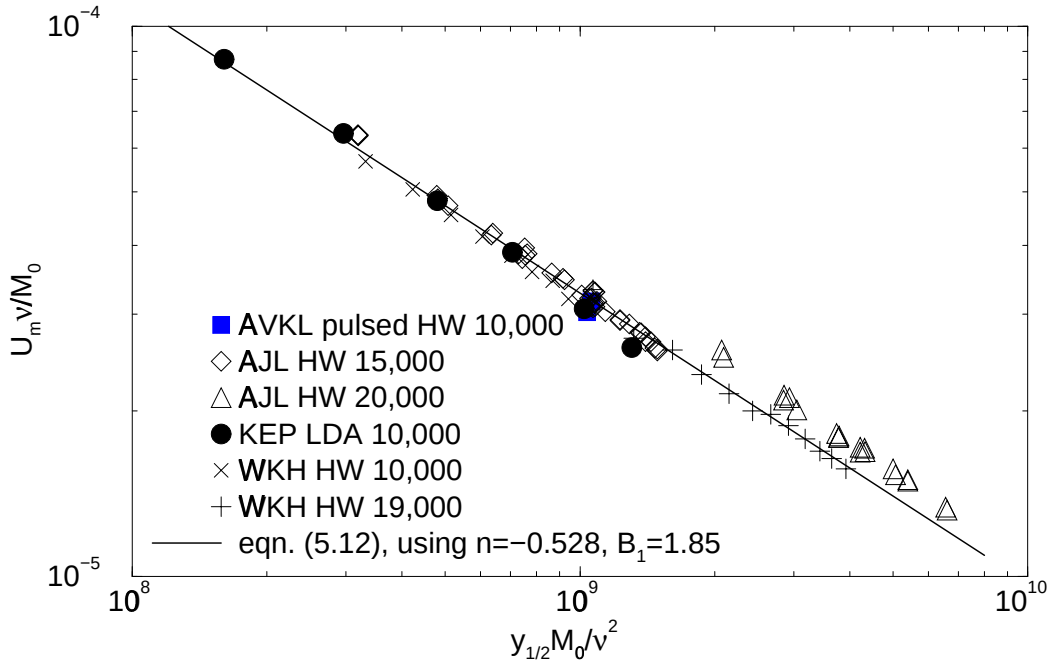

Figure 14: Log-log plot of $\nu U_m/M_o$ versus $y_{1/2}M_o/\nu^2$, KEP, AJL and WKH data.

numbers of $10,000$ and $19,000$[3]. Note that the values inferred from the WKH data would be a percent or two higher if the momentum had been based on the actual exit profile instead of the top-hat inferred values. Also all of the hot-wire values of B_1 may already be about eight percent too high because of the hot-wire errors in the determination of U_m and $y_{1/2}$ (about 2% and 12% respectively using the EKP results). Therefore it is impossible to tell whether these curves should indeed collapse, or whether each contains a unique dependence on its source. If the latter, the effect is not large, but (as will be seen later) still causes a noticeable variation in the rate at which the wall jet boundary layer grows.

As expected, the coefficient B_1 in the momentum/viscosity scaling shows a somewhat weaker source dependence than B_0 using the source parameters b and U_o. Whether or not all of the sets of data are unique, it is obvious that *they all individually satisfy the proper similarity power law relation between* U_m *and* $y_{1/2}$. Moreover,

[3]These were the only WKH runs for which there was no imposed external stream.

even though the coefficient B_1 may show a slight dependence on the particular source and experiment, the value of n appears to be nearly (if not exactly) the same for all experiments.

In fact, B_1 should at least be exactly the same for a family of similar sources (i.e., same exit profile, Reynolds number, etc.) Combining equations 5.30 and eq:wj-Umyhalf2, B_0 and B_1 are seen to be related by (for any source profile)

$$B_0 = B_1 \left(\frac{U_o b}{\nu}\right)^n \left(\frac{M_o}{\nu U_o}\right)^{n=1} \tag{5.32}$$

For a top-hat source B_0 and B_1 are related by

$$B_0 = B_1 \left(\frac{U_o b}{\nu}\right)^{(1+2n)} = B_1 R_o^{(1+2n)} \tag{5.33}$$

since $M_o = U_o^2 b$ (c.f. figure 3). All the experiments considered had approximately top-hat sources, which may explain why there is not a greater difference between figure 13 and 14

All of the estimates for n from the individual data sets are within a few percent of each other. It will be argued later using the similarity form of the momentum integral, equation 5.97, that $n = -1/2$ must represent a limiting value, so for finite Reynolds numbers at least, $-n > 1/2$. Since n is close to $-1/2$ and enters the momentum balance as $(1+2n)$, the momentum balance is very sensitive to very small errors in n; hence the value of determining n from the momentum balance. The actual estimates for the individual downstream locations of the KEP data vary from $n = -0.526$ to $n = -0.536$, depending on how $dy_{1/2}/dx$ is estimated. The latter value is exactly the value obtained if the $M_o x/\nu^2$-dependence of the power law curve fits of WKH for $\nu U_m/M_o$ and $M_o y_{1/2}/\nu^2$ is eliminated to obtain equation 5.31, although the value of B_1 so obtained is lower by about 25%. Whether this variation represents a source Reynolds number dependence, or is just an artifact of the method of analysis will require further investigation. Regardless of its precise value, the concurrent collapse

of the normalized velocity profiles from *all* experiments suggests that the value of n may be universal, as noted above.

In summary, the collapse of the profiles as suggested by the theory (especially the Reynolds shear stress), the success of the similarity relation between $U_m \sim y_{1/2}^n$, and even the differences among different experiments provide strong experimental support for the proposed outer scaling. The latter point is especially important in view of the increasing number of flows which appear to retain asymptotically a dependence on initial conditions. Although George & Castillo (1997) suggested the possibility of such a dependence for the outer part of the zero-pressure gradient boundary layer, the data were insufficient to make a judgement (although there were clues). There are, however, numerous examples of homogeneous and free shear flows which do appear to behave in this manner; e.g., isotropic decay George (1992), homogeneous shear flow George & Gibson (1992), plane wake Wygnanski, Champagne & Marasli (1986), time-dependent wake Moser, Rogers & Ewing (1996). But the wall jet appears to be the first wall-bounded flow for which it can be substantiated that initial conditions may matter, at least to the outer flow. And if the initial conditions matter, as will be seen in section 5.15, they can have an effect on the asymptotic spreading rate.

5.6 Scaling of the Other Turbulence Quantities

For the *inner layer*, there is only one velocity scale, u_*, which enters the *single point* equations; therefore all *single point* statistical quantities must scale with it. This is, of course, the conventional wisdom, but with an important difference: The inner layer *ends about* $y^+ \approx 7$, not far from where the velocity profile ceases to be linear ($y^+ \approx 3$)! This is contrary to the usual practice to include the overlap layer as part of the wall layer. As shown before, the dependent variables in the overlap layer are expected to be functions of both inner and outer scales, and thus Reynolds number dependent. (Note that different considerations must be applied to the multi-point equations since

conditions at a point can depend on those at another, and in particular those at a distance.)

From the preceding analysis, it is apparent that the *outer wall jet* at finite Reynolds numbers is governed by not one, but two velocity scales. In particular, the mean velocity and its gradients scale with U_m, while the Reynolds shear stress scales with u_*^2. Therefore it is not immediately obvious how the remaining turbulence quantities should scale. In particular, do they scale with U_m or u_*, or both? If the latter, then quantities scaled in the traditional way with only one of them will exhibit a Reynolds number dependence and will not collapse, even in the limit of infinite Reynolds number. It has already been noted in the plots of the previous section that this is indeed the case.

In view of the plots of the preceding section, it is reasonable to inquire under what conditions the equations for other turbulence quantities admit to fully similar solutions. For the outer part of the wall jet at high Reynolds number, the equation for $< u^2 >$ can be written (Tennekes & Lumley, 1972) as

$$U\frac{\partial < u^2 >}{\partial x} + V\frac{\partial < u^2 >}{\partial y} = 2 < \frac{p}{\rho}\frac{\partial u}{\partial x} > + \frac{\partial}{\partial y}\left\{ - < u^2 v > \right\} - 2 < uv > \frac{\partial U}{\partial y} - 2\epsilon_u \tag{5.34}$$

where ϵ_u is the energy dissipation rate for $< u^2 >$ and the viscous transport term has been neglected.

An order of magnitude analysis reveals the mean convection and turbulence transport terms to be of second order in the turbulence intensity u'/U, so to first order the equation reduces to simply a balance between production, dissipation and pressure strain rate. It could then be argued that these second order terms should be neglected in the subsequent analysis, cf. Townsend (1976). It is precisely these second order terms, however, that distinguish one boundary layer type flow from another, or from homogeneous flows (like channels and pipes) for that matter. Therefore, for a theory which purports to represent growing shear layers like the wall jet, they must

be retained.

Similarity representations are sought for the new moments of the form

$$\frac{1}{2} < u^2 > = K_u(x) k_u(\overline{y}) \tag{5.35}$$

$$< \frac{p}{\rho} \frac{\partial u}{\partial x} > = P_u(x) p_u(\overline{y}) \tag{5.36}$$

$$-\frac{1}{2} < u^2 v > = T_{u^2 v}(x) t_u(\overline{y}) \tag{5.37}$$

$$\epsilon_u = D_u(x) d_u(\overline{y}) \tag{5.38}$$

Similarity of the $< u^2 >$-equation is possible only if[4]

$$K_u \sim U_m^2 \tag{5.39}$$

$$P_u \sim \frac{U_m^3}{\delta} \frac{d\delta}{dx} \tag{5.40}$$

$$T_{u^2 v} \sim U_m^3 \frac{d\delta}{dx} \tag{5.41}$$

$$D_u \sim \frac{U_m^3}{\delta} \frac{d\delta}{dx} \tag{5.42}$$

All of these are somewhat surprising: The first (even though a second moment like the Reynolds stress) because the factor of $d\delta/dx$ is absent; the second, third and fourth because it is present.

Similar equations can be written for the $< v^2 >$ and $< w^2 >$ equations; i.e.,

$$U \frac{\partial < v^2 >}{\partial x} + V \frac{\partial < v^2 >}{\partial y} = 2 < \frac{p}{\rho} \frac{\partial v}{\partial y} > + \frac{\partial}{\partial y} \left\{ - < v^3 > -2 < pv > \right\} - 2\epsilon_v \tag{5.43}$$

$$U \frac{\partial < w^2 >}{\partial x} + V \frac{\partial < w^2 >}{\partial y} = 2 < \frac{p}{\rho} \frac{\partial w}{\partial z} > + \frac{\partial}{\partial y} \left\{ - < w^2 v > \right\} - 2\epsilon_w \tag{5.44}$$

When each of the terms in these equations is expressed in similarity variables, the

[4]Recall that the symbol '$\sim$' is used herein to mean 'has the same x-dependence as', and should not be confused with 'order of magnitude'.

resulting similarity conditions are:

$$D_v \sim P_v \sim \frac{U_m K_v}{\delta}\frac{d\delta}{dx} \tag{5.45}$$

$$D_w \sim P_w \sim \frac{U_m K_w}{\delta}\frac{d\delta}{dx} \tag{5.46}$$

$$T_{v^3} \sim \frac{U_m K_v}{\delta}\frac{d\delta}{dx} \tag{5.47}$$

$$T_{w^2 v} \sim \frac{U_m K_w}{\delta}\frac{d\delta}{dx} \tag{5.48}$$

There is an additional equation which must be accounted for; namely that the sum of the pressure strain-rate terms in the component energy equations be zero (from continuity). Thus, in similarity variables,

$$P_u(x)p_u(\overline{y}) + P_v(x)p_v(\overline{y}) + P_w(x)p_w(\overline{y}) = 0 \tag{5.49}$$

This can be true for all $\overline{y}$ only if

$$P_u \sim P_v \sim P_w \tag{5.50}$$

An immediate consequence is that

$$D_u \sim D_v \sim D_w \sim D_s \sim \frac{U_m u_*^2}{\delta} \tag{5.51}$$

where D_s is the scale for the entire dissipation.

From equations 5.40, 5.45 and 5.46 it follows that the constraint imposed by 5.50 can be satisfied only if

$$K_u \sim K_v \sim K_w \sim U_m^2 \tag{5.52}$$

Thus all of the Reynolds *normal* stresses scale with U_m^2, and not with u_*^2 like the Reynolds *shear* stresses. But this is exactly what was observed in figures 10 and 11.

The remaining equation for the Reynolds shear stress is given by

$$U\frac{\partial < uv >}{\partial x} + V\frac{\partial < uv >}{\partial y} = < \frac{p}{\rho}\left(\frac{\partial u}{\partial y} + \frac{\partial v}{\partial x}\right) > + \frac{\partial}{\partial y}\left\{- < uv^2 >\right\} - < v^2 > \frac{\partial U}{\partial y} \tag{5.53}$$

This does not introduce any new similarity functions, but as in the boundary layer analysis of GC, it does create an interesting problem. The x-dependence of the last term (which is the leading order term) is proportional to $(U_m R_{so}/\delta)d\delta/dx \sim (U_m^3/\delta)(d\delta/dx)^2$. If both terms are required to have the same x-dependence, a new constraint is imposed on the ones which already exist; namely,

$$K_v \sim R_{so}\frac{d\delta}{dx} \sim U_m^2\left(\frac{d\delta}{dx}\right)^2 \sim u_*^2\frac{d\delta}{dx} \tag{5.54}$$

Recall that R_{so} is only *asymptotically* equal to u_*^2 (from the matching), so the entire Reynolds shear stress scale evolves to this limit with increasing Reynolds number. Regardless, there is an apparent contradiction between equation 5.54 and equation 5.52. There are two possibilities for its resolution:

- *Either*, the two conditions together require that in the limit of infinite Reynolds number,

$$\frac{d\delta}{dx} \sim \frac{u_*^2}{U_m^2} \sim constant \tag{5.55}$$

- *Or*, the term which creates the contradiction must go to zero faster than the other terms so the offending condition does not remain in the analysis. In fact, as for the boundary layer, the possibility for this occurs since the terms on the left hand side of equation 5.53 are of order $(d\delta/dx)^2 \sim (u_*/U_m)^4$ relative to the leading term, whereas the highest order terms in the normal stress equations are of order $(d\delta/dx) \sim (u_*/U_m)^2$. Therefore the mean convection terms in the Reynolds shear stress equation will vanish faster in the limit of infinite Reynolds number than the remaining terms in any of the Reynolds stress equations if $d\delta/dx \to 0$.

It will be seen later that $d\delta/dx \to 0$ *is a necessary condition for insuring that the proper infinite Reynolds number dissipation limits can be satisfied; namely that the local dissipation rate be finite.* Therefore equation 5.55 is *not* relevant, nor must it be satisfied.

It is clear from the above that the outer Reynolds stress equations indeed admit to similarity solutions in the infinite Reynolds number limit (to second order in u_*/U_m), just as the mean momentum equations (and just as for the boundary layer). It is also clear from the figures shown earlier that the Reynolds stresses show a trend toward collapse in a manner consistent with the analysis above, even for the modest Reynolds numbers of the experiments. As noted earlier, nothing in the analysis or the data suggests that this similarity state should be independent of upstream and source conditions.

5.7 The Overlap Layer

Since both inner and outer similarity forms are non-dimensional profiles with different scales and the ratio of the scales is Reynolds number dependent, any region between the two similarity regimes cannot be Reynolds number independent, except asymptotically. As noted earlier, however, both inner and outer scaled profiles, f_i and f_o, describe the entire flow as long as the argument $\delta^+ = \delta/\eta$ is finite. Therefore at finite Reynolds numbers, *both* equations 5.16 and 5.28 must describe the region between the two similarity regimes. Thus the situation here is quite different from the usual asymptotic matching problem where infinite Reynolds number inner and outer solutions are extended and matched in an overlap region. Here both solutions are valid everywhere, at least for finite Reynolds numbers. Hence the objective is *not* to see if they overlap and match them if they do; rather, it is to determine whether the fact that they degenerate at infinite Reynolds number in different ways determines their functional forms in the common region they describe.

There are several pieces of information about the two profiles which can be utilized in this determination without further assumptions. They are:

- First, since both inner and outer forms of the velocity profile must describe the flow everywhere as long as the ratio of length scales, $\delta^+ = \delta/\eta$, is finite, it follows from equations 5.16 and 5.28 that

$$f_o(\overline{y}, \delta^+) = g(\delta^+) f_i(y^+, \delta^+) \tag{5.56}$$

  where $g(\delta^+)$ has been defined as

$$g(\delta^+) \equiv u_*/U_m \tag{5.57}$$

- Second, for finite values of δ^+, the velocity derivatives from both forms of the velocity must also be the same everywhere. This requires

$$\frac{\overline{y}}{f_o}\frac{df_o}{d\overline{y}} = \frac{y^+}{f_i}\frac{df_i}{dy^+} \tag{5.58}$$

  for all values of δ^+ and y.

- Third, both f_o and f_i must become asymptotically independent of δ^+. Thus $f_o(\overline{y}, \delta^+) \rightarrow f_{o\infty}(\overline{y})$, and $f_i(y^+, \delta^+) \rightarrow f_{i\infty}(y^+)$ as $\delta^+ \rightarrow \infty$ (otherwise the velocity scales have been incorrectly chosen). This is, in fact, the application of the *Asymptotic Invariance Principle* (section 2.3).

Now the problem is that in the limit as $\delta^+ \rightarrow \infty$, the outer form fails to account for the behavior close to the wall while the inner fails to describe the behavior away from it. The question then is: In this limit (as well as for all finite values approaching it) does there exist an "overlap" region where equation 5.56 is still valid? This question can be answered in the affirmative using the Near Asymptotics methodology of George (1995) and GC. The details are the same as for the zero pressure gradient turbulent

boundary layer (c.f. chapter 3, and are presented in Appendix B. There it is shown that, to leading order in δ^+, an overlap region exits in which

$$\left.\frac{y^+}{f_i}\frac{\partial f_i}{\partial y^+}\right|_{\delta^+} = \gamma(\delta^+) \tag{5.59}$$

and

$$\left.\frac{\overline{y}}{f_o}\frac{\partial f_o}{\partial \overline{y}}\right|_{\delta^+} = \gamma(\delta^+) \tag{5.60}$$

where $\gamma(\delta^+)$ has been defined as

$$\gamma \equiv -\frac{\delta^+}{g}\frac{dg}{d\delta^+} = -\frac{d\ln g}{d\ln \delta^+} \tag{5.61}$$

Both equations 5.59 and 5.60 must be invariant to transformations of the form $y \to y + a$ where a is arbitrary (since the equation must be valid for any choice of the origin of y). Therefore, the most general solutions are of the form:

$$\frac{U}{U_m} = f_o(\overline{y}, \delta^+) = C_o(\delta^+)[\overline{y} + \overline{a}]^{\gamma(\delta^+)} \tag{5.62}$$

$$\frac{U}{u_*} = f_i(y^+, \delta^+) = C_i(\delta^+)[y^+ + a^+]^{\gamma(\delta^+)} \tag{5.63}$$

where the parameters C_o, C_i and γ are functions of δ^+ and must be determined in addition to a. It will be argued later that a^+ is approximately constant. It is interesting to note that the power law form of equations 5.62 and 5.63 was one of those derived by Oberlack (1997) from a Lie group analysis of the equations for parallel shear flows.

It follows immediately from equation 5.56 that the friction law is given by

$$\frac{u_*}{U_m} = g(\delta^+) = \frac{C_o(\delta^+)}{C_i(\delta^+)}\delta^{+\,-\gamma(\delta^+)} \tag{5.64}$$

However, equation 5.61 must also be satisfied. Substituting equation 5.64 into equa-

tion 5.61 implies that γ, C_o, and C_i are constrained by

$$ln\delta^+ \frac{d\gamma}{d\ln\delta^+} = \frac{d}{d\ln\delta^+} \ln\left[\frac{C_o}{C_i}\right] \tag{5.65}$$

This constraint equation must be invariant to scale transformations of the form $\delta^+ \rightarrow D\delta^+$ since the physical choice of $\delta^+ = y^+_{1/2}$ is arbitrary. Thus the Reynolds number dependence of γ and C_o/C_i is independent of the particular choice of $\delta \sim y_{1/2}$ made earlier; any other choice would simply be reflected in the coefficient D. This will be of considerable importance in relating the wall jet parameters to those for the boundary layer obtained earlier by GC. From equation 5.65 we see that both γ and C_o/C_i can be most conveniently expressed as functions of $\ln\delta^+ = \ln Dy^+_{1/2}$.

Since by the AIP, equations 5.62 and 5.63 must be asymptotically independent of Reynolds number, the coefficients and exponent must be asymptotically constant; i.e.,

$$\begin{aligned} \gamma(\delta^+) &\rightarrow \gamma_\infty \\ C_o(\delta^+) &\rightarrow C_{o\infty} \\ C_i(\delta^+) &\rightarrow C_{i\infty} \end{aligned}$$

as $\delta^+ \rightarrow \infty$. Moreover, $C_{o\infty}$ and $C_{i\infty}$ must be non-zero, or else the solutions are trivial. Also, GC have argued that γ_∞ must also be non-zero to insure a finite local energy dissipation rate at infinite Reynolds number. Therefore none of these three important constants can be zero.

Following GC, it is convenient to write the solution to equation 5.65 as

$$\frac{C_o}{C_i} = \exp[(\gamma - \gamma_\infty)\ln\delta^+ + h] \tag{5.66}$$

where $h = h(\ln \delta^+)$ remains to be determined, but must satisfy

$$\gamma - \gamma_\infty = -\delta^+ \frac{dh}{d\delta^+} = -\frac{dh}{d \ln \delta^+} \tag{5.67}$$

The conditions that both $C_{o\infty}$ and $C_{i\infty}$ be finite and non-zero require that:
Either

- C_o, C_i and γ remain constant always;

or

- (i) $\gamma \to \gamma_\infty$ faster than $1/\ln \delta^+ \to 0$

and

- (ii) $h(\ln \delta^+) \to h_\infty = constant.$

It follows immediately that

$$\frac{C_{o\infty}}{C_{i\infty}} = exp[h_\infty] \tag{5.68}$$

Note that condition (i) together with equation 5.67 requires that $dh/d \ln \delta^+ \to 0$ faster than $1/\ln \delta^+$. Thus, regardless of the exact functional form of h, the leading term must be $h \sim (ln\delta^+)^\alpha$ where $\alpha > 0$ to satisfy condition (i) .

The behavior of u_*/U_m obviously is determined by both γ and the ratio C_o/C_i, which are themselves inter-related by equation 5.65. By substituting equations 5.66, 5.67, and 5.68 into equation 5.64, the friction law can be expressed as

$$\frac{u_*}{U_m} = \exp[-\gamma_\infty \ln \delta^+ + h] \tag{5.69}$$

Using equation 5.68 this can be re-written as

$$\frac{u_*}{U_m} = \frac{C_{o\infty}}{C_{i\infty}} \delta^{+-\gamma_\infty} \exp(h - h_\infty) \tag{5.70}$$

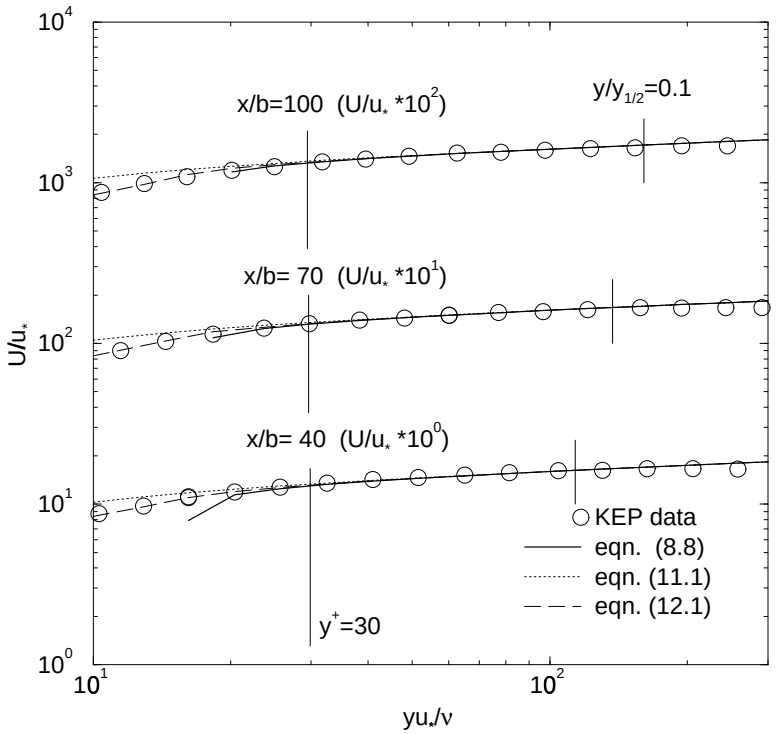

Figure 15: KEP data ($x/b = 40, 70$, and 100) and overlap solutions in inner variables.

Figures 15 and 16 show the mean velocity data in inner and outer variables for three positions of the KEP data ($x/b = 40, 70$, and 100), together with the overlap solutions of equations 5.62 and 5.63 using the h-function of CG and the parameters discussed in Section 5.11 below. Also plotted are two curves described in the following sections used to extend the overlap solution to the wall. The overlap solution provides an excellent fit to the LDA data from approximately $y^+ = 30$ to $\overline{y} = 0.1$. Note that the overlap region is not a straight line on a log-log plot because of the offset parameter a^+ (or $\overline{a}$).

The KEP data for u_*/U_m are plotted in Figure 17 as a function of $y^+_{1/2}$. Also shown is equation 5.70, again using the h-function of GC and the parameters given below. The agreement between theory and experiment is excellent.

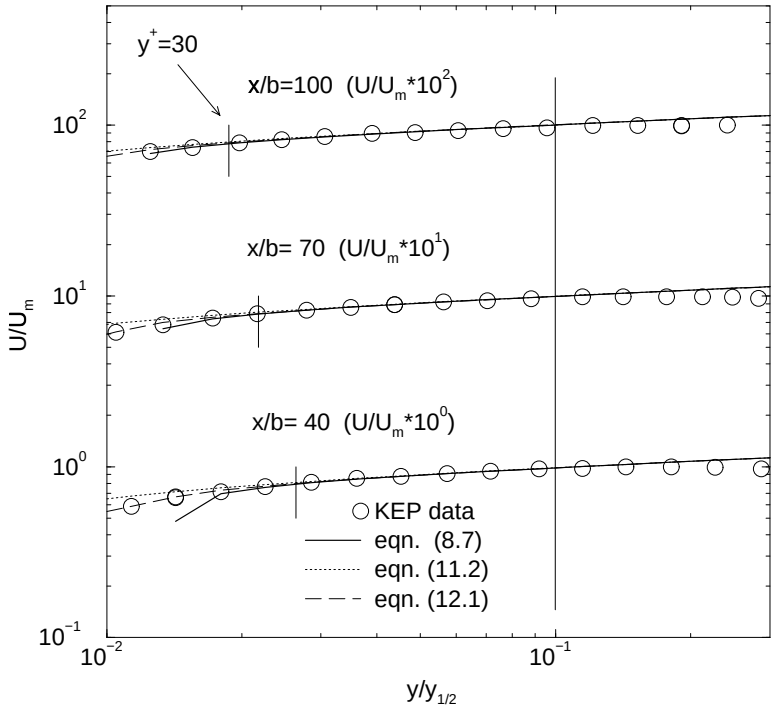

Figure 16: KEP data ($x/b = 40, 70$, and 100) and overlap solutions in outer variables.

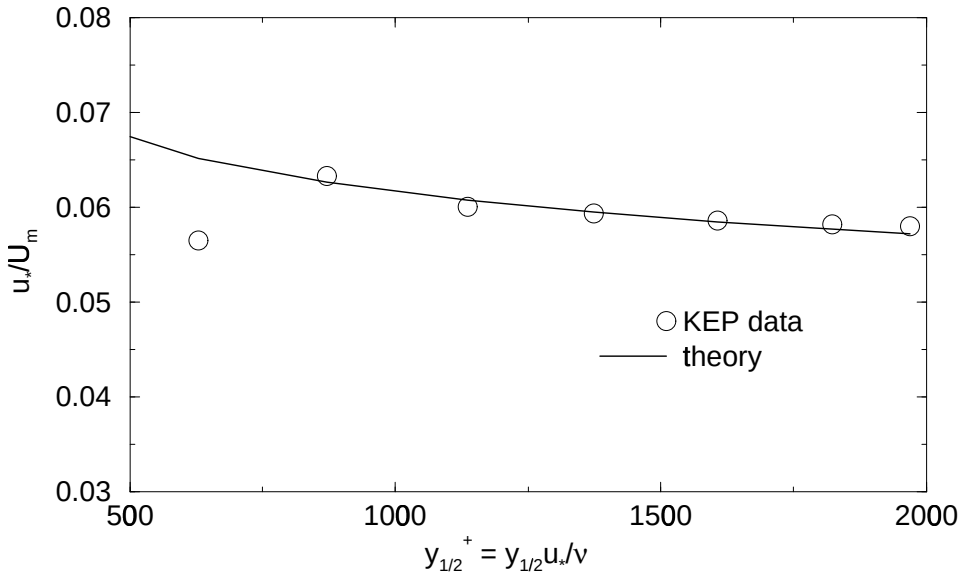

Figure 17: u_*/U_m versus $y^+_{1/2}$. KEP data.

5.8 The Reynolds Stress in the Overlap Layer

By following the same procedure as for the velocity (v. appendix B), the outer and inner Reynolds stress profile functions for the overlap region can be obtained (just as for the boundary layer by GC). Here, the Reynolds shear stress is given by,

$$r_o(\overline{y};\delta^+) = D_o(\delta^+)\overline{y}^{\beta(\delta^+)} \tag{5.71}$$

$$r_i(y^+;\delta^+) = D_i(\delta^+)y^{+\beta(\delta^+)} \tag{5.72}$$

where a solution is possible only if

$$\frac{R_{so}}{R_{si}} = \frac{D_i}{D_o}\delta^{+\beta} \tag{5.73}$$

and

$$\ln\delta^+\frac{d\beta}{d\delta^+} = \frac{d}{d\delta^+}\ln\left[\frac{D_o}{D_i}\right] \tag{5.74}$$

Unlike the velocity, however, more information about the Reynolds stress is available from the averaged momentum equation for the overlap layer since both equations 5.4 and 5.5 reduce to

$$\frac{\partial}{\partial y} < -uv >= 0 \tag{5.75}$$

in the limit of infinite Reynolds number. Thus,

$$\beta R_{so} D_o \overline{y}^{\beta-1} \to 0 \tag{5.76}$$

and

$$\beta R_{si} D_i y^{+\beta-1} \to 0 \tag{5.77}$$

Since both D_o and D_i must remain finite and be asymptotically constant (if the

Reynolds stress itself is non-zero), these conditions can be met only if

$$\beta \to 0 \tag{5.78}$$

From equation 5.75 for large values of y^+, the Reynolds stress in inner variables in the matched layer is given to first order (exact in the limit) by

$$r_i \to 1 \tag{5.79}$$

Since $R_{si} = u_*^2$, this can be consistent with equation 5.72 only if $D_i \to 1$ as $\delta^+ \to \infty$. It follows immediately that

$$R_{so} \to \frac{D_i}{D_o} u_*^2 \tag{5.80}$$

in the infinite Reynolds number limit, just as suggested in Section 5.4.

5.9 The Effect of Reynolds Number on the Overlap Range

This section also parallels closely George & Castillo (1997), but is included here since it is also important to understanding the wall jet. The overlap layer can be related directly to the averaged equations for the mean flow and the Reynolds stresses. The latter will be seen to be of particular interest since it is through them that the local Reynolds number influences the approach to the asymptotic state. Of particular interest is the question of how large the Reynolds number must be before the wall jet begins to show the characteristics of the asymptotic state.

The averaged momentum equation from about $y^+ > 30$ out to $\overline{y} < 0.1$ is given approximately by

$$0 = \frac{\partial}{\partial y} < -uv > \tag{5.81}$$

It has no obvious Reynolds number dependence; and the stress is effectively constant

throughout this region. This is, however, not the entire story because of the Reynolds transport equations. For this "constant shear stress region" the viscous diffusion and mean convection terms are negligible (as in the mean momentum equation), so the equations reduce approximately to (Tennekes & Lumley, 1972),

$$0 = -\left(< p\frac{\partial u_i}{\partial x_k} > + < p\frac{\partial u_k}{\partial x_i} > \right) \quad - \quad \left[< u_i u_2 > \frac{\partial U_k}{\partial x_2} \right.$$
$$\left. + < u_k u_2 > \frac{\partial U_i}{\partial x_2} \right] \quad - \quad \frac{\partial < u_i u_k u_2 >}{\partial x_2} - 2\epsilon_{ik} \qquad (5.82)$$

where $U_i = U\delta_{i1}$. Thus the viscosity does not appear directly in any of the single point equations governing this region, nor does it appear in those governing the outer boundary layer.

In spite of the above, viscosity continues to play a crucial role in at least a portion of the constant stress layer, even at infinite Reynolds number. The reason for this is that the scales at which the dissipation, ϵ_{ik}, takes place depend on the *local* turbulence Reynolds number, $R_t = u'L/\nu$. For $R_t > 10^4$ approximately, the energy dissipation is completely controlled by the large energetic scales of motion. These are effectively inviscid, but transfer energy through non-linear interactions (the energy cascade) to the much smaller viscous scales where the actual dissipation occurs (v. Tennekes & Lumley, 1972). When this is the case, the dissipation is nearly isotropic so $\epsilon_{ik} \approx \epsilon\delta_{ik}$. Moreover, ϵ can be approximated by the infinite Reynolds number relation: $\epsilon \sim q^3/L$ where L is a scale characteristic of the energy-containing eddies. Thus the entire Reynolds stress equations are effectively inviscid. Note that in this limit the Reynolds shear stress has no dissipation at all, i.e., $\epsilon_{12} = 0$.

At very low turbulence Reynolds number, however, the dissipative and energy-containing scales nearly overlap, and so the latter (which also produce the Reynolds shear stress) feel directly the influence of viscosity. In this limit, the energy and dissipative ranges nearly overlap, and the dissipation is more reasonably estimated by $\epsilon \sim \nu q^2/L^2$, where the constant of proportionality is of order 10. The dissipation

tensor, ϵ_{ik}, is anisotropic and ϵ_{12}, in particular, is non-zero (Hanjalic & Launder, 1974).

For turbulence Reynolds numbers between these two limits, the dissipation will show characteristics of both limits, gradually making a transition from $\epsilon \sim \nu q^2/L^2$ to $\epsilon \sim q^3/L$ as R_t increases. Thus the Reynolds stresses themselves will feel directly this, and will show a strong Reynolds number dependence. Obviously, in order to establish when (if at all) parts of the flow become Reynolds number independent, it is necessary to determine how the local turbulence Reynolds number varies downstream and across the flow.

Over the outer boundary layer (which is most of it) and excluding the overlap region, $L \approx 0.65 y_{1/2}$ and $u' \approx 0.2 U_m$. So when $U_m y_{1/2}/\nu > 7000$, the dissipation in the outer flow is effectively inviscid. The data of KEP vary from 14×10^3 at $x/b = 20$ to 31×10^3 at $x/b = 150$. Hence the mean and turbulence quantities in the outer flow should show little Reynolds number dependence, and this is indeed the case — when they are scaled properly! They can, of course, not be entirely Reynolds number independent because of the boundary conditions imposed by the inner flow on the outer. This residual dependence manifests itself in the overlap layer in the slow variations of C_i and γ, for example.

The near wall region is considerably more interesting, however, since in it the scales governing the energy-containing eddies are constrained by the proximity of the wall. Hence, the turbulence Reynolds number, R_t, depends on the distance from the wall, y. In fact, $R_t \sim y^+$ with a coefficient of about 18, so in effect y^+ is the turbulence Reynolds number. Because of this, two things are immediately obvious:

- First, since the physical distance from the wall for a fixed value of y^+ does not increase with downstream distance as rapidly as the jet spreads, then more and more of the wall jet will become effectively inviscid and will be governed by the inviscid dissipation relation. And correspondingly, the mean and turbulence quantities in the overlap layer will become Reynolds number independent, al-

beit very slowly. This is exactly the physical reason why C_o, C_i, and γ become asymptotically constant as described above. And clearly these limiting values cannot be reached until the entire 'inertial' layer is governed by the infinite Reynolds number dissipation relation. Obviously this can happen only when there is a substantial range satisfying $y^+ > 300$ and for which the mean convection terms are negligible. Thus the asymptotic limits are realized only when $300\nu/u_* << 0.1y_{1/2}$ or $u_* y_{1/2}/\nu >> 3000$, which corresponds approximately to $U_m y_{1/2}/\nu >> 50,000$. This is well above the range of the data considered here, or available elsewhere. Therefore the overlap layer, to the extent that it is identifiable at all, should (and does) display a Reynolds number dependence, not only in C_o, C_i, and γ, but correspondingly in the behavior of $< u^2 >$, $< uv >$, etc. This is directly analogous to the observations in the zero pressure gradient boundary layer (cf. Gad-el-Hak & Bandyopadhyay, 1994, , GC).

- Second, there will always be a *mesolayer* [5] a region below about $y^+ \approx 300$ in which the dissipation can *never* assume the character of a high Reynolds number flow. Hence, the dissipation can never become independent of viscosity, no matter how high the Reynolds number becomes — and even though the mean momentum equation itself is inviscid above $y^+ \approx 30$! This is well-known to turbulence modellers, but the consequences for similarity theory and asymptotic analyses do not seem to have been noticed previously. It is particularly important for experimentalists who have routinely (and wrongly) tried to apply asymptotic formulas to data from to this region.

Thus the constant stress layer is really four separate regions, each having their own unique character. The 'inertial' layer ($y^+ > 300, \overline{y} < 0.1$) obtained in the preceding section which can ultimately become inviscid; an 'in-between layer' ($30 < y^+ < 300$), in which the viscous stresses are negligible, but in which viscosity acts directly on

[5] This appropriates a term from Long & Chen (1981) who argued for its existence, but from entirely different physical and scaling arguments which we find untenable.

the turbulence scales producing the Reynolds stresses; a buffer layer ($3 < y^+ < 30$ approximately) where the Reynolds stress and viscous stress both control the mean flow, and the linear sublayer near the wall ($y^+ < 3$ approximately) where the viscous stresses dominate. It seems appropriate to call this 'in-between layer' the mesolayer since it is clearly not the buffer layer, nor is it the overlap region. And unlike the 'mesolayer' proposed by Long & Chen (1981), it needs no new length scale to describe it since its characteristics and extent are measured entirely by y^+. Interestingly, the application of Near-Asymptotics to the overlap region appears to capture the functional dependence of both the inertial and mesolayer regions, with the offset parameter a as noted in section 5.12.

5.10 The Inertial and Mesolayer Subregions

The mathematical character of the overlap region has been derived above and is seen to follow directly from first principles without assumptions. It remains to interpret these results physically. The overlap region is essentially the region of the flow where neither convection by the mean motion nor viscous shear stress are of major importance in the mean momentum balance. In the wall jet, it is clear from the profiles presented earlier that these conditions are satisfied approximately in the region bounded by $30 < y^+ < 0.1 y^+_{1/2}$ (or $30/y^+_{1/2} < \overline{y} < 0.1$), or from just outside the buffer region (where the total stress has evolved from primarily viscous to Reynolds stress only) to just inside the velocity maximum which is near $\overline{y} = 0.17$ as noted earlier. This is illustrated schematically in Figure 4. It is important to note that neither mean convection nor viscous effects are completely negligible in the overlap region *at finite Reynolds number*, and this is the origin of the Reynolds number dependence of the overlap solutions obtained above. In fact, GC have argued using the spectral energy equations that even if viscous effects were small in the single point equations, they could *never* be negligible in the two-point equations in the lower part of the overlap

region, a subregion which they called the *mesolayer*. Below a value of $y^+ < 300$ approximately, they argued that viscosity directly affects the multi-point Reynolds stress equations, and hence the dissipation and Reynolds stress. Above $y^+ \approx 300$, inertial effects dominate the non-linear turbulence energy transfer; hence the term *inertial sublayer* is used to describe it.

Thus the overlap region itself has two sublayers within it: the mesolayer and the inertial sublayer. Obviously the latter can exist only when there is a substantial region in the flow satisfying $0.1y^+_{1/2} > 300$ or $y^+_{1/2} > 3000$. Few wall jet experiments satisfy this criterion, and of those, none have been made with techniques which could measure the near wall region with sufficient accuracy to determine the wall shear stress. In the KEP data, for example, the mesolayer comprises all of the overlap region. Note that this is still substantially better than current DNS capability where even the conditions for a mesolayer are not satisfied; namely, $0.1y^+_{1/2} > 30$! In such cases the velocity maximum itself does not even occur in the outer region of the flow, and hence is dependent on flow Reynolds number. Obviously the overlap analysis above should not be expected to apply to such low Reynolds number flows. It is clear then that experiments and/or simulations at much higher Reynolds numbers are necessary before the above theory can be completely tested and the function $h(ln\delta^+)$ determined beyond doubt.

In spite of the problems presented by the lack of data to test the overlap arguments at sufficiently high Reynolds numbers, equivalent arguments have previously been made for the turbulent boundary layer by GC for which there is at least some data. In fact, the overlap profiles, friction law, and constraint equation for both wall jet and boundary layer are all of the same form. Therefore there is reason to hope that the function $h(\ln \delta^+)$ might be the same for boundary layers and wall jets, at least to within the scale factor D as noted above. These ideas will be formalized and tested below.

5.11 Wall Jet versus Boundary Layer: A Common Inner Region?

While the outer flows of the zero pressure gradient boundary layer and the wall jet are, of course, entirely different, there is reason to suspect that the inner flows may be the same. First, both scale with the same inner variables, u_* and ν. Second, all the governing equations are exactly the same at infinite Reynolds number, and even the terms which begin to appear at finite Reynolds number are the same. Third, the overlap profiles *in inner variables* have exactly the same form. Fourth, for both flows the leading term in the Taylor expansion around $y = 0$ is $u^+ = y^+$ and the next non-zero term is the fourth order term $c_4 {y^+}^4$; i.e., $u^+ = y^{+} + c_4 {y^+}^4 + \ldots$. And finally, as the success of the GC h-function above makes clear, there is experimental evidence. Figures 18 and 19 show the mean velocity and Reynolds stress profiles in inner variables for the Johansson & Karlsson (1989) boundary layer experiment ($R_\theta = 2.4 \times 10^3$) and the KEP wall jet profile for $x/b = 70$ ($y^+_{1/2} = 1.8 \times 10^3$). The mean velocity profiles are nearly identical for $y^+ < 100$, while the Reynolds stress profiles coincide for $y^+ < 35$. Also shown on the figures are the composite velocity given by equation 5.89 and the Reynolds stress profile derived by substituting its derivative into equation 5.15. (The discontinuity arises from the splice described in Section 5.13). These make it clear that the departure of the wall jet profiles from the boundary layer profiles is indeed attributable to the outer flow which penetrates to relatively low values of y^+ at these Reynolds numbers.

Therefore it seems reasonable *to hypothesize* that:

- The inner variable parameters $C_{i\infty}$, γ_∞, a^+ and c_4 are the same for both the wall jet and the zero pressure gradient boundary layer.

- The Reynolds number dependence of the parameters C_i and γ is the same, *to within the scale factor D discussed in the preceding section.*

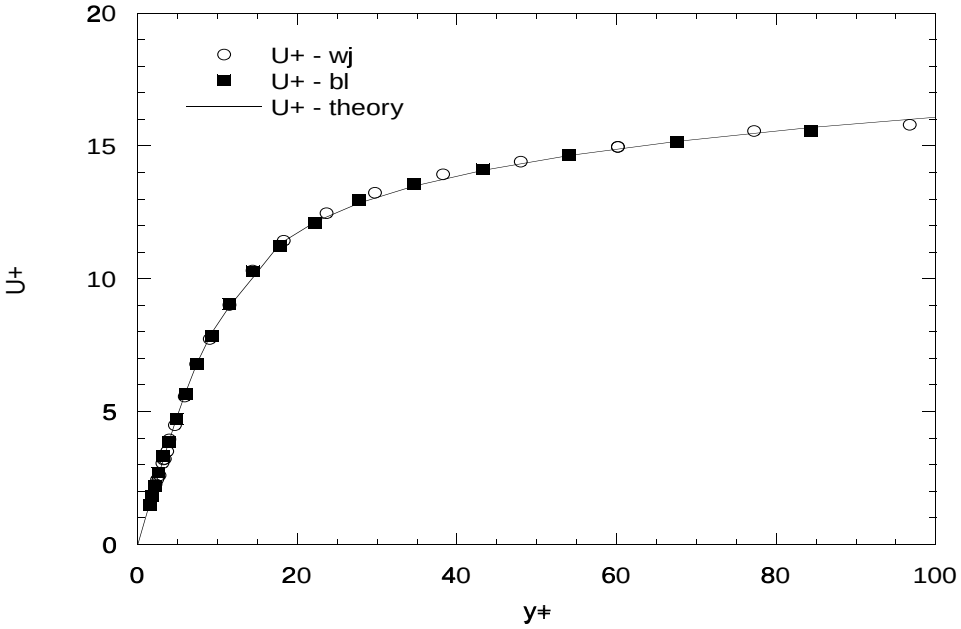

Figure 18: Velocity in inner variables for boundary layer and wall jet. Data of Johansson and Karlsson 1989 and KEP.

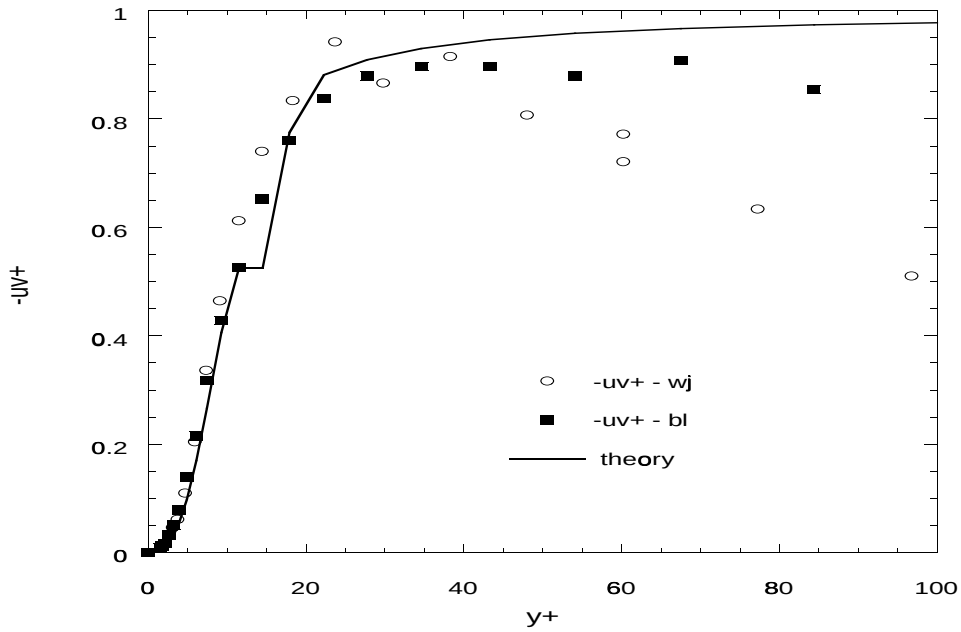

Figure 19: Reynolds shear stress in inner variables for boundary layer and wall jet. Data of Johansson and Karlsson 1989 and KEP.

It follows immediately from equation 5.65 that the outer parameter C_o for the wall jet can at most differ by a constant multiplicative factor from the boundary layer values, since any other difference would change γ. Because this multiplicative factor must also be reflected in $C_{o\infty}$, the *only* differences between the wall jet and the boundary layer can be $C_{o\infty}$ and the scale factor D; otherwise the second hypothesis is wrong. Finally, the all-important function, $h(\delta^+) - h_\infty$, must be the same for both boundary layers and wall jets, since it determines the Reynolds number behavior of both γ and C_o/C_i. (Recall that $\delta^+ = Dy^+_{1/2}$.) (Note that a similar line of reasoning was applied by Castillo (1997) the pressure gradient boundary layer.)

Thus, as discovered above, the GC empirical form for h for the boundary layer can be incorporated directly here in the form:

$$h = \frac{A}{(\ln Dy^+_{1/2})^\alpha} \tag{5.83}$$

Note that while this may appear to be an arbitrary empirical equation, it is really much more general. Since $h \to h_\infty$ as $\ln Dy^+_{1/2} \to \infty$, only negative powers are possible in an expansion of $h - h_\infty$ for large values, of which equation 5.83 is at least the leading term.

It follows from equations 5.67, 5.66, and 5.70 that

$$\gamma - \gamma_\infty = \frac{\alpha A}{\left(\ln Dy^+_{1/2}\right)^{1+\alpha}} \tag{5.84}$$

$$\frac{C_o}{C_i} = \frac{C_{o\infty}}{C_{i\infty}} \exp[(1+\alpha)A/(\ln Dy^+_{1/2})^\alpha] \tag{5.85}$$

and

$$\frac{u_*}{U_m} = \frac{C_o}{C_i}\left(Dy^+_{1/2}\right)^{-\gamma} = \frac{C_{o\infty}}{C_{i\infty}}[Dy^+_{1/2}]^{-\gamma_\infty} \exp[A/(\ln Dy^+_{1/2})^\alpha] \tag{5.86}$$

For the boundary layer, GC found $\alpha = 0.46$, $A = 2.90$, $C_{i\infty} = 55$, $\gamma_\infty = 0.0362$, and $a^+ \approx -16$. *If the hypothesis is correct*, these values should be the same for the

wall jet. Alternatively, if the parameters or the empirical form for h have been more accurately determined for the wall jet, then they should also describe the boundary layer, to within the scale factor D and $C_{o\infty}$ which must be determined for each flow separately. In fact, the CG parameters describe the KEP wall jet velocity profiles data to within five percent between $y^+ = 30$ and $\overline{y} = 0.1$ using $C_o = C_{o\infty} = 1.26$ and $D = 1.0$. But as illustrated in Figures 15 to 17 above, a slight change to $C_o = C_{o\infty} = 1.30$ and $C_{i\infty} = 56.7$ (so $C_{o\infty}/C_{i\infty} = 0.023$ is unchanged) reduces the maximum error in the overlap range of the mean velocity profiles to less than two percent, which is within the experimental uncertainty. Both sets of parameters predict the friction data to within 1% (since u_*/U_m depends only on the ratio of $C_{o\infty}$ to $C_{i\infty}$, and not their individual values). As shown later, a subtle consequence of this will be that *all* of the differences in spreading rate among the various experiments can be attributed to the parameter B_1 defined in equation 5.31.

5.12 A Mesolayer Interpretation of a^+

The a appearing in equations 5.63 and 5.62 has been interpreted by GC as arising from the effect of the turbulence Reynolds number near the wall on the two-point Reynolds stress equations. A useful form of the inner velocity profile can be obtained by expanding the inner velocity profile of equation 5.63 for $y^+ >> a^+$. The result is

$$\frac{U}{u_*} = C_i {y^+}^{\gamma} + \gamma C_i a^+ {y^+}^{\gamma-1} + \frac{1}{2}\gamma(\gamma-1) C_i {a^+}^2 (y^+)^{\gamma-2} + \ldots \tag{5.87}$$

Equation 5.87 can also be written in outer variables as

$$\frac{U}{U_m} = C_o \overline{y}^{\gamma} + \gamma \overline{a} C_o \overline{y}^{\gamma-1} + \frac{1}{2}\gamma(\gamma-1) C_o \overline{a}^2 (\overline{y})^{\gamma-2} + \ldots \tag{5.88}$$

where $\overline{a} = a^+/y^+_{1/2}$.

These forms are useful for two reasons: First, they are excellent approximations

to equation 5.63 for all values of $y^+ > -a^+$ (or $\overline{y} > -\overline{a}$). Second, it is easier to incorporate them into a composite solution for the inner region since they do not have the singularity at $y^+ = -a^+$. These profiles have been included on Figures 15 and 16 using the GC value of $a^+ = -16$.

5.13 Composite Velocity Profiles for the Inner and Overlap Regions

A velocity profile valid over the entire inner and overlap regions can be obtained using equation 5.87 if empirical relations are introduced to account for the variation of $f_i(y^+, \delta^+)$ inside the overlap region. This is analogous to the near wall and buffer layer empirical profiles employed by GC for boundary layers which use an empirical relation to splice together the various regions of the flow so that a continuous profile is obtained.

The term "buffer layer" was used by GC to refer to the region of adjustment from linear to the meso/overlap region. They proposed splicing the near wall and expanded form of the overlap solutions using

$$\begin{aligned} \frac{U}{u_*} = f_i(y^+) &= (y^+ + c_4 {y^+}^4 + c_5 {y^+}^5) \exp(-d {y^+}^6) \\ &+ C_i {y^+}^{\gamma} [1 + \gamma a^+ {y^+}^{-1} + \frac{1}{2}\gamma(\gamma-1) {a^+}^2 {y^+}^{-2}][1 - exp(-d {y^+}^6)] \end{aligned} \quad (5.89)$$

The ${y^+}^6$-dependence of the exponentials allows not only the no-slip condition to be satisfied at the wall, but also the boundary conditions on the first three velocity derivatives. The damping parameter is chosen as $d = 8 \times 10^{-8}$ to fix the changeover at $y^+ \approx 15$. A constant value of $c_4 = -0.0003$ is in good agreement with both the velocity data of KEP and the corresponding expansion for the Reynolds shear stress near the wall (i.e., $< -uv >^+ = 4c_4 {y^+}^3$). The value of c_5 can not be determined with any accuracy from the data, so was arbitrarily chosen as $c_5 = 1.35 \times 10^{-5}$ to provide

the best splice between the near wall and mesolayer profiles. The value of a^+ was determined by GC to be approximately -16.

Figure 18 shows equation 5.89 together with the velocity data in inner variables for the KEP profile ($x/b = 70$) and the boundary layer data of Johansson & Karlsson (1989). Figure 19 shows the corresponding Reynolds stress profile calculated using equation 5.89 and equation 5.15, together with the measured Reynolds stress from these experiments. The calculated profiles use the modified GC values described earlier for the inner parameters ($\gamma_\infty = 0.0362$, $C_{i\infty} = 56.7$, $a^+ = -16$, $\alpha = 0.46$, and $A = 2.9$) with $D = 1.00$ and $C_{o\infty} = 1.30$. The agreement between experiment and theory is remarkable. The slight difference in $C_{i\infty}$ (from the boundary layer value) is undoubtedly attributable to the higher quality of the wall jet data. Overall, the agreement between the composite profile and the velocity data is within one percent for $\overline{y} < 0.1$.

5.14 The Asymptotic Friction Law

As noted above, it has long been customary to present friction data plotted against the local Reynolds number based on the velocity maximum and half-width (or location of velocity maximum). Such a plot is not naturally suggested by the theory presented here since the parameters depend on $y^+_{1/2}$, and not on $U_m y_{1/2}/\nu$ or $U_m y_m/\nu$. It can easily be generated on a spreadsheet, however, by assuming a value for $y^+_{1/2}$, then calculating u_*/U_m and from the two, R_m. To facilitate comparison with earlier empirical friction laws and data, such a plot is presented here as Figure 20, where it has again been assumed that $y_m/y_{1/2} = 0.17$. Representative values are shown in table 5.1.

Since there is no new information, it is not surprising that the same good agreement noted above is achieved. Also shown is the Bradshaw & Gee (1960) correlation. This was originally given by the authors in terms of c_f as a power law in

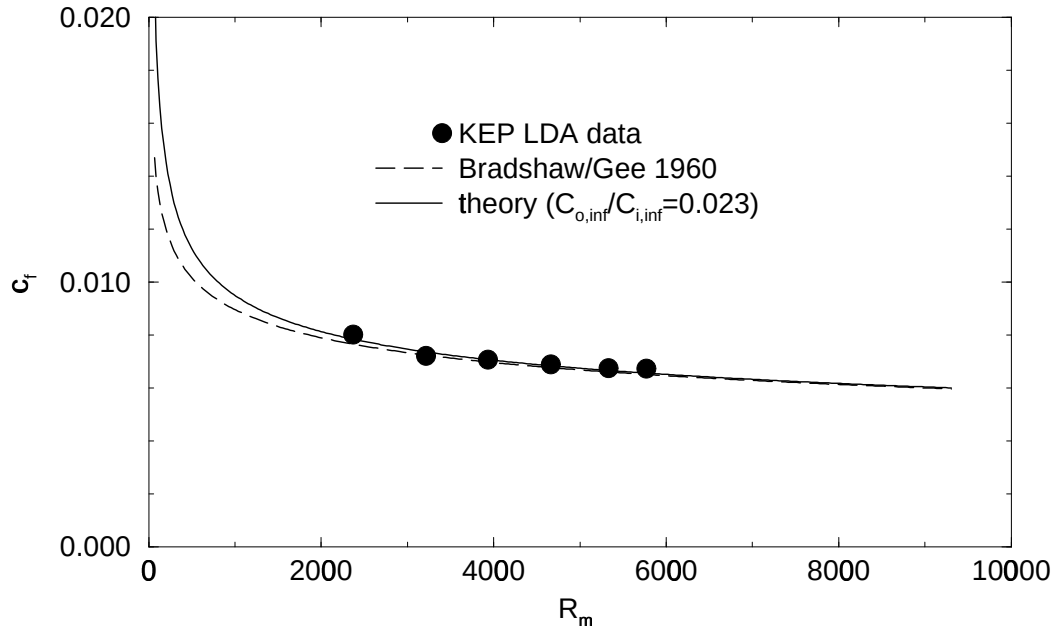

Figure 20: Skin friction coefficient versus $R_m = U_m y_m/\nu$.

$y^+_{1/2}$ (given)	C_o ($\approx C_{o\infty}$)	C_i (eqn. 5.85)	γ (eqn. 5.84)	u_*/U_m (eqn. 5.64 or 5.86)	$R_m = y_m U_m/\nu$ ($y_m/y_{1/2} = 0.17$)
800	1.3	9.30	0.1189	0.0633	2,149
1,000	1.3	9.53	0.1151	0.0616	2,758
1,200	1.3	9.72	0.1122	0.0604	3,379
1,500	1.3	9.95	0.1089	0.0589	4,329
2,000	1.3	10.25	0.1050	0.0571	5,952
2,500	1.3	10.47	0.1022	0.0558	7,614
3,000	1.3	10.65	0.1000	0.0548	9,307
4,000	1.3	10.93	0.0968	0.0533	12,765
5,000	1.3	11.14	0.0946	0.0521	16,301
6,000	1.3	11.31	0.0928	0.0513	19,899
8,000	1.3	11.57	0.0902	0.0499	27,239
10,000	1.3	11.77	0.0884	0.0489	34,734

Table 5.1: Wall jet parameters calculated as a function of $y^+_{1/2}$

$R_m \equiv U_m y_m/\nu$; in particular, $c_f = 0.0315 R_m^{-0.182}$. This transforms to $u_*/U_m = 0.122(y^+_{1/2})^{-0.100}$ using the KEP estimate of $y_m/y_{1/2} = 0.17$. There is a remarkable correspondence between the theoretical curve and the empirical relation of Bradshaw & Gee (1960). Note that the theoretical and empirical curves diverge as the Reynolds number increases since the power exponent continues to drop in the former, but is fixed in the latter. Obviously the empirical expressions should not be used outside of the limited range for which they were established by experiment, but the theory is not so limited.

As shown in equation 5.86, u_*/U_m is entirely determined by the two constants, γ_∞ and $C_{o\infty}/C_{i\infty}$, and the function $h(Dy^+_{1/2})$. In the limit of infinite Reynolds number, however, even the function h must be constant, so the asymptotic friction law is indeed a power law with constant coefficients; i.e.,

$$\frac{u_*}{U_m} \rightarrow \frac{C_{o\infty}}{C_{i\infty}} (Dy^+_{1/2})^{-\gamma_\infty} \tag{5.90}$$

Some idea of when this limiting power law is valid can be obtained by expanding the exponential of equation 5.86 in powers of $A/(\ln(Dy^+_{1/2})^\alpha$

$$\exp[A/(\ln Dy^+_{1/2})^\alpha] = 1 + \frac{A}{(\ln Dy^+_{1/2})^\alpha} + \ldots \tag{5.91}$$

Clearly the second term must be negligible for the power law limiting behavior to dominate; thus the limiting power law behavior is obtained when

$$\ln Dy^+_{1/2} >> [A]^{1/\alpha} \tag{5.92}$$

For the values above this would require $y^+_{1/2} >> 2.4 \times 10^4$, which is an order of magnitude above the existing experiments.

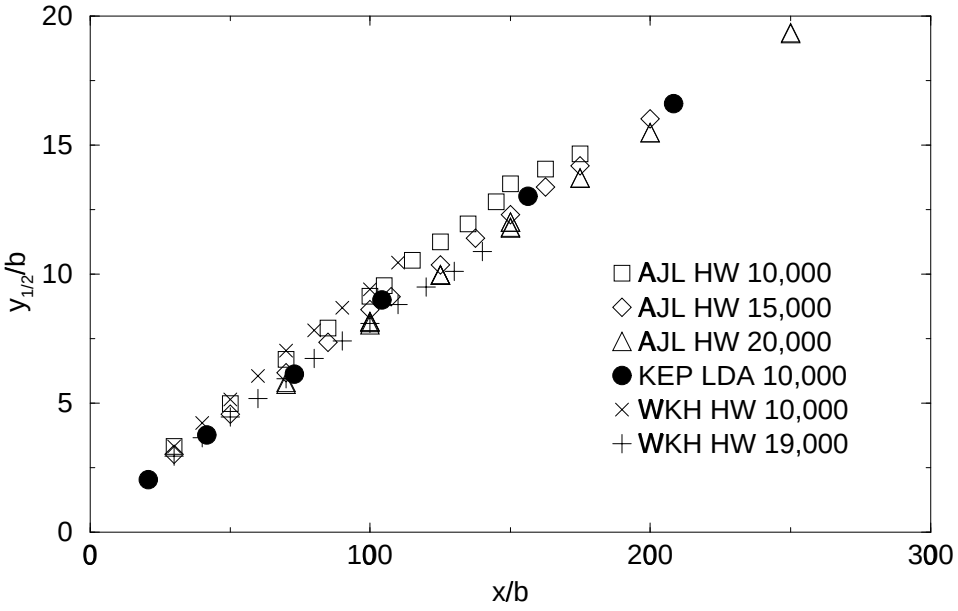

Figure 21: Variation of half-width with downstream distance, $y_{1/2}/b$ versus x/b. KEP, AJL and WKH data.

5.15 Implications for $y_{1/2}$ and U_m versus x

Figures 21 through 24 show the variation of the half-width, $y_{1/2}$, and the velocity maximum, U_m, with downstream distance, x, for the KEP, AJL and WKH data. These data are plotted using both the traditional normalization using b and U_o (cf. Launder & Rodi, 1981), and using M_o and ν (cf. Narasimha *et al.*, 1973, WKH). Also shown on the latter are the theoretical curves derived below.

It is not entirely clear whether the data collapse or not even when plotted using the momentum/viscosity scaling (which is seen to work somewhat better than the scaling using U_m and b). The same lack of collapse was observed by by WKH who attempted to remove the trends with a virtual origin, with limited success. These differences between data sets were noted in Section 5.5 in the normalized plots of U_m versus $y_{1/2}$. Clearly source Reynolds number alone cannot explain the differences since the WKH source Reynolds numbers overlap those of AJL and KEP. As noted earlier there is nothing in the single point similarity equations themselves to suggest that

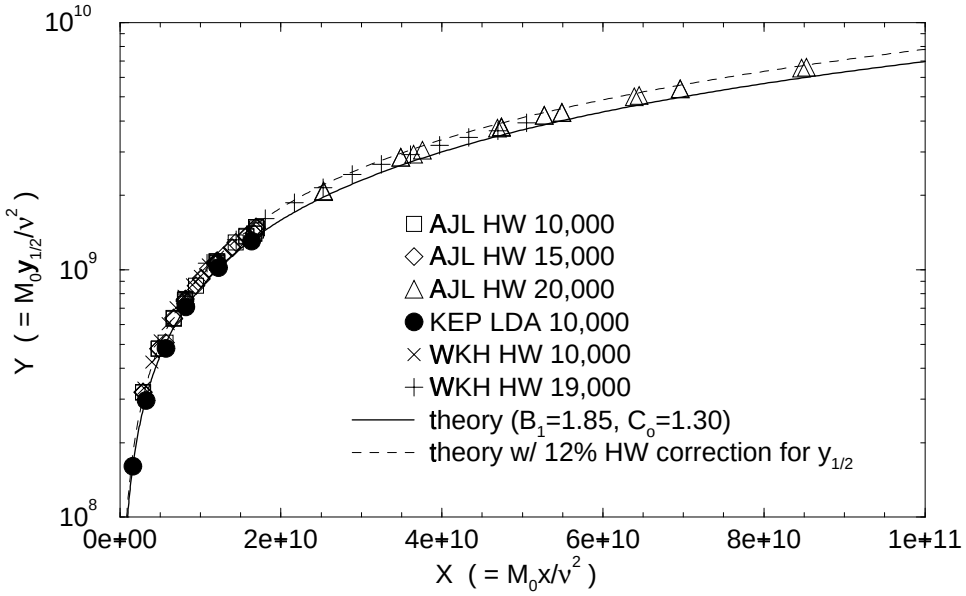

Figure 22: $Y = M_o y_{1/2}/\nu^2$ versus $X = M_o x/\nu^2$. KEP, AJL and WKH data.

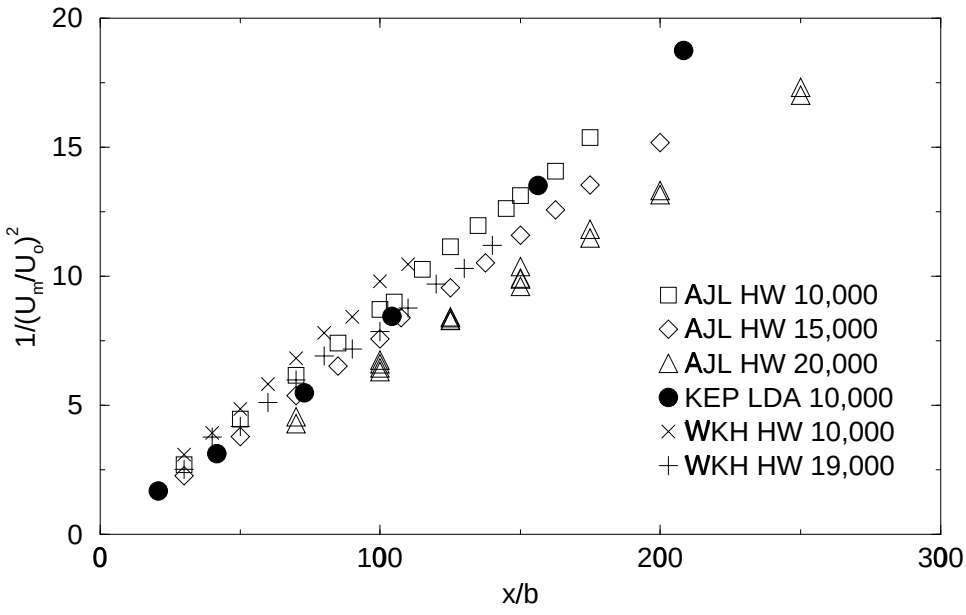

Figure 23: Variation of centerline velocity with distance, $1/(U/U_o)^2$ versus x/b. KEP, AJL and WKH data.

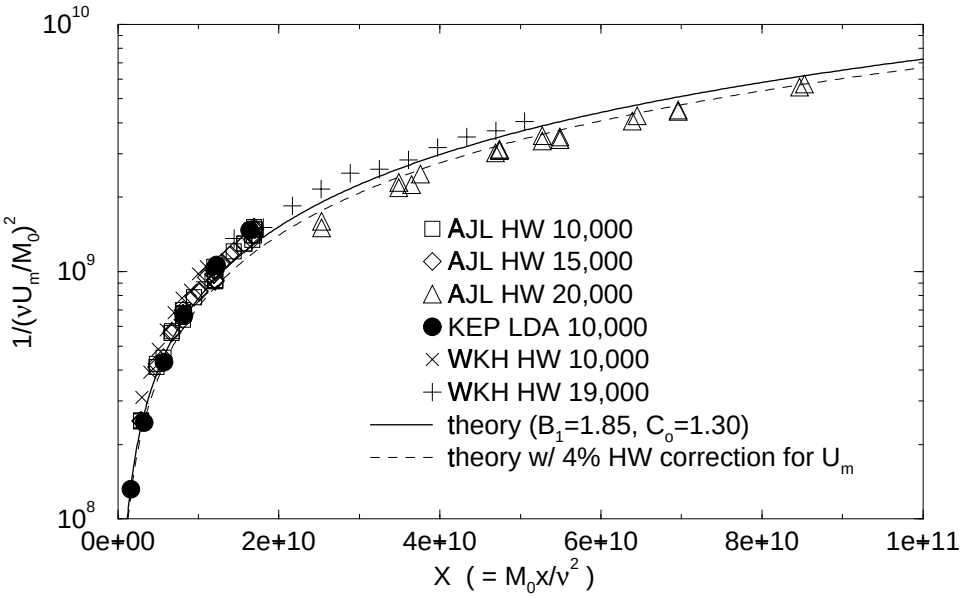

Figure 24: $1/(\nu U_m/\nu)^2$ versus $X = M_o x/\nu^2$. KEP, AJL and WKH data.

the effect of initial conditions dies off. It is precisely here in B_1, $dy_{1/2}/dx$ and dU_m/dx where the differences appear. Nonetheless, the cross-flow and rectification errors in the hot-wire measurements due to the turbulence intensity at least account for some of the observed differences. All of the hot-wire estimates of $y_{1/2}$ are about 10% to 15% higher than the LDA and theoretical results, consistent with the error estimate of EKP. Near the velocity maximum, the hot-wire obtained mean velocity measurement are 3 to 5% too high, which means that the plotted HW data in Figure 24 should be 6 to 10% too low. This is at least in the correct direction for the AJL data, but can not account for the WKH data. As noted in Section 5.5, however, we might have overestimated the WKH values of M_o by about the same amount which would have the opposite effect. So the role of the initial conditions, if any, must remain unresolved for now.

It has regularly been conjectured (e.g. Launder & Rodi, 1981) that the half-width of the plane wall jet grows linearly with distance. It will be argued below that $dy_{1/2}/dx$ is proportional to the shear stress, and it has already been shown that the only possible asymptotic limit for this is zero. However, $dy_{1/2}/dx \to 0$ does *not* imply

that the wall jet stops growing, only that it cannot grow faster than linear. For example, if $dy_{1/2}/dx \sim x^p$ where $0 > p > -1$, then clearly $dy_{1/2}/dx \to 0$ as $x \to \infty$, but $y_{1/2} = x^{1+p}/(1+p)$ continues to increase. The growth is not linear, however, unless $p \equiv 0$, which we shall see it is not. In fact, most experiments which have attempted to establish empirical power laws for the x-dependence of the half-width conclude the growth rate is slightly less than linear. For example, WKH and Narasimha *et al.* (1973) suggest on empirical grounds that $y_{1/2} \sim (x - x_o)^{0.88}$ and $y_{1/2} \sim (x - x_o)^{0.91}$, respectively. As will be shown below, there is no theoretical justification for such power laws *in* x except for very large values of the Reynolds number, and well above any experiments to-date.

The x-dependence of $y_{1/2}$ can be considered using the momentum integral equation in outer similarity variables, which can be written as

$$U_m^{-2} \frac{d}{dx} \left[U_m^2 y_{1/2} I_2 \right] = -\frac{u_*^2}{U_m^2} \tag{5.93}$$

where I_2 is defined by

$$I_2 = \int_0^\infty [f_o^2 + 2(k_u - k_v)] d\overline{y} \tag{5.94}$$

The turbulence normal stress term, $(k_u - k_v)$ is of second order, and could have been omitted with no loss of generality but an error of approximately 5% would be introduced. Note that I_2 becomes asymptotically independent of the Reynolds number in the limit as $y_{1/2}^+ \to \infty$.

The similarity condition of equation 5.24 (i.e., $U_m \sim y_{1/2}^n$) implies that

$$\frac{y_{1/2}}{U_m} \frac{dU_m}{dx} = n \frac{dy_{1/2}}{dx} \tag{5.95}$$

It follows after some manipulation that

$$\left\{ (1 + 2n) I_2 + \frac{dI_2}{d \ln y_{1/2}^+} \right\} \left[\frac{dy_{1/2}}{dx} \right] = -\frac{u_*^2}{U_m^2} \tag{5.96}$$

In the limit as $y^+_{1/2} \to \infty$, this reduces to

$$(1+2n)I_2\left[\frac{dy_{1/2}}{dx}\right] = -\frac{u_*^2}{U_m^2} \tag{5.97}$$

Note the appearance of the exponent n from the similarity condition of equation 5.24.

The value $n = -1/2$ is a special case since the corresponding shear stress must be zero, and hence the growth rate either becomes undefined or must be exactly zero. In fact, from equation 5.24 it is clear that $n = -1/2$ would require that that $U_m^2 y_{1/2}$ be constant, which is exactly the momentum conservation condition for a free plane jet (cf. George, 1989), and this makes sense only if there is no momentum loss to the boundary. Given the presence of the wall, this would be a possibility only at infinite source Reynolds number, if at all. For finite source Reynolds numbers, the presence of the wall dictates a continuing momentum loss to the wall so that $n < -1/2$, and as a consequence $y_{1/2}$ must grow slower than linearly with x, exactly as suggested by Narasimha *et al.* (1973), WKH and AJL on empirical grounds. But there is, to this point at least, nothing in the equations to indicate that the value of n is universal, although the experiments cited earlier in Section 5.5 suggest that it might be.

The derivative, $dy_{1/2}/dx$, in equation 5.97 can be replaced by either $d(y_{1/2}/b)/d(x/b)$ or $dY_{1/2}/dX$ with no loss of generality where $Y_{1/2}$ is defined as before and X by $X \equiv xM_o/\nu^2$. The momentum-viscosity scaled version is used below to derive the X-dependence of $Y_{1/2}$ and $\nu U_m/M_o$.

Since n, I_2 and u_*/U_m can be determined directly from the data, equation 5.97 can be used to calculate $dy_{1/2}/dx$. Alternatively, n can be determined if I_2, u_*/U_m, and $dy_{1/2}/dx$ are known. In fact, this is probably the best way to determine n since $2n$ is very close to -1, so the difference between n and $-1/2$ is magnified. The value so obtained can then be used together with the continuity equation developed in the next section to provide an overall consistency check on the flow and data. From the KEP data, the value of I_2 for $x/b = 40$, 70, 100 (and even 150) is 0.78 (0.745 if

$y^+_{1/2}$ (given)	$dy_{1/2}/dx$ (eqn. 5.97)	$X = M_0 x/\nu^2$ (eqn. 5.101)	$Y = M_0 y_{1/2}/\nu^2$ (eqn. 5.98)	$1/(\nu U_m/M_0)^2$ (eqn. 5.31)
800	0.0917	1.31E+09	1.33E+08	1.11E+08
1,000	0.0870	2.35E+09	2.26E+08	1.94E+08
1,200	0.0835	3.77E+09	3.47E+08	3.05E+08
1,500	0.0794	6.72E+09	5.87E+08	5.31E+08
2,000	0.0747	1.41E+10	1.15E+09	1.08E+09
2,500	0.0713	2.49E+10	1.94E+09	1.88E+09
3,000	0.0687	3.96E+10	2.97E+09	2.94E+09
4,000	0.0650	8.21E+10	5.80E+09	5.97E+09
5,000	0.0622	1.44E+11	9.74E+09	1.03E+10
6,000	0.0602	2.28E+11	1.49E+10	1.61E+10
8,000	0.0571	4.68E+11	2.89E+10	3.25E+10
10,000	0.0548	8.17E+11	4.84E+10	5.61E+10

Table 5.2: Wall jet development as a function of $y^+_{1/2}$. (See table 5.1 for parameters)

the turbulence terms are neglected). Using this, the measured values of u_*/U_m and $dy_{1/2}/dx$, and averaging the result yields $n = -0.528$, which is the value cited earlier in Section 5.4.

Since the values of n and I_2 can now be assumed known, then the x-dependence of $Y_{1/2}$ (or $y_{1/2}/b$) can be calculated numerically using equation 5.97 together with the friction law of equation 5.86. The local value of $y^+_{1/2}$ must be determined for each value of x before the integration can be performed, so an inverse procedure was carried out using a spreadsheet, the results of which are summarized in Table 5.2. It follows after some manipulation that

$$\frac{M_o y_{1/2}}{\nu^2} = Y_{1/2} = \left[\frac{1}{B_1}\left(\frac{C_i D^\gamma}{C_o}\right)\right]^{1/(1+n)} [y^+_{1/2}]^{(1+\gamma)/(1+n)} \tag{5.98}$$

so $Y_{1/2}$ can be obtained directly for each selected value of $y^+_{1/2}$. Moreover, from equations 5.97, 5.86, and 5.31 it can also be shown that

$$\frac{dY_{1/2}}{dX} = \left[\frac{-1}{(1+2n)I_2}\right]\left(\frac{C_o}{C_i}\right)^{2/(1+\gamma)} [DB_1 Y_{1/2}^{(1+n)}]^{-2\gamma/(1+\gamma)} \tag{5.99}$$

Note especially the appearance of B_1 in equation 5.99. This is the only way for the source dependence of $y_{1/2}$ and U_m to influence the growth rate calculation if n is assumed universal. As noted in Section 5.5, it is not at all clear whether B_1 is universal.

A finite difference estimate of $dY_{1/2}/dX$ is given by

$$\frac{dY_{1/2}(X)}{dX} \approx \frac{Y_{1/2}(X+\Delta X) - Y_{1/2}(X)}{\Delta X} \tag{5.100}$$

From this $X - X_o$ can be readily obtained by summing the ΔX estimated from

$$\Delta X = \frac{Y_{1/2}(X+\Delta X) - Y_{1/2}(X)}{dY_{1/2}/dX} \tag{5.101}$$

where for each incremental increase in the value of $y^+_{1/2}$ from a small value, the values of $Y_{1/2}$ are obtained from equation 5.98 and $dY_{1/2}/dX$ from equation 5.100. Note that X_o is a possible virtual origin chosen to be zero for the computations shown in Figure 22. The results shown were obtained by starting at $y^+_{1/2} = 40$ and using increments of $\Delta y^+_{1/2} = 10$.

Figure 22 shows the calculated variation of $Y_{1/2}$ versus X for the using the values of $B_1 = 1.85$ and $n = -0.528$ determined in Section 5.5. Also shown are the KEP, AJL and WKH data. There is excellent agreement between data and theory[6]. It is straightforward to convert this $Y_{1/2}$ versus X information to $y_{1/2}/b$ versus x/b using equation 5.33 and the definitions of $Y_{1/2}$ and X, at least for a top-hat profile source, but the results depend B_1 and hence on source Reynolds number as noted in Section 5.5.

The velocity maxima can readily be calculated as a function of x once the x-variation of $y_{1/2}$ is known using equation 5.31. The calculated results using $B_1 = 1.85$ are shown in Figure 24, along with the experimental data of KEP, AJL and WKH. The experiments and theory are in reasonable agreement. Note that the agreement

[6]Especially if the errors for hot-wires in high intensity turbulence are taken into account.

for each individual data set is considerably improved if the optimum values of B_1 for each data set are used. As noted above, the uncertainty of the hot-wire data does not seem to warrant this tinkering.

As noted above, it has long been customary to fit power laws to wall jet data. In fact, power law expressions for $y_{1/2}$ and U_m as functions of x can be obtained by assuming the parameters C_i, C_o and γ to be *locally constant*. These, of course, are not valid for the entire range of x, but are useful in understanding such fits from earlier experiments. If this assumption is made, then the dependence of C_i, C_o and γ on y^+ can be ignored, and equation 5.99 can be integrated directly to yield

$$Y_{1/2} = B_{2,local}(X - X_o)^{(1+\gamma)/(1+3\gamma+2n\gamma)} \tag{5.102}$$

where

$$B_{2,local} \equiv \left\{ \frac{-(1+3\gamma+2n\gamma)}{(1+\gamma)(1+2n)I_2} \left(\frac{C_o}{C_i}\right)^{2/(1+\gamma)} (DB_1)^{-2\gamma/(1+\gamma)} \right\}^{(1+\gamma)/(1+3\gamma+2n\gamma)} \tag{5.103}$$

and X_o is a virtual origin which depends on the Reynolds number range under consideration. Note that there would be an additional Reynolds number dependence in the coefficient if $y_{1/2}/b$ and x/b had been used instead of $Y_{1/2}$ and X.

If the parameters are evaluated at $y^+_{1/2} = 1500$ (which corresponds approximately to the KEP experiment at $x/b = 100$), then $C_o/C_i = 0.12$, and $\gamma = 0.109$. Thus *locally*, $Y_{1/2} = 0.515(X - X_o)^{0.915}$. This exponent is exactly that obtained by AJL, and very much in the range observed by WKH and Narasimha et al. 1973. The coefficient is quite different, however, indicating that the virtual origin must be quite large and negative, in fact nearly as large as x/b itself to achieve estimates in reasonable agreement with the data. The fact that these are only *local* estimates means that the power will increase as higher local Reynolds numbers are achieved, as will the magnitude of the virtual origin required. Recall that no virtual origin at all was required in the numerical integration above which made no assumptions about the

constancy of the parameters, but evaluated them at each step in the integration.

Finally, it is easy to show that the true asymptotic behavior is indeed a power law. Like the friction law, however, this asymptotic will be achieved at Reynolds numbers far above those of current experiments. In the limit as $y^+_{1/2} \to \infty$, all the parameters are exactly constant, so *in this limit equation 5.103 represents the exact asymptotic variation of* $Y_{1/2}$. Using $n = -0.528$, $I_2 = 0.78$, $\gamma_\infty = 0.0362$, $C_{o\infty}/C_{i\infty} = 0.023$ and $B_1 = 1.85$ yields $B_{2\infty} = 0.019$ and the exponent is 0.97. Thus the asymptotic variation of $Y_{1/2}$ with X is nearly linear, but not quite. The difference from linear behavior is quite important, however, since as shown above it is a consequence of the continuing momentum loss to the wall. And even this relation depends on the value of B_1, and hence perhaps the source conditions. Note that this limiting power law growth rate cannot be achieved until the friction law has achieved its asymptotic power law; namely when the inequality of equation 5.92 is satisfied.

5.16 Implications of the Continuity Equation

The averaged continuity equation can be integrated from the wall to y to obtain

$$V = -\int_0^y \frac{\partial U}{\partial x} dy' \tag{5.104}$$

It follows immediately that

$$V_\infty = -\int_0^\infty \frac{\partial U}{\partial x} dy' \tag{5.105}$$

Obviously any attempt to realize a plane wall jet must satisfy these equations. In general they are difficult to apply, however, because of the x-derivatives. As will be shown below, similarity simplifies this process considerably so that continuity can be used both to verify the two-dimensionality of the flow and to provide further evidence that the flow is indeed similar and the measurements of it are correct.

The *outer variables* version of the continuity equation can be easily derived by

substituting equation 5.28 to obtain

$$\frac{V}{U_m} = \left[\frac{dy_{1/2}}{dx}\right]\overline{y}f_o(\overline{y}, y^+_{1/2}) \quad - \quad \left[\frac{y_{1/2}}{U_m}\frac{dU_m}{dx} + \frac{dy_{1/2}}{dx}\right]\int_0^{\overline{y}} f_o(\xi, y^+_{1/2})d\xi \quad (5.106)$$
$$- \quad \left[y_{1/2}\frac{dy^+_{1/2}}{dx}\right]\frac{\partial}{\partial y^+_{1/2}}\int_0^{\overline{y}} f_o(\xi, y^+_{1/2})d\xi$$

Note that this equation is valid for all values of $\overline{y}$ as long as $y^+_{1/2}$ is finite.

Since f_o is a similarity solution of the outer equations as $y^+_{1/2} \to \infty$ (i.e., $f_o \to f_{o\infty}$) the last integral is Reynolds number independent in the limit; hence the last term vanishes in the limit. Thus in the limit, the velocity profile in the outer region of the flow must satisfy

$$\frac{V}{U_m}\left[\frac{dy_{1/2}}{dx}\right]^{-1} = \overline{y}f_{o\infty}(\overline{y}) - (1+n)\int_0^{\overline{y}} f_{o\infty}(\xi)d\xi \quad (5.107)$$

where equation 5.95 has been to used to relate dU_m/dx to $dy_{1/2}/dx$. It follows immediately that in the same limit, the entrainment velocity is given by

$$\frac{V_\infty}{U_m} = -(1+n)I_1\left[\frac{dy_{1/2}}{dx}\right] \quad (5.108)$$

where

$$I_1 \equiv \int_0^\infty f_{o\infty}(\xi)d\xi \quad (5.109)$$

Note that since from equation 5.97 $dy_{1/2}/dx$ depends on $y^+_{1//2}$, so does V_∞/U_m. On the other hand, if the value of n (and hence the corresponding mean velocity profiles) are universal, then the ratio $(V_\infty/U_m)/[dy_{1/2}/dx]$ must be a universal constant.

The integral, I_1, in equation 5.109 was estimated from the KEP data by averaging the integral of U/U_m for $x/b = 40, 70$, and 100; the result was $I_1 \approx 1.05$ to within 2%. The value of $n = -0.528$ was obtained using the integral momentum equation as described in Section 5.15 above. Using these, the calculated value of $(V_\infty/U_m)/[dy_{1/2}/dx]$ for the KEP data is 0.50, This can be compared to the ratios

inferred from the measurements using the local estimates of V_∞/U_m and $dy_{1/2}/dx$ which were $-0.47, -0.48, -0.55$, and -0.71 for positions $x/b = 40, 70, 100$, and 150 respectively. Clearly the value for $x/b = 150$ differs substantially from the rest, but so does the value of I_1 there which increases to 1.10. Both of these are clear indicators that similarity is breaking down because of either a lack of two-dimensionality, or a return flow, or both.

If the flow satisfies the similarity conditions, then the profile of V/U_m in the *outer region* should collapse when normalized by either $dy_{1/2}/dx$ or u_*^2/U_m^2. In the KEP experiment the latter are determined with more accuracy than the former because the excellent resolution of the measurements near the wall. Figure 25 shows the actual profiles of $(V/U_m)/(u_*^2/U_m^2)$. Also shown are the profiles calculated from equation 5.107 using the values of n and I_1 cited above, and from integrating the U/U_m profile for the $x/b = 70$ position. The agreement between the measured and calculated peak values is within 10% for $x/b = 40, 70$ and 100, but the relative error increases to nearly 30% for $x/b = 150$. Also shown on the plot as a horizontal dashed line is the theoretical limiting value given by

$$\frac{V_\infty/U_m}{u_*^2/U_m^2} = \frac{(1+n)I_1}{(1+2n)I_2} \tag{5.110}$$

Using the values cited above yields $(V_\infty/U_m)/(u_*^2/U_m^2) = -11.3$ (which corresponds to the value estimated above of $(V_\infty/U_m)/[dy_{1/2}/dx] = -0.50$).

The discrepancy between the measured and calculated profiles at $y/b = 40$ can in part be attributed to the Reynolds number dependent terms in equation 5.107 which are not yet negligible since the flow is still developing. Such is not the case beyond $x/b = 100$ where the outermost data show substantial development with distance, thus providing additional evidence that the return flow in the facility is beginning to affect the wall jet part of the flow as noted above.

Another part of the discrepancies must be attributed to measurement errors. EKP have noted that since the values of V are very small compared to U, a very tiny

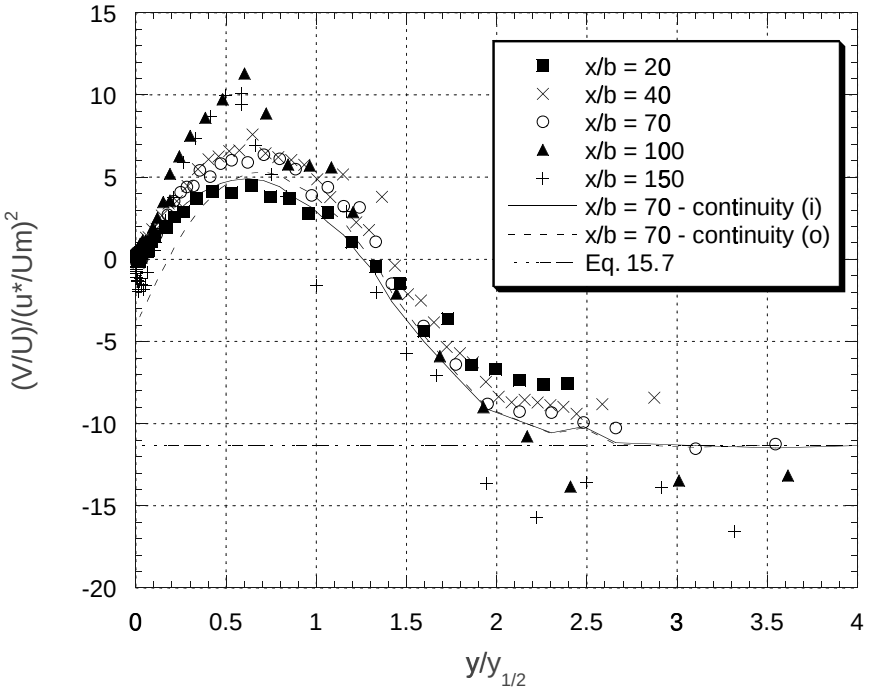

Figure 25: Profiles of $V/U_m/(u_*^2/U_m^2)$; KEP data, theory: $n = -0.528, I_1 = 1.05$. Figure provided by J. Eriksson (see also George *et al.* 2000).

error in the angle between the beams of an LDA system can make a large error in the determination of V. For example, a change in the beam angle of only 0.3 degrees makes about a 10% difference in the V-profiles. Therefore, in cases where similarity behavior has been established using the U-velocity profile, the V-profiles calculated from similarity may be considered more accurate than those measured. This is a wonderful example of how the theory can be used to refine the measurement parameters, *as long as both two-dimensionality and similarity have been established.*

The inner part of the wall jet can also be considered by using the inner scaled profile of equation 5.16. It is straightforward to show that

$$\frac{V}{u_*} = -\left[\frac{\eta}{u_*}\frac{du_*}{dx}\right] y^+ f_i(y^+) - \eta \frac{dy_{1/2}^+}{dx}\frac{d}{dy_{1/2}^+}\int_0^{y^+} f_i(\xi, y_{1/2}^+)d\xi \qquad (5.111)$$

In the limit as $y^+_{1/2} \to \infty$ this reduces to

$$\frac{V}{u_*} = -\left[\frac{\eta}{u_*}\frac{du_*}{dx}\right] y^+ f_i(y^+) \tag{5.112}$$

It is easy to show that from a Taylor expansion and the inner momentum equation that the velocity very near the wall is given by $u^+ = y^+ + c_4 y^{+4} + \cdots$ and $v^+ = e_2 y^{+2} + e_3 y^{+3} + \cdots$ (v. Monin and Yaglom 1971). It follows immediately from equation 5.112 that

$$v^+ = -\left[\frac{\eta}{u_*}\frac{du_*}{dx}\right] [y^{+2} + c_4 y^{+5} + \cdots] \tag{5.113}$$

Thus $e_2 = [(\eta/u_*)/(du*/dx)]$, $e_3 = e_4 = 0$ and $e_5 = c_4[(\eta/u_*)/(du*/dx)]$. Interestingly, e_2 and e_5 are Reynolds number dependent, contrary to the usual assumptions that they are constant.

By using the friction law derived, equation 5.86, together with the similarity condition of equation 5.24, it can be shown after some manipulation that

$$\frac{\eta}{u_*}\frac{du_*}{dx} = \left[\frac{n-\gamma}{1+\gamma}\right]\frac{1}{y^+_{1/2}}\frac{dy_{1/2}}{dx} \tag{5.114}$$

or using equation 5.97 derived in Section 5.15,

$$\frac{\eta}{u_*}\frac{du_*}{dx} = -\left[\frac{n-\gamma}{1+\gamma}\right]\left[\frac{1}{(1+2n)I_2 y^+_{1/2}}\right]\left(\frac{u_*}{U_m}\right)^2 \tag{5.115}$$

Given the experimental difficulties in obtaining mean V-velocity data so close to the wall (both because of its very small magnitude and the proximity of the wall), the velocity calculated from equations 5.112 using 5.115 is probably the only way V can be obtained here. This is an excellent example of how theory can be used to obtain indirectly a result which is not measurable at all.

5.17 Summary and Conclusions

A new theory has been set forth based on the Asymptotic Invariance Principle in which the outer wall jet is governed by different scaling parameters than commonly believed. In particular, the Reynolds shear stress in the outer layer scales to first order with u_*^2, so that the outer layer is governed by two velocity scales, U_m and u_*. Both inner and outer regions become asymptotically independent of the Reynolds number, and reduce to similarity solutions of the inner and outer boundary layer equations in the limit of infinite Reynolds number. A consequence of this is that *no scaling laws can perfectly collapse the data at finite Reynolds number.*

By examining the inner and outer velocity profiles using Near-Asymptotics, the velocity in the overlap layer was shown to exhibit power law behavior, but with an exponent which was only asymptotically constant. This overlap region is not Reynolds number invariant in either inner or outer variables, contrary to common belief, but consistent with recent experimental findings. Another consequence of the analysis was that the friction coefficient varied as a power of the local Reynolds number, the power and coefficients being entirely determined by the velocity parameters, or vice versa. New scaling laws for the turbulence quantities in the outer layer were also derived from similarity considerations of the turbulence Reynolds stress equations. The theory was shown to be in excellent agreement with the all the experimental data. In addition, the hypothesis that the inner flow of the zero pressure gradient boundary layer and the wall jet are the same appears to be supported.

At the very least, a strong motivation has been provided for a careful re-analysis of the older experiments, and perhaps a new generation of experiments over the entire range of Reynolds numbers. Of particular interest will be determining whether there are features of the initial conditions which are preserved, and what exactly are the asymptotic values of the parameters. The success of the theory in correlating the observations to-date, all of which were made before the theory was deduced, lends considerable credibility to the AIP approach to similarity.

Chapter 6

Thermal Boundary Layers

From an endless beach of reality, we take a grain of sand and call it the world.

– Robert Pirsig, author of "Zen and the Art of Motorcycle Maintenance"

6.1 Introduction

In this chapter, the similarity analysis of appendix A (see also George & Castillo (1997), George *et al.* (1996)) for the isothermal zero pressure-gradient turbulent boundary layer on a flat plate will be extended to the thermal boundary layer of forced convection.

The classical scaling laws for the forced convection boundary layer temperature profile (c.f. Monin & Yaglom, 1971) are:

$$\frac{T - T_w}{T_i} = f_i(y^+, Pr) \tag{6.1}$$

$$\frac{T - T_\infty}{T_o} = f_o(\overline{y}, Pr) \tag{6.2}$$

where

$$y^+ \equiv \frac{y}{\eta} \quad \text{with: } \eta = \frac{\nu}{u_*} \qquad \text{and } T_i = T_o = \frac{F_w}{u_*} \tag{6.3}$$

This scaling leads to a logarithmic temperature profile in the overlap region

$$\frac{T_w - T}{T_i} = \frac{1}{\alpha_T \kappa} \ln y^+ + A_i' \tag{6.4}$$

$$\frac{T - T_\infty}{T_o} = \frac{1}{\alpha_T \kappa} \ln \overline{y} + A_o' \tag{6.5}$$

and to a logarithmic heat transfer law

$$St_*^{-1} = \frac{(T_w - T_\infty) u_*}{F_w} = \frac{1}{\alpha_T \kappa} \ln \delta^+ + (A_i' - A_o') \tag{6.6}$$

There have been problems with the classical scaling laws. For example, Bradshaw & Huang (1995) summarize mounting evidence that the classical theory is, in fact, wrong. The most serious evidence is that a logarithmic region of the temperature profile is very limited and does not increase with Reynolds/Péclét number, as a proper overlap solution should[1]. Moreover, the constants appear not to be universal constants.

These problems have been very difficult to detect, because almost no experiments measure τ_w or $F_w = q_w/\rho\ c_p$ directly. They instead assume the classical theory to be correct, the constants to be universal, and adjust τ_w and F_w to get the best log fits to velocity and temperature profiles. As for the ZPG-TBL, this is clearly a logical fallacy.

In the following sections, the new theory for the thermal boundary layer will be outlined. It is a straightforward extension of the results for the momentum boundary layer, which is presented in chapter 3. This work shows that

- The classical theory is *inconsistent* with the Reynolds-averaged Navier-Stokes and thermal energy equations. Therefore the suspicions of Bradshaw and Huang were justified – the classical theory *cannot* be correct!

[1] Bradshaw & Huang (1995) note that although a point of tangency to the log law can always be found, that point is moving with Reynolds number.

- A new theory is proposed which is consistent with the averaged Navier-Stokes and thermal energy equations.
- The new theory appears to be in excellent agreement with the limited data available where the heat flux was actually measured.

6.1.1 A Note on Thermal Boundary Layer Data

Unfortunately, there are not many thermal boundary layer data sets where temperature is a passive scalar in a zero pressure pressure gradient flow. Of the ones available, only one was found to have measured the heat flux directly *and* have all the necessary velocity and temperature information. This was the experiment performed by Reynolds *et al.* (1958). Even in this experiment the boundary layer flow was not exactly zero pressure gradient — it exhibited a slight adverse pressure gradient.

Fortunately, Castillo & George (2000) (see also Castillo, 1997) extended the theory to include boundary layers with imposed pressure gradient. These boundary layers were shown to be uniquely described by a single equilibrium parameter[2], $\Lambda = [\delta/\rho U_\infty^2 d\delta/dx] dP_\infty/dx$, derived from a similarity condition on the Euler equation outside the boundary layer, which reduces to the Clauser parameter in the limit of infinite Reynolds number. This will be of importance here, since the weak pressure gradients the analyzed data sets exhibited were nonetheless strong enough to introduce a 12-15% error into the momentum integral, when not accounted for. The shear stress data of Reynolds *et al.* (1958) were corrected using the momentum integral for the change in free stream velocity (pressure gradient), then parameters were calculated according to the theory outlined in appendix A (see also Castillo, 1997).

[2]Surprisingly — and contrary to earlier attempts to analyze such boundary layers —nearly all the measurements either conform to the new equilibrium definition, or show evidence of moving from one equilibrium state to another. Thus similarity techniques, with the definition of the equilibrium parameter used here, seem to describe a large portion of the available measurements, contrary to the conventional wisdom.

6.2 The Thermal Boundary Layer Equations

Consider the thermal boundary layer formed by flow over a heated surface (c.f. Figure 1). The effects of buoyancy will be assumed negligible, as will those due to the variation of thermal properties with temperature. The temperature effectively acts as a passive scalar entirely driven by conduction and the velocity field.

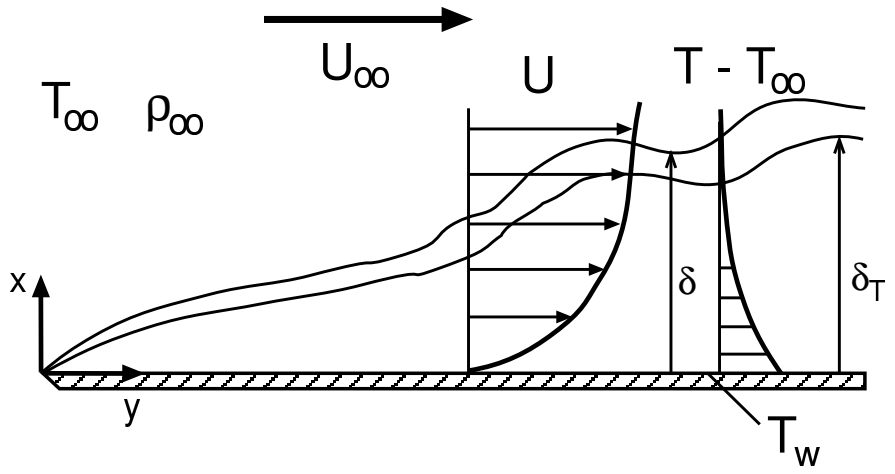

Figure 1: Definition sketch for the thermal boundary layer.

It is well-known that at high Reynolds and Péclét numbers, the conduction term is negligible over most of the boundary layer, so the outer thermal equation reduces to

$$U\frac{\partial(T-T_\infty)}{\partial x}+V\frac{\partial(T-T_\infty)}{\partial y}=-\frac{\partial<vt>}{\partial y} \tag{6.7}$$

where the ambient field is assumed to be at uniform temperature and can thus be subtracted $T_\infty = const.$.

Near the wall the conduction term must remain so that the wall boundary condition can be satisfied. A consequence of the re-scaling necessary to keep it is that the convection terms can be shown to be negligible near the near wall, so the thermal

equation there reduces to

$$0 = \frac{\partial}{\partial y}\left[- < vt > + \alpha \frac{\partial (T - T_\infty)}{\partial y} \right] \tag{6.8}$$

The inner and outer equations, equations 6.7 and 6.8, are exact in the limit as the Reynolds and Peclet numbers go to infinity ($Re \to \infty$, $Pe \to \infty$).

Equation 6.8 can be integrated from the wall to yield

$$-F_w = - < vt > + \alpha \frac{\partial (T - T_\infty)}{\partial y} \tag{6.9}$$

where F_w is the flux parameter defined by

$$F_w = \frac{q_w}{\rho c_p} = -\frac{k}{\rho c_p} \left. \frac{\partial T}{\partial y} \right|_{y=0} \tag{6.10}$$

and q_w represents the wall heat flux. In general, q_w and the wall temperature T_w are x-dependent.

6.3 Similarity Analysis of the Near-wall Region

The Asymptotic Invariance Principle (AIP, section 2.3) requires that properly scaled inner and outer profiles reduce to similarity solutions of the inner and outer equations in the limit as Reynolds and Peclet numbers go to infinity (i.e., the limit in which the equations themselves are valid). Thus for the inner equations similarity solutions are sought of the form

$$T - T_\infty = T_{si} g_i({y^+}_T, \delta_T^+, Pr) \tag{6.11}$$

$$- < vt > = F_{si} h_i({y^+}_T, \delta_T^+, Pr) \tag{6.12}$$

where

$$y^+{}_T \equiv \frac{y}{\eta_T} \tag{6.13}$$

and η_T is a length scale which remains to be determined. The parameter δ_T^+ is the ratio of outer to inner length scales and remains to be defined. It can be shown *a posteriori* that $\delta_T^+ \to \infty$ as $R_x \to \infty$. The non-zero boundary conditions are given by

$$T - T_\infty = T_w - T_\infty \equiv \Delta T_w \tag{6.14}$$

at $y = 0$, and

$$-\overline{vt} \to F_w \tag{6.15}$$

as $y \to \infty$. The last condition is only true in the limit as $\delta_T^+ \to \infty$, which insures that the outer flow is never reached so the inner equation is never invalid (at least in inner variables).

Substitution into equation 6.9 and dividing by F_w shows that similarity solutions are possible only if

$$F_{si} \sim F_w, \tag{6.16}$$

$$T_{si} \sim \Delta T_w \tag{6.17}$$

and

$$\eta_T \sim \frac{\alpha \Delta T_w}{F_w} \tag{6.18}$$

Note that the symbol '$\sim$' does not mean order of magnitude, but rather 'has the same x-dependence as'. These can be taken as equalities without loss of generality, and thus the inner scales are defined.

These results are quite different from the classical law of the wall for thermal boundary layers; here it is deduced and does not depend simply on dimensional analysis or empirical scaling. Note that as long as the argument δ_T is finite, the profile of equation 6.11 is simply a scaled temperature profile for the entire boundary

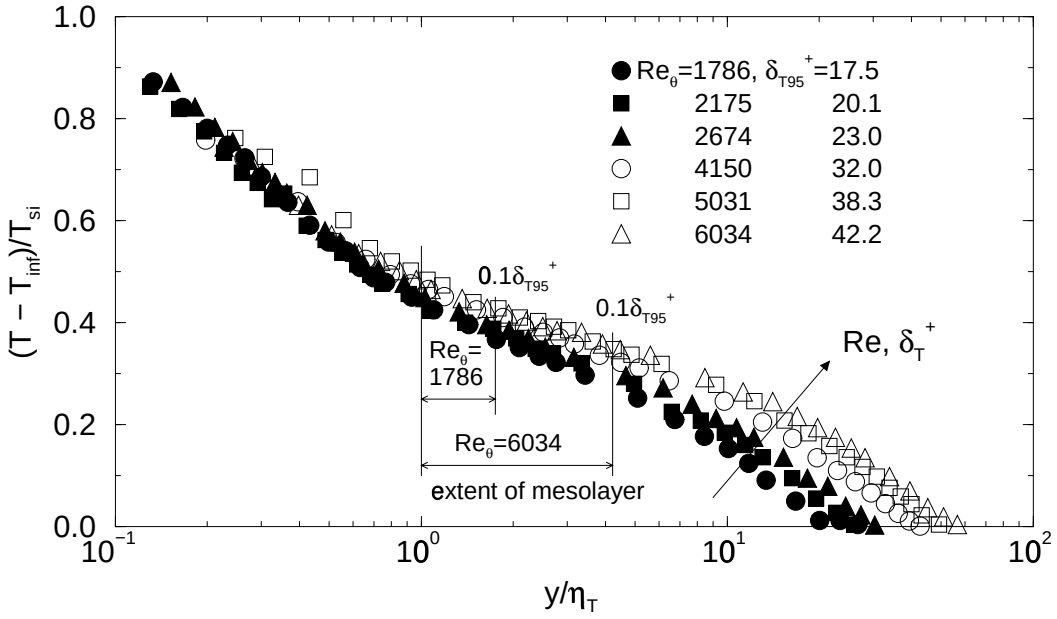

Figure 2: Mean temperature data for thermal boundary layer in inner variables. Data of Reynolds *et al.* (1958)

layer. Only in the limit of infinite δ_T^+ does it lose the ability to describe the outer flow and become an inner solution.

Figure 2 shows six of the temperature profiles measured by Reynolds, Kays & Kline (1958) normalized in the inner variables derived here. The data were taken at two different values of the free stream velocity for three positions along the surface. Note the excellent collapse near the wall for all the data, the slight dependence on Reynolds number in what will be identified later as the overlap region, and the departure from similarity in the outermost region. Particularly noteworthy is the dramatic difference between the two sets of measurements outside the near wall region, clearly suggesting a dependence on initial conditions.

6.4 Similarity Analysis of the Outer Flow

Application of the AIP to the outer flow is carried out in the same manner. Solutions are sought of the form

$$T - T_\infty = T_{so} g_o(\overline{y}_T, \delta_T^+, Pr) \tag{6.19}$$

$$- < vt > = F_{so} h_o(\overline{y}_T, \delta_T^+, Pr) \tag{6.20}$$

where

$$\overline{y}_T = y/\delta_T \tag{6.21}$$

and δ_T remains to be determined. Note that the dependence of the outer solutions on δ_T^+ might be expected to vanish in the limit as $\delta_T^+ \to \infty$, and that of the Prandtl number as well. The result for the outer velocity from George & Castillo (1997) must also be utilized; it is

$$U = U_\infty[1 + f_o(\overline{y}, \delta^+)] \tag{6.22}$$

where

$$\overline{y} = \frac{y}{\delta} \tag{6.23}$$

Substitution into equation 6.7 and dividing by $U_\infty T_{so}/\delta_T$ shows that the necessary conditions for similarity are:

$$\frac{d\delta}{dx} \sim \frac{d\delta_T}{dx} \sim \frac{F_{so}}{U_\infty T_{so}} \sim \frac{\delta_T}{T_{so}} \frac{dT_{so}}{dx} \sim \frac{\delta}{U_\infty} \frac{dU_\infty}{dx} \tag{6.24}$$

The last condition involving U_∞ applies only if the free stream speed is varying (i.e., $dP_\infty/dx \neq 0$).

Thus it is clear that both the thermal and momentum boundary layer thickness have the same x-dependence, and can at most differ by a constant (or alternatively, have different virtual origins). Again, note that there is no suggestion in either the outer thermal or the momentum boundary governing equations that the outer flow

might be independent of initial (or upstream) conditions.

Also it is immediately obvious that

$$F_{so} \sim U_\infty T_{so} \frac{d\delta}{dx} \sim U_\infty T_{so} \frac{d\delta_T}{dx} \tag{6.25}$$

This condition on T_{so} will be examined later and shown to yield the outer temperature scale.

6.5 The Outer Temperature Scale

Equation 6.25 is the thermal counterpart to the similarity condition on the Reynolds stress in the outer layer of the momentum boundary layer; namely, $R_{so} \sim U_\infty^2 d\delta/dx$ (eqn. A.39). Since the heat flux across the inner layer is constant and equal to F_w (but only in the limit of infinite Peclet number), it provides an inner boundary condition on the heat flux, so

$$U_\infty T_{so} \frac{d\delta_T}{dx} \sim F_{so} \sim F_w \tag{6.26}$$

The coefficient in equation 6.26 is dependent on Peclet number, but asymptotically constant. A similar argument for the Reynolds stress in the outer layer yielded

$$R_{so} \sim U_\infty^2 \frac{d\delta}{dx} \sim u_*^2, \tag{6.27}$$

again with a Reynolds number dependent coefficient which was constant in the limit. An interesting consequence of this is that for finite U_∞ and finite T_{so}, $F_w \sim u_*^2$ is the only possibility as $x \to \infty$. Thus $F_w \to f(\Delta T)\ \tau_w$.

It follows immediately from equations 6.24, 6.26 and 6.27 that the outer temperature scale which reduces to the proper limit (as the Péclét number $Pe \to \infty$) is given by

$$T_{so} = T_{si} \frac{U_\infty}{u_*} = \frac{F_w}{u_*} \left(\frac{U_\infty}{u_*} \right) \tag{6.28}$$

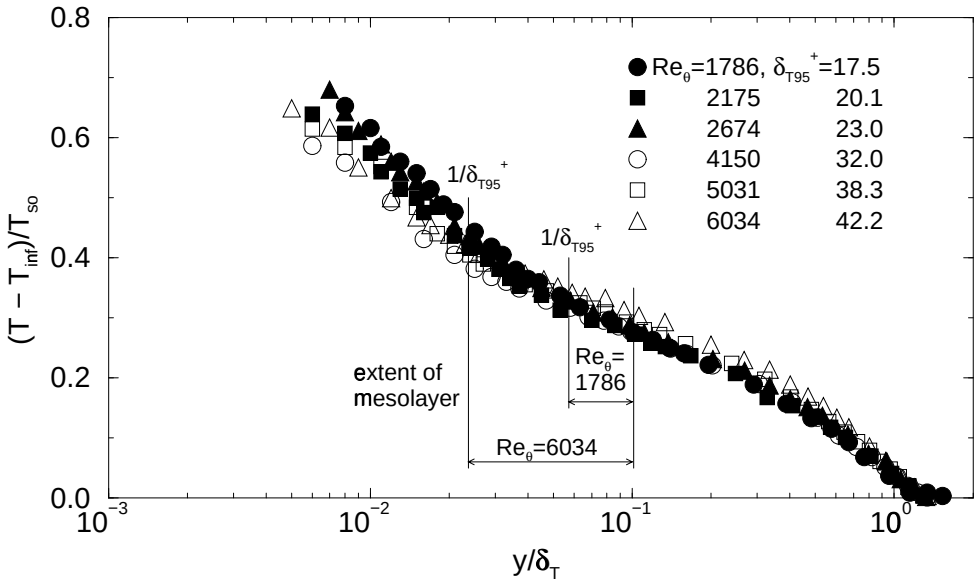

Figure 3: Mean temperature data for thermal boundary layer in outer variables. Data of Reynolds *et al.* (1958)

Thus

$$\frac{T_{so}}{T_{si}} = \frac{F_w}{u_* \Delta T_w} \frac{U_\infty}{u_*} \equiv H \tag{6.29}$$

The parameter H can easily be shown to be related to the Stanton number star, St_*, and the Stanton number, St, by

$$H = St_* \sqrt{\frac{2}{c_f}} = \frac{2St}{c_f} \tag{6.30}$$

where c_f is the friction coefficient.

Figure 3 shows the same data as figure 2, now normalized in outer variables. The value of δ_T was taken as the y-location where the temperature had dropped to $0.10(T_w - T_\infty)$. The friction velocity was computed from the momentum integral equation, which included a correction for the slight adverse pressure gradient in the tunnel. The data clearly collapse well over the outer part of the flow as long as the upstream conditions are fixed. They show the same differences in the overlap region for the two different sets, however, just as for the inner scaled profiles above. Whether

this is a consequence of the Reynolds number dependence of the overlap region, or the effect of upstream conditions was discussed in chapter 3.

6.6 The Overlap Region of the Temperature Profiles

In the limit as the Péclét number becomes infinite, the ratio of outer to inner length scale also becomes infinite. Thus, although at finite Péclét numbers, both of the scaled profiles of equation 6.11 and 6.19 can describe the temperature profile everywhere (because of their dependence on δ_T^+), in the limit the inner cannot describe the outer region, nor the outer the region closest to the wall. There might, however, exist an overlap region in which both inner and outer scalings work in the limit. This can indeed be shown to be the case by the methodology of George and Castillo 1997 which makes clear the Reynolds and Prandtl number dependence of the parameters.

By applying the Asymptotic Invariance Principle (AIP) and Near-Asymptotics (methodoloy as outlined in chapter 2) it can be shown (after some manipulation) that the inner temperature profile is given by

$$g_i({y^+}_T, \delta_T^+, Pr) = A_i({y^+}_T + a^+)^{\gamma_T} \tag{6.31}$$

where $A_i = A_i(\delta_T^+, Pr)$ and $\gamma_T(\delta_T^+)$ is defined as

$$\gamma_T \equiv \frac{\delta_T^+}{H}\frac{dH}{d\delta_T^+} \qquad \text{with:} \quad H \equiv \frac{T_{so}}{T_{si}} \tag{6.32}$$

The parameter a arises from the fact that the results must be independent of the origin in y. The exact behavior of a must be established from experiment (at least at this point), but it is certainly related to the mesolayer and the effects of the low turbulence Reynolds number on the thermal dissipation. For the momentum boundary layer, $a^+ \approx -16$, so that it might be constant for the thermal layer as well.

Similarly, the outer temperature profile can be shown to be given by

$$g_o(\overline{y}_T, \delta_T^+) = A_o(\overline{y}_T + \overline{a})^{\gamma_T} \tag{6.33}$$

where $A_o = A_o(\delta_T^+, Pr)$.

Thus the temperature profile in the overlap region is described by a power law, but not a simple one because of the dependence of the coefficients on δ_T^+. In the limit as $\delta_T^+ \to \infty$, $A_i \to A_{i\infty}$ and $A_o \to A_{o\infty}$. The AIP requires that both $A_{i\infty}$ and $A_{o\infty}$ be asymptotically finite and non-zero, just as for the velocity profile parameters. Moreover, the limiting value of γ_T must be zero to insure a finite local dissipation of temperature fluctuations.

The parameters A_i, A_o, and γ_T must also satisfy a constraint equation given by

$$\ln \delta_T^+ \frac{d\gamma_T}{d \ln \delta_T^+} = \frac{d \ln A_o/A_i}{d \ln \delta_T^+} \tag{6.34}$$

which is similar to the analogous requirement for the momentum boundary layer parameters. The various regions of the turbulent thermal boundary layer are shown in figure 4.

6.7 The Heat Transfer Law

The heat transfer law governing the forced boundary layer can readily be derived by substituting the overlap solutions for g_i and g_o into equations 6.11 and 6.19, then equating the temperatures. The result is:

$$H = \frac{T_{so}}{T_{si}} = \frac{A_i}{A_o} \delta_T^{+\gamma_T} \tag{6.35}$$

or

$$St_* \frac{U_\infty}{u_*} = St \left(\frac{U_\infty}{u_*} \right)^2 = \frac{A_i}{A_o} \delta_T^{+\gamma_T} \tag{6.36}$$

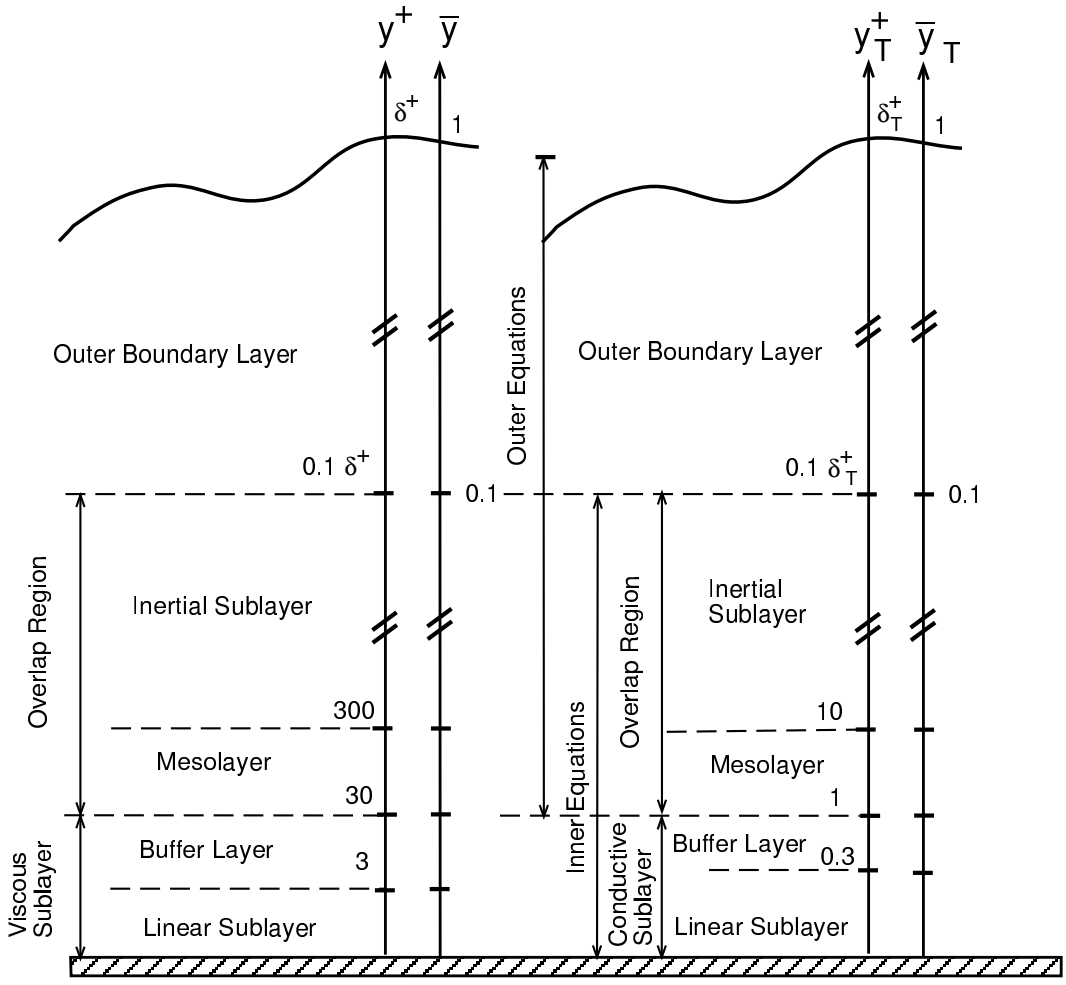

Figure 4: Regions of the turbulent thermal boundary layer.

or using equation A.73

$$St_* = \frac{A_i}{A_o}\frac{C_o}{C_i}\delta_T^{+\gamma_T}\delta^{+-\gamma} \tag{6.37}$$

The ratio of temperature scales H is related to the Stanton number and the friction coefficient c_f by

$$H = St_*\sqrt{\frac{2}{c_f}} = \frac{2St}{c_f} \tag{6.38}$$

It is clear from equation 6.37 that the exact behavior of the Stanton number based on the friction velocity is an interesting interaction between the momentum and thermal boundary layer parameters. If $\gamma_T > \gamma$, St_* increases as the boundary layer grows, whereas St_* decreases if $\gamma_T < \gamma$. On the other hand, if $\gamma_T = \gamma$, then St_* does not change downstream

$$St_* = \frac{F_w}{u_*\Delta T_w} = const. \tag{6.39}$$

There is reason to suspect that this may indeed be the case, at least when both boundary layers have the same effective origin. If so, then the Stanton number is proportional to the friction coefficient, at least asymptotically, just as in the classic Reynolds analogy.[3]

6.8 The Variation of the Parameters with δ_T^+

A solution to equation 6.34 can be written as

$$\frac{A_o}{A_i} = \exp[(\gamma_T - \gamma_{T\infty})\ln\delta_T^+ + h_T] \tag{6.40}$$

[3]These possibilities need to be explored further as more data where both wall shear stress and wall heat flux were measured directly become available.

where the single unknown new function h_T is at most a function of δ_T^+ and the Prandtl number. It follows immediately from equations 6.32 and 6.35 that

$$\gamma_T - \gamma_{T\infty} = -\frac{dh_T}{d\ln\delta_T^+} \tag{6.41}$$

and

$$H = {\delta_T^+}^{\gamma_{T\infty}} e^{-h_T} \tag{6.42}$$

Thus the entire problem is reduced to finding either theoretically or empirically the function h_T.

It is possible to proceed by analogy with the momentum boundary layer and take

$$h_T - h_{T\infty} = \frac{A_T}{(\ln\delta_T^+)^{\alpha_T}} \tag{6.43}$$

where $h_{T\infty} = \ln A_{o\infty}/A_{i\infty}$. If so, then

$$\gamma_T - \gamma_{T\infty} = \frac{\alpha_T A_T}{(\ln\delta_T^+)^{1+\alpha_T}} \tag{6.44}$$

$$\frac{A_o}{A_i} = \frac{A_{o\infty}}{A_{i\infty}} \exp[(1+\alpha_T)A_T/(\ln\delta_T^+)^{\alpha_T}] \tag{6.45}$$

and

$$H = \frac{A_{i\infty}}{A_{o\infty}} {\delta_T^+}^{\gamma_{T\infty}} \exp[-A_T/(\ln\delta_T^+)^{\alpha_T}] \tag{6.46}$$

The heat transfer law and overlap profiles are then entirely specified by $\gamma_{T\infty}$, $A_{i\infty}$, $A_{o\infty}$ and the constants A_T and α_T.

It appears from the data that dependence on δ_T^+ (or δ^+) is of the same form as for the velocity profile, therefore

$$A_i = A_{i\infty} \exp[(1+\alpha)A/(\ln\delta^+)^{\alpha}] \tag{6.47}$$

$$A_o = A_{o\infty} \exp[(1+\alpha)A'/(\ln\delta^+)^{\alpha}] \tag{6.48}$$

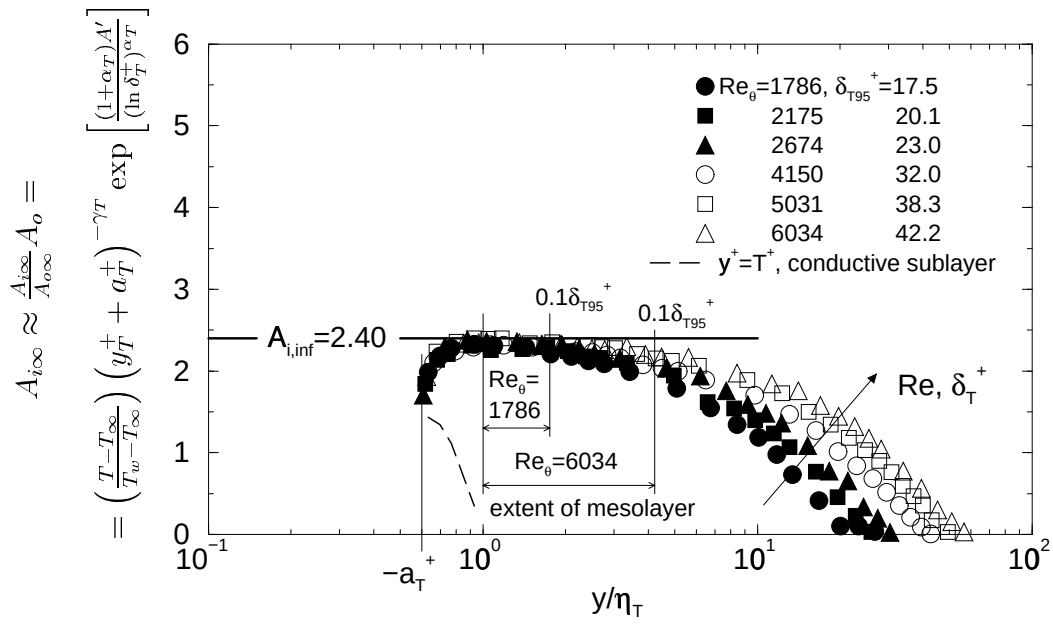

Figure 5: Determination of thermal boundary layer parameter $A_{i\infty}$. Data of Reynolds *et al.* (1958).

The same values as for the momentum boundary layer are used for A and α. Even for the mesolayer constant

$$a_T^+ \approx a^+ \frac{\eta}{\eta_T} \qquad . \tag{6.49}$$

For $C_{i\infty}$, $C_{o\infty}$, γ_∞, A and α the values of George & Castillo (1997) were used. From the data examined here (c.f. Figures 5 and 6) it is found that $A_{i\infty} \approx 2.4$, $A_{o\infty} \approx 2.17$ and $A' = 1.3A$. With $A_{i\infty}$ and $A_{o\infty}$ determined, there are no more adjustable parameters!

A theoretical heat transfer law can then be expressed as:

$$St^{1+\gamma} = \frac{A_{i\infty}}{A_{o\infty}} \left(\frac{\delta_T}{\delta} Pr\right)^{-\gamma} \left(\frac{u_*}{U_\infty}\right)^{2+\gamma} \exp\left[\frac{(1+\alpha)(A'-A)}{(\ln \delta^+)^\alpha}\right] \quad \delta^{+-\gamma} \tag{6.50}$$

with

$$\frac{u_*}{U_\infty} = \frac{C_{o\infty}}{C_{i\infty}} \delta^{+\gamma_\infty} \exp\left[\frac{A}{(\ln \delta^+)^\alpha}\right] \tag{6.51}$$

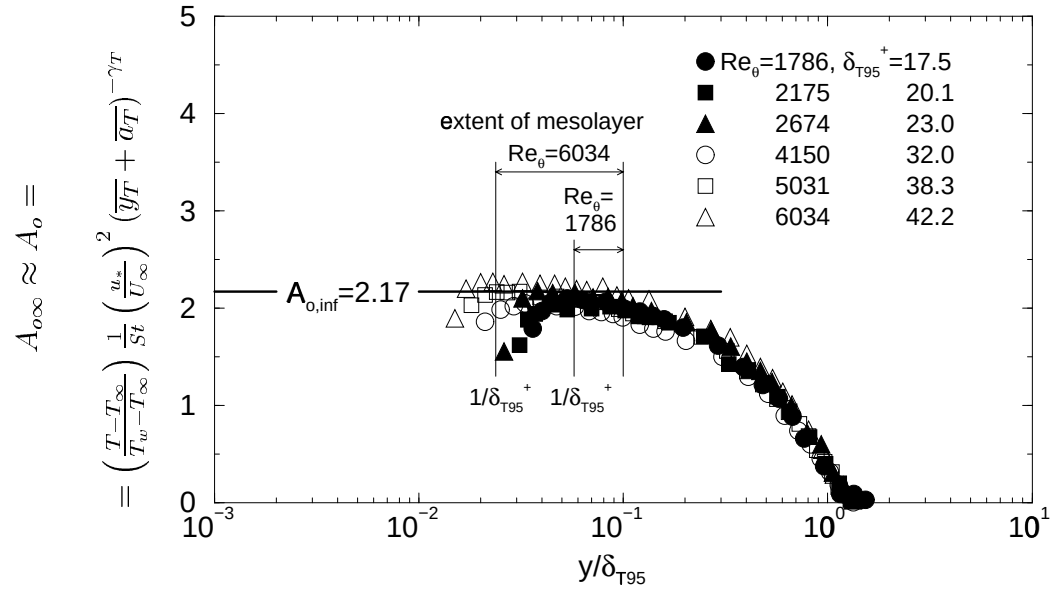

Figure 6: Determination of thermal boundary layer parameter $A_{o\infty}$. Data of Reynolds *et al.* (1958).

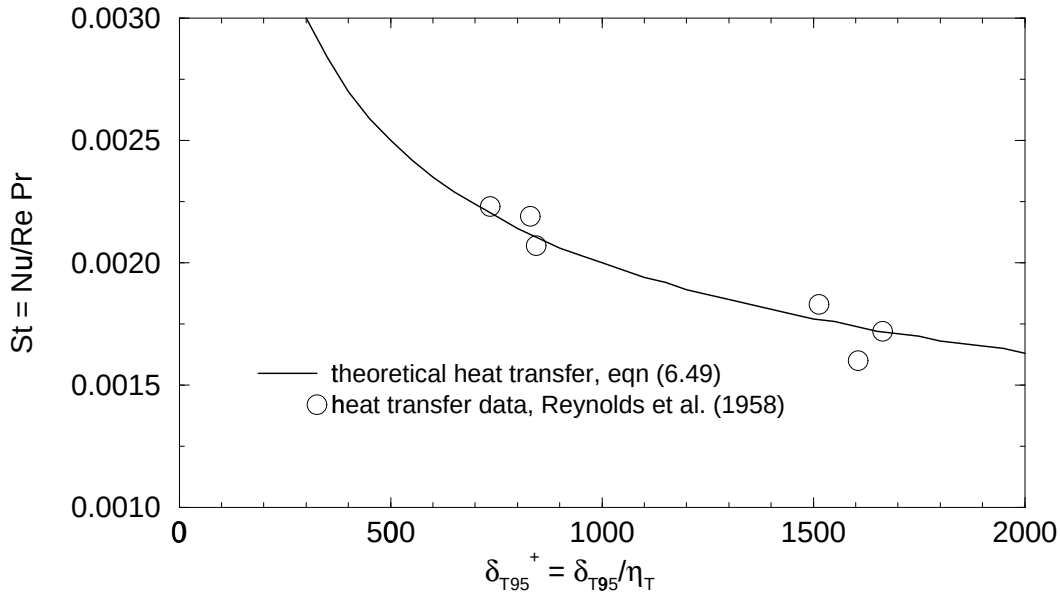

Figure 7: Comparison of heat transfer prediction to data of Reynolds *et al.* (1958).

and

$$-\gamma_T = \gamma = \gamma_\infty + \frac{\alpha A}{(\ln \delta^+)^{1+\alpha}} \qquad . \tag{6.52}$$

Figure 7 shows the heat transfer law of equation 6.50 compared to the data of Reynolds *et al.* (1958).

Future work should attempt to determine the necessary constants to greater accuracy as more and better data and/or simulations become available. In addition, if turbulence data become available, the implications for the scaling of the turbulence quantities should be explored.

Chapter 7

Summary and Conclusions

The eye sees only what the mind is prepared to comprehend.

– Henri-Louis Bergson (1859-1941), French philosopher

7.1 Thesis Summary

The turbulent wall-bounded flows treated in this work were pipe and channel flows, plane wall jets, thermal boundary layers and zero pressure gradient boundary layers.

7.1.1 Pipe and Channel Flow

A new theory for turbulent pipe and channel flows has been developed. Application of the Asymptotic Invariance Principle and deductions from Near-Asymptotics lead to Reynolds number dependent *logarithmic* overlap profiles and a *logarithmic* friction law. These provided an excellent description of the mean velocity and skin friction data from fully-developed channel and pipe flows over more than three and a half decades in Reynolds number.

Unlike developing wall-bounded flows, the Reynolds number dependence of the solution parameters for pipe and channel flows was found to be slight. The *mesolayer* concept, together with the offset a^+, proved crucial in understanding where to apply

the theory. In particular, the overlap mean velocity profile was found not to be a simple logarithm in y, but instead a logarithm in $y+a$. Therefore attempts to establish $\ln y$ behavior using velocity profile data inside $y^+ \approx 300$ are doomed to failure and the results misleading unless the mesolayer (and the offset a^+ in particular) are explicitly accounted for.

7.1.2 Plane Wall Jet

A new theory has been put forth for the plane turbulent wall jet based on a similarity analysis of the governing equations and the Asymptotic Invariance Principle. In this new theory the outer wall jet is governed by different scaling parameters than those commonly believed. In particular, the Reynolds shear stress in the outer layer scales to first order with u_*^2, so that the outer layer is governed by two velocity scales, U_m and u_*. Both inner and outer regions become asymptotically independent of the Reynolds number, and reduce to similarity solutions of the inner and outer boundary layer equations in the limit of infinite Reynolds number. A consequence of this is that *no scaling laws can perfectly collapse the data at finite Reynolds number.* Velocity profiles in the overlap region and the friction law exhibit *power law* behavior, with coefficients which depend on the local Reynolds number.

New scaling laws for the turbulence quantities in the outer layer were also derived from similarity considerations of the turbulence Reynolds stress equations. The theory was shown to be in excellent agreement with the all the experimental data. In addition, the hypothesis that the inner flow of the zero pressure gradient boundary layer and the wall jet are the same, appears to be supported.

7.1.3 Thermal Boundary Layer

The similarity analysis of George & Castillo (1997) for the isothermal zero pressure-gradient turbulent boundary layer on a flat plate has been extended to the thermal boundary layer of forced convection, where temperature acts as passive scalar. In

contrast to the classical scale, a new outer temperature scale was derived, which also depends on the friction law. Temperature profiles in the overlap region and the heat transfer law were *power laws* with Reynolds number dependent coefficients.

A surprising result was — provided the power exponent for the temperature field, γ_T is equal to the γ found by George & Castillo (1997) — that a modified heat transfer law can be written as $St_* = St/(U_\infty/u_*) = const.$, thus asymptotically recovering Reynolds' analogy. Thermal data suited for the determination of the overlap solution parameters is of very limited availability. The values put forth here were based on a single experiment and await confirmation.

7.1.4 Zero Pressure Gradient Turbulent Boundary Layer

The "base case" originally treated by George & Castillo (1997) has been revisited and several new developments have been explored. It was shown that the displacement thickness scaling introduced by Zagarola & Smits (1998*b*) is consistent with the fundamental scaling laws. The Zagarola/Smits scaling was then derived from a separability hypothesis of the George/Castillo velocity deficit.

It was suggested that a modified (outer flow only) displacement thickness, $\tilde{\delta}_*$, integrated for $\overline{y} > 0.1$, might be a better choice for collapsing data in the outer layer. It was shown that δ_*/δ is independent of the local Reynolds number and uniquely determined by the initial/upstream conditions. This implies that fixing a downstream position and varying the free stream velocity is *not* a good way to conduct a boundary layer survey. Even in view of the Zagarola/Smits scaling, the overlap analysis of George/Castillo remains unchanged.

The consequences of a higher order approximation to the solution for the Reynolds number dependence were explored, and shown to have little effect on the friction law.

A modified "power law diagnostic function" much better suited to test the George & Castillo (1997) theory has been suggested, but it was subsequently shown that even this new form is of limited usefulness when sorting boundary layer theories.

7.2 Outlook

While quite a few questions were answered — some quite surprisingly so — other interesting questions arise from the results of this work:

- Is the *mesolayer* parameter a^+ indeed constant as it appears it might be? This will require accurate measurements of the velocity profile near $y^+ = 30$ at considerably higher Reynolds numbers than has been possible to-date. The problem here is not with the overall flow Reynolds number, but with the inability to resolve the flow near the wall at the higher Reynolds numbers due to probe size limitations. An obvious solution is to increase Reynolds number by increasing the size of the experiment — and not by decreasing viscosity or increasing the pressure drop — so less absolute resolution is required at a given Reynolds number.

- The Reynolds number dependence seems to be nearly negligible for channel and pipe, but crucial for boundary layer flows. Is this a subtle consequence of the homogeneity of the former and inhomogeneity of the latter, or is it simply a reflection of the differing inner and outer velocity scales for the boundary layer with the consequent Reynolds number dependence?

- Since there is very little Reynolds number dependence in pipe and channel flows, does the parameter $R^+ = Ru_*/\nu$ contain all the initial/upstream dependence for these flows?

- There are — of course — numerous possibilities to extend the ideas presented here to other flows (e.g., heat transfer in pipe/channel, temperature fluctuations in isotropic turbulence, fully developed turbulent Taylor/Couette flow, buoyancy-driven flows, to name but a few).

- For turbulent boundary layers, does the finding that δ_*/δ is constant for fixed initial/upstream conditions imply that everything that determines the fully de-

veloped turbulent boundary layer is in the transition process? (This certainly destroys the classical view of turbulence theory, i.e. that turbulence always settles into an asymptotic state which is independent of its initial/upstream conditions ...) This could also be of great practical interest, since it implies that we can predict turbulence from knowing how it was generated. It also implies that flow control in turbulent flows, including separation control, should be focused on how a turbulent boundary layer is created (*passive* control, transition process), not on trying to influence the flow downstream (*active* control).

- Why was it not noticed earlier that $\delta_*/\delta = const.$ for fixed initial/upstream conditions?

- Are CTA hot wire and Pitot tube errors in turbulent flows the reason we were lead to believe that δ_*/δ was decreasing with increasing Reynolds number (since measurements are moving through different regions of turbulence intensity)? Both Hussein *et al.* (1994) (using LDA and CTA in free jets) and Eriksson *et al.* (1998) *vs.* Abrahamsson *et al.* (1994) (using LDA and CTA, respectively, in plane wall jets) showed that even a modest turbulence intensity can result in significant differences between the two measuring techniques. This is especially troubling looking at the small differences between competing theories which need to be sorted out.

- In view of the importance of the initial conditions for the outer region of the boundary layer, it is puzzling that it does not seem to have any effect on the overlap region (more investigation is needed here).

- The data in the overlap region of *all* of the wall-bounded flows considered are very much in dispute...

It would be very pleasant if we had simple answers to all these questions, but this does not seem to be the nature of the subject, turbulence...

Appendix A

Review of George/Castillo Theory for Zero Pressure-Gradient Turbulent Boundary Layers

A.1 Introduction

This dissertation largely builds upon the theoretical concepts developed by George and co-workers over the past decade. In this appendix, important results of this approach as applied to the zero pressure-gradient boundary layer are reviewed, closely following George & Castillo (1997). The zero pressure-gradient turbulent boundary layer (a schematic is shown in Figure 1, chapter 3) has been extensively investigated. It has very simple boundary conditions, yet contains the essential physics of the subject of wall-bounded turbulent flows, and is therefore the canonical problem. George & Castillo (1997) state: "... any general principles which apply to it should be applicable to all [wall-bounded flows] — if they are in fact principles and general..."

The problem of the overlap region in this flow and its scaling laws had been generally regarded as solved. For recent reviews of ZPG-TBL, see e.g. Sreenivasan (1989); Gad-el-Hak & Bandyopadhyay (1994); Smits & Dussauge (1996). The analysis of

channel and pipe flow by Millikan (1938), where inner and outer scaling laws (the Law of the Wall and the Velocity Deficit Law) were matched at infinite Reynolds number to obtain logarithmic velocity and friction laws is widely considered to be a classical result of turbulence theory. Clauser (1954), Hama (1954), Coles (1962) and others extended Millikan's arguments to boundary layers — with pressure gradients, roughness and compressibility. These extensions had been accepted without much question for the past few decades. One reason for this has been the apparent agreement of experimental data with the theoretical results[1], although the reviews cited above point out several disagreements and inadequacies.

A.1.1 The Classical Theory and its Shortcomings

The classical approach usually lumps together boundary layers *and* pipe and channel flows and can be found in almost every textbook on fluid mechanics (e.g. White, 1991; Tennekes & Lumley, 1972). It is based on the analysis by Millikan (1938). The inner layer is governed by the *law of the wall* (Prandtl, 1932)

$$\frac{U}{u_*} = f_{i\infty}\left(\frac{yu_*}{\nu}\right) \qquad , \tag{A.1}$$

and for the outer layer a velocity deficit is assumed at the outset as

$$\frac{U - U_\infty}{u_*} = F_{o\infty}\left(\frac{y}{\delta}\right) \qquad . \tag{A.2}$$

Clauser (1954), following Millikan (1938), matched both profiles in the limit of infinite Reynolds number to obtain the familiar logarithmic overlap velocity profile in the

[1] As shown in chapter 3, the difference bewteen a logarithmic overlap velocity profile with constant coefficients, and a power-law (with Reynolds number dependent coefficients) with a mesolayer offset 'a' is smaller than the spread between various sets of data. This is also the case for the velocity derivative, usually plotted as a "power law diagnostic function", Γ, when a modified form, including the off set 'a' $\Gamma^* = (y^+ + a^+)/U^+ dU^+/dy^+$ is used.

overlap region in inner and outer variables

$$\frac{U}{u_*} = \frac{1}{\kappa} ln \left(\frac{y u_*}{\nu} \right) + B \tag{A.3}$$

$$\frac{U - U_\infty}{u_*} = \frac{1}{\kappa} ln \left(\frac{y}{\delta} \right) + B_1 \tag{A.4}$$

and a friction law given by

$$\frac{U_\infty}{u_*} = \sqrt{\frac{2}{c_f}} = \frac{1}{\kappa} ln \delta^+ + (B - B_1) \tag{A.5}$$

where κ, B, and B_1 are presumed to be universal constants, and $\delta^+ \equiv u_* \delta / \nu$.

Some peculiar features of the Millikan/Clauser theory are:

(i) When multiplying equation A.4 by u_*/U_∞

$$\frac{U - U_\infty}{u_*} \frac{u_*}{U_\infty} = F_{o\infty} \left(\frac{y}{\delta} \right) \frac{u_*}{U_\infty} \tag{A.6}$$

substituting equation A.5 and taking the limit $Re \to \infty$

$$\frac{U}{U_\infty} = 1 - F_{o\infty} \left(\frac{y}{\delta} \right) \frac{u_*}{U_\infty} = 1 - F_{o\infty} \left(\frac{y}{\delta} \right) \left[\frac{1}{\kappa} \ln \delta^+ + (B - B_i) \right] \to 1 \tag{A.7}$$

the velocity profile disappears, i.e. $U/U_\infty \to 1$, since $U_\infty / u_* \to \infty$. This might be considered plausible if the limit is approached by increasing the free stream velocity or by decreasing the viscosity,[2] but not if the limit is approached by simply increasing the streamwise distance (i.e., by proceeding along the plate).

(ii) Substituting the inner (A.1) and outer (A.2) scaling laws into the defining integrals for the displacement thickness δ_* and the momentum thickness θ, the

[2]It is, in fact, a zero-viscosity solution.

result is (for large δ^+, contributions from inner layer can be neglected)

$$\frac{\delta_*}{\delta} = \int_0^\infty F_{o\infty} \frac{u_*}{U_\infty} d\left(\frac{y}{\delta}\right) = D_1 \frac{u_*}{U_\infty} \tag{A.8}$$

$$\frac{\theta}{\delta} = \int_0^\infty \left[F_{o\infty} \frac{u_*}{U_\infty} - F_{o\infty}^2 \left(\frac{u_*}{U_\infty}\right)^2\right] d\left(\frac{y}{\delta}\right) = D_1 \frac{u_*}{U_\infty}\left[1 - D_2 \frac{u_*}{U_\infty}\right] \tag{A.9}$$

where D_1 and D_2 should be universal constants. Therefore, as $Re \to \infty$, the outer length scale does not remain proportional to any integral length scale, and blows up relative to them. Boundary layer profiles seem to collapse as well with momentum or displacement thickness as they do when normalized with the boundary layer thickness δ determined from the velocity profile (e.g., δ_{99}).

(iii) The shape factor H

$$H^{-1} = \frac{\theta}{\delta_*} = 1 - \frac{u_*}{U_\infty} \frac{\int_0^\infty F_{o\infty}^2 d\left(\frac{y}{\delta}\right)}{\int_0^\infty F_{o\infty} d\left(\frac{y}{\delta}\right)} \to 1 \tag{A.10}$$

approaches unity in the infinite Reynolds number limit (i.e., $H \equiv \delta_*/\theta \to 1$). No shape factors below about 1.2 have been reported in experiments.

A.2 Governing Equations and Boundary Conditions

George & Castillo (1997) reconsidered the theoretical foundations of the classical analysis (often referred to as the Millikan/Clauser analysis). Using the AIP (c.f. section 2.3) the classical velocity deficit law for the outer layer is shown to be inconsistent with the equations of motion.

The equation governing streamwise mean momentum and boundary conditions of a zero-pressure-gradient turbulent boundary layer (with constant properties) at high

Reynolds number are given by (c.f. Tennekes & Lumley, 1972)

$$U\frac{\partial U}{\partial x}+V\frac{\partial U}{\partial y}=\frac{\partial}{\partial y}\left[-<uv>+\nu\frac{\partial U}{\partial y}\right]-\left\{\frac{\partial}{\partial x}\left[<u^2>-<v^2>\right]\right\} \qquad (A.11)$$

where $U \rightarrow U_\infty$ as $y \rightarrow \infty$ and $U = 0$ at $y = 0$. The $< v^2 >$ term arises from integrating the y-momentum equation to obtain the mean pressure variation explicitly, then substituting for the pressure in the x-momentum equation. Both of the Reynolds normal stress terms in curly brackets are of second order in the turbulence intensity and are usually neglected. However, they do not necessarily become vanishingly small as the Reynolds number increases, therefore they are kept here.

The presence of the turbulence terms — or, vice-versa, the viscous term — precludes the possibility of a similarity solution for the entire boundary layer. If the fluctuating terms are neglected, the laminar boundary equations are recovered, and a Blasius solution can be applied. If the viscous term is neglected, the solutions lose the ability to satisfy the no-slip condition. Then there is no momentum loss to the wall (drag) and no boundary layer at all.[3] The zero pressure-gradient boundary layer therefore is a singular perturbation problem where a small, inner length scale must be defined to ensure that the viscous term remains in the equation in a region close to the wall, even in the limit of infinite Reynolds number. The use of two length scales creates a "boundary layer inside of a boundary layer" (c.f. Tennekes & Lumley, 1972), which divides the turbulent boundary layer (and any other turbulent wall-bounded flow) in two distinct regions: An outer region comprising most of the boundary layer where the single point Reynolds-averaged equations are effectively inviscid; and an inner region very close to the wall where the viscous term is dominant.

When an order of magnitude analysis is performed with an outer and an inner length scale, one obtains two sets of reduced equations. Therefore solutions are sought

[3]Classical laminar boundary layer theory was invented by Prandtl to account for momentum loss to solid surfaces, which could not be accounted for by potential flow theory, which was well-developed by his time (c.f. Lamb (1932).

which asymptotically (at infinite Reynolds number) satisfy the following outer equations and boundary conditions:

$$U\frac{\partial U}{\partial x}+V\frac{\partial U}{\partial y}=\frac{\partial}{\partial y}\left[-<uv>\right]-\left\{\frac{\partial}{\partial x}\left[<u^2>-<v^2>\right]\right\} \tag{A.12}$$

where $U \to U_\infty$ as $y \to \infty$. For the inner (or near wall) region

$$0=\frac{\partial}{\partial y}\left[-<uv>+\nu\frac{\partial U}{\partial y}\right] \tag{A.13}$$

where $U = 0$ at $y = 0$.

These equations are exact only at infinite Reynolds number.[4] This is of considerable importance in the analysis repeated here (and applied to different flows in chapters 3 through 6), since properly scaled profiles will reduce to similarity solutions only in this limit. However, these equations are approximately valid as long as the Reynolds number is large.[5]

Equation A.13 for the inner region can be integrated from the wall w.r.t. y to obtain

$$-<uv>+\nu\frac{\partial U}{\partial y}=\nu\left.\frac{\partial U}{\partial y}\right|_{y=0}\equiv\frac{\tau_w}{\rho}\equiv u_*^2 \tag{A.14}$$

where τ_w is the wall shear stress and u_* is the corresponding friction velocity defined by this equation. In the limit of infinite Reynolds number, the total stress across the inner layer is constant, hence it is called the "constant stress layer" (Monin & Yaglom, 1971). The appearance of u_* in equation A.14 does not imply that the wall shear stress is an independent parameter (like ν or U_∞, section A.3). It enters the problem only because it measures the forcing of the inner flow by the outer; or alternatively, it can be viewed as measuring the retarding effect of the inner flow on the outer. Thus u_* is a *dependent* parameter which must be determined by matching solutions of the

[4] This can most easily be shown *a posteriori* by substituting the scaled solutions into the full equations, then using the friction law to get the asymptotic dependence.

[5] What constitutes "large" remains to be determined, c.f. section A.11.

inner and outer equations.

The inner layer occurs only because of the necessity of including viscosity in the problem so that the no-slip condition at the wall can be met. The outer layer, on the other hand, is dominated by inertia and the effects of viscosity enter only through the matching to the inner layer. The outer flow is effectively governed by inviscid equations, but has viscous-dominated inner boundary conditions set by the inner layer.

A.3 Dimensional Analysis and Velocity Scaling Laws

Solutions to the governing equations are sought which depend only on the streamwise coordinate through a local length scale $\delta(x)$, c.f. Monin & Yaglom (1971). Parameters occurring in the governing equations and boundary conditions are the free stream velocity, U_∞, the kinematic viscosity, ν, and the friction velocity, u_*. The friction velocity, u_*, is a dependent parameter, since it can be determined by the rest; i.e., $u_* = u_*(U_\infty, \delta, \nu)$. In other words, placing a smooth flat plate in a flow of viscosity ν and velocity U_∞ uniquely determines the wall shear stress τ_w (and therefore u_*) at a given position x (expressed as $\delta(x)$), if the upstream conditions are not varied. The "Buckingham Pi Theorem" (c.f. Sedov, 1959; Spurk, 1992) can be used to show that there can be only two independent dimensionless ratios. Convenient choices are u_*/U_∞ and $u_*\delta/\nu \equiv \delta^+$, so that the functional dependence can be written as

$$\frac{u_*}{U_\infty} = g\left(\delta^+\right) \tag{A.15}$$

and the ratio u_*/U_∞ can be expressed as a "skin friction coefficient"

$$c_f \equiv \frac{\tau_W}{\frac{1}{2}\rho U_\infty^2} = 2\frac{u_*^2}{U_\infty^2} \tag{A.16}$$

A consequence of equation A.15 is that either (but not both) u_* or U_∞ can be used be for scaling in the mean momentum equation as long as δ^+ is retained and is finite.

The asymptotic value of u_*/U_∞ is of considerable interest, because it determines if $\delta^+ \to \infty$ and $U_\infty \delta/\nu \to \infty$ as $U_\infty x/\nu \to \infty$. For now, it will be *assumed* that this is the case, so that any of the limits can be used interchangeably. It will be shown *a posteriori* that this assumption is consistent with the derived friction law, the momentum integral equation, and a boundary layer which continues to grow while the skin friction becomes vanishingly small.

The cross-stream variation of the local mean velocity profile must be described by $U = U(y, \delta, U_\infty, \nu)$. Application of the Buckingham Pi Theorem to the velocity profile yields a number of possibilities, especially since equation A.15 can be used to switch among them. In general, inner and outer Reynolds number dependent profiles can be written as

$$\frac{U}{U_{si}(x)} = f_i\left(\frac{y}{\eta}, \delta^+\right) \tag{A.17}$$

$$\frac{U - U_\infty}{U_{so}(x)} = f_o\left(\frac{y}{\delta}, \delta^+\right) \tag{A.18}$$

These profiles describe the variation of the velocity across the entire boundary layer at finite Reynolds number (since δ^+ has been retained as a parameter). Velocity and length scales remain to be determined, from dimensional analysis they can be either u_* or U_∞, or ν/u_* or δ, respectively. Note that since u_*/U_∞ and δ^+ (or $u_*\delta/\nu$) are related by equation A.15, only one of them needs to be retained[6] in equations A.17 – A.18.

For a similarity solution it is of interest how these scaled profiles behave as δ^+ (or any other Reynolds number for that matter, e.g., $U_\infty\delta/\nu$ or $U_\infty x/\nu$), becomes large. In the asymptotic limit as $\delta^+ \to \infty$, a properly scaled profile must produce finite values of the scaled velocity (the left hand side) for finite values of the scaled distance

[6]This fact seems to have escaped Monin & Yaglom (1971), who dismiss a separate dependence on u_*/U_∞, only on empirical grounds.

from the wall (the remaining argument on the right hand side). As the dimensionless profiles becomes asymptotically independent of δ^+, they degenerate to

$$\frac{U}{U_{si}} = f_i\left(\frac{y}{\eta}, \delta^+\right) \longrightarrow f_{i\infty}\left(\frac{y}{\eta}\right) \tag{A.19}$$

and

$$\frac{U - U_\infty}{U_{so}} = f_o\left(\frac{y}{\delta}, \delta^+\right) \longrightarrow f_{o\infty}\left(\frac{y}{\delta}\right) \tag{A.20}$$

As mentioned above, U_{so} can be either u_* or U_∞, which gives two different velocity deficits. Only one of them, not both, can be Reynolds number independent (and finite) in the limit as $\delta^+ \to \infty$ if the ratio u_*/U_∞ continues to vary (as the Millikan/Clauser theory requires, see below).

A.4 Full Similarity of the Inner Equations

Following the Asymptotic Invariance Principle introduced in section 2.3, solutions are sought which reduce to similarity solutions of the inner momentum equation and boundary conditions in the limit of infinite Reynolds number ($\delta^+ \to \infty$).

$$U = U_{si}(x) f_{i\infty}(y^+) \tag{A.21}$$

$$- < uv > = R_{si}(x) r_{i\infty}(y^+) \tag{A.22}$$

where the "inner variable" y^+ is defined by

$$y^+ \equiv \frac{y}{\eta} \tag{A.23}$$

and the length scale $\eta = \eta(x)$ remains to be determined. The subscript "$i\infty$" is used to distinguish the scaled velocity and Reynolds shear stress profiles at finite Reynolds number, $f_i(y^+, \delta^+)$ and $r_i(y^+, \delta^+)$, from their limiting forms used here. Obviously f_i and r_i, which will be used later in the overlap analysis, are dependent on δ^+, while

$f_{i\infty}$ and $r_{i\infty}$ are not.

Substitution into equation A.14, nondimensionalizing and clearing terms yields

$$\left[\frac{u_*^2}{U_{si}^2}\right] = \left[\frac{R_{si}}{U_{si}^2}\right] r_{i\infty} + \left[\frac{\nu}{\eta U_{si}}\right] f_{i\infty}' \tag{A.24}$$

A similarity solution can only exist if η, U_{si}, and R_{si} can be determined so that all the terms in brackets have the same x-dependence; i.e.,

$$\left[\frac{u_*^2}{U_{si}^2}\right] \sim \left[\frac{R_{si}}{U_{si}^2}\right] \sim \left[\frac{\nu}{\eta U_{si}}\right] \tag{A.25}$$

To this point only a transformation of variables has been performed[7].

Three scaling functions are to be determined from only two independent constraints, so one can be chosen freely. A convenient (and obvious) choice for the inner length scale η is

$$\eta = \nu / U_{si} \tag{A.26}$$

from which it follows immediately that similarity solutions are possible only if the velocity scale is the friction velocity

$$U_{si} \equiv u_* \tag{A.27}$$

It then further follows that

$$\eta = \nu / u_* \tag{A.28}$$

$$R_{si} = u_*^2 \tag{A.29}$$

Substitution into equation A.24 yields the integrated inner equation at infinite Reynolds

[7]Note that the symbol "$\sim$" will be used in this analysis to mean "*has the same x-dependence as*", and does not refer to the order of magnitude of the quantities involved.

number (i.e., $\delta^+ \to \infty$)

$$1 = r_{i\infty} + f_{i\infty}' \tag{A.30}$$

For finite values of δ^+, this equation is only approximately valid because of the neglected mean convection terms.

Note that the similarity variables *derived* above are the usual choices[8] for the inner layer, and the familiar *Law of the Wall* expressed in inner variables as originally proposed by Prandtl (1932) is recovered. The *Law of the Wall*[9] is thus consistent with a similarity solution of the inner equations, *in the limit of infinite Reynolds number*. For any finite (but large) Reynolds number, solutions for the inner layer will retain a Reynolds number dependence (as discovered from the Pi-theorem in deriving equation A.17) since the governing equations themselves do so.

Equation A.17 can now be written as

$$\frac{U}{u_*} = f_i\left(\frac{yu_*}{\nu}, \delta^+\right) \tag{A.31}$$

It reduces to the proper limiting form of a similarity solution for the inner layer as $\delta^+ \to \infty$, and thus is "Law of the Wall for finite Reynolds numbers." At finite Reynolds numbers however, it describes the velocity profile over the entire boundary layer. These ideas are not incompatible since in inner variables the outer layer can never be reached in the limit of infinite Reynolds number (i.e., as $\delta^+ \to \infty$, $y^+ \to \infty$ for finite values of the physical variable y).

[8]One could argue that too much space and effort were put into getting the 'old' results. It is not just the resulting scales which are important here, but the formal procedure used to find them.

[9]The word 'law' is formally incorrect since the result has been derived, and no longer depends on experimental results alone to establish its validity.

A.5 Full Similarity of the Outer Equations

Again, no scaling laws will be assumed at the outset (in particular, it is *not* assumed that $R_{so} = U_{so}^2$). In accordance with the Asymptotic Invariance Principle, solutions are sought which reduce to similarity solutions of the outer momentum equation and boundary conditions in the limit of infinite Reynolds number

$$U - U_\infty = U_{so}(x) f_{o\infty}(\overline{y}) \tag{A.32}$$

$$- < uv > = R_{so}(x) r_{o\infty}(\overline{y}) \tag{A.33}$$

where the "outer variable" $\overline{y}$ is defined by

$$\overline{y} = y/\delta(x) \tag{A.34}$$

and U_{so}, R_{so}, and δ are functions of x only[10]. The velocity has been written as a deficit to avoid the necessity of accounting for an offset arising from viscous effects across the inner layer. This is, of course, not a problem for the Reynolds stress since it vanishes outside the boundary layer. As in the previous section, the subscript "$o\infty$" distinguishes $f_{o\infty}$ and $r_{o\infty}$ from the the δ^+-dependent profiles scaled with U_{so} and R_{so} used later.

The V-component can be eliminated by integrating the continuity equation from the wall (integration by parts), thus introducing a contribution from the inner layer which vanishes identically at infinite Reynolds number.

$$V = - \left[\frac{dU_{so}}{dx}\delta + U_{so}\frac{d\delta}{dx} \right] \int_0^{\overline{y}} f_{o\infty}(\hat{\overline{y}}) d\hat{\overline{y}} - \left[\frac{dU_\infty}{dx}\delta \right] \overline{y} + \left[U_{so}\frac{d\delta}{dx} \right] \overline{y} f_{o\infty}(\overline{y}) \tag{A.35}$$

[10]Note that extra arguments can be included in the functional dependence of $f_{o\infty}$ and $r_{o\infty}$ to account for the effects of upstream conditions, as shown in section 3.2.

Substitution into equation A.12 and clearing terms yields

$$\left[\left(\frac{U_\infty}{U_{so}}\right)\frac{\delta}{U_{so}}\frac{dU_{so}}{dx}\right] f_{o\infty} \;+\; \left[\frac{\delta}{U_{so}}\frac{dU_{so}}{dx}\right] f_{o\infty}^2 - \left[\frac{U_\infty}{U_{so}}\frac{d\delta}{dx}\right]\overline{y} f_{o\infty}{}' - \left[\frac{d\delta}{dx}+\frac{\delta}{U_{so}}\frac{dU_{so}}{dx}\right] f_{o\infty}{}' \int_0^{\overline{y}} f_{o\infty}(\xi)d\xi = \left[\frac{R_{so}}{U_{so}^2}\right] r_{o\infty} \quad \text{(A.36)}$$

Note that the streamwise gradient of the normal stresses (the last term of equation A.12) has been neglected (for now, but with no loss of generality. This will be shown in section A.6 where the Reynolds stress component equations are considered individually).

For a similarity solution to be possible, the bracketed terms must all have the same $x-$dependence (or be identically zero, the trivial solution). Therefore, full similarity is possible only if

$$\left(\frac{U_\infty}{U_{so}}\right)\frac{\delta}{U_{so}}\frac{dU_{so}}{dx} \sim \frac{\delta}{U_{so}}\frac{dU_{so}}{dx} \sim \left(\frac{U_\infty}{U_{so}}\right)\frac{d\delta}{dx} \sim \frac{d\delta}{dx} \sim \frac{R_{so}}{U_{so}^2}. \quad \text{(A.37)}$$

It follows immediately from the third and fourth terms that

$$U_{so} = U_\infty, \quad \text{(A.38)}$$

at least to within a constant of proportionality which can be chosen as unity with no loss of generality. Thus, the proper velocity scale for the velocity deficit[11] law must be U_∞, and not u_* as suggested by Von Kármán (1930) and widely utilized since (e.g. Clauser, 1954; Coles, 1956, 1962).

Since, from Euler's equation outside the boundary layer, U_∞ is constant in a zero pressure gradient flow, the first two terms of the similarity conditions of equation A.37 are identically zero and with equation A.38 the third is equal to the fourth. The

[11]If the velocity were not written as a deficit, the first and third terms in equation A.37 would drop out. Then outer velocity scale then is not automatically equal to the reference velocity in the velocity deficit, but could be chosen as proportional to any velocity occurring in the outer layer. It could be chosen as U_∞, but *not* as u_*.

remaining two can be satisfied only — to within a constant of proportionality — if

$$R_{so} = U_\infty^2 \frac{d\delta}{dx}, \tag{A.39}$$

The limiting form of the outer equation governing the mean flow then becomes

$$-\overline{y} f_{o\infty}{}' - f_{o\infty}{}' \int_0^{\overline{y}} f_{o\infty}(\xi) d\xi = \left[\frac{R_{so}}{U_{so}^2 d\delta/dx} \right] r_{o\infty}{}'. \tag{A.40}$$

This equation can not be solved without a turbulence model and will not receive further attention in this chapter (except to obtain the Reynolds shear stress). Nonetheless, it has served a very important role, since the outer scaling parameters were determined from it according to the AIP.

The analysis above leads to the conclusion, that only the profile using $U_{so} = U_\infty$ (c.f. equation A.18) is Reynolds number invariant in the limit. Therefore it must be the appropriate scaling for finite Reynolds numbers as well[12]. Equation A.18 can now be written as

$$\frac{U - U_\infty}{U_\infty} = f_o \left(\frac{y}{\delta}, \delta^+ \right) \tag{A.41}$$

A deficit profile using u_* as velocity scale[13], $F_o(\overline{y}, \delta^+)$, can not be Reynolds number invariant in the limit (unless u_*/U_∞ is non-zero in the limit), since $F_o = (u_*/U_\infty) f_o$. Conversely, the fact that f_o is Reynolds number invariant in the limit explains why F_o vanishes in this limit if $u_*/U_\infty \to 0$,[14] as shown under item (i) in section A.1.1.

The Reynolds stress scale, on the other hand, is *not* U_∞^2, but an entirely different scale depending on the growth rate of the boundary layer, $d\delta/dx$. In effect, $d\delta/dx$ is acting as a Reynolds number dependent correlation coefficient, just as for free shear flows (George, 1989). This will be shown later to be related to the fact that as the

[12] This is, of course, the whole idea behind the Asymptotic Invariance Principle.

[13] Here the capital'F' in $F_o(\overline{y}, \delta^+)$ refers to the finite Reynolds number version of $F_{o\infty}(\overline{y})$ introduced in equation A.2. Analogous to equation A.41, but the velocity has been normalized with u_*.

[14] as required in the classical theory and as derived in section A.8

Reynolds number increases, less and less of the energy is dissipated at the scales at which the Reynolds stress is adding energy to the flow so they become effectively inviscid (c.f. George, 1995). It will also be shown below that R_{so} can be determined by matching the outer Reynolds stress to the inner Reynolds stress. The need for such a matching is intuitively obvious, since the only non-zero boundary condition on the Reynolds stress in the outer flow is that imposed by the inner.

Millikan (1938) and others have objected to the type of similarity analysis employed here as leading to unphysical results for the boundary layer. There is nothing unphysical about the velocity deficit law using U_∞ (it occurs in the outer layer!), and a case for such a deficit law could have been made, even with the data available at the time. Thus the objection must have come from the condition on the Reynolds stress. However, this would have been a problem only if it were also required or *assumed at the outset* that $R_{so} = U_{so}^2$, for then it would have also been necessary that $d\delta/dx = constant$. Since the boundary layer was believed not to grow linearly, Millikan (and many before and after him as well) was forced to conclude that full self-preservation (in the assumed sense) was not possible, and therefore had to settle for what was termed a *locally* self-preserving solution.

Contrary to how most texts present self-preservation, George (1989) pointed out that there is no reason to insist *a priori* that $R_{so} = U_{so}^2$. If this arbitrary requirement is relaxed, similarity become feasible since there no longer is the requirement for linear growth. The outer flow is then governed by two velocity scales, U_∞ and a second governing the Reynolds stress which is determined by the boundary conditions imposed on the Reynolds stress by the inner layer. It will be shown below that the inner and outer Reynolds stresses can overlap asymptotically only if

$$R_{so} \sim U_\infty^2 \frac{d\delta}{dx} \sim u_*^2 \tag{A.42}$$

which resembles closely the momentum integral equation. This relationship will be discussed further later on.

That the outer (and inner) equations admit to similarity solutions (in the sense of George, 1989) should come as no surprise to the experimentalists who had recognized that the mean velocity data in outer variables collapses with only U_∞ and δ (especially if the upstream conditions such as e.g. trip wire and free stream velocity remain fixed). Hinze (1975) and Schlichting (1968), for example, show profiles normalized by U/U_∞ and plotted as a function of y/δ. Even the fact that the outer Reynolds shear stress scales with u_* (but only to first order) is in accord with common practice, since it is assumed in the old theory — but in a way which could not account for the observed weak dependence on Reynolds number. Millikan's conclusions might have been different had he (and several generations after him) not been locked into the too restrictive idea of self-preservation (i.e., single velocity scale).

A.6 Scaling of the Other Turbulence Quantities

For the inner layer, there is only one velocity scale, u_*, which enters the *single point* equations; therefore all *single point* statistical quantities must scale with it. This is, of course, the conventional wisdom, but with an important difference: *The inner layer does not include the overlap layer* — the region between the inner and outer regions — which is Reynolds number dependent. Since the inner and outer scales are different, the dependent variables in the overlap layer are expected to be functions of both, and thus Reynolds number dependent.[15]

From the preceding analysis, it is apparent that the outer layer at finite Reynolds numbers is governed by not one, but two velocity scales. In particular, the mean velocity and its gradients scale with U_∞, while the Reynolds shear stress scales with $U_\infty^2 d\delta/dx \sim u_*^2$. Therefore it is not immediately obvious how the remaining turbulence quantities should scale. In particular, do they scale with U_∞ or u_*, or both? If the latter, then quantities scaled in the traditional way with only one of them will exhibit a

[15]Note that different considerations must be applied to the multi-point equations since conditions at a point can depend on those at another, and in particular those at a distance.

Reynolds number dependence and will not collapse. Note that if the ratio of velocity scales, u_*/U_∞, approaches an asymptotic limit, this Reynolds number dependence would appear to reduce with increasing downstream distance and could lead to the erroneous conclusion that certain quantities scaled with only one of them take longer to reach equilibrium than others.

In view of the possible similarity of the outer equations for the mean flow, it is reasonable to inquire whether the equations for other turbulence quantities also admit to fully similar solutions. For the outer part of the boundary layer at high Reynolds number the equation for $< u^2 >$ can be written as (c.f. Tennekes & Lumley, 1972)

$$\begin{aligned} U\frac{\partial < u^2 >}{\partial x} + V\frac{\partial < u^2 >}{\partial y} &= 2 < p\frac{\partial u}{\partial x} > \\ &+ \frac{\partial}{\partial y}\left(- < u^2 v >\right) - 2 < uv > \frac{\partial U}{\partial y} - 2\epsilon_u \end{aligned} \quad \text{(A.43)}$$

where ϵ_u is the energy dissipation rate for $< u^2 >$ and the viscous transport term has been neglected. An order of magnitude analysis of the governing equations reveals the mean convection and turbulence transport terms to be of second order in the turbulence intensity u'/U, so to first order the equation reduces to simply a balance among the production, dissipation and pressure strain rate terms. It could be argued that these second order terms should be neglected in the subsequent analysis, as in Townsend (1976). It is precisely these second order terms, however, that distinguish one boundary layer type flow from another, or from homogeneous flows (like fully-developed channels and pipes, chapter 4) for that matter. Therefore, for a theory describing growing shear layers — like the boundary layer — they must be retained.

By considering similarity forms for the new moments like

$$< u^2 > = K_u(x) k_{u\infty}(\overline{y}) \quad \text{(A.44)}$$

$$< p\frac{\partial u}{\partial x} > = P_u(x) p_{u\infty}(\overline{y}) \quad \text{(A.45)}$$

$$< -u^2 v > = T_{u^2 v}(x) t_{u\infty}(\overline{y}) \quad \text{(A.46)}$$

$$\epsilon_u = D_u(x) d_{u\infty}(\overline{y}) \tag{A.47}$$

and using $R_s = U_\infty^2 d\delta/dx$, it can be shown that similarity of the $< u^2 >$-equation is possible only if

$$K_u \sim U_\infty^2 \tag{A.48}$$

$$P_u \sim \frac{U_\infty^3}{\delta}\frac{d\delta}{dx} \qquad \left(\sim \frac{U_\infty u_*^2}{\delta} \right) \tag{A.49}$$

$$T_{u^2v} \sim U_\infty^3 \frac{d\delta}{dx} \qquad \left(\sim U_\infty u_*^2 \right) \tag{A.50}$$

$$D_u \sim \frac{U_\infty^3}{\delta}\frac{d\delta}{dx} \qquad \left(\sim \frac{U_\infty u_*^2}{\delta} \right) \tag{A.51}$$

All of these are somewhat surprising: The first (even though a second moment like the Reynolds stress) because the factor of $d\delta/dx$ is absent; the second, third and fourth because it is present. The mixed forms using u_* and U_∞ instead of $d\delta/dx$ should be especially useful for scaling experimental data at low to moderate Reynolds numbers where u_*/U_∞ shows considerable variation.

Similar equations can be written for $< v^2 >$ and $< w^2 >$; i.e.,

$$U\frac{\partial < v^2 >}{\partial x} + V\frac{\partial < v^2 >}{\partial y} = 2 < p\frac{\partial v}{\partial y} > + \frac{\partial}{\partial y}\Big(- < v^3 > -2 < pv > \Big) - 2\epsilon_v \tag{A.52}$$

and

$$U\frac{\partial < w^2 >}{\partial x} + V\frac{\partial < w^2 >}{\partial y} = 2 < p\frac{\partial w}{\partial z} > + \frac{\partial}{\partial y}\Big(- < w^2 v > \Big) - 2\epsilon_w \tag{A.53}$$

When each of the terms in these equations is expressed in similarity variables, the

resulting similarity conditions are:

$$D_v \sim P_v \sim \frac{U_\infty K_v}{\delta}\frac{d\delta}{dx} \tag{A.54}$$

$$D_w \sim P_w \sim \frac{U_\infty K_w}{\delta}\frac{d\delta}{dx} \tag{A.55}$$

$$T_{v^3} \sim \frac{U_\infty K_v}{\delta}\frac{d\delta}{dx} \tag{A.56}$$

$$T_{w^2 v} \sim \frac{U_\infty K_w}{\delta}\frac{d\delta}{dx} \tag{A.57}$$

The continuity equation requires that the sum of the pressure strain-rate terms occurring in the component energy equations must be zero. Thus, in similarity variables,

$$P_u(x)p_u(\overline{y}) + P_v(x)p_v(\overline{y}) + P_w(x)p_w(\overline{y}) = 0 \tag{A.58}$$

This can be true for all $\overline{y}$ only if

$$P_u \sim P_v \sim P_w \tag{A.59}$$

An immediate consequence from equations A.54 and A.55 is that

$$D_u \sim D_v \sim D_w \sim D_s \sim \frac{U_\infty^3}{\delta}\frac{d\delta}{dx} \qquad \left(\sim \frac{U_\infty u_*^2}{\delta} \right) \tag{A.60}$$

where D_s is the scale for the entire dissipation, and

$$K_u \sim K_v \sim K_w \sim U_\infty^2 \tag{A.61}$$

Therefore all of the Reynolds *normal* stresses scale with U_∞^2, but the Reynolds *shear* stress scales with u_*^2. Note that this does *not* imply that the normal stresses are the same order of magnitude as U_∞^2 which clearly can not be the case, only that they are proportional. It is easy to show that relations of equation A.61 are consistent with

similarity of the neglected normal stress terms in the mean momentum equation A.36; hence the equation for the mean flow is consistent with similarity to the second order, exactly as is being required here.

The remaining equation for the Reynolds shear stress is given by

$$\begin{aligned} U\frac{\partial < uv >}{\partial x} + V\frac{\partial < uv >}{\partial y} &= < p\left(\frac{\partial u}{\partial y} + \frac{\partial v}{\partial x}\right) > \\ &+ \frac{\partial}{\partial y}\left\{- < uv^2 >\right\} - < v^2 > \frac{\partial U}{\partial y} \end{aligned} \qquad \text{(A.62)}$$

This does not introduce any new similarity functions, but it does create an interesting problem. The x-dependence of the last term (which is the leading order term) is proportional to $K_v U_\infty/\delta$, while the first term is proportional to $(U_\infty R_{so}/\delta)d\delta/dx \sim (U_\infty^3/\delta)(d\delta/dx)^2$. If both terms are required to have the same x-dependence, a new constraint is imposed on the ones which exist already, namely,

$$K_v \sim R_{so}\frac{d\delta}{dx} \sim U_\infty^2(\frac{d\delta}{dx})^2 \qquad \left(\sim u_*^2\frac{d\delta}{dx}\right)dx \qquad \text{(A.63)}$$

R_{so} is only *asymptotically* equal to u_*^2 (see Section A.10 below), so the outer Reynolds shear stress scale only evolves to this value with increasing Reynolds number. Regardless, there is an apparent contradiction between equation A.63 and equation A.61. It can be resolved two ways:

(i) *Either*, the two conditions together require that in the limit of infinite Reynolds number,

$$\frac{d\delta}{dx} \sim \frac{u_*^2}{U_\infty^2} \rightarrow constant \qquad \text{(A.64)}$$

(ii) *Or*, the term which creates the contradiction must go to zero faster than the other terms so that the offending condition can be removed from the analysis. In fact, the possibility for this occurs since the terms on the left hand side of equation A.62 are of order $(d\delta/dx)^2 \sim (u_*/U_\infty)^4$ relative to the leading term, whereas the highest order terms in the normal stress equations are of

order $d\delta/dx \sim (u_*/U_\infty)^2$ relative to the remaining terms. Obviously the mean convection terms in the Reynolds shear stress equation will vanish in the infinite Reynolds number limit faster than the remaining terms in any of the Reynolds stress equations if $d\delta/dx \to 0$.

It will be argued later that the $d\delta/dx \to 0$ is a necessary consequence of insuring that the proper infinite Reynolds number dissipation limits can be satisfied,[16] i.e., that the local energy dissipation rate be finite. Therefore the mean convection terms in the Reynolds shear stress equation vanish faster than the remaining terms in the limit, and so to order $d\delta/dx \sim (u_*/U_\infty)^2$, equation A.64 does not enter the analysis.

Therefore similarity solutions to the infinite Reynolds number outer turbulence Reynolds stress equations are possible to at least order $d\delta/dx \sim (u_*/U_\infty)^2$, with the leading neglected terms being of order $(d\delta/dx)^2 \sim (u_*/U_\infty)^4$. Section A.11below establishes approximate bounds where each part of the boundary layer can be Reynolds number independent. Again, it is noted that nothing in the equations indicates whether the similarity state achieved in the outer part of the boundary layer is independent of upstream conditions.

A.7 The Overlap Layer

Since both the outer and inner profiles are non-dimensional profiles with different scales and the ratio of the scales is Reynolds number dependent, then any region between the two similarity regimes cannot be Reynolds number independent, except possibly in the limit. The actual mean velocity profile at any Reynolds number is the average of the instantaneous solutions to the Navier-Stokes equations and boundary conditions. Both scaled forms of this solution, $f_i(y^+, \delta^+)$ and $f_o(\overline{y}, \delta^+)$ (equations A.31 and A.41, respectively), represent the velocity everywhere, at least as long as the

[16] Note that this does *not* imply that the boundary layer stops growing, only that it grows more slowly than linearly.

Reynolds number is finite (as discussed in section 2.4). In fact, the parameter δ^+ uniquely labels the fanning out of the inner scaled profiles in the outer region and the outer scaled profiles near the wall. These scaled finite Reynolds number solutions (to the whole flow) degenerate in different ways at infinite Reynolds number, and this can be used to determine their functional forms in the common region they retain in the limit.

Analytical forms for these Reynolds number dependent solutions are not available and are only known *in principle*. But there are several pieces of information about the two profiles which can be utilized without further assumptions:

- First, since both inner and outer forms of the velocity profile must describe the flow everywhere as long as the ratio of length scales, $\delta^+ = \delta/\eta$, is finite, it follows from equations A.31 and A.41 that

$$1 + f_o(\overline{y}, \delta^+) = g(\delta^+) f_i(y^+, \delta^+) \tag{A.65}$$

  where $g(\delta^+) = u_*/U_\infty$ is defined by equation A.15.

- Second, for finite values of δ^+, the velocity derivatives from both inner and outer forms of the velocity must also be the same everywhere. It is easy to show that this requires that

$$\frac{\overline{y}}{1 + f_o} \frac{df_o}{d\overline{y}} = \frac{y^+}{f_i} \frac{df_i}{dy^+} \tag{A.66}$$

  for all values of δ^+ and y.

- Third, in the limit, both f_o and f_i must become asymptotically independent of δ^+. Thus $f_o(\overline{y}, \delta^+) \to f_{o\infty}(\overline{y})$ only, and $f_i(y^+, \delta^+) \to f_{i\infty}(y^+)$ only as $\delta^+ \to \infty$, or otherwise the velocity scales have been incorrectly chosen. (This is the *Asymptotic Invariance Principle*, introduced in section 2.3.)

Now the problem is that *in the limit* as $\delta^+ \to \infty$, the outer form fails to account for the behavior close to the wall while the inner fails to describe the behavior away

from it. The question then is: In this limit (as well as for all finite values approaching it) does there exist an "overlap" region where equation A.65 is still valid? It does indeed, and it can be shown using the Near Asymptotics methodology of George (1995) and GC. The details of this particular overlap analysis are the same for all developing wall-bounded turbulent flows. They have been presented in George & Castillo (1997) (see also Castillo (1997)) or, in an earlier version in George (1995) or Wosnik & George (1995). For completeness, the analysis is presented in Appendix B.

Since both δ and η are increasing with streamwise distance along the surface, this "overlap" region will not only increase in extent (in inner or outer variables), it will also move away from the wall in physical variables (this is different for fully-developed pipe and channel flows, c.f. section 4.4).

In Appendix B it is shown that, to leading order in δ^+, an overlap region exits in which

$$\frac{\overline{y}}{1+f_o^{(1)}}\frac{\partial(1+f_o^{(1)})}{\partial\overline{y}}\Big|_{\delta^+} = \gamma(\delta^+) \tag{A.67}$$

The solution to equation A.67 can be denoted as $f_o^{(1)}$ since it represents a first order approximation to f_o. It is *not*, however, simply the same as $f_{o\infty}$ because of the δ^+ dependence of γ, but reduces to it in the limit. Thus, by regrouping into the leading term all of the y-independent contributions, the method applied here has yielded a more general result than the customary expansion about infinite Reynolds number[17]

From equations A.66 and A.67, it follows that (c.f. appendix B)

$$\frac{y^+}{f_i^{(1)}}\frac{\partial f_i^{(1)}}{\partial y^+}\Big|_{\delta^+} = \gamma(\delta^+) \tag{A.68}$$

An interesting feature of these first order solutions is that the inequalities given by equations B.12 and B.13 determine the limits of validity of both equations A.67 and A.68 since either S_o or S_i will be large outside the overlap region. Clearly the extent

[17]It is also easy to see why the usual matching of infinite Reynolds number inner and outer solutions will not work since the limiting value of γ might be zero.

of this region will increase as the Reynolds number (or δ^+) increases.

Both equations A.68 and A.67 must be invariant to transformations of the form $y \to y + a$ where a is arbitrary, since the equation must be valid for any choice of the origin of y (c.f. Oberlack, 1997). Therefore, the most general solutions are of the form:

$$1 + f_o^{(1)}(\overline{y}, \delta^+) = C_o(\delta^+)(\overline{y} + \overline{a})^{\gamma(\delta^+)} \tag{A.69}$$

$$f_i^{(1)}(y^+, \delta^+) = C_i(\delta^+)(y^+ + a^+)^{\gamma(\delta^+)} \tag{A.70}$$

or in physical variables,

$$\frac{U}{U_\infty} = C_o(\frac{y+a}{\delta})^\gamma \tag{A.71}$$

$$\frac{U}{u_*} = C_i(\frac{y+a}{\eta})^\gamma \tag{A.72}$$

The velocity profile in the overlap layer of this flow is thus algebraic — a power law in $(y + a)$ — with coefficients and exponent which depend on the local Reynolds number, δ^+. It is reasonable to expect that a^+ be nearly constant since any shift of the overlap layer in y must be accomplished by the inner layer; regardless it is closely related to the *mesolayer* discussed below.[18] Earlier versions of this theory (George et al. 1992, George and Castillo 1993) included additive constants which were believed to be zero only on experimental grounds. The derivation here makes it clear that these constants are indeed zero. In the remainder of this paper, the superscript '(1)' will be dropped; these first order solutions will be referred to unless otherwise stated.

The relation between u_* and U_∞ follows from equation A.65; i.e.,

$$\sqrt{\frac{c_f}{2}} = \frac{u_*}{U_\infty} = g(\delta^+) = \frac{C_o(\delta^+)}{C_i(\delta^+)}\delta^{+-\gamma(\delta^+)} \tag{A.73}$$

[18] From the data it appears that $a^+ \approx -16$.

Thus the friction law is also a power law entirely determined by the velocity parameters for the overlap region. However, equation B.11 must also be satisfied. Substituting equation A.73 into equation B.11 implies that γ, C_o, and C_i are constrained by

$$ln\delta^+ \frac{d\gamma}{d\ln\delta^+} = \frac{d\ln[C_o/C_i]}{d\ln\delta^+} \tag{A.74}$$

This constraint equation must be invariant to scale transformations of the form $\delta^+ \rightarrow D\delta^+$ since the physical choice of δ^+ must be arbitrary (e.g., δ_{99}, δ_{95}, etc.). Thus the Reynolds number dependence of γ and C_o/C_i must also be independent of the particular choice of δ, since any other choice (say from δ_{99}) would simply be reflected in the constant coefficient D. This will be important in relating the boundary layer parameters to other wall-bounded flows (chapters 4, 5 and 6). Also obvious from equation A.74 is that both γ and C_o/C_i are functions of $\ln\delta^+$.

Equation A.74 is exactly the criterion for the neglected terms in equation B.9 to vanish identically (i.e., $S_i - S_o \equiv 0$). Therefore the solution represented by equations A.69 – A.74 is, indeed, the first order solution for the velocity profile in the overlap layer at *finite*, but large, Reynolds number. Clearly when y^+ is too big or $\overline{y}$ is too small for a given value of δ^+, the inequalities of equations B.12 and B.13 cannot be satisfied. Since all the derivatives with respect to δ^+ must vanish as $\delta^+ \rightarrow \infty$ (the AIP), the outer range of the inner overlap solution is unbounded in the limit, while the inner range of the outer is bounded only by $\overline{y} = -\overline{a}$.

The parameters $C_i(\delta^+)$, $C_o(\delta^+)$, and $\gamma(\delta^+)$ as well as the constant D can be determined empirically or from a turbulence closure model. However, the results must be consistent with equation A.74. Also, equations A.69 and A.70 must be asymptotically independent of Reynolds number, since f_i and f_o are. Therefore the coefficients and exponent must be asymptotically constant; i.e.,

$$\begin{aligned} \gamma(\delta^+) &\rightarrow \gamma_\infty \\ C_o(\delta^+) &\rightarrow C_{o\infty} \end{aligned}$$

$$C_i(\delta^+) \;\rightarrow\; C_{i\infty}$$

as $\delta^+ \rightarrow \infty$. These conditions are powerful physical constraints and together with equation A.74 will be seen to rule out some functional forms for γ, like that suggested by Barenblatt 1993 (see below). Therefore it is important to note that they are a direct consequence of the AIP and the assumption that scaling laws should correspond to similarity solutions of the equations of motion.

A.8 A Solution for the Reynolds Number Dependence

It is convenient to write the solution to equation A.74 as

$$\frac{C_o}{C_i} = \exp[(\gamma - \gamma_\infty)\ln\delta^+ + h] \tag{A.75}$$

where $h = h(\delta^+)$ remains to be determined, but must satisfy

$$\gamma - \gamma_\infty = -\delta^+\frac{dh}{d\delta^+} = -\frac{dh}{d\ln\delta^+} \tag{A.76}$$

The advantage of this form of the solution is easily seen by substituting equation A.75 into equation A.73 to obtain

$$\frac{u_*}{U_\infty} = \exp[-\gamma_\infty \ln\delta^+ + h] \tag{A.77}$$

Thus u_*/U_∞ is entirely determined by γ_∞ and $h(\delta^+)$.

It is easy to show the conditions that both $C_{o\infty}$ and $C_{i\infty}$ be finite and non-zero require that:

Either

- C_o, C_i and γ remain constant always;

or

- (i) $\gamma \to \gamma_\infty$ faster than $1/\ln\delta^+ \to 0$

and

- (ii) $h(\delta^+) \to h_\infty = constant.$

It follows immediately that

$$\frac{C_{o\infty}}{C_{i\infty}} = exp[h_\infty] \tag{A.78}$$

Note that condition (i) together with equation A.76 requires that $dh/d\ln\delta^+ \to 0$ faster than $1/\ln\delta^+ \to 0$.

Condition (ii) rules out solutions of the form suggested by Barenblatt 1993 who proposed power law profiles with $\gamma = a/\ln\delta^+$ for which $h = \ln b - a\ln\ln\delta^+$ where $\ln b$ is the integration constant. Obviously this h is unbounded in the limit as $\delta^+ \to \infty$. Substitution into equation A.75 yields $C_o/C_i = b(e/\ln\delta^+)^a$. Thus, either $C_o \to 0$ or $C_i \to \infty$ or both. Both of these are unacceptable alternatives in that they are inconsistent with similarity of even the mean velocity.[19]

It is interesting to examine the relation between the asymptotic value of γ and u_*/U_∞. Since γ must be asymptotically independent of δ^+, the only possible values for γ_∞ are either a finite constant, or zero. For the former, $u_*/U_\infty \to 0$, while for the latter the limiting value is finite and non-zero. Note that both of these satisfy the conditions from Section A.6 for similarity of the Reynolds stress equations in the outer layer.

A zero limit for γ itself can be considered by using Equation A.77 to obtain

$$\frac{u_*}{U_\infty} = \exp[h] \tag{A.79}$$

[19]Barenblatt's form does produce a logarithmic drag law which is desirable for pipe/channel flow, but not necessarily for a boundary layer. A logarithmic drag (friction) law can be obtained for pipe/channel flow in another way as shown in chapter 4.

Recall that if $\gamma \to 0$ faster than $1/\ln \delta^+$ and $h \to const$ as required, this insures a finite asymptotic value of u_*/U_∞. Hence there would be no question about whether the turbulence moments in the *outer* layer approach a state of asymptotic similarity; they would, since the limiting values of both $d\theta/dx$ and $d\delta/dx$ are finite. A finite and non-zero limiting value for u_*/U_∞ is certainly contrary to traditional thinking, and would have important implications for the engineer.

So there would seem to be a strong argument for $\gamma \to 0$. But this presents another problem. In the overlap region in the limit of infinite Reynolds number, the production of turbulence energy is exactly balanced by the rate of dissipation. Thus, in inner variables, $\epsilon^+ = P^+ = \gamma C_i (y^+ + a^+)^{\gamma - 1}$ since $< -uv >= u_*^2$ in this limit. If there is indeed an energy dissipation law (Frisch 1995) which demands that the *local* rate of dissipation be finite and non-zero in the limit of infinite Reynolds number, then γ_∞ must also be finite and non-zero since C_i must be finite and non-zero for similarity as noted earlier. Note that Goldenfeld (1996) has suggested that the integrated energy dissipation across the flow should be finite, which would lead to the opposite conclusion if applied here. Finite total energy in the infinite Reynolds number limit does not appear to be physical no matter how the limit is approached[20], since the flow is unbounded in inner variables, as is the energy in outer; so only the *local* dissipation need be finite. In fact, the data shown in Part II are most consistent with a non-zero value of γ_∞, but the experimental evidence is not conclusive, so the dissipation argument is crucial.

A.8.1 George/Castillo Solution for the Constraint Equation

George & Castillo (1997) found on empirical grounds that the variation of $\gamma - \gamma_\infty$ and C_o/C_i with δ^+ was described to a very good approximation by (for the data sets

[20] Certainly no homogeneous flow could satisfy this criterion.

investigated)

$$h - h_\infty = \frac{A}{(\ln \delta^+)^\alpha} \tag{A.80}$$

where $\alpha = 0.46$, $A = 2.90$ and $D = 1$ for δ chosen to be δ_{99}. This can easily be shown to satisfy the constraints above. It follows immediately from equations A.76 and A.75 that

$$\gamma - \gamma_\infty = \frac{\alpha A}{(\ln \delta^+)^{1+\alpha}} \tag{A.81}$$

$$\frac{C_o}{C_i} = \frac{C_{o\infty}}{C_{i\infty}} \exp[(1+\alpha)A/(\ln \delta^+)^\alpha] \tag{A.82}$$

and

$$\frac{u_*}{U_\infty} = \frac{C_{o\infty}}{C_{i\infty}} [\delta^+]^{-\gamma_\infty} \exp[A/(\ln \delta^+)^\alpha] \tag{A.83}$$

The variation of C_o is described by an empirical expression with two constants found from experimental data,

$$\frac{C_o}{C_{o\infty}} = 1 + 0.283 \exp(-0.00598\delta^+) \tag{A.84}$$

The data of Purtell *et al.* (1981) and Smith and Walker (1959), were found to be consistent with $C_{o\infty} = 0.897$, $C_{i\infty} = 55$ and $\gamma_\infty = 0.0362$. The variation of C_i and γ with δ^+ was satisfactory. C_o (eqn. A.84) reached its asymptotic value too fast, at least for the boundary layer data examined.[21] A solution to the constraint equation which obtains h (and therefore γ and C_o) in higher orders of $A/(\ln \delta^+)^\alpha$ was derived in section 3.3.

A.9 The Asymptotic Friction Law

The relation between u_*/U_∞ and δ^+ is given by equation A.73, or equation 3.32. From the above conditions on γ and $h(\delta^+)$ it is clear that the asymptotic friction law

[21] For the plane wall jet, on the other hand, the assumption of $C_o \approx C_{o\infty} = 1.3$ worked well for the limited range of Reynolds numbers for which experimental data was available.

is also power law given by

$$\frac{u_*}{U_\infty} \rightarrow \frac{C_{o\infty}}{C_{i\infty}} \delta^{+-\gamma_\infty} \tag{A.85}$$

The asymptotic behavior of u_*/U_∞ can be investigated by rewriting the friction law as

$$\frac{u_*}{U_\infty} = \frac{C_o}{C_i} \delta^{+-\gamma} = \frac{C_o}{C_i} e^{-\gamma \ln \delta^+} \tag{A.86}$$

To get an idea when the infinite Reynolds number limit might be achieved, the exponential of equation A.83 is expanded in powers of $A/(\ln \delta^+)^\alpha$ to obtain

$$exp[A/(\ln \delta^+)^\alpha] = 1 + \frac{A}{(\ln \delta^+)^\alpha} + \ldots \tag{A.87}$$

The second term must be negligible for the power law behavior to dominate; thus the limiting power law behavior is obtained when

$$\ln \delta^+ >> [A]^{1/\alpha} \tag{A.88}$$

For the values A and α of George & Castillo (1997) this would require $\delta^+ >> 2.4 \times 10^4$, or at least an order of magnitude above the existing experiments (currently $\delta^+ \approx 18,000$ is the highest, c.f. Fernholz *et al.* (1995)).

The friction laws written above all use u_* on both sides of the equation. This can be cast in an alternative form by eliminating the dependence of the right-hand side of equation A.73 on u_*; i.e.,

$$\frac{u_*}{U_\infty} = \left(\frac{C_o}{C_i}\right)^{1/1+\gamma} \left(\frac{U_\infty \delta}{\nu}\right)^{-\gamma/(1+\gamma)} \tag{A.89}$$

or

$$c_f = 2 \left(\frac{C_o}{C_i}\right)^{2/(1+\gamma)} \left(\frac{U_\infty \delta}{\nu}\right)^{-2\gamma/(1+\gamma)} \tag{A.90}$$

Unfortunately, because C_o/C_i is itself a function of Reynolds number, this form is less useful than it might appear to be. In section A.14 the relation of R_δ to R_θ and

R_{δ_*} will be determined so that the friction law can be expressed in terms of any of the convenient Reynolds numbers.

A.10 The Reynolds Stress in the Overlap Layer

By following the same procedure[22] as for mean velocity, the outer and inner Reynolds stress profiles for the overlap region are also obtained as power laws. For example, the Reynolds *shear* stress is given by,

$$r_o(\overline{y};\delta^+) = D_o(\delta^+)(\overline{y}+\overline{a})^{\beta(\delta^+)} \tag{A.91}$$

$$r_i(y^+;\delta^+) = D_i(\delta^+)(y^+ + a^+)^{\beta(\delta^+)} \tag{A.92}$$

where a solution is possible only if

$$\frac{R_{so}}{R_{si}} = \frac{D_i}{D_o}\delta^{+\beta} \tag{A.93}$$

and

$$ln\delta^+ \frac{d\beta}{d\ln\delta^+} = \frac{d}{d\ln\delta^+} ln\left[\frac{D_o}{D_i}\right] \tag{A.94}$$

Note that the last equation must also be invariant to transformations of the form $\delta \rightarrow D\delta$, just as for the corresponding velocity constraint. It has been assumed that the scale factor D and the origin shift represented by a is the same as for the velocity, since any other choice does not seem to make sense physically.

Unlike the velocity, however, more information about the Reynolds stress is available from the averaged momentum equation for the overlap layer since both equations A.12 and A.13 reduce to

$$\frac{\partial}{\partial y}\left(- < uv >\right) = 0 \tag{A.95}$$

[22]Sections A.10 through A.16 closely follow George & Castillo (1997)

in the limit of infinite Reynolds number. Thus,

$$\beta R_{so} D_o (\overline{y} + \overline{a})^{\beta - 1} \to 0 \tag{A.96}$$

and

$$\beta R_{si} D_i (y^+ + a^+)^{\beta - 1} \to 0 \tag{A.97}$$

Since both D_o and D_i must remain finite and be asymptotically constant (if the Reynolds stress itself is non-zero), these conditions can be met only if

$$\beta \to 0 \tag{A.98}$$

From equation A.30 for large values of y^+, the Reynolds stress in inner variables in the matched layer is given to first order (exact in the limit) by

$$r_i \to 1 \tag{A.99}$$

Since $R_{si} = u_*^2$, this can be consistent with equation A.92 only if $D_i \to 1$ as $\delta^+ \to \infty$. It follows immediately that

$$R_{so} \to \frac{D_i}{D_o} u_*^2 \tag{A.100}$$

in the infinite Reynolds number limit, just as suggested in Section A.5.

Some insight into the behavior of $D_o(\delta^+)$ and $D_i(\delta^+)$ can be obtained by introducing the momentum integral equation defined by

$$\frac{d\theta}{dx} = \frac{u_*^2}{U_\infty^2} \tag{A.101}$$

Using this, equation A.100 and the similarity relation for R_{so} from equation A.39 yields

$$\frac{D_o(\delta^+)}{D_i(\delta^+)} = \frac{d\theta/dx}{d\delta/dx} \tag{A.102}$$

The relationship between θ and δ will be explored in more detail below, and it will be shown that θ/δ is asymptotically constant. Thus the scale for the outer Reynolds shear stress is asymptotically proportional to u_*^2 as noted earlier, and the outer layer is indeed governed by two velocity scales. Note that for *finite* Reynolds numbers, both D_o and D_i are Reynolds number dependent. Hence, u_*^2 *alone* should not be able to perfectly collapse the Reynolds shear stress in either the overlap or outer layers, except in the limit of infinite Reynolds number. This has been observed by numerous experimenters (e.g., Klewicki and Falco 1993) who show persistent Reynolds number trends in the Reynolds shear stress measurements.

The interrelation of the Reynolds stress and velocity parameters can be examined by considering the production term $< -uv > \partial U/\partial y$. Since this must be the same whether expressed in inner or outer variables, it follows that

$$C_o D_o U_\infty^2 \frac{d\delta}{dx} \sim C_i D_i u_*^2 \tag{A.103}$$

or asymptotically, $D_o \sim C_i(D_i/C_o)$. The experiments considered in Part II show that C_o and D_i achieve a nearly constant value for relatively low values of R_θ, while C_i only approaches a constant value for much higher Reynolds numbers. Obviously the outer Reynolds stress parameter, D_o, follows the inner velocity, thus emphasizing the role of the boundary condition provided by the Reynolds stress on the outer flow by the inner.

A.11 The Effect of Reynolds Number

The question arises: How large must the Reynolds number be before the boundary layer begins to show the characteristics of the asymptotic state.

The averaged momentum equation from about $y^+ > 30$ out to $\overline{y} < 0.1$ is given

approximately by

$$0 = -\frac{\partial < uv >}{\partial y} \tag{A.104}$$

It has no explicit Reynolds number dependence; and the Reynolds shear stress is effectively constant throughout this region. Unfortunately many low Reynolds number experiments do not have a region where this is even approximately true because the convection terms are not truly negligible. Hence it is unreasonable to expect these experimental profiles to display any of the characteristics of the overlap described above, except possibly in combination with the characteristics of the other regions. (For example, the composite velocity profile of section A.13 can be used to obtain the Reynolds stress by integrating the complete momentum equation from the wall.)

Even when there is a region of reasonably constant Reynolds stress, however, this is not the entire story because of the Reynolds number dependence of $< -uv >$ itself. The origin of this weak Reynolds number dependence can be seen by considering the Reynolds transport equations. For this "constant shear stress region", the viscous diffusion and mean convection terms are negligible (as in the mean momentum equation), so the equations reduce approximately to (c.f. Tennekes & Lumley, 1972),

$$0 \approx -(< p\frac{\partial u_i}{\partial x_k} > + < p\frac{\partial u_k}{\partial x_i} >) - \left[< u_i u_2 > \frac{\partial U_k}{\partial x_2} + < u_k u_2 > \frac{\partial U_i}{\partial x_2}\right] - \frac{\partial < u_i u_k u_2 >}{\partial x_2} - \epsilon_{ik} \tag{A.105}$$

where $U_i = U\delta_{i1}$. Thus viscosity does not appear directly in any of the single point equations governing this region, nor does it appear in those governing the outer boundary layer.

In spite of the above, however, viscosity can be shown to play a crucial role in at least a portion of the constant stress layer, even at infinite Reynolds number. The reason is that the scales of motion at which the dissipation, ϵ_{ik}, actually takes place depend on the *local* turbulence Reynolds number, $R_t = q^4/\nu\epsilon$. At $R_t \sim 5000$, the energy-containing scales of motion, say L, are about 20 times larger than the Kolmogorov microscale, η_K (since $L/\eta_K = (R_t/9)^{3/4}$). The peak in the dissipation spec-

trum is at about $6\eta_K$, and most of the dissipation occurs at smaller scales (Tennekes & Lumley, 1972). Thus for $R_t > 5000$ approximately, the energy and Reynolds stress producing scales are effectively inviscid,but they control the energy transfer through the energy cascade to the much smaller dissipative scales. When this is the case, the dissipation is nearly isotropic so $\epsilon_{ik} \approx 2\epsilon\delta_{ik}$. Moreover, ϵ can be approximated by the infinite Reynolds number relation, $\epsilon \sim q^3/L$, where L is a scale characteristic of the energy-containing eddies. The coefficient has a weak Reynolds number dependence, but is asymptotically constant. Thus, the Reynolds stress equations are effectively inviscid, but only exactly so in the limit. And in this limit the Reynolds shear stress has no dissipation at all[23], i.e., $\epsilon_{12} = 0$.

At very low turbulence Reynolds number, however, the dissipative and energy-containing ranges nearly overlap (c.f. Figurefig:zpg-spectra), and so the latter (which also produce the Reynolds shear stress) feel directly the influence of viscosity. In this limit, the energy and dissipative scales are about the same, so the dissipation is more reasonably estimated by $\epsilon \sim \nu q^2/L^2$, where the constant of proportionality is of order 10. The dissipation tensor, ϵ_{ik} is anisotropic and ϵ_{12}, in particular, is non-zero (Launder 1993). (Hanjalic and Launder 1972, for example, take $\epsilon_{12} = \epsilon < -u_1 u_2 > /q^2$.)

For turbulence Reynolds numbers between these two limits, the dissipation will show characteristics of both limits, gradually making a transition from $\epsilon \sim \nu q^2/L^2$ to $\epsilon \sim q^3/L$ as R_t increases. Thus the Reynolds stresses themselves will feel this directly through their balance equations, and will consequently show a Reynolds number dependence. Obviously, in order to establish when (if at all) parts of the flow become Reynolds number independent, it is necessary to determine how the local turbulence Reynolds number varies downstream and across the flow.

Over the outer boundary layer (which is most of it), $L \approx 3\theta$ and $q \approx 0.1U_\infty$.

[23]Note that these are nearly the same conditions required to observe a $k^{-5/3}$-range in the energy spectrum, (c.f. Batchelor, 1953).

So when $U_\infty\theta/\nu > 15,000$, the dissipation in the outer flow is effectively inviscid. Alternatively, $L \approx 0.3\delta$ and $q \approx 2.5u_*$ so this corresponds to $\delta^+ > 5,000$. Above these values the mean and turbulence quantities in the outer flow should show little Reynolds number dependence, and this is indeed the case — when they are scaled properly! This outer region can, of course, not be entirely Reynolds number independent, except in the limit, and this residual dependence manifests itself in the overlap layer in the slow variation of γ, for example.

The near wall region is considerably more interesting since in it the scales governing the energy-containing eddies are constrained by the proximity of the wall. Hence, the turbulence Reynolds number, R_t, depends on the distance from the wall and $R_t \approx 18y^+$ (Gibson 1997); so, in effect, y^+ is the turbulence Reynolds number. Because of this, two things are immediately obvious:

- First, since a fixed value of y^+ does not move away from the wall as fast as δ, then as the Reynolds number increases more and more of the boundary layer (in outer variables) will become effectively inviscid and will be governed by the inviscid dissipation relation. And correspondingly, the mean and turbulence quantities in the overlap layer will become Reynolds number independent, albeit very slowly. Clearly this limiting behavior cannot be reached until at least part of overlap layer, say the *inertial sublayer*, is governed by the infinite Reynolds number dissipation relation and its coefficient has reached the limiting value. Obviously this can happen only when there is a substantial *inertial subrange* satisfying $y^+ > 300$ and for which the mean convection terms are negligible, typically $\overline{y} < 0.1$. Thus the asymptotic limits are realized only when $300\nu/u_* << 0.1\delta$ or $u_*\delta/\nu >> 3000$, which corresponds approximately to $U_\infty\theta/\nu >> 10,000$. Note that a choice of $\overline{y} < 0.15$ would bring these numbers into coincidence with those for the outer flow, but at most all of these choices are approximate. Regardless, all estimates for where inertial effects dominate the dissipation and Reynolds stress in the near wall region are near the highest

range of the available data which end at about $R_\theta \approx 50,000$. Therefore the inertial sublayer, to the extent that it is identifiable at all, should display a Reynolds number dependence, not only in C_o, C_i, and γ, but correspondingly in the behavior of $< u^2 >$, $< uv >$, etc.

- Second, there will always be a region, hereafter referred to as the *mesolayer*[24], below about $y^+ \approx 300$ in which the dissipation (and Reynolds stress) can *never* assume the character of a high Reynolds number flow, no matter how high the Reynolds number for the boundary layer becomes. This is because the dissipation (and Reynolds stress) can never become independent of viscosity — even though the mean momentum equation itself is inviscid above $y^+ \approx 30$! This fact is well-known to turbulence modelers (v. Hanjalic and Launder 1972), but the consequences for similarity theory and asymptotic analyses do not seem to have been noticed previously. It is particularly important for experimentalists who have routinely tried to apply asymptotic formulas to this region, wrongly believing the mesolayer to be the *inertial sublayer*.

Thus, as illustrated in Figure 1, the constant stress layer is really two separate regions, an '*overlap* (or constant Reynolds stress) region' and a '*viscous sublayer*' where the viscous stress directly affects the mean momentum equation. Each of these has two subregions. The overlap region obtained in the preceding section consists of an '*inertial sublayer*' ($y^+ > 300$, $\overline{y} < 0.1$) which is nearly inviscid; and a '*mesolayer*' ($30 < y^+ < 300$) in which the viscous stresses are negligible, but in which viscosity acts directly on the turbulence scales producing the Reynolds stresses. The viscous sublayer consists of a '*buffer layer*' ($3 < y^+ < 30$) where the Reynolds stress and viscous stress both act directly on the mean flow; and a '*linear sublayer*' near the wall ($y^+ < 3$) where the viscous stresses dominate. And of these four sub-regions, the

[24] This appropriates a term from Long 1976 (see also Long and Chen 1982) who argued strongly for its existence, but from entirely different physical and scaling arguments which we find untenable. Nonetheless, despite the skepticism which greeted his ideas, Long's instincts were correct.

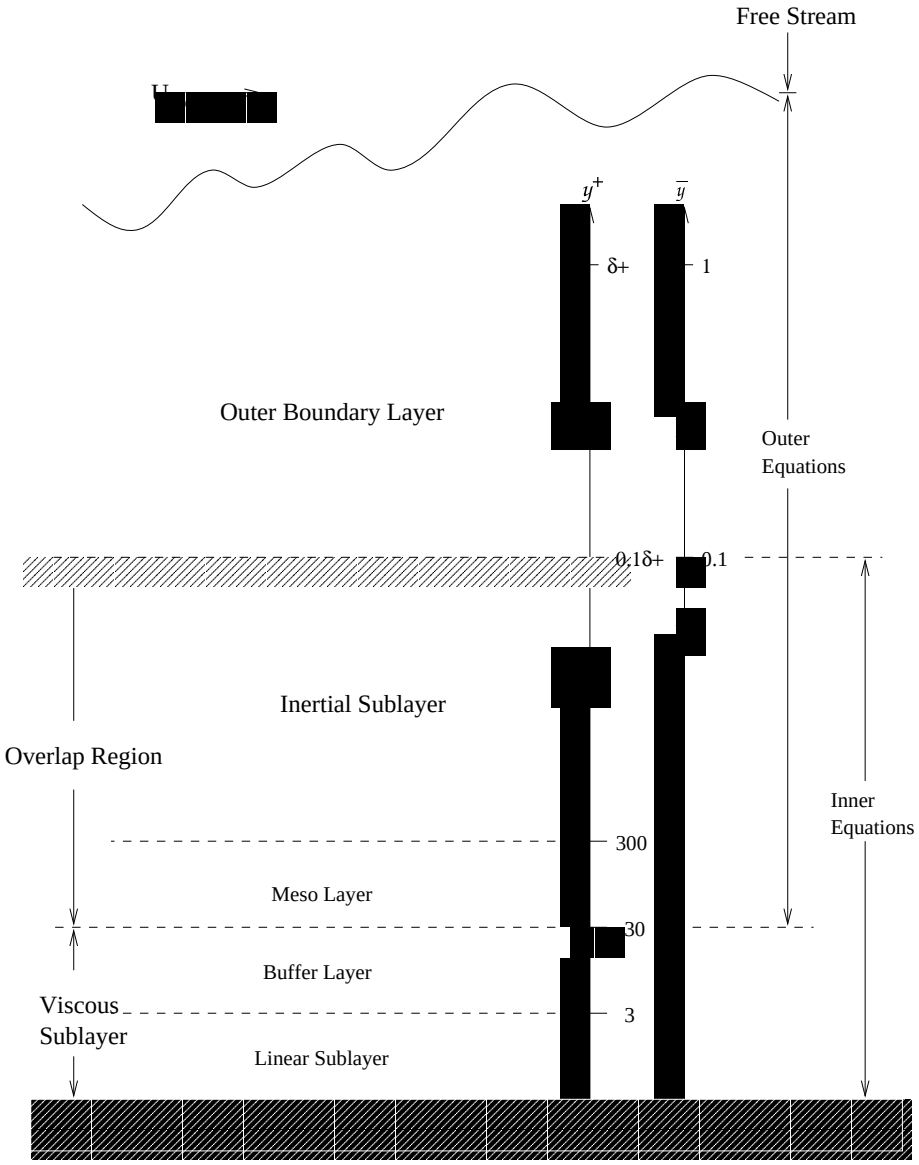

Figure 1: Schematic showing inner and outer regions of a zero pressure gradient turbulent boundary layer together with subregions ($\delta^+ = \delta u_*/\nu$).

'*inertial sublayer*' will be the *last* to appear as the flow develops or as the Reynolds number is increased. Thus it will be the most difficult to identify at the modest Reynolds numbers of laboratory experiments. Identification will be easier if the properties of the mesolayer are known. Fortunately, as demonstrated in the next section, its essential features have been captured by the overlap analysis; in particular the parameter a^+.

A.12 A *Mesolayer* Interpretation of a^+

The overlap solution of equation A.70 can be expanded for values of $y^+ >> |a^+|$ to obtain

$$\frac{U}{u_*} = C_i y^{+\gamma} + \gamma C_i a^+ y^{+\gamma-1} + \frac{1}{2}\gamma(\gamma-1) C_i a^{+2} y^{+(\gamma-2)} + \frac{1}{6}\gamma(\gamma-1)(\gamma-2) C_i a^{+3} y^{+(\gamma-3)} + \ldots \tag{A.106}$$

For $y^+ >> |(2-\gamma)a^+|/3$, this can be approximated by the first three terms as

$$\frac{U}{u_*} = C_i y^{+\gamma}[1 + \gamma a^+ y^{+-1} + \frac{1}{2}\gamma(\gamma-1) a^{+2} y^{+-2}] \tag{A.107}$$

An equivalent expansion in outer variables is given by

$$\frac{U}{U_\infty} = C_o \overline{y}^{\gamma}[1 + \gamma \overline{a}\,\overline{y}^{-1} + \frac{1}{2}\gamma(\gamma-1)\overline{a}^2 \overline{y}^{-2}] \tag{A.108}$$

Equations A.107 and A.108 are useful for three reasons: First, they are an excellent approximation to the overlap solutions for values of $y^+ > 2|a^+|$ (or $\overline{y} > 2|\overline{a}|$). Second, they are easier to incorporate into a composite solution than the overlap solution itself since they do not have the singularity at $y^+ = -a^+$; and they will be used for this purpose when comparing to experimental data. Third, the inner variable version will be shown below to offer a useful insight into the role of the parameter a^+ as accounting for the mesolayer identified in the previous section.

In the overlap region the turbulence energy balance reduces to production equals dissipation; i.e., in inner variables, $P^+ \approx \epsilon^+$. This is exactly true in the limit of infinite Reynolds number, but is approximately true even at finite Reynolds numbers for $30 < y^+ < 0.1\delta^+$. The overlap solutions for the velocity and Reynolds stress have already been obtained. The same methodology applied to the dissipation yields

$$\epsilon^+ = E_i(y^+ + a^+)^{\vartheta} \tag{A.109}$$

It follows immediately by substitution for P^+ and ϵ^+ that

$$\gamma C_i D_i (y^+ + a^+)^{\beta+\gamma-1} = E_i(y^+ + a^+)^{\vartheta} \tag{A.110}$$

Hence $\vartheta = \beta + \gamma - 1$ and $E_i = \gamma C_i D_i$, at least in the limit as $\delta^+ \to \infty$. So the dissipation is given by

$$\epsilon^+ = \gamma C_i D_i (y^+ + a^+)^{\beta+\gamma-1} \tag{A.111}$$

But in section A.10 it was shown that $\beta \to 0$ and $D_i \to 1$ as $\delta^+ \to \infty$. Therefore in this limit, the dissipation profile and the velocity derivative profile are identical and equal to the derivative of equation A.70 with respect to y^+; i.e.,

$$\epsilon^+ \to \frac{du^+}{dy^+} = \gamma C_i (y^+ + a^+)^{\gamma-1} \tag{A.112}$$

Equation A.111 can also be expanded for $y^+ >> a^+$ to obtain

$$\epsilon^+ \approx \gamma C_i D_i y^{+\gamma+\beta-1}[1 + (\gamma + \beta - 1)\frac{a^+}{y^+}] \tag{A.113}$$

This can be re-written into the form

$$\epsilon^+ = \epsilon_o^+ f_T(y^+) \tag{A.114}$$

where

$$\epsilon_o^+ = \gamma C_i D_i y^{+\gamma+\beta-1} \tag{A.115}$$

and

$$f_T = [1 + (\gamma + \beta - 1)\frac{a^+}{y^+}] \tag{A.116}$$

But this is identical to the form used by most turbulence modellers for wall- bounded flows (cf. Reynolds 1976). In fact, if $R_t = 18y^+$ as noted earlier, the function f_T is exactly that used by Hanjalic and Launder 1972 to account empirically for the change in the character of the dissipation near the wall. Thus the interpretation of a^+ as a mesolayer parameter is obvious since it, in effect, modifies the dissipation (and hence the velocity profile) near the wall.

The same form of f_T is obtained if the log profile of Appendix I for fully-developed pipe and channel flow is expanded in a similar fashion, even though the form of ϵ_o is different (v. George, Castillo & Knecht, 1996). However, interestingly, if the order of argument is reversed and any of the simple dissipation models (e.g., Reynolds 1976) are used to deduce the mesolayer contribution to the velocity profile, they produce a y^{+-1} additive term for both types of flows instead of the $y^{+\gamma-1}$ required for the developing flow here. This form of the mesolayer contribution was used by George et al. (1996) and Castillo (1997), and is nearly indistinguishable from the expanded form of the overlap solution given by equation A.107. Obviously these simple turbulence models, as currently posed, are inconsistent with the theory developed here, although the difference is slight. Also note that the common practice of choosing the model constants to produce a log profile at $y^+ \approx 30$ is clearly wrong if the theory proposed herein is correct.

Note that equation A.114 offers an insight into why the familiar log profile has survived so long. As noted earlier, the high Reynolds number dissipation is approximately proportional to q^{+3}/y^+ in inner variables. Suppose there were a region in the boundary layer for which the kinetic energy is nearly constant, but at sufficiently

large values of y^+ so that the a^+ could be neglected. Then to a first approximation, $du^+/dy^+ \sim y^{+^{-1}}$, and the profile corresponds exactly to that originally deduced by Prandtl (1932) from an eddy viscosity hypothesis. These assumptions above are only satisfied over a very narrow region for boundary layer flows ($50 < y^+ < 150$), but this is exactly the region where the log law is known to work best (v. Bradshaw and Huang 1995). These same authors note the seemingly paradoxial fact that the log profile is remarkably 'resilient', but its range of validitly does not seem to increase with increasing Reynolds number like a proper overlap solution as it does for fully-developed pipe and channel flows. In fact, the mesolayer/overlap profile derived above and the old log law are nearly indistinguishable over this limited range. All of these observations are consistent with the interpretation that the 'log' region in a boundary layer is just a portion of the mesolayer. Thus Prandtl's original log law is valid, *but* only over a limited range. Clauser's identification of this region with Millikan's matched layer is, however, clearly incorrect.

A.13 Construction of a Composite Velocity Profile

It is possible to use the information obtained in the preceding sections to form a composite velocity profile which is valid over the entire boundary layer. This is accomplished by expressing the inner profile in outer variables, adding it to the outer profile and subtracting the common part (Van Dyke, 1964), which is the profile for the overlap region. Alternatively, the outer profile could be expressed in inner variables, etc.

The composite velocity profile in outer variables is given by

$$\frac{U}{U_\infty} = \left[1 + f_o(\overline{y}, \delta^+)\right] + \frac{u_*}{U_\infty}\left[f_i(\overline{y}\delta^+, \delta^+) - C_i\left(\overline{y}\delta^+ + a^+\right)^\gamma\right] \tag{A.117}$$

Recall that f_o, f_i, C_i and γ are all functions of δ^+, as is u_*/U_∞.

The composite velocity solution has the following properties:

- As $\delta^+ = \delta/\eta \to \infty$, $U/U_\infty \to 1 + f_{o\infty}(\overline{y})$ for finite values of $\overline{y}$. Thus there is a boundary layer profile even in the limit of infinite Reynolds number and it corresponds to the outer scaling law. This can be contrasted with the Millikan approach for which $U/U_\infty \to 1$, a limit remarkably like no boundary layer at all, even in its own variables.

- As $\overline{y} \to 0$, $U/U_\infty \to (u_*/U_\infty) f_i(\overline{y}\delta^+, \delta^+)$ for all values of δ^+. This is because the small $\overline{y}$ behavior of $[1 + f_o(\overline{y}, \delta^+)]$ is cancelled out by the last term leaving only the inner solution.

- As $\overline{y}\delta^+ \to \infty$, $U/U_\infty \to 1 + f_o(\overline{y}, \delta^+)$ for all values of δ^+. This is because the large $\overline{y}\delta^+$ behavior of f_i is cancelled by the last term.

- In the overlap region, only the power law profile remains.

It is an interesting exercise to substitute the composite solution into the full boundary layer equation given by equation A.11. As expected, it reduces to equation A.12 for infinite Reynolds number and to equation A.13 as the wall is approached. This can be contrasted with the substitution of the Millikan/Clauser log law plus wake function (v. Coles 1956) in which the outer equation vanishes identically in the limit of infinite Reynolds number.

An alternative composite solution can be obtained by multiplying the inner and outer solutions together and dividing by the common part; i.e.,

$$\frac{U}{U_\infty} = \frac{[1 + f_o(\overline{y}, \delta^+)] f_i(\overline{y}\delta^+, \delta^+)}{C_o(\overline{y} + \overline{a})^\gamma} \tag{A.118}$$

For the zero-pressure-gradient boundary layer, this composite solution is nearly indistinguishable from equation A.117 when plotted against the experimental data.

A.14 Displacement and Momentum Thickness

The displacement thickness, δ_*, is defined by

$$U_\infty \delta_* \equiv \int_0^\infty (U_\infty - U) dy \tag{A.119}$$

This can be expressed using equation A.117 as

$$\frac{\delta_*}{\delta} = -I_1 - I_2 {R_\delta}^{-1} \tag{A.120}$$

or

$$\frac{\delta}{\delta_*} = -\frac{1}{I_1}(1 + \frac{I_2}{R_{\delta_*}}) \tag{A.121}$$

where

$$I_1 \equiv \int_0^\infty f_o(\overline{y}, \delta^+) d\overline{y} \tag{A.122}$$

$$I_2 \equiv \int_0^\infty \left[f_i(y^+, \delta^+) - C_i(y^+ + a^+)^\gamma \right] dy^+ \tag{A.123}$$

and the Reynolds numbers R_δ and R_{δ_*} are defined by

$$R_\delta = \frac{U_\infty \delta}{\nu} \tag{A.124}$$

and

$$R_{\delta_*} = \frac{U_\infty \delta_*}{\nu} \tag{A.125}$$

The integrals I_1 and I_2 are functions only of the Reynolds number and become asymptotically constant.

The momentum thickness, θ, is defined by

$$U_\infty^2 \theta \equiv \int_0^\infty U(U_\infty - U) dy \tag{A.126}$$

Again using equation A.117, the result is

$$\frac{\theta}{\delta} = -(I_1 + I_3) - R_\delta{}^{-1}\left[I_2 + 2I_4 + I_5\frac{u_*}{U_\infty}\right] \tag{A.127}$$

or

$$\frac{\delta}{\theta} = -\frac{1}{I_1 + I_3}\left\{1 + R_\theta^{-1}\left[I_2 + 2I_4 + I_5\frac{u_*}{U_\infty}\right]\right\} \tag{A.128}$$

where

$$R_\theta = \frac{U_\infty \theta}{\nu} \tag{A.129}$$

and

$$I_3 \equiv \int_0^\infty \left[f_o(\overline{y}, \delta^+)\right]^2 d\overline{y} \tag{A.130}$$

$$I_4 \equiv \int_0^\infty \left[f_i(y^+, \delta^+) - C_i(y^+ + a^+)^\gamma\right] f_o(y^+/\delta^+, \delta^+) dy^+ \tag{A.131}$$

$$I_5 \equiv \int_0^\infty \left[f_i(y^+, \delta^+) - C_i(y^+ + a^+)^\gamma\right]^2 dy^+ \tag{A.132}$$

Since u_*/U_∞ varies in the limit as $(U_\infty \delta/\nu)^{-\gamma/(1+\gamma)}$ and $\gamma \geq 0$, all terms but the first vanish in the limit of infinite Reynolds number. Thus, as for the displacement thickness, the momentum thickness is also asymptotically proportional to the outer length scale, but with a different constant of proportionality. This limit is approached very slowly, and the limiting value is achieved at Reynolds numbers well above those at which experiments have been performed.

The shape factor can be computed by taking the ratio of equations A.120 and A.127. The result is

$$\begin{aligned} H &\equiv \delta_*/\theta \\ &= \frac{I_1 + I_2 R_\delta^{-1}}{(I_1 + I_3) + R_\delta^{-1}(I_2 + 2I_4 + I_5 u_*/U_\infty)} \end{aligned} \tag{A.133}$$

For large values of Reynolds number, the asymptotic shape factor is easily seen to be

given by

$$H \rightarrow \frac{I_1}{I_1 + I_3} \tag{A.134}$$

Note that since $f_o \leq 1$ always, it follows from their definitions that $I_1 < 0$, $I_3 > 0$ and $|I_1| > I_3$. Therefore the asymptotic shape factor is greater than unity, in contrast to the old result, but consistent with all experimental observations.

It is obvious from equations A.120 and A.127 that both the displacement and momentum boundary layer thicknesses are asymptotically proportional to the outer length scale (or boundary layer thickness) used in the analysis. Note that it does not matter precisely how this outer length scale is determined experimentally, as long as the choice is consistent and depends on the velocity profile in the outer region of the flow (e.g., $\delta_{0.99}$ or $\delta_{0.95}$). This is quite different from the Millikan/Clauser theory (with finite κ) where the displacement and momentum thicknesses vanish relative to the unspecified outer length scale.

A.15 Streamwise Dependence of the Boundary Layer

The friction coefficient can be written entirely in terms of R_θ by using equations A.128 and A.90; i.e.,

$$c_f = 2(\frac{C_o}{C_i})^{2/(1+\gamma)}[\left(\frac{-1}{I_1 + I_3}\right)(R_\theta + I_2 + 2I_4)]^{-2\gamma/(1+\gamma)} \tag{A.135}$$

where the term involving $I_5 u_*/U_\infty$ has been neglected. Also I_2 and I_4 are much less than R_θ, so that

$$c_f \approx 2(\frac{C_o}{C_i})^{2/(1+\gamma)}[\left(\frac{-1}{I_1 + I_3}\right)R_\theta]^{-2\gamma/(1+\gamma)} \tag{A.136}$$

This theoretical result provides a point of reference with Schlichting (1968) who noted that a 1/7-power law fit the velocity profile reasonably over a range of Reynolds

numbers. Using $\gamma = 1/7$ leads immediately to $c_f \sim R_\theta^{-1/4}$ which was his corresponding friction law. Note that for higher Reynolds numbers Schlichting suggested $c_f \sim R_\theta^{-1/5}$ which corresponds to $\gamma = 1/9$, consistent with the idea that γ is indeed Reynolds number dependent and decreases with increasing Reynolds number. The asymptotic value of $\gamma_\infty = 0.0362$ suggested in Part II gives $c_f \sim R_\theta^{-0.07}$ as the limiting power law.

The integral of equation A.11 across the entire boundary yields the momentum integral equation for a zero-pressure gradient boundary layer as

$$\frac{d\theta}{dx} = \frac{1}{2} c_f \tag{A.137}$$

Thus the x-dependence of θ can be obtained by integrating

$$\{ \left(\frac{-1}{I_1 + I_3} \right) \left(\frac{C_i}{C_o} \right)^{1/\gamma} [1 + R_\theta^{-1}(I_2 + 2I_4)] \}^{2\gamma/(1+\gamma)} R_\theta^{2\gamma/(1+\gamma)} dR_\theta = dR_x \tag{A.138}$$

where $R_x \equiv U_\infty x/\nu$.

If the values of C_i, C_o, γ and the I's can be evaluated as functions of R_θ, equation A.138 can be integrated numerically to yield the variation of R_θ as a function of $R_x - R_{x_o}$ where R_{x_o} is a virtual origin which will be determined by how the boundary layer is generated. The x-dependence of H, and the other boundary layer parameters can be similarly determined by substituting the results of the integration into the appropriate equations.

It is interesting to note that if γ can be considered to be constant over some range of Reynolds numbers, then equation A.138 can be integrated analytically to obtain

$$R_\theta = \left(\frac{C_o}{C_i} \right)^{2/(1+3\gamma)} \{ \left(\frac{1+3\gamma}{1+\gamma} \right) \left[\frac{-1}{I_1 + I_3} \right] (R_x - R_{x_l}) \}^{(1+\gamma)/(1+3\gamma)} \tag{A.139}$$

where x_l is the virtual origin for the section of the flow under consideration. Thus the boundary layer thickness is proportional to $x^{(1+\gamma)/(1+3\gamma)}$. For example, if $\gamma \to 1/10$, $\theta \to x^{11/14}$. The suggested infinite Reynolds number limit for γ corresponds to

$\delta \sim x^{0.935}$. Because of the slow approach of γ to its limiting value, a most important experimental clue that the present analysis is correct will be whether the exponent increases toward unity (or some limiting value close to it, like 0.935) as data points are added from distances farther from the leading edge, especially if data from points close to leading edge are successivelly dropped.

A.16 Power Law versus Log Law

The asymptotic approach of γ to a small value makes it possible to approximately recover the logarithmic relations of the classical theory. Ignoring for the moment the mesolayer parameter a^+, the power law velocity profiles of equations A.69 and A.70 can be expanded for small values of γ as

$$\frac{U}{u_*} = f_i(y^+;\delta^+) = C_i e^{\gamma ln y^+} \approx C_i(1 + \gamma ln y^+ + \ldots) \tag{A.140}$$

and

$$\frac{U}{U_\infty} = 1 + f_o(\overline{y};\delta^+) = C_o e^{\gamma ln \overline{y}} \approx C_o(1 + \gamma ln \overline{y} + \ldots) \tag{A.141}$$

So the asymptotic boundary layer profiles would appear logarithmic to leading order, even for finite values of γ.

From these "log" profiles and the asymptotic friction value of equation A.73 it follows that the effective von Karman/Millikan "constants" of equations A.3 and A.4 are given by

$$1/\kappa \equiv \gamma_\infty C_{i\infty} \tag{A.142}$$

$$B_i \equiv C_{i\infty} \tag{A.143}$$

and

$$B_o \equiv C_{i\infty}(1 - \frac{1}{C_{o\infty}}) \tag{A.144}$$

Thus the Millikan/Clauser log profile result is recovered as the first term in an expan-

sion. It will be shown below, however, that this is not a useful approximation since the higher order terms vanish at Reynolds numbers well above those encountered in the experiments.

It is easy to see why the mean velocity profile could have been accepted for so long by experimentalists as logarithmic: it is very difficult to tell a logarithm from a weak power using experimental data alone since one can always be expanded in terms of the other. Suppose for the moment that it is indeed the overlap region which is being examined and that the present theory is correct, but that an experimenter believed the log theory to be correct with a constant and finite value of κ. The values for C_i and γ at $R_\theta = 50,000$, the limits of experimental data, will be estimated later in Part II to be about 12 and 0.09 respectively. These yield a value of $1/\kappa = 1.1$ which is nowhere close to the generally accepted value of about 2.5, believed to be the asymptotic value for both boundary layers and pipes. Over the range of most experiments, however, $R_\theta \sim 10^4$ and $\gamma \approx 1/7$ while $C_i \approx 10$, which yields about an estimate of $1/\kappa \approx 1.4$. However, the logarithmic expansion converges rather slowly and terms above first order are not negligible (nor were they in the calculation above). To third order in $\gamma \ln y^+$, the effective value of κ is given by

$$\frac{1}{\kappa} \approx \gamma C_i[1 + \gamma \ln y^+ + \frac{1}{2}(\gamma \ln y^+)^2 + \frac{1}{6}(\gamma \ln y^+)^3] \qquad \text{(A.145)}$$

Now the presence of y^+ in this expansion is interesting since it is well-known that attempts to fit the log law to boundary layer velocity profiles at modest Reynolds numbers depend on where the point of tangency is chosen. If κ is evaluated by fitting a log profile which is tangent to the data at $y^+ = 100$ (as suggested by Bradshaw 1993), using the above values in the expansion yields an estimate of $1/\kappa \approx 2.36$ or $\kappa \approx 0.42$, which is the value usually assumed. Most often in practice, the experimenter picks his point to obtain the "right" value of κ (hence its *universal* value), and accepts whatever value of the other universal (but highly variable!) *constant* which comes out. In view of this and equation A.145, the seemingly paradoxical variability of B_i

and constancy of κ is not at all surprising since the 'right' point of tangency can always be found.

As noted above, there is considerable debate in the literature about the value of B_i with cited values (for boundary layers) ranging from 4 to 12. From equation A.143 it is equal to C_i. C_i will be seen later to vary from about 7 to 10 over the range of the low Reynolds number experiments. This is higher than the value of 4.9 suggested by Coles 1968, but well in the range of recent experiments, some of which also show much higher values and a Reynolds number dependence (Nagib and Hites 1995). There is no consensus value for the outer 'constant' B_o, and it is seldom reported at all. Perhaps equation A.144 suggests a reason for this in that it is quite small since C_o is never very far from unity. Hence estimates for it would vary widely since the errors might be larger than its value.

In summary, at least some of the general satisfaction (and dissatisfaction as well) with the log law over the range of most experiments can be explained with the new theory. Even the sensitivity noted by experimentalists to the choice of the point of tangency can be explained because of the $\ln y^+$-terms in the expansion of κ for finite values of γ. The power law profiles (and the parameters in them) resulting from the present theory, if correct, should be much less sensitive to the actual range of the data used, especially if the limits imposed by the mesolayer are honored.

The considerations above apply only to boundary layers and other developing flows, and not to homogeneous wall-bounded flows like fully-developed pipes and channels. These homogeneous flows are indeed described theoretically by logarithmic profiles, the recent arguments of Barenblatt et al. (1997) notwithstanding. These naturally occuring log profiles could, of course, be expanded approximately as power laws, but with all the problems of Reynolds number dependencies and tangency points noted above. This undoubtedly explains the success of Barenblatt et al. (1997) in fitting power laws to the data of Nikuradse (1932), as well as their difficulty in extending their results to the much higher Reynolds numbers of the Zagarola and

Smits (1996) superpipe data[25].

Before leaving this section it is interesting to consider one aspect of a finite and non-zero limit for u_*/U_∞, however unlikely it may be in view of the requirement for a finite *local* energy dissipation rate discussed earlier. If both u_* and U_∞ were the same in the limit, shouldn't an asymptotic theory based on either alone (like the Millikan/Clauser theory) be correct? An asymptotic approach of γ to zero indeed makes the expansions above exact, and the definitions of equations A.142 and A.143 must be exactly the Millikan/Clauser constants. The problem is that in the limit as $R_\theta \to \infty$, κ will blow up if $\gamma \to 0$ since $C_{i\infty}$ must be constant (to satisfy the requirements for similarity of the mean momentum equation). This unseemly behavior of κ is not just a consequence of the theory here but can readily be seen from the old log friction law of equation A.5 by requiring that the limiting value of u_*/U_∞ be a non-zero constant. In fact, if the Millikan/Clauser scaling arguments are applied to the turbulence moment equations, then it is easy to show that similarity of the Reynolds stress equations is possible only if $d\delta/dx = constant$ and $u_*/U_\infty = constant$, consistent with the analysis presented herein. And the only possibility of satisfying equation A.5 with a finite value of u_*/U_∞ is for κ to increase without bound, exactly as derived here. Note that this problem has been rationalized in the past by simply ignoring all the second order terms as noted in Section A.6. Interestingly, the terms which must be ignored are those associated with the streamwise growth of the boundary layer. These second-order terms vanish identically for flows homogeneous in x, providing yet another indicator that the inner and outer region of fully-developed pipe and channel flows indeed scale with u_* as argued in Appendix I.

Therefore, either the old theory is not the limit of the new (if $u_*/U_\infty \to 0$), or it is but with an infinite von Karman constant (if the limiting value of u_*/U_∞ is finite). Obviously the latter possibility makes little sense. Note that precisely the

[25]They 'explained' this failure by suggesting the superpipe data was tainted by roughness. It is shown in Wosnik *et al.* (2000), and in chapter 4 that this it not the case.

same arguments which have been applied to the boundary layer here lead to a *finite* limiting value of the von Karman 'parameter', κ_∞, in the log profile for fully-developed pipe and channel flows (see Appendix I). Thus the *principles* applied to both flows are the same; only the *results* are different; and this is clearly because one flow is developing in x while the other is homogeneous.

"Part II. Experimental Data" of George & Castillo (1997) has not been included due to its length. The reader is referred to the original article.

Appendix B

Details of the Overlap Analysis for Developing Flows

The methodology used to determine the overlap characteristics was introduced by George (1995) and was termed "Near-Asymptotics". It is necessary because the traditional approaches to asymptotic matching cannot account for the possibility of a power exponent tending to zero, which cannot be ruled out without additional arguments. Here the overlap analysis is performed for the mean velocity profile, its adoption to any statistical quantity is straightforward. This appendix closely follows George & Castillo (1997) (see also Wosnik & George (1995) for an application to the natural convection boundary layer), and is included here for completeness. The details of this particular overlap analysis are the same for all developing wall-bounded turbulent flows, like turbulent boundary layers and wall jets. There is a slight difference depending on whether there is a need for a reference velocity in the outer layer (boundary layer) or not (wall jet, natural convection boundary layer), which will be pointed out where necessary. This analysis is somewhat different — especially in its results — for flows which are homogeneous in the streamwise direction, such as fully developed pipe and channel flows, therefore it is discussed separately in chapter 4.

The question of whether there is a common region of validity can be investigated by examining how rapidly f_o and f_i are changing with δ^+. From the Taylor expansion of the velocity derivatives in equation A.66,5.58 about a fixed value of δ^+,

$$\frac{f_i(y^+;\delta^+ + \Delta\delta^+) - f_i(y^+;\delta^+)}{\Delta\delta^+ f_i(y^+;\delta^+)} \approx \frac{1}{f_i(y^+;\delta^+)} \frac{\partial f_i(y^+;\delta^+)}{\partial \delta^+}\bigg|_{y^+} \equiv S_i(\delta^+, y^+) \qquad \text{(B.1)}$$

and

$$\frac{f_o(\overline{y};\delta^+ + \Delta\delta^+) - f_o(\overline{y};\delta^+)}{\Delta\delta^+ f_o(\overline{y};\delta^+)} \approx \frac{1}{f_o(\overline{y};\delta^+)} \frac{\partial f_o(\overline{y};\delta^+)}{\partial \delta^+}\bigg|_{\overline{y}} \equiv S_o(\delta^+, \overline{y}) \qquad \text{(B.2)}$$

Thus S_i and S_o are measures of the Reynolds number dependences of f_i and f_o respectively. Both vanish identically in the limit as $\delta^+ \to \infty$. If ${y^+}_{max}$ denotes a location where outer flow effects begin to be strongly felt on the inner scaled profile, then for $y^+ < {y^+}_{max}$, S_i should be much less than unity (or else the inner scaling is not very useful). Similarly, if $\overline{y}_{min}$ measures the location where viscous effects begin to be strongly felt (e.g., as the linear velocity region near the wall is approached), then S_o should be small for $\overline{y} > \overline{y}_{min}$. Obviously either S_i or S_o should increase as these limits are approached. Outside these limits, one or the other should increase dramatically.

The quantities S_i and S_o can, in fact, be used to provide a formal definition of an "overlap" region where both scaling laws are valid. Since S_i will increase drastically for large values of y for given δ^+ and S_o will increase for small values of y, an "overlap" region exists only if there exists a region for which both S_i and S_o remain small simultaneously. In the following paragraphs, this condition will be used in conjunction with equation 5.56 to derive the functional form of the velocity in the overlap region *at finite Reynolds number.*

Because of the movement of the matched layer away from the wall with increasing x, it is convenient and necessary to introduce an intermediate variable $\tilde{y}$ which can be fixed in the overlap region all the way to the limit, regardless of what is happening

in physical space (v. Cole & Kevorkian, 1981). A definition of $\tilde{y}$ which accomplishes this is given by

$$\tilde{y} = y^+ \delta^{+-m} \tag{B.3}$$

or

$$y^+ = \tilde{y} \delta^{+m} \tag{B.4}$$

Since $\overline{y} = y^+/\delta^+$, it follows that

$$\overline{y} = \tilde{y} \delta^{+m-1} \tag{B.5}$$

For all values of m satisfying $0 < m < 1$, $\tilde{y}$ can remain fixed in the limit as $\delta^+ \to \infty$ while $\overline{y} \to 0$ and $y^+ \to \infty$. Substituting these into equation 5.56 yields the matching condition on the velocity as

$$f_o(\tilde{y}\delta^{+m-1}, \delta^+) = g(\delta^+) f_i(\tilde{y}\delta^{+m}, \delta^+) \tag{B.6}$$

Now equation B.6 can be differentiated with respect to δ^+ *for fixed* $\tilde{y}$ to yield equations which explicitly include S_i and S_o. The result is

$$\left.\frac{\partial f_o}{\partial \overline{y}}\right|_{\delta^+} \frac{\partial \overline{y}}{\partial \delta^+} + \left.\frac{\partial f_o}{\partial \delta^+}\right|_{\overline{y}} = \frac{dg}{d\delta^+} f_i + g \left\{ \left.\frac{\partial f_i}{\partial y^+}\right|_{\delta^+} \frac{\partial y^+}{\partial \delta^+} + \left.\frac{\partial f_i}{\partial \delta^+}\right|_{y^+} \right\} \tag{B.7}$$

Carrying out the indicated differentiation of y^+ and $\overline{y}$ by δ^+ (for fixed $\tilde{y}$), and multiplying by δ^+/f_o yields (after some rearranging)

$$(m-1)\frac{\overline{y}}{f_o}\left.\frac{\partial f_o}{\partial \overline{y}}\right|_{\delta^+} - m\frac{y^+}{f_i}\left.\frac{\partial f_i}{\partial y^+}\right|_{\delta^+} = \frac{\delta^+}{g}\frac{dg}{d\delta^+} + \delta^+ \left\{ \frac{1}{f_i}\left.\frac{\partial f_i}{\partial \delta^+}\right|_{y^+} - \frac{1}{f_o}\left.\frac{\partial f_o}{\partial \delta^+}\right|_{\overline{y}} \right\} \tag{B.8}$$

It follows immediately from equation 5.58 that

$$\frac{\overline{y}}{f_o}\left.\frac{\partial f_o}{\partial \overline{y}}\right|_{\delta^+} = -\frac{\delta^+}{g}\frac{dg}{d\delta^+} - \delta^+ \left\{ \frac{1}{f_i}\left.\frac{\partial f_i}{\partial \delta^+}\right|_{y^+} - \frac{1}{f_o}\left.\frac{\partial f_o}{\partial \delta^+}\right|_{\overline{y}} \right\} \tag{B.9}$$

Equation B.9 can be rewritten as

$$\left.\frac{\overline{y}}{f_o}\frac{\partial f_o}{\partial \overline{y}}\right|_{\delta^+} = \gamma(\delta^+) - \delta^+(S_i - S_o) \tag{B.10}$$

where $\gamma = \gamma(\delta^+)$ is defined by

$$\gamma(\delta^+) \equiv -\frac{\delta^+}{g}\frac{dg}{d\delta^+} = -\frac{d\ln g}{d\ln \delta^+} \tag{B.11}$$

Note that the first term on the right hand side B.10 is at most a function of δ^+ alone, while the second term contains all of the residual y-dependence.

Now it is clear that if both

$$|S_o| << \left|\frac{1}{\delta^+}\frac{d\ln g}{d\ln \delta^+}\right| = \left|\frac{\gamma}{\delta^+}\right| \tag{B.12}$$

and

$$|S_i| << \left|\frac{1}{\delta^+}\frac{d\ln g}{d\ln \delta^+}\right| = \left|\frac{\gamma}{\delta^+}\right| \tag{B.13}$$

then the first term on the right-hand side of equation B.9 dominates. If $\gamma \rightarrow constant$ as $\delta^+ \rightarrow \infty$, the inequalities are satisfied. Note that a much weaker condition can be applied which yields the same result; namely that both inner and outer scaled profiles have the same dependence on δ^+, i.e., $S_i = S_o$ in the overlap range.

Since these inequalities are satisfied over some range in y, then to leading order, equation B.9 can be written as

$$\left.\frac{\overline{y}}{f_o^{(1)}}\frac{\partial f_o^{(1)}}{\partial \overline{y}}\right|_{\delta^+} = \gamma(\delta^+) \tag{B.14}$$

The solution to equation B.14 can be denoted as $f_o^{(1)}$ since it represents a first order approximations to f_o. It is *not*, however, simply the same as $f_{o\infty}$ because of the δ^+ dependence of γ, but reduces to it in the limit. Thus, by regrouping into the leading term all of the y-independent contributions, the method applied here has yielded a

more general result than the customary expansion about infinite Reynols number. It is also easy to see why the usual matching of infinite Reynolds number inner and outer solutions will not work if the limiting value of γ is zero.

From equation 5.58, it also follows that

$$\left.\frac{y^+}{f_i^{(1)}}\frac{\partial f_i^{(1)}}{\partial y^+}\right|_{\delta^+} = \gamma(\delta^+) \tag{B.15}$$

An interesting feature of these first order solutions is that the inequalities given by equations B.12 and B.13 determine the limits of validity of both equations B.14 and B.15 since either S_o or S_i will be large outside the overlap region. Clearly the extent of this region will increase as the Reynolds number (or δ^+) increases.

Both equations B.14 and B.15 must be independent of the origin for y; i.e. invariant to transformations of the form $y \to y + a$. Therefore, the most general solutions are of the form:

$$f_o^{(1)}(\overline{y}, \delta^+) = C_o(\overline{y} + \overline{a})^\gamma \tag{B.16}$$

$$f_i^{(1)}(y^+, \delta^+) = C_i(y^+ + a^+)^\gamma \tag{B.17}$$

where the parameters C_o, C_i and γ are functions of δ^+ and must be determined along with the constant a. *In the remainder of this chapter, the superscript '(1)' will be dropped; however it is these first order solutions that are being referred to unless otherwise stated.*

The relation between u_* and U_m follows immediately from equation 5.56; i.e.,

$$g(\delta^+) = \frac{C_o(\delta^+)}{C_i(\delta^+)}\delta^{+-\gamma(\delta^+)} \tag{B.18}$$

However, equation B.11 must also be satisfied. Substituting equation B.18 into

equation B.11 implies that γ, C_o, and C_i are constrained by

$$\ln \delta^+ \frac{d\gamma}{d\delta^+} = \frac{d}{d\delta^+} \ln \left[\frac{C_o}{C_i} \right] \tag{B.19}$$

or equivalently,

$$\ln \delta^+ \frac{d\gamma}{d \ln \delta^+} = \frac{d}{d \ln \delta^+} \ln \left[\frac{C_o}{C_i} \right] \tag{B.20}$$

Equation B.19 is exactly the criterion for the neglected terms in equation B.9 to vanish identically (i.e., $S_i - S_o \equiv 0$). Therefore the solution represented by equations B.16 – B.19 is, indeed, the first order solution for the velocity profile in the overlap layer at *finite*, but large, Reynolds number. Clearly when y^+ is too big or $\overline{y}$ is too small for a given value of δ^+, the inequalities of equation B.12 and B.13 cannot be satisfied. Since all the derivatives with respect to δ^+ must vanish as $\delta^+ \to \infty$ (the A.I.P.), the inner range of the outer overlap solution is unbounded in the limit, as is the outer range of the inner.

Since equation B.20 must be satisfied regardless of the precise choice of δ^+, solutions to it must be invariant to transformations of the type $\delta^+ \to D\delta^+$ where D is a scale factor. Also, equations B.16 and B.17 must be asymptotically independent of Reynolds number, since f_i and f_o are. Therefore the coefficients and exponent must be asymptotically constant; i.e.

$$\begin{aligned} \gamma(\delta^+) &\to \gamma_\infty \\ C_o(\delta^+) &\to C_{o\infty} \\ C_i(\delta^+) &\to C_{i\infty} \end{aligned}$$

as $\delta^+ \to \infty$. Also, as noted in in section 5.7, γ_∞, $C_{o\infty}$ and $C_{o\infty}$ cannot be zero. These conditions are powerful constraints; and together with equation B.19 rule out some functional forms for γ (like that suggested by Barenblatt (1993), for example).

Therefore it is important to note that they are a direct consequence of the AIP and the assumption that scaling laws should correspond to similarity solutions of the equations of motion.

... and two quotes for the road:

Remember, son, trying is the first step towards failure.
– Homer Simpson (immortal), animated couch potato, counseling Bart

There is no comparison between that which is lost by not succeeding and that lost by not trying.
– Francis Bacon (1561-1626), English philosopher

Bibliography

Abrahamsson, H., Johansson, B. & Löfdahl, L. 1994 A turbulent plane two-dimensional wall-jet in a quiescent surrounding. *Eur. J. Mech. B/Fluids* **13** (5), 533–556.

Barenblatt, G. I. 1993 Scaling laws for fully developed shear flow. Part 1. Basic hypotheses and analysis. *Journal of Fluid Mechanics* **248**, 513–520.

Barenblatt, G. I. 1996 *Scaling, Self-Similarity, and Intermediate Asymptotics*. Cambridge University Press, Cambridge, UK.

Barenblatt, G. I. & Chorin, A. J. 1998 Scaling of the intermediate region in wall-bounded turbulence: The power law. *Physics of Fluids* **10** (4), 1043–1044.

Barenblatt, G. I., Chorin, A. J. & Prostokishin, V. M. 1997 Scaling laws for fully developed flow in pipes. *Applied Mech. Rev.* **50** (7), 413–429.

Barenblatt, G. I. & Prostokishin, V. M. 1993 Scaling laws for fully developed shear flow. Part 2. Processing of experimental data. *Journal of Fluid Mechanics* **248**, 521–529.

Batchelor, G. K. 1953 *The Theory of Homogeneous Turbulence*. Cambridge University Press, Cambridge, UK.

Blake, W. K. 1983 *Fluid Mechanics Measurements*, chap. Differential Pressure Measurement, pp. 61–97. Hemisphere Publishing Co., Washington.

Blasius, H. 1908 Grenzschichten in Flüssigkeiten mit kleiner Reibung. *Z. Math. u. Phys.* **56**, 1–37.

Bradshaw, P. & Gee, M. 1960 Turbulent wall jets with and without an external stream. In *Aero. Res. Council R and M*.

Bradshaw, P. & Huang, G. 1995 Law of the wall in turbulent flows. In *Reynolds Anniversary Symposium*. Univ.Manchester, UK.

Bush, W. B. & Fendell, F. E. 1974 Asymptotic analysis of turbulent boundary layer and channel flow. *Journal of Fluid Mechanics* **56**, 657–681.

Castillo, L. 1997 Similarity analysis of turbulent boundary layers. PhD thesis, University at Buffalo.

Castillo, L. & George, W. K. 2000 Boundary layers with pressure gradient. *accepted for publication in AIAA Journal* .

Castillo, L., Walker, D. & Wosnik, M. 2000 The effect of the upstream conditions on the mean velocity deficit of turbulent boundary layers. In *AIAA Fluids 2000 Meeting*, , vol. AIAA 2000-2309. Denver, CO.

Clauser, F. H. 1954 The turbulent boundary layer. *Adv. Appl. Mech.* **IV**, 1–51.

Cole, J. D. & Kevorkian, J. 1981 *Perturbation Methods in Applied Mathematics*. New York: Springer-Verlag.

Coles, D. C. 1956 The law of the wake in turbulent boundary layers. *Journal of Fluid Mechanics* **1**, 191–226.

Coles, D. C. 1962 The turbulent boundary layer in a compressible fluid. *Tech. Rep.* R-403-PR. Rand Report.

Duncan, W. J., Thom, A. S. & Young, A. D. 1970 *Mechanics of Fluids*, 2nd edn. New York, NY: American Elsevier.

Durst, F., Jovanovic, J. & Sender, J. 1995 LDA measurement in the near-wall region of a turbulent pipe flow. *Journal of Fluid Mechanics* **295**, 305–335.

Eriksson, J., Karlsson, R. & Persson, J. 1997 An experimental study of a two-dimensional plane turbulent wall jet. *Tech. Rep.* US91:17O. Vattenfall Utveckling AB.

Eriksson, J., Karlsson, R. & Persson, J. 1998 An experimental study of a two-dimensional plane turbulent wall jet. *Experiments in Fluids* **25**, 50–60.

Eriksson, J., Karlsson, R. & Persson, J. 1999 Some new results for the turbulent wall jet, with focus on the near-wall region. In *Proc. 8th Int. Conf. on Laser Anemometry - Advances and Applications, Rome, Italy, Sept. 6-8, 1999.*, pp. 327–334. Paper XIII:1.

Fernholz, H. H., Krause, E., Nockemann, M. & Schober, M. 1995 Comparative measurements in the canonical boundary layer at $Re_{\delta_2} \leq 6 \times 10^4$ on the wall of the German-Dutch windtunnel. *Phys. Fluids* **7** (6), 1275–1281.

Frisch, U. 1995 *Turbulence*. Cambridge University Press, Cambridge, UK.

Gad-el-Hak, M. & Bandyopadhyay, P. R. 1994 Reynolds number effects in wall-bounded flows. *Applied Mech. Rev.* **47**, 307–365.

Gamard, S. & George, W. K. 2000 Reynolds number dependence of energy spectra in the overlap region of isotropic turbulence. *Flow, Turbulence and Combustion* (9), 1982, special B.E. Launder Birthday Issue.

George, W. K. 1988 Another look at the log (or is it a power law?) velocity profile for a zero-pressure gradient boundary layer. *Bulletin of the American Physical Society* **33** (10), 2301.

GEORGE, W. K. 1989 The self-preservation of turbulent flows and its relation to initial conditions and coherent structures. In *Advances in Turbulence*, pp. 39–73. Hemisphere, NY.

GEORGE, W. K. 1990 Another look at the log (or is it a power law?) velocity profile for a zero-pressure gradient boundary layer. 3rd Joint ASME/ASCE Mech. Conf. LaJolla, CA July 9-12.

GEORGE, W. K. 1992 The decay of homogeneous isotropic turbulence. *Physics of Fluids A* **4** (7), 1492–1509.

GEORGE, W. K. 1995 Some new ideas for similarity of turbulent shear flows. In *Proc. ICHMT Symposium on Turbulence, Heat and Mass Transfer, Lisbon, Portugal (1994)* (ed. Hanjalic & Pereira). Elsevier, Amsterdam.

GEORGE, W. K., ABRAHAMSSON, H., ERIKSSON, J., KARLSSON, R., LÖFDAHL, L. & WOSNIK, M. 2000 A similarity theory for the turbulent plane wall jet without external stream. *under consideration for publication in J.Fluid Mechanics* .

GEORGE, W. K. & CASTILLO, L. 1993 Boundary layers with pressure gradient: Another look at the equilibrium boundary layer. In *Near Wall Turbulent Flows* (ed. R. M. C. So, C. G. Speziale & B. E. Launder), pp. 901–910. Elsevier, NY.

GEORGE, W. K. & CASTILLO, L. 1997 Zero-pressure-gradient turbulent boundary layer. *Applied Mech. Rev.* **50** (12), 689–729.

GEORGE, W. K., CASTILLO, L. & KNECHT, P. 1996 The zero pressure-gradient turbulent boundary layer. *Tech. Rep.* TRL-153. Turbulence Research Laboratory, University at Buffalo.

GEORGE, W. K., CASTILLO, L. & WOSNIK, M. 1997 A theory for turbulent pipe and channel flows. *Tech. Rep.* TAM 872, UILU-ENG-97-6033. Theoretical and Applied Mechanics, University of Illinois at Urbana-Champaign.

George, W. K. & Gibson, M. M. 1992 The self-preservation of homogeneous shear flow turbulence. *Experiments in Fluids* **13**, 229–238.

George, W. K., Knecht, P. & Castillo, L. 1992 The zero pressure-gradient boundary layer revisited. In *13th Symposium on Turbulence* (ed. X. B. Reed). Rolla, MO.

Gibson, M. M. 1997 private communication to WKG.

Hama, F. R. 1954 Boundary layer characteristics for smooth and rough surfaces. *Trans. Soc. Nav. Archt. Marine Engrs.* **62**, 333–358.

Hanjalic, K. & Launder, B. E. 1974 Contribution towards a Reynolds stress closure for low-Reynolds number turbulence. Rept. HTS/74/24. Imperial College.

Hinze, J. O. 1975 *Turbulence*. McGraw-Hill, New York, NY.

Hussein, H. J., Capp, S. P. & George, W. K. 1994 Velocity measurements in a high-reynolds-number, momentum-conserving, axisymmetric, turbulent jet. *Journal of Fluid Mechanics* **258**, 31–75.

Irwin, H. 1973 Measurements in a self-preserving plane wall jet in a positive pressure gradient. *Journal of Fluid Mechanics* **61**, 33–63.

Johansson, G. & Castillo, L. 2000 New measurements in a zero pressure gradient boundary layer using LDA.

Johansson, T. & Karlsson, R. 1989 Energy budget in the near-wall region of a turbulent boundary layer. In *Applications of Laser Anemometry to Fluid Mechanics* (ed. R. A. et al.), pp. 3–22. Springer Verlag.

Karlsson, R., Eriksson, J. & Persson, J. 1993*a* An experimental study of a two-dimensional plane turbulent wall jet. *Tech. Rep.* VU-S93-B36. Vattenfall Utveckling AB, Älvkarleby Laboratory, Sweden.

KARLSSON, R., ERIKSSON, J. & PERSSON, J. 1993*b* LDV measurements in a plane wall jet in a large enclosure. In *Laser Techniques and Application in Fluid Mechanics* (ed. R. A. et al.), pp. 311–332. Springer Verlag.

KIM, J. 1989 On the structure of pressure fluctuations in simulated turbulent channel flow. *Journal of Fluid Mechanics* **205**, 421–451.

KIM, J. 1997 private communication.

KIM, J., MOIN, P. & MOSER, R. T. 1987 Turbulence statistics in fully developed channel flow at low reynolds number. *Journal of Fluid Mechanics* **177**, 133–166.

KNECHT, P. 1990 An investigation of the matched layer in a turbulent boundary layer with zero pressure gradient. Master's thesis, University at Buffalo.

KULFAN, B. 2000 Assessment of CFD predictions of viscous drag. In *AIAA Fluids 2000 Meeting*, , vol. AIAA 2000-2391. Denver, CO.

LAUNDER, B. E. & RODI, W. 1981 The turbulent wall jet. *Prog. Aerosp. Sci.* **19**, 81–128.

LAUNDER, B. E. & RODI, W. 1983 The turbulent wall jet – measurements and modelling. In *Ann. Rev. Fluid Mech.*, , vol. 15, pp. 429–459. Annual Reviews, Inc.

LONG, R. R. 1976 presentation at Naval Hydrodynamics Mtg., Wash., DC.

LONG, R. R. & CHEN, T.-C. 1981 Experimental evidence for the existence of the 'mesolayer' in turbulent systems. *Journal of Fluid Mechanics* **105**, 19–59.

MILLIKAN, C. B. 1938 A critical discussion of turbulent flow in channels and circular tubes. In *Proceedings of the 5th Int. Congress on Applied Mechanics, Cambridge, MA*, pp. 386–392. John Wiley and Sons, New York, NY.

MONIN, A. S. & YAGLOM, A. M. 1971 *Statistical Fluid Mechanics*. MIT Press, Cambridge,MA.

Moser, R., Rogers, M. & Ewing, D. 1996 Self-similarity of time-evolving plane wakes. *Tech. Rep.* TAM 829, UILU-ENG-96-6016. Theoretical and Applied Mechanics, University of Illinois at Urbana-Champaign.

Moser, R. T., Kim, J. & Mansour, N. N. 1999 Direct numerical simulation of turbulent channel flow up to $Re_\tau = 590$. *Phys. Fluids* **11** (4), 943–945.

Narasimha, R., Yegna Narayan, K. & Parthasarathy, S. 1973 Parametric analysis of turbulent wall jets in still air. *Aeronautical Journal* pp. 355 – 359.

Navier, M. 1827 Mémoire sur les lois du movement des fluides. *Mém. de l'Acad. de Sci.*. **6**, 389–416.

Oberlack, M. 1997 Unified theory for symmetries in plane parallel turbulent shear flows. manuscript 163. Center for Turbulence Research, NASA Ames/Stanford University (also submitted to jfm).

Österlund, J. M. 1999 Experimental studies of zero pressure-gradient turbulent boundary layer flow. PhD thesis, Royal Institute of Technology, Sweden.

Österlund, J. M., Johansson, A. V., Nagib, H. M. & Hites, M. H. 2000 A note on the overlap region in turbulent boundary layers. *Phys.Fluids* **12** (1), 1–4.

Panton, R. 1990 Scaling turbulent wall layers. *J. Fluids Engr.* **112**, 425–432.

Perry, A. E. & Abell, C. J. 1975 *Journal of Fluid Mechanics* **67**, 257.

Prandtl, L. 1932 Zur turbulenten Stroemung in Rohren und laengs Platten. *Ergeb. Aerodyn. Versuch Goettingen* **IV. Lieferung**, 18.

Reynolds, W. C. 1976 *Computation of Turbulent Flows*, , vol. 8, pp. 183–208. Ann. Rev. of Fluid Mech.

Reynolds, W. C., Kays, W. M. & Kline, S. J. 1958 Heat transfer in the turbulent incompressible boundary layer, i – constant wall temperature. *Tech. Rep.* 12-1-58W. NASA Memorandum, Washington, DC.

Schlichting, H. 1968 *Boundary-Layer Theory*. McGraw-Hill, New York, NY.

Sedov, L. I. 1959 *Similarity and Dimensional Methods in Mechanics*. Academic Press, New York, NY.

Smith, D. W. & Walker, J. H. 1959 Skin-friction measurements in incompressible flow. *Tech. Rep.* Technical Report R 26. NACA Report, Washington, DC.

Smith, R. W. 1994 Effect of Reynolds number on the structure of turbulent boundary layers. PhD thesis, Princeton University.

Smits, A. J. & Dussauge, A. P. 1996 *Turbulent shear layers in supersonic flows*. AIP Press.

Smits, A. J. & Zagarola, M. V. 1998 Response to: Scaling of the intermediate region in wall-bounded turbulence: The power law (Phys.Fluids 10, 1043 (1998)). *Physics of Fluids* **10** (4), 1045–1046.

Spurk, J. H. 1992 *Dimensionsanalyse in der Strömungslehre*. Berlin: Springer-Verlag.

Squire, H. B. 1948 Reconsideration of the theory of free turbulence. *Philosphical Magazine* **39** (288), 1–20.

Sreenivasan, K. R. 1989 The turbulent boundary layer. In *Frontiers in Experimental Fluid Mechanics* (ed. M. Gad-el-Hak), pp. 159–209.

Stanton, T. E. & Pannell, J. R. 1914 Similarity of motion in relation to the surface friction of fluids. *Phil. Trans. Roy. Soc. A* **214**, 199.

STOKES, G. G. 1845 On the theories of internal friction of fluids in motion. *Trans. Cambr. Phil. Soc.* **8**, 287–305.

TENNEKES, H. 1968 Outline of a second-order theory of turbulent pipe flow. *AIAA Journal* **6**, 1735–1740.

TENNEKES, H. & LUMLEY, J. L. 1972 *A First Course in Turbulence*. MIT Press, Cambridge,MA.

TOWNSEND, A. A. 1976 *The Structure of Turbulent Shear Flow*, 2nd edn. Cambridge University Press, Cambridge, UK.

VON KÁRMÁN, T. 1930 Mechanische Aehnlichkeit und Turbulenz. In *Nachr. Ges. Wiss.*, p. pp.68. Göttingen.

WHITE, F. M. 1991 *Viscous Fluid Flow*. McGraw-Hill, Inc., New York.

WIEGHARDT, K. 1943 Über die Wandschubspannung in turbulenten Reibungsschichten bei veränderlichem Aussendruck. *Tech. Rep.* U M-6603. Kaiser Wilhelm Institut für Strömungsforschung, Göttingen, Germany.

WOSNIK, M., CASTILLO, L. & GEORGE, W. K. 2000 A theory for turbulent pipe and channel flows. *under consideration for publication in J.Fluid Mechanics* .

WOSNIK, M. & GEORGE, W. K. 1995 Another look at the turbulent natural convection boundary layer. In *Proc. ICHMT Symposium on Turbulence, Heat and Mass Transfer, Lisbon, Portugal (1994)* (ed. Hanjalic & Pereira). Elsevier, Amsterdam.

WYGNANSKI, I., CHAMPAGNE, F. & MARASLI, B. 1986 On the large-scale structures in two-dimensional, small-deficit, turbulent wakes. *Journal of Fluid Mechanics* **168**, 31–71.

WYGNANSKI, I., KATZ, Y. & HOREV, E. 1992 On the applicability of various scaling laws to the turbulent wall jet. *Journal of Fluid Mechanics* **234**, 669–690.

ZAGAROLA, M. V. 1996 Mean flow scaling in turbulent pipe flow. PhD thesis, Princeton University.

ZAGAROLA, M. V., PERRY, A. E. & SMITS, A. J. 1997 Log laws or power laws: The scaling in the overlap region. *Phys. Fluids* **9**, 2094.

ZAGAROLA, M. V. & SMITS, A. J. 1998*a* Mean-flow scaling of turbulent pipe flow. *Journal of Fluid Mechanics* **373**, 33–79.

ZAGAROLA, M. V. & SMITS, A. J. 1998*b* A new mean velocity scaling for turbulent boundary layers. In *Proceedings of FEDSM'98, ASME*. Wash., DC.